An Electrochemical Investigation into the Corrosion Protection Properties of Coatings for the Active Metal Copper

Ursula Carragher

NUI MAYNOOTH

Ollscoil na hÉireann Má Nuad

A thesis submitted in partial fulfilment
of the requirements for
Doctor of Philosophy

Department of Chemistry
National University of Ireland, Maynooth
Ireland

Head of the Department: Dr. John Stephens
Supervisor of the Research: Prof. Carmel Breslin

Declaration Of Authorship

I hereby certify that this thesis, which I now submit for assessment on the programme of study leading to the award of PhD has not been submitted, in whole or part, to this or any other University for any degree and is, except where otherwise stated the original work of the author.

Signed: .....

Date: February 12, 2013

Abstract

In the research presented in this thesis, corrosion protection films were synthesised and characterised. The films were based on polypyrrole (PPy) coatings doped with combinations of tartrate, oxalate and dodecylbenzene sulfonate (DBS) along with the incorporation of multi-walled carbon nanotubes (MWCNT), and viologen films adsorbed at copper. The corrosion protective properties of these films were studied and compared to the uncoated copper substrate. They were assessed and studied using a combination of cyclic voltammetry, polarisation curves, Tafel analysis, open-circuit potential measurements and electrochemical impedance spectroscopy.

Polypyrrole films were successfully deposited at copper from a 0.10 mol dm^{-3} oxalate solution at a pH of 8.0 and a 0.10 mol dm^{-3} tartrate solution at a pH of 7.0 to generate PPy-Tartrate and PPy-Oxalate films on copper. SEM micrographs confirmed that the polymers were homogeneous, defect and crack-free. In addition, bi-layers comprising PPy-Tartrate/PPy-Oxalate and PPy-Oxalate/PPy-Tartrate were successfully formed at the copper interface. The bi-layer provided the better corrosion protective coatings. Higher breakdown potentials were observed with the bi-layer. In an attempt to further improve the corrosion protective properties of the bi-layer coatings, MWCNT, were incorporated into the polymer films. The MWCNT were successfully dispersed using DBS. The concentration ratio of the MWCNT to DBS was important in forming a stable and well dispersed solution. This was achieved using 0.05 mol dm^{-3} DBS and 0.02 mg MWCNT. The MWCNT-modified polypyrrole films were deposited as bi-layers and multi-layers and showed excellent corrosion protection for copper. The PPy-Tartrate/PPy-DBS bi-layer films also showed potential as a corrosion protective coating.

An alternative approach was then considered. The electrochemical deposition of three viologens, methyl viologen (MV), benzyl viologen (BV) and ethyl viologen (EV) at copper in the presence of a 0.10 mol dm^{-3} NaCl supporting electrolyte was studied. The formation of the viologen films was achieved by cycling the copper electrode from -0.20 to 1.00 V vs. SCE at a

scan rate of 1 mV s^{-1}. For comparison, the copper was cycled under the same conditions in the 0.10 mol dm^{-3} NaCl solution, but in the absence of the viologens. Significant dissolution of the copper was observed in the absence of the viologens. However, considerably lower currents were measured in the presence of the viologens, indicating a reduction in the rate of dissolution and the formation of a protective film.

Acknowledgements

Firstly, I would like to express my sincere and heartfelt thank you to my supervisor Prof. Carmel Breslin for her continuous support throughout my PhD research. Carmel has been both a friend and a mentor. She has always been there to offer encouragement and guidance, her door was always open. Carmel had belief in me when I doubted myself and showed me how to approach my research problems and the need to be persistent with my goal. She was always there to proofread and correct my chapters and I really appreciate all you have done for me. I thank you for all your help, I could not have finished my thesis without you.

During the course of this work I was funded by Science Foundation Ireland (SFI) and Monaghan County Council.

I'd also like to thank Dr. Denise Rooney, Dr. Bernadette Alcock and Dr. John Colleran for their help, encouragement and support over the last few years. To the technical staff, especially Ken, Ria, Orla, Barbara, Ann and Ollie, thanks for all the help and expertise throughout the years. A special thank you to Mr. Noel Williams, who was always there to help out with all computer glitches, the department would be lost without him. I would also like to extend my gratitude to the executive staff, Niamh and Donna for all their help.

Louise thank you for your support and encouragement over the last few years especially in the last few weeks. Thank you for amusing me and coming with me for our extracurricular activities to the business campus, you will thanks me some day for those bruises, we have had some good memories and laughs over the last few years, the christmas parties, Slane 2011 to name a few. You are a good friend and I wish you every success in the future. Likewise, Anita and Paul thank you for friendship, your support and help over the last number of years, I hope you both are successful in whatever path you both choose. A special thank you to my lab colleagues Orla (the random conversations to yourself were always amusing), Emer, Dave, Lynn, Sam and Gama, you are some of the kindest, generous people I know and are always there to offer your support, best of luck in the future. To my fellow postgraduate students both

past and present, a special mention to Conor, thank you for all your help with the SEM, Trish, John and Saidhbhe, thanks for the banter and laughs in the reading room, best of luck in the future.

To my friends outside college who have been so understanding, supportive and have kept me sane over the last few months, a special thanks you to Angela, Orlaith, Eileen, Michelle, Deirdre, Catherine and Emma. Thank you for the keeping me grounded and always putting a smile on my face no matter how tough things were, especially in the last few months. The phone calls and text messages of encouragement were always welcome and much appreciated even though it might not of appeared that way at the time.

I would like to extend a special thank you to my wonderful boyfriend and best friend John, John has always been there for me since day one, through thick and thin. He has encouraged me and supported me. No matter how tough things got, he was always there. He has helped with so much in the last few years, months and weeks I will never forget the endless hours and days spent helping my with my thesis, he would not hesitate, my happiness was his priority. Thank you for being there, for your love, hugs, motivation, your understanding and for your constant support. You were always there when I needed someone to talk to, when I was having a bad day, no matter how busy you would be with your own PhD you would always make time to clam me down and make me see sense. Even after a long day at the office John would still be there for me to help me fix any problems or glitches I had, regardless of the time. I would not be here today if it was not for all your help, support and encouragement and I definitely would not have finished my thesis without you. You mean the world to me; I will never forget what you have done for me.

I would also like to extend a special thanks to John's family for their endless support, encouragement and help over the last few years, Kathleen, Eddie, Catherine, Emma and Edward and the extended family of Brendan, James and Emma, thank you for all the words of advice, the constant phone calls and text messages, the support was much appreciated. To John's nieces and nephew, Kathlyn (BFF), Jasmine, Amber, Rachel and Seamus, thank you for all the laughs and fun over the last few months, I love you all.

Finally, I would like to thank my own family for all their support over the last few years in particular. My parents Paddy and Margaret for your unconditional love, your understanding and the many words of encouragement. My brothers Padraig, Stephen and Ferghal and my sisters Fiona, Aoife and Orfhlaith. Thank for the much needed distractions and phone calls. Thank you for all the support, love and hugs especially when I needed them the most.

Dedicated to both John and my parents with Love.

Contents

List of Figures

List of Tables

CHAPTER 1

Introduction

The objective of this thesis is to develop and analyse anti-corrosive coatings based on polypyrrole (PPy) and modified polypyrrole coatings for non-inert metals, namely copper (Cu) [1, 2]. Copper is widely used in industry and is particularly well known for its use in piping and in the electronics industry [3]. The use of copper has been growing continuously for over a century. However, the activity of copper and copper alloys depends on the surrounding environment [4, 5, 6, 7, 8]. This activity can change dramatically under certain conditions resulting in corrosion of the metal. Corrosion is a naturally occurring phenomenon which affects the performance of materials used in many technological fields, ranging from light-weight aluminium alloys, used in the aerospace industry, materials used in the electronics industry, materials used in transportation, petroleum, pipeline, waste water, coatings and linings, food, pulp and paper, power, fuel cell and refining industries [9, 10]. Many of the traditional corrosion protective strategies, for example those employing chromates, are no longer viable due to environmental considerations. Consequently, there is an ever-increasing interest in developing new and environmentally acceptable corrosion-control technologies. This is a multidisciplinary and technologically important field of research affecting metals and alloys and attracting the interest of Chemists, Physicists, Engineers and Material Scientists.

In this introductory chapter, information on corrosion and the electrochemical stability

and corrosion of copper is first presented [11]. Then, the concept of conducting polymers is introduced and the electrochemistry of PPy [12, 13] and its applications are described in detail, followed by a section on the application of conducting polymers in corrosion protection [14]. This is followed with information on carbon nanotubes [15] and dodecylbenzene sulfonate [16]. Finally, the chapter ends with a section on the electrochemistry of viologen compounds [17]. These topics are all relevant to the work presented in this thesis.

The results and main findings are presented and discussed in Chapters 3 - 7. The properties and characteristics of copper and the electrosynthesis of PPy at copper are outlined and discussed in Chapter 3, where an extensive section is devoted to the synthesis of the polymer, PPy [18, 19], at the corrosion-susceptible copper substrate. Strategies to enhance the corrosion protection properties of the coating are presented in Chapter 4. In particular, promising results were obtained by incorporating multi-walled carbon nanotubes (MWCNTs), dispersed in dodecylbenzene sulfonate (DBS), [20, 21] within the polymer matrix. In view of the successful results obtained in Chapter 4, the results presented in Chapter 5 are focussed on a comprehensive study to determine if the DBS or the MWCNTs are responsible for the good corrosion protection observed and which is the key factor in the corrosion-protection coatings. In Chapters 6 and 7, viologens are introduced and their various properties are discussed and highlighted. No prior work has been reported in the literature on corrosion protection of copper by viologens. Accordingly the viologens were adsorbed onto the copper surface and their corrosion protection properties are highlighted in Chapter 7.

The work presented in this thesis is significant in terms of its contribution to the scientific field of conducting polymers and protective coatings. To date, conducting polymers have been deposited at copper [1], iron [22], steels [23, 24] and various aluminium alloys [25, 26, 27] and have been reported to give corrosion protection. Recently, conducting polymers and their protective abilities have been featured in Science Daily, Science Centric and Nanowerk News as 'conductive plastic fights against corrosion'. This clearly illustrates the interest in using these materials as environmentally acceptable corrosion protective coatings. Indeed, there are now a number of industrial companies concentrating on marketing conductive polymers. For example, Panipol Ltd. sell polyaniline emeraldine base, Panipol PA, as a pigment for paint to shield steel structures against climatic corrosion, while Ormecon Chemie GmbH, have dispersed polyaniline in paint for the production of industrially applicable and effective

corrosion prevention primers.

At a more fundamental level, a number of different mechanisms have been proposed to explain the corrosion protection afforded by these polymers and modified polymer coatings [28, 29]. These include the so-called 'ennobling mechanism', which is based on the fact that the conducting polymer may act as an oxidiser, enhancing the formation of the oxide layer at the polymer/metal interface. Another proposed mechanism is that conducting polymers shift the reaction site of oxygen reduction, the key reaction during delamination of protective coatings. More recent studies have explored the release of corrosion inhibitors from the conducting polymer. For example, Barisci *et al.* [30] were the first to point out that as a result of the galvanic coupling between the corroding metal and the conducting polymer, the polymer is reduced and consequently dopants could be released. If dopants with corrosion inhibiting properties were chosen, then these inhibitors could be released at the corroding site to slow down the corrosion event. However, with the presence of oxygen in the environment, the polymers are subsequently oxidised and will then, most likely, be doped with chlorides or other corrosion promoting anions.

1.1 Corrosion

Corrosion can be defined as an irreversible reaction of a material with the environment, which usually (but not always) results in the degradation of the material, or as the chemical and/or electrochemical reaction between a material and its environment that produces a deterioration of the material and its properties. There are several parameters that influence the rate and nature of the corrosion reactions and these include the material, the properties of the material and the environment, the chemical composition, the constituents, and the temperature.

1.1.1 Fundamental Corrosion Reaction

Corrosion involves the oxidation of the metal to form ionic species with a higher oxidation state and the liberation of electrons [31, 32], as depicted in Equation 1.1 for a generic metal [M].

$$M \rightarrow M^{z+} + ze^{-} \tag{1.1}$$

This equation corresponds to the oxidation half-cell reaction and the electrons liberated must be consumed by a reduction reaction occurring on the same surface. The sites for the oxidation reaction are known as anodes, and the sites for the reduction reactions are called cathodes. Anodes and cathodes can be spatially separated at fixed locations associated with heterogeneities on the electrode surface. Alternatively, the locations of the anodic and cathodic reactions can fluctuate randomly across the sample surface. The former case results in a localised form of corrosion, such as pitting, crevice corrosion, intergranular corrosion, or galvanic corrosion, and the latter case normally results in uniform corrosion. In all cases, the anodic and cathodic sites must be electrically connected, to facilitate electron transfer [33, 34, 35]. The environment in which the corrosion reaction takes place is also very important and completes the electrochemical cell [36, 37, 38]. This is often a solution or an electrolyte with solvated ions. For the corrosion reaction to proceed, the electrolytes must have sufficient conductivity to allow the transport of ions and minimise the resistance. Accordingly, the properties of the electrolyte solution, particularly conductivity and mobility of the ions, can influence the rate of the corrosion reaction [36, 39].

1.1.2 Structure of the Electrode-Solution Interface

As corrosion occurs at the interface of the metal and an electrolyte, the structure of this interface is important in controlling the initiation and propagation of the corrosion reactions. At the electrode surface there is an excess of charge of one sign and in the solution there is an excess of charge of the opposite sign. As a consequence there is a potential drop at the metal solution interface. The separation of charge at an electrode-electrolyte interface may be viewed as a capacitor, as first suggested by Helmholtz [39, 40, 41]. The solution side of the double layer is thought to be made up of several layers. This theory was first put forward by Helmholtz in the 1850s. In this model he proposed that the interactions between the ions in solution and the electrode surface were electrostatic in nature and resulted from the fact that the electrode holds a charge density (q^m) which arises from either an excess or deficiency of electrons at the electrode surface. In order for the interface to remain neutral the charge held on the electrode is balanced by the redistribution of ions close to the electrode surface.

The attracted ions are assumed to approach the electrode surface and form a layer balancing the electrode charge. The distance of approach is limited to the radius of the ion and a single

sphere of solvation round each ion. The overall result is two layers of charge (the double layer) and a potential drop which is confined to only this region (termed the outer Helmholtz Plane, OHP) in solution [40]. The result is analogous to an electrical capacitor which has two plates of charge separated by some distance (d) with the potential drop occurring in a linear manner between the two plates. It is perhaps no surprise that when impedance analysis is performed on electrochemical systems the response due to the electrolyte redistribution is modelled in terms of a capacitance [41, 42, 43].

The model of Helmholtz, while providing a basis for rationalising the behaviour of this region, does not account for many factors such as, diffusion/mixing in solution, the possibility of adsorption on to the surface and the interaction between solvent dipole moments and the electrode. A later model put forward by Stern begins to address some of these limitations [39, 43], Figure 1.1. Now the ions are assumed to be able to move in solution and so the electrostatic interactions are in competition with Brownian motion. The result is still a region close to the electrode surface (100×10^{-10} m) containing an excess of one type of ion but now the potential drop occurs over the region called the diffuse layer. Many modifications and improvements have been made to these early models with the latest approaches using numerical modelling to follow the redistribution effects as the electrode potential is varied [39, 44, 45, 46].

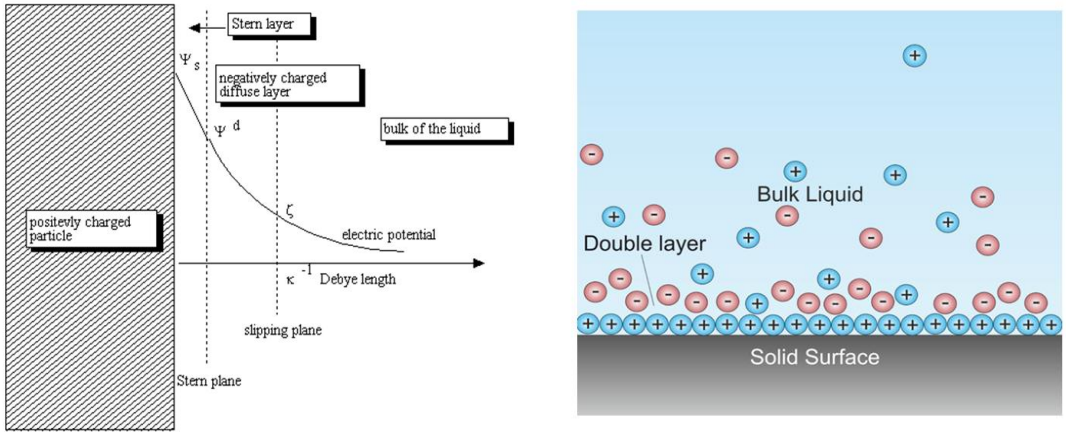

(a) **(b)**

Figure 1.1: Schematic of the electrical double layer showing most of Stern's adjustments to the Helmholtz analysis: (a) detailed illustration of interfacial double layer and (b) schematic of double layer in a liquid in contact with a negative charged solid.

1.2 Forms of Corrosion

Corrosion occurs at this electrode-solution interface, Figure 1.1, and there are many types of corrosion, ranging from uniform to localised corrosion. For convenience, these are usually categorised into eight different forms, namely galvanic, crevice, pitting, intergranular, leaching, erosion-corrosion stress corrosion cracking and hydrogen embrittlement [33, 34, 35, 47, 48].

Galvanic corrosion [23] can result when a metal is in contact with another dissimilar metal to give distinct cathodes and anodes. Dissolution of the anode occurs, while the cathode is protected and not dissolved, leading to the preferential dissolution of one of the metals. Some examples include copper and zinc, iron and brass, or mild steel and cast iron. Crevice corrosion occurs when a differential aeration, or oxygen concentration cell, is established. It results from a difference in the composition of the electrolyte under the crevice, or restricted area, and that outside of the crevice. Moreover, there is a higher oxygen concentration in the solution that surrounds the crevice than contained within the crevice, and this gives rise to accelerated corrosion inside the crevice [49, 50].

Many passive electrodes suffer from pitting corrosion, where the pit is considered to be a self-catalysing cell. Pits are nucleated on the surface, usually at some surface defect, and this gives rise to high dissolution of the metal at the site of the pit, while the reduction reactions proceed on the passive surface [51, 52, 53]. Intergranular corrosion occurs at the boundaries of the metallic grains that make up the metal, while selective leaching corrosion is due to the selective leaching of an alloying element out of the alloy matrix [35, 54, 55]. The most common form of this type of corrosion is dezincification, the selective leaching of zinc from a brass matrix [45, 56]. In general, embrittlement is corrosion that causes a ductile material to fail without localised yielding or shearing. More specifically, hydrogen embrittlement assumes several different forms with a general similarity. This damage takes place at the cathode. Hydrogen ions are adsorbed and reduced to hydrogen molecules at the cathode. These molecules bubble off as hydrogen gas. However, some metals are very susceptible to the permeation of hydrogen atoms into the grains and this gives rise to embrittlement [57, 58].

Copper is less affected by galvanic reactions, compared to most other metals. As a result, the electrical industry generally considers copper to be corrosion resistant in virtually all environments while regarding steel and aluminium as non-resistant. However, this is an over

generalisation. In contact with more noble metals such as passive nickel, passive stainless steel or titanium, copper is galvanically depleted just as readily as steel [59] or aluminium [27, 54]. Copper and copper alloys [35, 58, 60] are widely used in many environments and applications because of their excellent corrosion resistance, which is coupled with combinations of other desirable properties, such as superior electrical and thermal conductivity, ease of fabricating, wide range of attainable mechanical properties, and resistance to biofouling. Copper corrodes at negligible rates in unpolluted air, water, and deaerated non-oxidising acids [39]. Copper alloy artifacts have been found in nearly pristine condition after having been buried in the earth for thousands of years, and copper roofing in rural atmospheres has been found to corrode at rates of less than 0.4 mm in 200 years. Copper alloys resist many saline solutions, alkaline solutions, and organic chemicals. However, copper is susceptible to more rapid attack in oxidising acids, oxidising heavy-metal salts, sulfur, ammonia (NH_3), and some sulfur and NH_3 compounds [39, 61, 62, 63]. Copper develops a strongly adhering oxide layer [64, 65, 66, 67], which thickens to acquire the familiar green patina. In the presence of atmospheric sulfur dioxide (SO_2) the transition from oxide layer to patina is accelerated [68]. In applications such as roofing where the green patina has aesthetic value, the increase in formation of patina is desirable. This is definitely not the case in electrical system applications where the formation of this thick non-conductive patina is undesirable. There are various methods of corrosion prevention or control that are generally used in an attempt to avoid or minimise these corrosion reactions. The approach depends on the form of corrosion, but in general includes the use of corrosion inhibitors, cathodic protection, anodic protection and coatings, which range from metallic to various types of non-metallic coatings [3, 69, 70, 71, 72].

1.3 Electrochemical Stability and Corrosion Protection of Copper

In this section the electrochemical stability of copper is discussed. This analysis is performed with the aid of Pourbaix diagrams, which were first constructed by Marcel Pourbaix, and the stable domains of copper are discussed as a function of pH and potential. Also reviewed in this section are some of the documented procedures for the corrosion control of copper using benzotriazole (BTA). BTA is a well known corrosion inhibitor used to protect copper from corrosion [7].

1.3.1 Electrochemical Stability of Copper

The Pourbaix diagram of copper [73] is shown in Figure 1.2, giving the stable domains of copper oxide, copper metal and oxidised copper species, Cu^{2+} and Cu^{+}.

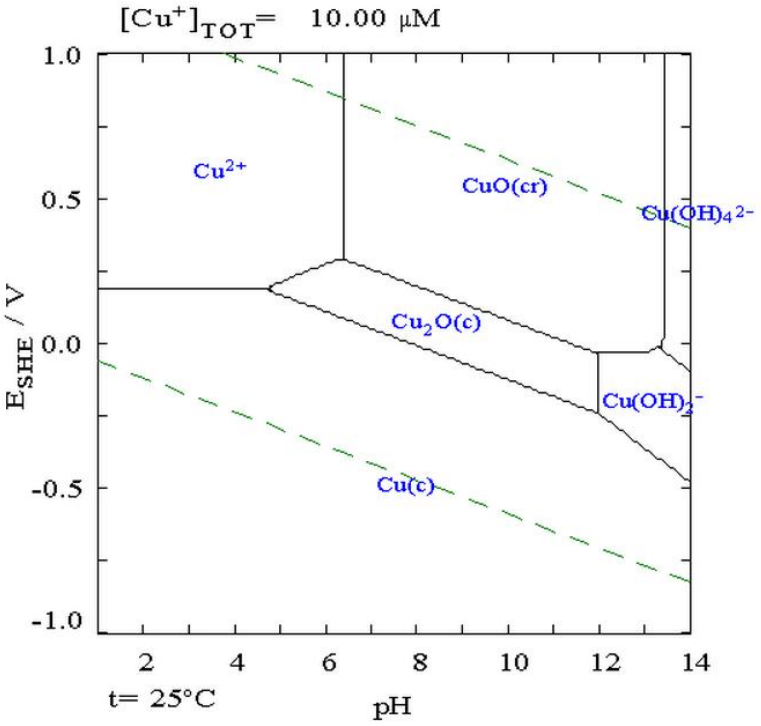

Figure 1.2: Pourbaix diagram of copper.

Some of the equations used to construct the diagram are given in Equations 1.2 to 1.4, while in the presence of chloride anions, Equations 1.5 and 1.6 can occur to generate corrosion products, such as CuCl and $Cu_2(OH)_3Cl$.

$$Cu_2O + 2H^+ + 2e^- \rightleftharpoons 2Cu + H_2O$$
$$E = E^0\ 0.471 - 0.0591pH \tag{1.2}$$

$$2CuO + 2H^+ + 2e^- \rightleftharpoons Cu_2O + H_2O$$
$$E = E^0\ 0.669 - 0.0591pH \tag{1.3}$$

$$2Cu(OH)_2 + 2H^+ + 2e^- \rightleftharpoons Cu_2O + 3H_2O$$
$$E = E^0\ 0.747 - 0.0591pH \tag{1.4}$$

$$CuCl + e^- \rightleftharpoons Cu + Cl^-$$
$$E = E^0\ 0.1575 \tag{1.5}$$

$$Cu_2(OH)_3Cl + Cl^- + 3H^+ + 2e^- \rightleftharpoons 2CuCl + 3H_2O$$
$$E = E^0\ 0.778 - 0.08865pH \tag{1.6}$$

It is clear from this diagram that relatively high pH values are required for the formation of copper oxides and that at values below pH 6.0, free copper, Cu^{2+}, ions are the stable form. At higher pH values, and depending on the electrode potential, the formation of two copper oxides is possible. The Cu_2O is formed at lower applied potentials, while the CuO is stable at higher potentials.

These oxides have been studied extensively. For example, Feng *et al.* [32] have summarised the corrosion products formed on the copper electrode during anodic polarisation. It is generally thought that a Cu_2O phase initially is deposited during anodic oxidation, followed by electroformation of Cu(II) compounds, such as cupric hydroxide ($Cu(OH)_2$) and cupric oxide (CuO) at higher potentials. It is thought that passivation is primarily caused by the electroformation of a $Cu(OH)_2$ film filling the pores of the base film. Shoesmith *et al.* [74, 75] have demonstrated that $Cu(OH)_2$ forms in two layers, a base layer grown by a solid-state mechanism and an upper layer of individual crystals nucleated and grown from solution. As previously reported by Feng *et al*. [32] this $Cu(OH)_2$ phase is in chemical equilibrium with the CuO and is transformed to CuO upon ageing. This in turn agrees with results reported by Pyun and Park [76] who have also shown, using an incidence reflectance spectrochemical technique, that hydroxides of Cu(I) and Cu(II) are first formed by anodic oxidation at corresponding potentials and then transform to oxides upon ageing. Burke *et al*. [65] have concluded that both Cu_2O and CuO can exist in both anhydrous and hydrated forms, however, Cu_2O appears to be poorly conducting and can act as a barrier and inhibit reduction of the Cu(II) species if

present in a thick film. In addition to the advances made Capobianco *et al*. [77] also verified the presence of Cu_2O and CuOH in the oxide layers and they have shown that the ratio of CuOH/Cu_2O increases on decreasing the anodic potential and on increasing the oxidation time. Sathiyanarayanan *et al.* [78] have recorded the photo potentials of the passive films formed on copper in sodium hydroxide showing that the oxides behave as *p*-type semi-conductors and that the composition of the film varies considerably with time. Also, Abrantes *et al.* [79] have recorded the presence of the *p*-type Cu_2O initially on oxidation of copper on the forward sweep of the cyclic voltammogram. The thickness of the layer increases on the reverse sweep as an over-layer of $Cu(OH)_2$ or CuO is reduced to Cu_2O.

Thomas and Tiller [80] have studied the effects of chloride on the passive film formed on copper and have shown that the oxide layer retains some protective character. However, when conditions favour interactions of chloride ions with the oxide, i.e., longer immersion times, or greater chloride concentration, the oxide layer becomes less protective, and the breakdown potential is displaced to more negative potentials and becomes less defined. This is expected as under acidic to near-neutral conditions, formation of Cu complexes is possible. Cornwell *et al.* [81] have also studied the effect of chloride ions on copper corrosion, however they have confined their study to that of supply waters. They have suggested that a clean copper surface immersed in aerated water containing chloride will form cuprous chloride by anodic dissolution of the copper electrode. Cuprous chloride is not stable at near-neutral pH ranges and hydrolyses to form cuprous oxide, which is precipitated on the metal surface. Using the hydroxyl ions created by the cathodic reaction and bicarbonate ions present in water supplies, a mixed calcium carbonate and basic copper carbonate scale precipitates to the surface. However, if the surface is unclean, i.e., such as carbon on the surface, an increase in the copper dissolution rate is seen. Consequently an increase in the formation of cuprous chloride is observed resulting in a contaminated oxide layer which is less adherent than that formed on clean copper.

1.3.2 Corrosion Protection of Copper

It is evident that the corrosion of copper gives unwanted corrosion products, such as cuprous chloride, and this leads to dissolution and attack of the copper structure. Over the last number of decades scientists have overcome this problem by the use of organic and inorganic inhibitors. Figure 1.3 depicts the chemical structure of BTA, this is one of the most common inhibitors

used in the protection of copper metal. Some of the earlier work was performed by Cotton and co-workers in the early 1960s [70, 82]. In these studies, Cotton and his co-workers showed that the products produced on the BTA treated surface are polymeric in nature and are chemically bonded to the metal oxide or metal surface. BTA also afforded good corrosion protection in both aqueous and gaseous environments polluted with sulfur dioxide, hydrogen sulfide and salt mist. These authors also discovered that benzotriazole could be applied as an aqueous solution or be incorporated in lacquers and polishes. Since then, BTA has been extensively studied, in an attempt to understand the mechanism of protection afforded to the underlying metal.

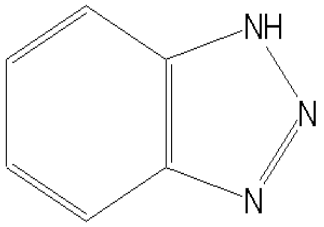

Figure 1.3: The chemical structure of BTA.

Modestov *et al*. [83] have studied the electrochemical formation of Cu(I)-BTA films on copper electrodes and the mechanism of corrosion inhibition in aqueous chloride/BTA solutions. Their results showed that in chloride solutions the Cu(I)-BTA film formation occurs according to the following reactions, Equations 1.7 and 1.8.

$$Cu + 2Cl^{-} \rightleftharpoons CuCl_2^{-} + e^{-} \tag{1.7}$$

$$CuCl_2^{-} + H - BTA \rightleftharpoons Cu - BTA + 2Cl^{-} + H^{+} \tag{1.8}$$

The formation of Cu(I)-BTA is accompanied by the deposition of Cu_2O as the under-layer. This layer is unstable. It regains stability through the formation of the Cu(I)-BTA over-layer, which maintains a high resistance by preventing the layer from being doped with Cl^- ions and preventing the formation of CuCl. The presence of Cu_2O has been confirmed by Modestov *et al*. [83] by SEM analysis and it is assumed that Cu_2O formed in the air at the copper surface is a source of Cu(I) oxide for the Cu(I)-BTA film. Barbic *et al.* [84] have verified the presence of a Cu_2O layer underneath the Cu-inhibitor over-layer.

However, there have been reports of the formation of BTA films on oxide free surfaces [85, 86]. In these works, Tromans and colleagues have shown that BTA can interact with oxide free surfaces to promote the corrosion inhibition of copper metal. The inhibition mechanism can be described by Equations 1.9, 1.10 and 1.11.

$$Cu + BTAH \rightarrow (Cu - BTAH)_{ads} \tag{1.9}$$

$$nCuCl_2^- + nBTAH \rightarrow (Cu - BTA)_n + nH^+ + 2nCl^- \tag{1.10}$$

$$(Cu - BATH)_{ads} + (Cu - BTA)_n \rightarrow [(Cu - BTAH) - (Cu - BTA)_n]_{ads} \tag{1.11}$$

The critical step is the adsorption of the BTAH onto the oxide-free surface, which is both time and potential dependent. Studies by Hope *et al.* [87] show that H-BTA is initially adsorbed on to clean copper by coordination through the nitrogen lone pair. Ashour *et al.* [88] have shown that the interaction of BTA with a Cu_2O covered CuZn alloy is faster than on a reduced alloy, although the protection efficiency on the latter is slightly better than on the former.

Sayed *et al.* [89] have shown the effects of BTA on stress corrosion cracking of α-brass and reported that BTA inhibits the dezincification process and hence reduces the corrosion cracking of the alloy. Mansfeld and Smith [90] have carried out studies on BTA as a corrosion inhibitor for copper and the mechanism of corrosion inhibition in acid chloride solutions and have reported an increase in breakdown potentials, an increase in the polarisation resistance and also the inhibition of the formation of CuCl containing corrosion products in the presence of BTA. Zhou *et al.* [91] studied the photo-response of copper electrodes in a borate buffer solution containing BTA and have observed the presence of both *n*-type and *p*-type conductivities in the Cu_2O film. They also recorded that the higher the inhibition efficiency the greater the anodic photocurrent allowing the photo-response to be used as a method of evaluating the corrosion efficiency of the inhibitor. Bellakhal and Dachraoui [92] studied BTA as an inhibitor for copper in humid air plasma. In this study it was shown that BTA limits the oxidation process induced by gaseous species. The organic layer remains active for at least 40 min. For longer exposures, the BTA molecules, which form a film at the surface of copper, begin to degrade to carbon dioxide or other volatile organic compounds. The results obtained from this study showed that the non-thermal gliding arc discharge can be used as a tool to study the efficiency of the organic

inhibitors present at metallic surfaces [92].

Allam *et al.* [38] carried out research on the effect of BTA on copper and its alloys in both clean and polluted environments. The chemistry of BTA was reviewed and was shown to be the crucial element in determining the inhibition ability of BTA. BTA was found to be a good corrosion inhibitor for copper and its alloys in clean environments. However, the presence of pollutants, such as sulfide ions, gave a damaging effect on the remarkable inhibition efficiency of BTA against the corrosion of copper and its alloys. The use of BTA derivatives were shown to increase the inhibition efficiency. On the other hand, the use of BTA blends was reported to be a good alternative in the case of an aggressive environment [38].

Many other types of organic inhibitors, apart from BTA, have been researched for the corrosion protection of copper and its alloys. Cicileo *et al*. [93] have reported that the organic inhibitors from the oxime group exhibit strong corrosion protection. Gomma [94] has observed the inhibition efficiencies of other azoles derivatives, including tolyltriazole and imidazole and has found that the inhibition efficiency follows the sequence: BTA > tolyltriazole > imidazole. Subramanian and Lakshminarayanan [95] have carried out research on the adsorption ability of azoles on copper oxides and have found them to be in the order: mercaptobenzothiazole > benzimidazole ≈ mercaptobenzothiazole> benzotriazole ≈ imidazole.

Figure 1.4 illustrates a typical self-assembled monolayer (SAM). Metikos-Hukovic *et al.* [96] investigated the corrosion protection of a SAM of alkanethiol and observed that the SAMs of dodecanethiol (DT) formed in the absence of oxygen were characterised by a high hydrophobicity, low capacitance, and high resistance, thus providing an excellent barrier against corrosive species from attacking the underlying copper substrate. Guenbour *et al.* [97] have carried out investigations on the corrosion protection properties of polyaminophenol films and have shown that the polymer film reduces the corrosion of copper, however, polymerisation in the presence of azole compounds further increases the protective character of the coating.

Zhang *et al.* [98] investigated highly reliable copper-based conductive adhesives using an amine curing agent for corrosion prevention. The coordination of the amine curing agent to the exposed copper of Ag-coated copper flakes prevents the oxidation of the exposed copper during the isotropically conductive adhesives (ICA) curing at 150 °C. Following the curing process, the secondary and tertiary amine groups could further protect the exposed copper surface from oxidation/corrosion in harsh environments [98]. Taneichi *et al.* [99] have carried

out studies on alkyl isocyanates modified 11-mercapto-1-undecanol (MUO) self-assembled monolayers as alternatives of chlorosilane modifiers for protective films and have reported protection efficiencies as high as 95.4%. Singh and Singh [100] have carried out research on the corrosion of copper in aqueous solutions of formic acid and have added organometallic inhibitors to reduce the rate of corrosion. Their results show that Ph_3SnCl has inhibition properties in both acids. Patel *et al.* [101] investigated the effect of 2-mercaptothiazoline as corrosion inhibitor for copper in acidic media. They observed that the inhibitive power of the 2-mercaptothiazoline among the acids tested is in the order: trichloracteic acid < dichloroacetic acid < monochloroacetic acid < acetic acid.

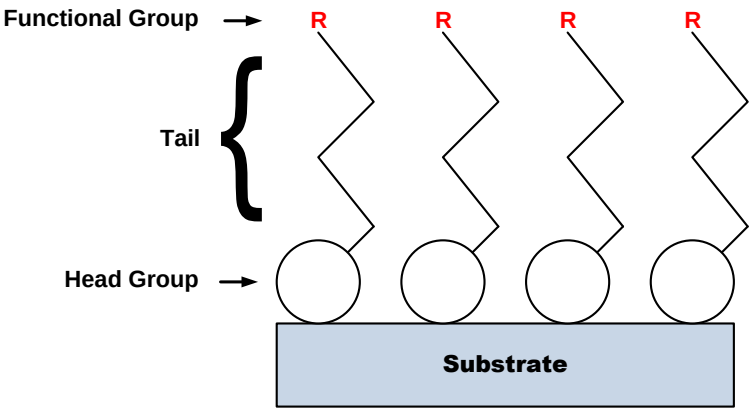

Figure 1.4: A schematic of a self-assembled monolayer (SAM).

However in recent years, conducting polymers have emerged as a potential corrosion-control and corrosion inhibition technology. This subsequent section is focused on an introduction to conducting polymers and details on the electropolymerisation of pyrrole and the formation of polypyrrole at inert electrodes. Finally, an overview of the application of conducting polymers in corrosion protection, with a particular focus on copper, is given in Section 1.5.

1.4 Introduction to Conducting Polymers

A polymer is made up of smaller repeating units, called monomers. Polymers are produced through the polymerisation of a monomer. This polymerisation step can be achieved by chemical or electrochemical methods. Originally polymers with basic carbon chains were

considered only as insulators. The first real interest in conducting polymers can be attributed to Walatka *et al.* [102] in 1973 with the report of highly conducting polysulfur nitride $(SN)_x$. Meanwhile, towards the late 1970s, MacDiarmid, Shirakawa and Heeger enhanced the discovery of the semi-conducting and metallic properties of the chemically synthesised organic polyacetylene [103]. As is well known, the Nobel Prize in Chemistry was awarded to Alan J. Heeger, Alan G. MacDiarmid and Hideki Shirakawa in 2000 for the discovery and development of conducting polymers (CPs). In the following years, a wide range of polymeric organic species have been prepared as stable inherent films on inert electrodes via both chemical oxidation and electropolymerisation from aqueous and organic solutions.

Conducting polymers consist of carbon, hydrogen and heteroatoms, such as nitrogen or sulfur, and contain conjugation across the polymer backbone. Typical conjugated conducting polymers include polyaniline (PANi), polypyrrole (PPy) and polythiophene, Figure 1.5. These and a number of other conducting polymers have been used in a variety of applications ranging from corrosion protection of materials, sensors to many biomedical applications, such as tissue engineering, nerve cell regeneration and drug delivery [104, 105, 106, 107].

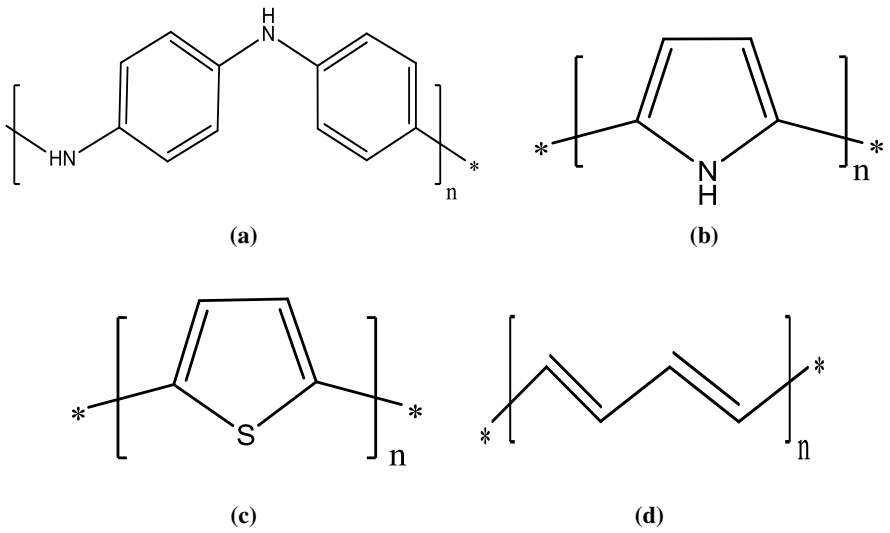

Figure 1.5: Structures of (a) polyaniline, (b) polypyrrole, (c) polythiophene and (d) polyacetylene all in their dedoped states.

Conducting polymers have very good conductivity, as shown in the logarithmic conductivity ladder presented in Figure 1.6, which compares the conductivity of PPy and other conducting polymers with copper. In general, materials are classed depending on their electrical

conductivity, where the electrical conductivity of insulators < semi-conductors < conductors. Bredas and Street [108] explained this phenomenon in terms of the band gap structure. Figure 1.7 illustrates the difference in each material using the band gap theory. The highest occupied molecular orbital is equivalent to the valence band (VB), while the lowest unoccupied molecular orbital may be equated to the conduction band (CB). The difference between each band is known as the band gap energy (Eg) and it is this energy gap that establishes the electrical properties of a material. If $Eg < 10\ eV$, it is difficult to excite electrons into the conduction band and an insulator is formed. If $Eg \sim 1.0\ eV$, then thermal energy is sufficient to promote the electrons into the conduction band and a semi-conductor is formed. If the gap vanishes, with overlap of the valence and conduction band, as shown in Figure 1.7, metallic conduction is observed. For most doped CPs the band gap energy is generally close to 1.0 eV, and consequently, CPs can be classified as semi-conductors.

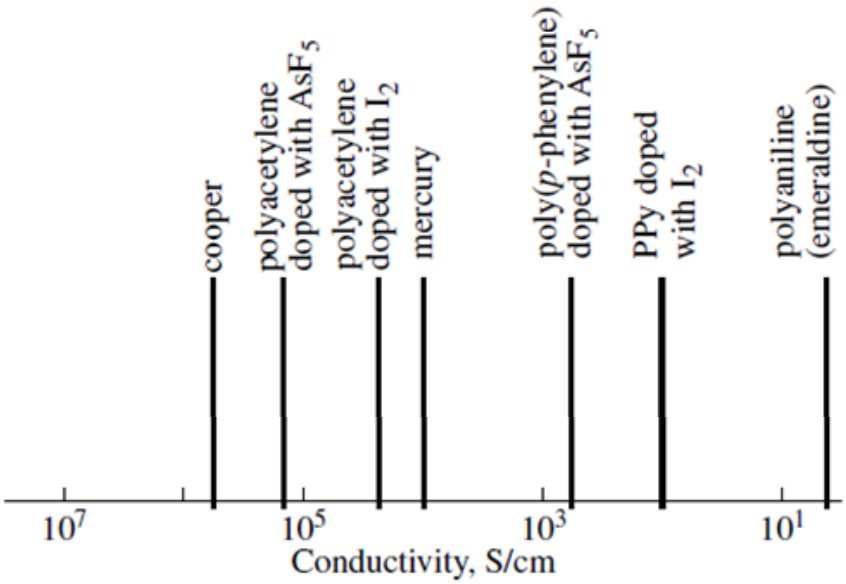

Figure 1.6: Logarithmic conductivity ladder.

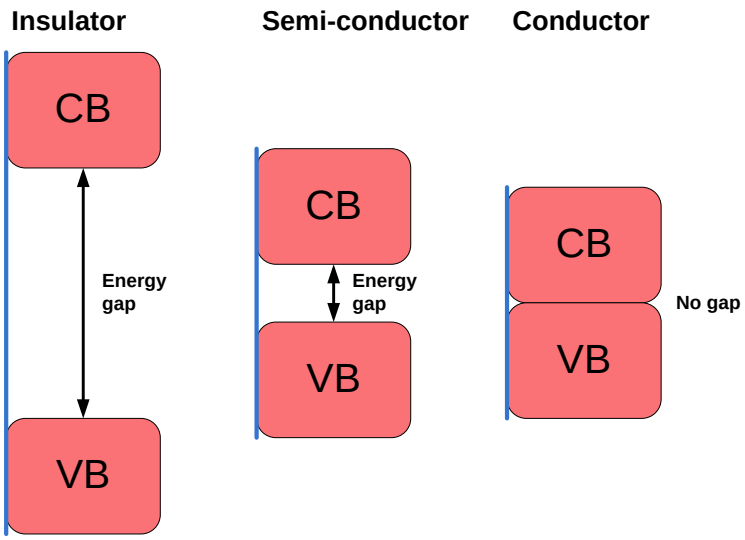

Figure 1.7: A schematic illustrating the band gap energy model, for insulators, semi-conductors and conductors.

As pointed out by Bredas and Street [108], the conductivity observed upon doping of the CPs was originally thought to be from the formation of unfilled electronic bands, however this idea was quickly dissipated upon experimental analysis of PPy and polyacetylene and now it is recognised that the conductivity is due to the formation of polarons and bipolarons, which are more energetically favoured [108, 109]. The π-bonded system of CPs, which comprises of alternating single and double bonds, enabling the delocalisation of electrons along the polymer backbone, is related to the conductivity of the system. The conductivity of these materials arises from a state of relative oxidation or reduction. Generally, it is said that this process occurs in 1 in every 4 monomer units [110]. In this state the polymer is charged and requires the introduction of counter ions (dopants) to compensate and reform the charge neutrality. The oxidation of the polymer in which an electron is removed from a π-bond, gives rise to a new energy state, which leaves the remaining electron in a non-bonding orbital. This energy level is higher than the valence band and behaves like a heavily doped semi-conductor [110]. This doping process enhances the conducting properties of the polymer. The extent of doping can be controlled during the polymerisation. The maximum doping level varies for different conducting polymers and with different dopants. For example, the doping level for PPy ranges from 20% to 50% depending on the dopant used [111]. The anionic doping can be described in Equation 1.12.

$$P + nXF \rightarrow P^{n+}nF^{-} + nX^{+} \tag{1.12}$$

Here, P indicates the polymer in the neutral state, P^{n+} is the polymer in its oxidised state, X^+ is any cation, F^- is any anion and n is the moles of the salt. Both the anionic and cationic doping processes enhance the conductive properties of the conducting polymer. This is because the conductivity increases as the doping level increases due to the creation of more mobile charges [112].

1.4.1 Synthesis of Conducting Polymers

Conducting polymers are synthesised through a method known as oxidative polymerisation. This can be generated either by chemical or electrochemical means. In both cases, the initial step of polymerisation involves the oxidation of the monomer to its radical cation [112]. Once formed, the radical cations react with each other in the case of electrochemical polymerisation, or with other monomers, in the case of chemical polymerisation, to form a radical dimer. This in turn, is transformed to a trimer and longer chain lengths.

Chemical polymerisation is achieved with the use of a chemical oxidant, such as ammonium peroxydisulfate (APS), ferric ions, permanganate, dichromate anions or hydrogen peroxide [113]. The oxidants not only oxidise the monomer but provide dopant anions to neutralise the positive charges formed on the polymer backbone. This is typically carried out in solution, although it can also be carried out directly onto a surface, using a technique known as vapour phase polymerisation [114]. This involves coating the desired surface with the oxidising agent and then subsequently treating the surface with the vapour of the monomer, which results in the deposition of the polymer film exclusively at the surface of preference. The chemical synthesis of a polymer in solution requires the polymer to be precipitated from a monomer solution upon the addition of an oxidising agent. This typically results in bulk polymerisation. The rate of polymerisation can be controlled by varying the reaction conditions, for example, varying the concentration of oxidant, monomer and the reaction temperature [115].

Electrochemical polymerisation is achieved by applying a suitable potential to an electrode in a monomer-containing electrolyte. This results in the electrochemical oxidation of the monomer. Electrochemical polymerisation, particularly potentiostatic and galvanostatic modes, has several advantages over chemical polymerisation because the precipitated polymer is deposited onto a conducting surface. Hence, an adherent polymer can be grafted directly onto an electrode surface in one simple step [116]. The film thickness can be controlled

by monitoring the charge passed during deposition, resulting in more reproducible films, and the films formed have fewer impurities as harsh oxidising agents are not used. It is also possible to perform in situ characterisation of the polymer while it is growing [117]. However, electrochemical polymerisation is limited to monomers which can be oxidised on the application of a potential to form the radical ion intermediates for polymerisation, whereas all polymers can be prepared using chemical synthesis.

1.4.1.1 Polypyrrole

Polypyrrole (PPy) is one of most intensively used and studied polymers due to its ease of preparation, inherent electrical conductivity, high stability, redox properties, and large surface area owing to its cauliflower-like structure [12, 14]. Accordingly, it is an ideal candidate for a number of advanced technologies such as corrosion protection, ion-selective electrodes, electrochromic displays, solar cells, drug delivery systems and actuators [1, 104, 118].

The first synthesis of PPy dates back to 1916, where records show that pyrrole was oxidised with hydrogen peroxide to give an amorphous black powder [119]. Following this revelation, Dall'Olio [120] and colleagues in 1968 were the first to synthesise polypyrrole on to a Pt substrate by the electrochemical polymerisation of pyrrole from a solution of sulfuric acid. In 1980 Diaz and Castillo [121], with the help of colleagues, modified Dall'Olio's approach and demonstrated the electropolymerisation of pyrrole onto platinum in acetonitrile, which led to a black, adherent film. Elemental analysis showed that the monomer unit was retained in the polymer [121].

PPy is an organic material comprised of C, H and a N heteroatom, but it is highly conducting, with an ideal planar ($\alpha - \alpha'$)-bonded chain in which the orientation of the pyrrole molecules alternate, as shown in Figure 1.8. PPy can be synthesised both chemically and electrochemically from the pyrrole monomer, as highlighted in Section 1.4.1.2.

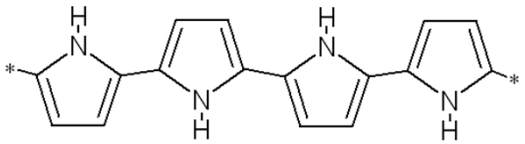

Figure 1.8: Structure of PPy in its neutral state.

1.4.1.2 Synthesis of Polypyrrole

As with all conducting polymers, PPy can be synthesised by either chemical or electrochemical methods. One of the easiest and most common ways of chemically synthesising PPy in large quantities is in solution. This involves exposing the pyrrole monomer to a strong oxidising agent, which yields a black precipitate. In chemical polymerisation, the propagation step is controlled by the fact that the monomer is in large excess of the radical cation that is formed upon oxidation, which then attacks another monomer generating a dimer radical cation which becomes further oxidised. Because of this, and coupled with the loss of hydrogen, the polymer chain grows until termination, as illustrated in the schematic presented in Figure 1.9. The most commonly used oxidising agents are salts, which include Fe^{3+}, Cu^{2+}, Cr^{6+}, Ce^{4+}, Ru^{3+} and Mn^{7+}. Several other oxidising agents including organic acids, have been used, however, films generated from these oxidants tend to exhibit lower conductivity [122] and as such, the salts of transition metal ions are generally used instead. An underlying disadvantage of this method is that PPy forms in bulk in the solution phase and only some of the polymer will cover the surface of any material that may be introduced into the solution.

An alternative way of chemically synthesising PPy is by directly depositing the polymer film onto a surface using vapour phase polymerisation. This involves applying the oxidant to the surface using a solvent coating process, and then exposing the coated surface to the vapour of the monomer. This vapour phase polymerisation process was initially reported by Mohammadi *et al.* [123] where the authors used $FeCl_3$ or H_2O_2 as oxidants in order to form PPy films. Since then the method has been altered slightly, with Fe(III) p-toluenesulfonic acid and a range of other Fe(III) sulfonates now generally being used as the oxidising agents [114, 124].

The electrochemical polymerisation of pyrrole occurs on the application of an anodic potential or current to a conducting substrate that has been immersed in a suitable electrolyte containing the monomer and the desired doping salt. This can be achieved using various electrochemical methods, e.g., potentiostatic, potentiodynamic or galvanostatic methods. There is still some debate on the exact mechanism of electropolymerisation, but the mechanism proposed initially by Diaz and Castillo [121] and later explained by Baker and Reynolds [125] is generally taken to be the accepted mechanism, and is the most commonly encountered mechanism in the literature. This mechanism is summarised in Figure 1.9. This process

involves the one-electron oxidation of the pyrrole monomer (1a), by which a radical cation is generated. This takes place at the electrode or substrate surface. The oxidation of pyrrole at the electrode surface is considered to be faster than the diffusion of the monomer from the bulk of the solution to the interface. In this way the monomer at the interface is predominantly present as a radical cation formed at potential E_1. This high concentration of radical cations gives rise to radical-radical coupling. This occurs at the α-position of each radical, forming a radical dication (1b), which subsequently loses two protons to generate a neutral dimer (1c). This dimer becomes further oxidised to generate another radical species (2a), which then couples with another radical monomer to form a trimer (2b and 2c). The propagation (ia, ib and ic) is continued via this sequence until the final polymer product is obtained. The chain growth is terminated either by reaction (t1) of the macromolecular radical cation with water or hydroxide anions, or by lack of reactivity of the radical cation (t2) due to delocalisation over a greater length as the polymer chain grows.

It is important to note that the final electrosynthesised polymer is oxidised. Intrinsic conductivity results from the formation of charge carriers upon oxidising the conjugated backbone, as discussed previously. Indeed, the final PPy chain is in an oxidised/doped state due to the incorporation of dopants that are present in order to maintain charge balance within the polymer [126]. The number of electrons taken from each monomer is equal to $2+p$, two electrons for the polymerisation and p electrons for the oxidation of the polymer chain. For PPy the value of p is usually 0.25 to 0.33 corresponding to one positive charge delocalised over every 3 to 4 monomeric units and accordingly one anionic dopant for every 3 to 4 monomeric units. The overall stoichiometry for the electropolymerisation of the pyrrole monomer is depicted in Figure 1.10.

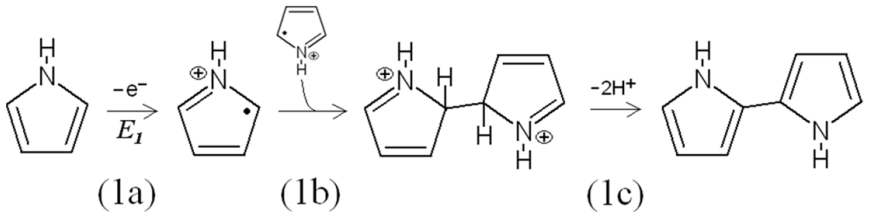

(a)

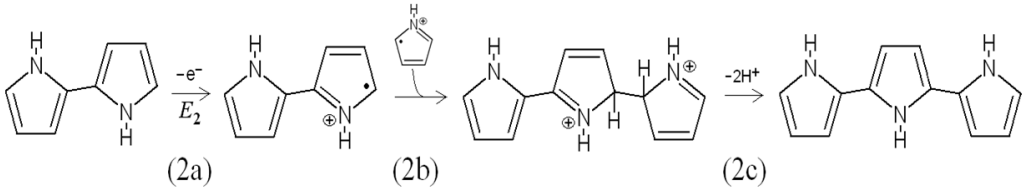

(b)

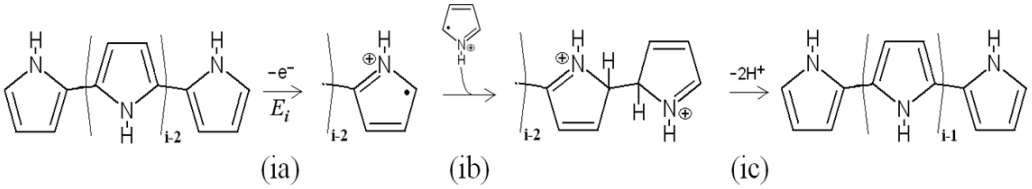

(c)

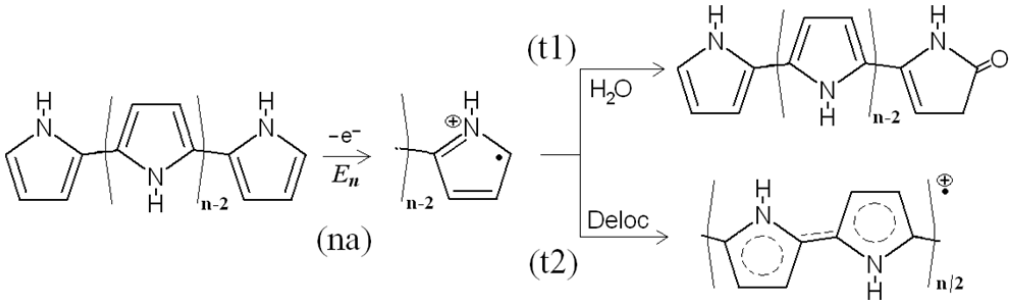

(d)

Figure 1.9: Electropolymerisation mechanism of pyrrole as proposed by Diaz and Castillo [121].

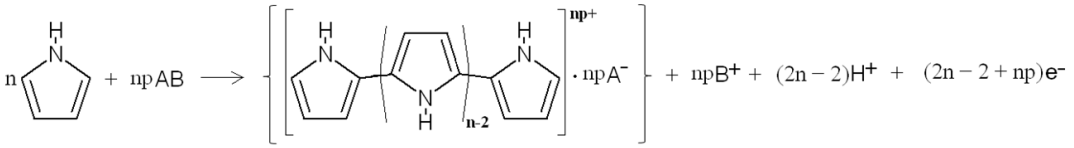

Figure 1.10: Stoichiometry of the electropolymerisation of pyrrole, where A^- and B^+ are the anion and cation from a simple AB salt dissolved in a suitable solvent with the monomer, pyrrole.

1.4.1.3 Factors Influencing the Electropolymerisation of Pyrrole

The electrochemical polymerisation of pyrrole is affected by a number of parameters used in the synthesis. These parameters can include, but are not limited to, the nature of the electrode, the concentration and nature of the electrolyte, the solvent, the applied potential or current density, the reaction temperature, thickness and pH and the mode of electropolymerisation. These will all have a strong effect on the rate of electropolymerisation and on the properties of the resulting polymer.

The electrode surface at which electrodeposition of PPy occurs must not be oxidisable as this would compete with the oxidation of the pyrrole monomer. If this were to happen the oxidation and polymerisation of pyrrole would be severely hindered. Consequently most studies have focused on using inert anodes such as platinum, gold or glassy carbon [127, 128, 129]. Apart from these metals, pyrrole has also been electropolymerised on silicon [130] and transparent indium tin oxide glass (ITO) [131], which is useful for spectroscopic applications.

The conductivity of the PPy films is usually related to the degree of doping by the counter-anions, which also contribute to the rate of formation. Provided the dopant is sufficiently conducting, it also serves as the supporting electrolyte. During oxidation of pyrrole, nucleation of the oligomers in solution occurs, followed by a rapid increase in charge density due to gradual PPy growth. According to Almario and Caceres [132], the doping agents play a key role in the polymerisation process, producing different induction times, mechanisms of nucleation and polymer growth. Therefore, the polymerisation rate varies with each dopant. Another key factor is the size of the dopant anion and this will influence various characteristics of the polymer film, including the redox properties and the porosity of the film. Also, the concentration of the electrolyte is important as the doping degree increases with increasing electrolyte concentration. Li *et al.* [133] reported that the higher the concentration of the electrolyte, the greater the conductivity and tensile strength of the polymer film. A PPy film that has initially high conductivity is less prone to attack by oxygen thus, the polymer matrix is increasingly stable with increasing doping levels and increasing conjugation.

Stankovic *et al.* [134] investigated the effect of preparation conditions on the properties of electrochemically synthesised thick films of PPy. Thick PPy layers (10-130 μm) were prepared electrochemically on Pt anodes under galvanostatic conditions. The effects of formation

parameters (e.g., electrolyte recycling, current density, temperature, solvent, the amount of water in the reaction mixture and film thickness) on the conductivity and morphology of the prepared PPy films were studied. In addition the effects of the nature of the counterion and of the nature and size of the cation associated with the counterion on the conductivity, morphology and electroactivity of the PPy films were examined. Vork and Janssen [135] also demonstrated that the polymer thickness could be controlled in a galvanostatic experiment by measuring the polymerisation time.

Another parameter that has a key influence on the electrochemical polymerisation of pyrrole is the nature of the chosen solvent. The main requirement of the solvent is that it has good ionic conductivity and a good electrochemical resistance against decomposition at the potentials necessary to oxidise the monomer. PPy films have been prepared using aqueous, organic and ionic liquid solutions [18, 127, 136]. A requirement for aqueous solutions is they generally need a reasonably high concentration of supporting electrolyte to achieve the desired conductivity, whereas organic solutions usually require a suitable organic salt. Vidanapathirana *et al.* [137] carried out investigations using aqueous and non-aqueous electrolytes to study the effect of solvent on the ion movement during redox processes. When PPy films are cycled in aqueous electrolytes transport of both the anions and cations occur during oxidation and reduction. However, when cycled in the non-aqueous electrolyte, propylene carbonate (PC), only anion movement takes place. The conductivity of PPy was also investigated. Samuelson and Druy [138] carried out a kinetic study of the degradation of the electrical conductivity of PPy. PPy was synthesised with a variety of anions including the p-toluenesulfonate, perchlorate, and tetrafluoroborate anions. Two different kinetic processes were found depending on the choice of anion. The degradation of the conductivity of PPy/toluenesulfonate was found to obey first-order reaction kinetics, while the other dopants investigated followed multi-order kinetics. Conductivity of PPy is well documented in the literature [121, 139, 140], Kassim *et al.* [140] carried out conductivity measurements on PPy, in order to investigate the effect of temperature on the conductivity. The polymer was grown from aqueous solutions employing a range of temperatures (l - 60 °C). It was found that with an increase in temperature the conductivity decreased and the optimum temperature was found to be between 10 and 30 °C.

The applied potential employed during electropolymerisation is also very significant in

the preparation and formation of the polymer films. Asavapiriyanont *et al*. [18] reported that the oxidation of pyrrole usually occurs between 0.65 and 0.90 V vs. SCE. At higher applied potentials the PPy formed is less conductive as the potential irreversibly over-oxidises the polymer. Over-oxidation is a gradual process occurring with increasing potential. The mechanism is still unclear. The most accepted mechanism is the nucleophilic attack of PPy by aqueous nucleophiles such as OH^- and H_2O. The nucleophilic attack leads to the formation of carbonyl groups on the α-carbons of the pyrrole ring which interrupt the conjugation of the polymeric chain [141]. Diaz *et al.* [142] observed that the potential for the oxidation reaction of PPy shifts towards more negative values as PPy growth proceeds. This is related to the reactivity of the PPy segments with air, which increases as the oxidation potential becomes more positive and the corresponding conjugation length becomes shorter. Ansari [143] suggested that conducting polymers have more limited stability (environmental, thermal, chemical) than conventional inert polymers due to the presence of dopants and their dynamic and electroactive nature. The effect of the counterion on the intrinsic and extrinsic stability is more indirect; the effect of the anion might be to alter the crystallinity of the polymer/dopant system, the number of chemical defects, or extent of backbone oxidation. All of these may affect the reactivity of the dopant/polymer system to the environment and its thermal stability. However, PPy shows good stability and undergoes only slow degradation in ambient atmosphere. Bof Bufon *et al.* [144] investigated the influence of polymerisation potential on the transport properties of PPy films. They prepared PPy films by potentiostatic electrochemical polymerisation at low temperatures. The cyclic voltammograms and the electronic transport properties of the films were investigated as a function of the polymerisation potential. A drop in the film conductivity was observed with higher polymerisation potentials.

Electropolymerisation can be carried out using cyclic voltammetry, potentiostatic or galvanostatic methods. It is well known that the electrochemical method controls the structural form of the electrodeposited PPy films. Herandez-Perez *et al.* [145] illustrated that potentiostatic methods give rise to smooth surfaces. The authors used atomic force microscopy (AFM) to investigate the surface morphology of PPy films prepared at platinum electrodes by potentiostatic and voltammetric methods. They concluded that the potentiostatic mode of growth was better for obtaining thin films with a smooth surface morphology. Furthermore, the PPy film growth was easier to control using this method, whereas galvanostatically prepared

polymer films are more rough and porous. Li *et al.* [133] investigated the effect of using various electrochemical techniques for the formation of PPy on the redox properties of PPy, and found that the galvanostatic deposition of PPy produced polymer films of higher electrochemical reactivity in comparison to those prepared using either potentiostatic or cyclic voltammetry methods. In addition, the electropolymerisation temperature has a considerable influence on the kinetics of the polymerisation, as well as on the conductivity, redox properties and mechanical characteristics of the polymer films. In general, as the temperature increases the rate of polymerisation will also increase, but there is a decrease in the conductivity and redox properties of the polymer. For instance, films prepared in propylene carbonate solution are much more conductive at -20 °C than those prepared at 20 °C. However, films produced at low temperatures have a rugged appearance and poor adhesion to the electrode substrate [140].

The pH of the monomer solution also has a significant influence on the conductivity and electropolymerisation of pyrrole. Asavapiriyanont *et al.* [18] investigated the electrodeposition of PPy onto platinum electrodes from acidic, neutral and basic aqueous solutions and found that polymerisation favours a neutral or weakly acidic pH. This is in close agreement with the work of Zhou and Heinze [146], who also found this to be the case when they investigated the effect of pH on the electropolymerisation of pyrrole from an acetonitrile solution. At high pH values, i.e., pH values greater than 7.0, the electropolymerisation of pyrrole is hindered due to the cation radicals being deprotonated to form neutral radicals. This interferes with radical-radical coupling and hence, the conductivity of the polymer film drops significantly. On the other hand, the electropolymerisation of pyrrole prepared in a highly acidic/low pH solution produces polymers with weak conductivity due to the acid catalysed formation of non conjugated trimers which react further to form only a partly conjugated PPy film.

1.4.1.4 Electroactivity and Redox Properties of Polypyrrole

PPy has been and is currently being studied due to its redox behaviour; it has high conductivity, stability in the oxidised form and the ability to be electrochemically switched between the conducting and insulating states. PPy can be easily switched between the neutral and oxidised states, as described in Figure 1.11. In the neutral state PPy exists as an insulator as the conduction band is empty as all the electrons remain in the valance band. Following oxidation, an electron is removed from a π-bond valence band and a polaron is formed. The separation

of the positive charge and the unpaired electron decreases during continual oxidation as the number of polarons increases.

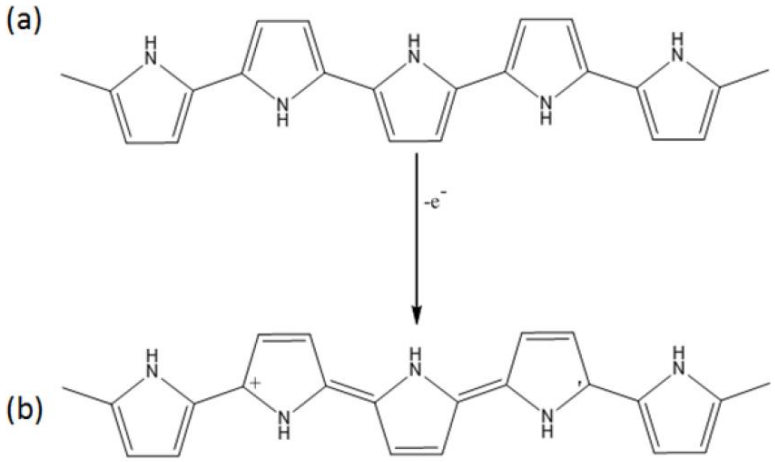

Figure 1.11: The formation of a polaron where (a) is the neutral PPy and (b) is the partially oxidised PPy (polaron).

During PPy oxidation, anions are incorporated into the polymer to neutralise the positive charges formed, Figure 1.12a. Furthermore, when PPy is reduced to its neutral state, dopant anions are expelled from the polymer matrix, Figure 1.12b. However, this scenario only works with small mobile dopants, such as chlorides. When larger anions are used to dope the polymer, they become permanently anchored into the polymer matrix. These anions may include large sulfonate groups, such as polyvinylsulfonate, dodecylbenzene sulfonate [147] and polystyrenesulfonate [148], and the reduction of the polymer doped with these does not result in the release of these dopants. Instead, the electroneutrality of the polymer is maintained by the influx of mobile cations from the electrolyte solution into the polymer. This cation exchange must take place in order to counterbalance the now overall negatively charged PPy matrix, Figure 1.13b. In the case of medium sized anions, they can exhibit both anionic and cationic exchange [147], as recorded by Ge and Wallace [149]. It is important to note that the ion-exchange properties of PPy are dependent on both the dopant present in the polymer and the ionic nature of the electrolyte in solution. PPy can also exchange OH^- ions when electrochemically switched in basic solutions. However, the hydroxyl anions have a deactivating effect on the conductivity of the polymer. This is due to the N-H ... OH hydrogen bonding which inhibits the generation of polar ionic positive charges on the nitrogen sites. This is the origin of the observed dramatic decrease in the conductivity of PPy after treatment

in base [150]. Generally, the rate-determining step in the doping/de-doping process in PPy is the ion migration. The rate of the electron transfer is usually much faster during the redox switching [151].

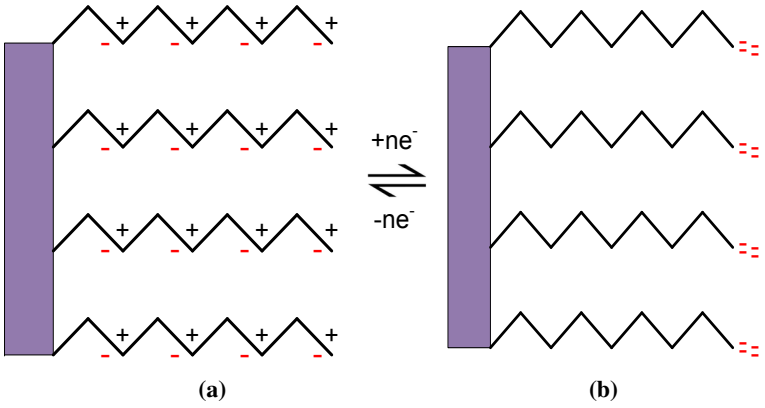

Figure 1.12: (a) The incorporation of anions into the PPy film and (b) the release of anions from the PPy film.

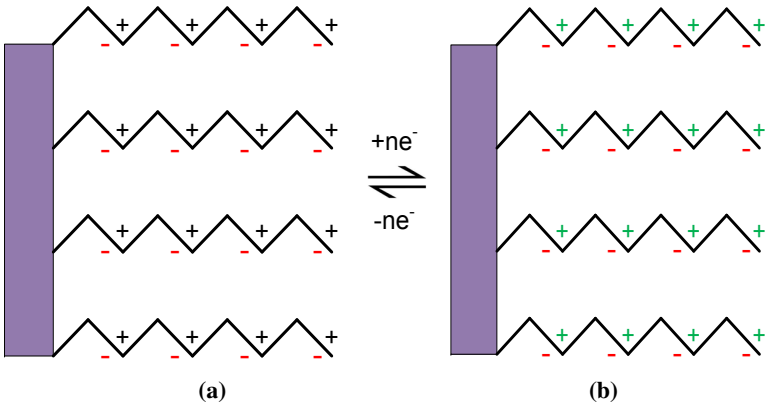

Figure 1.13: (a) The PPy film doped with a large anion and (b) the cation incorporation into the PPy film on reduction of the film, where + is the charge on the PPy, - is the anions and + is the cations.

1.5 Conducting Polymers and Corrosion Protection

Organic coatings are an efficient way to protect metal-based products from corrosion. However, over time even in the absence of defects a sufficient amount of ions may penetrate through the coating so that corrosion at the interfaces occurs. Such defects may be caused by external attack, such as through scratches, or by production steps. Since the discovery of conducting

polymers (CPs) in the late 1970s by Heeger, MacDiarmid and Shirakawa, [152, 153, 154], the unique combination of physical and chemical properties of CPs has drawn the attention of scientists and engineers from many different fields of research. One area where CPs are finding applications is in corrosion protection [155]. Rohwerder and Michalik [156] carried out a study on conducting polymers for corrosion protection, in order to determine if there was a difference between failure and success. They reported that continuous coatings of conducting redox polymer fails to provide corrosion protection in the presence of large defects. Tan and Blackwood [157] investigated corrosion protection by multi-layered conducting polymers, they found that the degree of protection was a function of the deposition order of the copolymer, with films consisting of a PANi layer over the top of a PPy layer yielding the best results. Scanning electron microscopy observations and adhesion measurements, along with the electrochemical data suggested that the ability of a conducting polymer film to act as electronic and chemical barriers were more important in providing corrosion protection than its ability to act as a physical barrier.

The electrodeposition of PPy and other conducting polymers has been achieved at corrosion-susceptible substrates [158], such as copper, copper alloys [19], iron [159, 160], mild steel [23, 161, 162, 163] and aluminium [164]. However, relative to an inert metal substrate, such as platinum or gold, the electrosynthesis is considerably more complex. This is due to the concurrent oxidation of the metal during the electropolymerisation reactions, as the monomers can only be electropolymerised at potentials higher than about 0.60 V vs. SCE. This normally gives rise to extensive dissolution of the underlying metal, as the stable phase is no longer the metal or alloy, Figure 1.1. This problem has generally been circumvented by the deposition of a passivating layer, over the electrode surface, which reduces the rate of substrate dissolution [165]. However, this layer must be sufficiently conducting to facilitate the electropolymerisation of the monomer and the generation of the conducing polymer film [157].

The electrodeposition of conducting polymers on active metals has been pioneered by Beck and co-workers. Much of Beck's early work was concerned with the electrodeposition of PPy on iron and aluminium [136, 166, 167, 168]. Smooth, adherent, PPy films were grown at a current density of 2.0 mA cm^{-2} on iron from an oxalic acid solution. Active dissolution of iron was observed, giving rise to the formation of Fe(II) oxalate. El-Shazly and Wazzan [161] have also reported PPy formation on steel, in order to improve the corrosion resistance of

steel buried in corrosive media. In another study, Aitout *et al.* [22] reported the successful electropolymerisation of pyrrole at iron in oxalic aqueous solution, while Petitjean *et al.* [116] have described the electropolymerisation of pyrrole onto zinc and other oxidisable metals in an aqueous medium containing the salicylate salt.

PPy has also been successfully deposited at copper and various copper alloys [1]. Fenelon and Breslin [1] have reported the in situ electropolymerisation of pyrrole on copper and copper alloys. The electrodeposition of PPy on copper was performed in a monomer solution containing sodium oxalate solutions by either cyclic voltammetry or potentiostatic techniques. The resultant layers were adherent, and offered good corrosion protection properties to the copper electrode. Potentiostatic techniques were used to deposit PPy from aqueous sodium oxalate and again the polymer layers showed promising results. Fenelon and Breslin [19] have also shown that reproducible PPy layers, giving good corrosion protection properties, can be deposited at CuNi alloys. In more recent studies, Duran and Bereket [169] have synthesised poly(N-methyl pyrrole) films onto copper from aqueous solutions containing the monomer and oxalic acid, using cyclic voltammetry. It was shown that the protection efficiency depends on the electrodeposition parameters, such as the applied potentials, scan rate and cycle number. The corrosion protection properties were assessed in 0.10 mol dm^{-3} H_2SO_4 and it was shown that the coatings were protective for 12 days in an acid rain corrosion medium. An oxalate medium was also employed by Redondo *et al.* [170] in the formation of poly(N-methyl pyrrole) films on copper.

In addition to oxalic acid and oxalate salts, a number of other salts have been employed successfully in the deposition of conducing polymers at copper and various copper alloys [1, 19]. For example, polyaniline coatings, showing good corrosion protection, have been galvanostatically deposited at copper from an aqueous solution of 0.30 mol dm^{-3} sodium benzoate [171], while poly(o-toluidine) coatings have been electrodeposited onto copper from a sodium oxalate solution [172]. Furthermore, Sharifirad *et al.* [14] have compared acetate, benzoate and citric acid as electrolytes for the deposition of PPy at copper. The electropolymerisation of pyrrole was observed in all three solutions, with the formation of a passive layer that was sufficiently protective to minimise further dissolution of copper, but enabling the efficient deposition of PPy at copper. Cascalheira *et al.* [173] have studied the formation of PPy at copper from aqueous salicylate solutions using in-situ AFM measurements.

Initially, a non-uniform copper-salicylate layer was deposited, which inhibits the copper dissolution reactions. Then, a thin layer of PPy was deposited, which follows the irregularities in the initial copper-salicylate layer. However, the influence of this initial layer was no longer evident as thick PPy films were deposited. Poly(o-anisidine) coatings have also been electrodeposited from salicylate solutions [174, 175]. Again, it was shown that passivation of the copper surface occurs with the formation of Cu_2O and / or a copper salicylate complex. It was found that the electropolymerisation of the poly(o-anisidine) only occurred after the passivation of the copper substrate.

Dodecylbenzene sulfonate (DBS), has also been used in electropolymerisation. For example, Wang *et al.* [16] have successfully formed a PPy-DBS film onto a copper surface by a galvanostatic method onto an under layer of PPy doped with oxalate as they could not achieve successful electropolymerisation directly onto the copper metal. Wang *et al.* [16] assessed the corrosion performance of this polymer coating in 3.5% NaCl and compared the results to that achieved with the PPy-Oxalate coating. The copper remained protected for a period exceeding 500 h. In addition, the corrosion current for the PPy-DBS film dropped by two orders of magnitude compared with the simpler PPy-oxalate film. It has been suggested that the DBS^- ion is difficult to eject from the polymer coating due to its large size. It obstructs the corrosion-inducing Cl^- ions from penetrating the PPy films and hinders the oxalate from escaping so that the healing ability of the PPy could be maintained for a longer term. DBS is considerably different to the relatively simple oxalate, benzoate or salicylate salts that have normally been used, as it has surfactant properties and the ability to form micelles [176, 177, 178]. These surfactant and micelle properties are highlighted in Section 1.7

The exact mechanism of how conducting polymers confer corrosion protection to the underlying substrate is still not fully understood [160, 179]. Conducting polymers are electroactive, with equilibrium potentials that are more electropositive than the substrate electrodes. Consequently, the polymer may preferentially undergo reduction keeping the metal in the oxidised state. Another variation on this mechanism is that the conducting polymer reacts with the surface of the metal to form a passivating layer, which inhibits further corrosion by setting up a barrier, or by changing the surface potential.

One of the most extensive studied models is the so called “ennobling mechanism”. It is based on the assumption that the conducting polymer acts as an oxidiser and maintains

the metal in the passivity domain. This may induce the oxidation of the free metal surface at small defects in the passive layer. Some publications report that this mechanism works, while others suggest it is only possible in chloride free media [25, 180, 181, 182]. An alternative mechanism is that, the electrons produced during the metal oxidation at the defect area can go in to the polymer and dislocate the oxygen reduction from the metal/polymer interface. This would hinder coating disbondment caused by interfacial oxygen radicals and / or hydroxide ions [183]. The typical polymeric coatings used as corrosion protection for non noble metals act as a barrier for ions and corrosion products. The coatings block their movement and do not allow the formation of a galvanic coupling between local anodes and cathodes. However, in the case of conducting coatings the good ionic conductivity could be an advantage. The "self-healing"mechanism proposed by Kendig *et al.* [29] and which is discussed in the literature [184], is based on the assumption that doping anions with corrosion inhibiting properties inside the polymer matrix are released during the reduction of the polymer and then migrate to the corroding defect. Once released these inhibitor anions could significantly decrease the corrosion rate. The influence of this inhibition is strongly dependent on the concentration of the inhibitor. The transport of the inhibitor must be fast enough to ensure a proper concentration [185].

These mechanisms are based on the unique properties of conducting polymers. In order to estimate the usability of conducting polymers as corrosion protective coatings all aspects of their electrochemical behaviour have to be taken in to account. A similar fate applies in relation to the viologens, which are discussed in Section 1.8, and the formation of corrosion protection films for highly reactive metals, namely copper. There is not much documented in the literature, however there has been some suggestions that the viologens bind to the metal interface through adsorption, [186].

1.6 Introduction to Carbon Nanotubes

1.6.1 History of Carbon Nanotubes

The history of carbon nanotubes appears to begin in 1952 when two Russian scientists published pictures of carbon tubes. They measured 50 nm in diameter. The findings of the Russian scientists were not given much publicity and it was not until 1976 that carbon fibers

with nanometer dimensions, and later images of a nanotube with a solitary graphene layer, were shown [187, 188].

In 1981, Russian scientists published more findings [187]. The carbon multi-layer tubular crystals were made by rolling graphene layers into cylindrical shapes. This was followed in 1991 by Sumio Lijima's unearthing of multi-walled carbon nanotubes in arc burned graphite rods [189]. In fact some accounts of the history of carbon nanotubes mistakenly point to Lijima as the discoverer of carbon nanotubes. The findings of Lijima led to more research and discovery. In 1995, Swiss scientists showed the electron emission property of the nanotubes. Two years later the carbon nanotube electronic transistors were demonstrated at Berkeley [187].

1.6.2 Carbon Nanotubes

The discovery of carbon nanotubes actually originates from fullerenes, a hollow spherical structure of an allotrope of carbon C-60 [190], which was discovered in 1985. The spherical structure is also called buckminsterfullerene. Some of the scientists who discovered this, including Harold Kroto, Robert Curl and Richard Smalley were awarded the 1996 Nobel Prize in Chemistry. Carbon nanotubes consist of pure carbon, and are long and thin and shaped like tubes, about 1-3 nm in diameter, and hundreds to thousands of nanometers in length. Carbon nanotubes are 100 times stronger than steel and one-sixth its weight. Some carbon nanotubes can be extremely efficient conductors of electricity and heat; depending on their configuration, some act as semi-conductors or have metal-like conductivity [187, 188, 191].

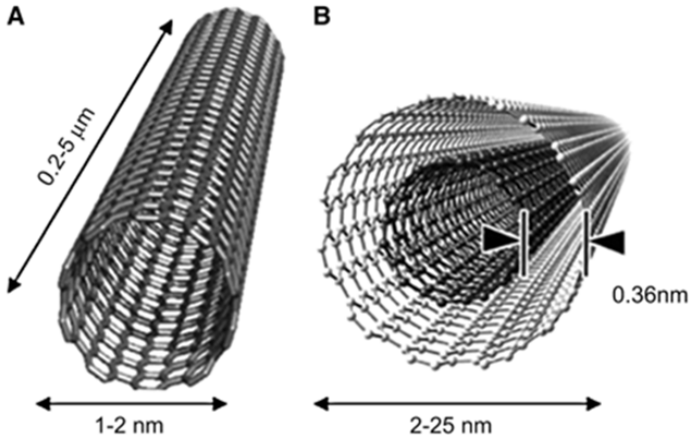

Figure 1.14: Diagram of a (a) single-walled nanotube (SWCNT) and (b) multi-walled nanotube (MWCNT) [192].

Carbon nanotubes, are an extended structure of a fullerene in length, and are composed of ultra thin carbon fiber with nanometer-size diameter and micrometer-size length, as illustrated in Figure 1.14. Basically, they are sheets of graphene rolled up into a tube. The manner in which the graphene sheet is folded leads to CNTs with different electrical and thermal conductivities, with armchair, chiral and zig-zag structures displaying different properties. Therefore, such characteristics have been employed in the semi-conductor industries. The difference in orientation can be determined using vectors. In particular, the chiral vector is used to distinguish between the armchair, zig-zag and chiral CNTs [193, 194].

1.6.3 Synthesis, Purification and Applications

CNTs can be prepared as multi-walled CNTs (MWCNT) and single-walled CNTs (SWCNT). MWCNT are comprised of 2 to 30 concentric graphitic layers, and the diameter ranges from 10.0 to 50.0 nm. SWCNT, on the other hand, has diameters from 1.0 to 1.4 nm.

The synthesis of CNTs has been studied extensively [191, 194, 195] and now they can be prepared by several methods, including arc-discharging, laser ablation and catalytic decomposition of hydrocarbons. Other methods such as electrolysis have been proposed. Regardless of the synthetic method, metal catalysts are used and these include Fe, Co, Ni and alloys, such as Fe/Co, Fe/Ni, Ni/Co, Ni/Cu. The length and diameter of the CNTs can be controlled, to some degree, by the synthetic method. For example, laser ablation results in shorter CNT lengths compared to arc-discharge, while high quality MWCNT can be mass produced using catalytic decomposition of hydrocarbons. Once synthesised the CNTs must be isolated from the metal catalysts, and carbon-containing structures that are produced as by-products in the synthesis. Centrifugation, micro-filtration and chromatography are employed to separate the CNTs of different lengths [196, 197, 198].

The unique, but flexible structure of carbon nanotubes, allow them to be applied to different scientific fields [187, 199], among them are nanotechnology and optics. For example, carbon nanotubes have been proposed in the development of waterproof clothing and they have been employed to augment the strength of concrete. They can also be used as chemical nanowires or conductive films (for use on LCD and computer monitors) and have potential as air pollution filters, water filters and electric circuits [193, 200].

1.7 Surfactants

Surfactants, also called surface active agents, are molecules composed of a polar hydrophilic group, the "head", attached to a non-polar hydrophobic group, the "tail". Surfactant molecules are amphiphilic in character, i.e., they possess hydrophilic and hydrophobic regions having a long hydrocarbon tail and a relatively small ionic or polar head group. Amphiphiles can be ionic (cationic, anionic), zwitterionic, or nonionic depending on the nature of their head groups. The surfactants have a tendency to accumulate at the interface of immiscible fluids resulting in a decrease in free energy which is reflected in a corresponding lowering of interfacial tension. This facilitates emulsification of the immiscible fluids, and hence such compounds are also known as emulsifiers [201, 202, 203]. A schematic diagram of a typical surfactant is shown in Figure 1.15.

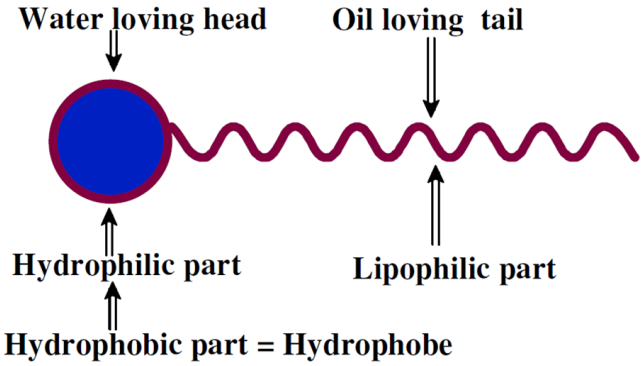

Figure 1.15: Illustration of a surfactant.

Depending on the charge of the head groups, the surfactants are classified as anionic, nonionic, cationic or zwitterionic. Sodium dodecyl sulfate (SDS) is one of the most important surfactants within the anionic category. In this case, the anion is the surface-active species. The counterions most frequently used are sodium, potassium, ammonium, calcium and various protonated alkyl amines. Sodium and potassium impart water solubility, whereas calcium and magnesium promote oil solubility [202]. Nonionic surfactants do not have any surface charge and have either a polyether or a polyhydroxyl unit as the non-polar group. This category continues to be dominated by ethylene oxide adducts of alkylphenols and fatty alcohols. In cationic surfactants, the cation is the surface-active species. The quaternary ammonium salts are the main compounds in this class. The majority of cationic surfactants are based on the nitrogen atom carrying the cationic charge. Both amine and quaternary ammonium-based

products are common. The amines only function as a surfactant in the protonated state; therefore, they cannot be used at high pH. Zwitterionic surfactants have two charged groups of different size. Zwitterionics are often referred to as 'amphoterics'and these surfactants can change from a net cationic to net anionic charge on going from a low to high pH. However, the compounds are only zwitterionic over a certain pH range [202].

1.7.1 Micelles, Micellar Structure and Properties

In polar solvents such as water, amphiphilic surfactant monomers assemble to form a micelle in such a way that their hydrocarbon tails are located in the core of the micelle [176, 204, 205]. The polar head groups project outwards into the polar bulk solution, as shown in Figure 1.16 [176, 206]. In this structure, the hydrophobic tails are shielded from water, giving a more stable arrangement. Micelles are in dynamic equilibrium with surfactant monomers in the bulk, which are frequently being exchanged with the surfactant molecule in the micelles [205]. The equilibrium between monomer and aggregate is established within a few milliseconds.

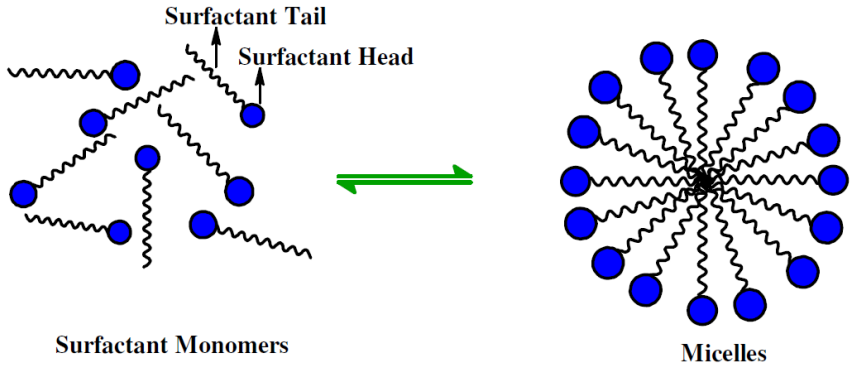

Figure 1.16: Schematic of the reversible monomer-micelle thermodynamic equilibrium.

The equilibrium depicted in Figure 1.16 can be expressed in Equation 1.13, where n represents the number of monomer units in solution, S represents the surfactant and S_n is a micelle formed from the surfactant monomers. The equilibrium is then given by Equation 1.14, where K_m is the micellar equilibrium constant, $[S]$ represents the surfactant concentration, $[S_n]$ indicates the micellar concentration of the surfactant and n is the number of monomers in the micelles, or the aggregation number.

$$nS \rightleftharpoons S_n \tag{1.13}$$

$$K_m = \frac{S_n}{[S]^n} \tag{1.14}$$

The surface layer of a micelle resembles a concentrated electrolyte solution with a dielectric constant lower than that of the bulk water. The micellar phase is less polar than water and the ionic micelles have polarity near to that of pure ethanol even at the stern layer [176]. The size and geometry of the micelle is determined by the number of monomers in a micelle, i.e., the aggregation number [202, 204]. In aqueous solutions, the aggregation numbers for surfactants generally range between 10 and 100. Surface polarity decreases with an increase in the aggregation number and this influences the solubility in water. In Figure 1.17, the charge distribution is shown, where the charge is neutralised by counterions to form an electrical double layer. The first layer immediately adjacent to the core corresponds to the stern layer. In this layer, the counterions are adsorbed [207]. According to the most widely accepted model, the head groups of the surfactant molecules are also located in this layer. The rest of the double layer corresponds to the diffuse (Gouy-Chapman) layer and diffusion of the ions into the bulk solution can occur due to thermal motion. The core radius is about the length of the fully extended alkyl chain of the amphiphile. The core is assumed to consist of two regions, namely the inner and outer core. The outer core contains approximately the first four methylene groups. There is also another defined region within micelles which is termed the palisade layer (mantle) which includes the head groups. Based on the Hartely model, the overall volume of a micelle is approximately twice that of the stern layer [202, 208].

1.7.2 Critical Micelle Concentration, CMC

The formation of the micelle, as shown in Figure 1.18, is controlled by a number of factors but depends particularly on the concentration of the surfactant [177, 202, 209]. The amphiphile molecules exist in dilute solutions as individual species with ideal physical and chemical properties. As the amphiphile concentration increases, these properties deviate gradually from ideality and at some critical concentration, where aggregation of monomers into micelles occurs, an abrupt change is observed (Figure 1.18) [202, 209]. On formation of the micelle, the head group repulsions are balanced by the hydrophobic attractions and for ionic micelles, also by attractions between head groups and counter ions. In some cases, hydrogen bonds can also be formed between adjacent head groups. This concentration is called the critical

micelle concentration (CMC). CMC is a key parameter for the optimisation of surfactants in chemical formulations [202, 204]. Various factors, such as temperature [210], the length of the hydrocarbon tail, the nature of the counter ions and the existence of salts and organic additives, influence the value of the CMC [211]. Hence, amphiphiles have characteristic CMC values only under given conditions [212].

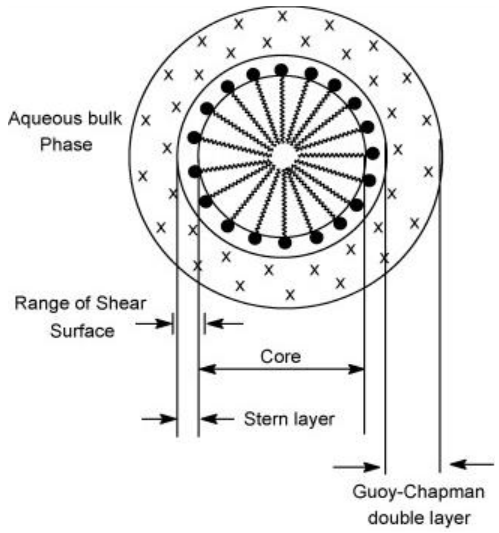

Figure 1.17: Model of a typical ionic micelle showing the location of head group, surfactant chain and counter ions (+).

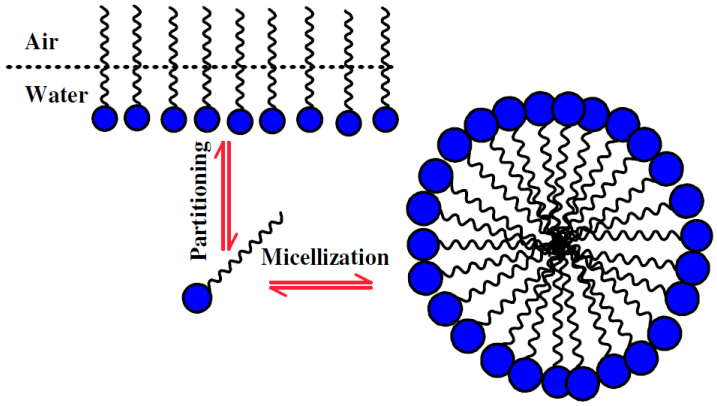

Figure 1.18: Representation of changes observed at the critical micelle concentration.

1.7.3 Dodecylbenzene Sulfonate (DBS)

The structure of DBS is shown in Figure 1.19, where the anionic SO_3^- groups comprise the head and the organic chain in the monomer forms the tail in a micelle structure. As detailed

earlier, DBS falls within the anionic category of surfactants.

Surfactants, such as DBS, are commonly used to disperse CNTs by sonicating in aqueous media. During this sonication period mechanical energy is provided to overcome the weak van der Waals interactions in the CNT aggregates and at the same time surfactant molecules adsorb on to the surface of the CNT walls [213, 214]. The organisation of surfactant molecules on the CNT surface has been extensively investigated [203, 215, 216, 217]. Three main arrangements have been considered [215]; structureless random adsorption on the CNT walls without any preferential arrangement of the head and tail, hemi-micellar adsorption on the CNT surface, and encapsulation of the CNTs in a cylindrical surfactant micelle [218, 216]. The majority of the experimental (AFM and adsorption measurements) and theoretical studies dealing with the organisation of surfactant molecules on the CNT walls supports the hemi-micelle configuration [216, 219, 220].

It is believed, that surfactants such as DBS, disperse CNTs in aqueous solutions mainly through hydrophobic/hydrophilic interactions. The hydrophobic tail of the DBS adsorbs on to the surface of the CNT aggregates while the hydrophilic head associates with water [217, 221]. CNTs can be encapsulated within cylindrical micelles or covered with either hemispherical micelles or randomly adsorbed molecules [21]. A further hypothesis is that the DBS disperses the CNTs due to the presence of the benzene ring, the smaller head group and the slightly longer alkyl chain. In addition, the higher charge in the head group strengthens the electrostatic repulsion among surface covered CNTs which prohibits the aggregation of the CNTs resulting in a more stable suspension [217, 222, 223]. In addition, DBS can be employed as a dopant in conducting polymers, as detailed in Section 1.5.

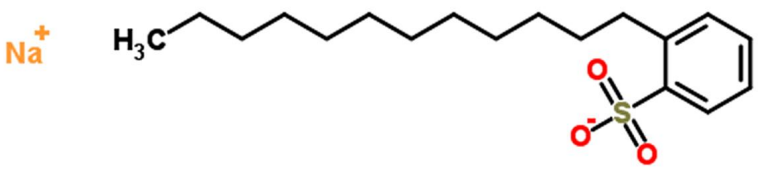

Figure 1.19: Structure of dodecylbenzene sulfonate (DBS).

1.7.4 The CMC and Aggregation Number of DBS

It has been reported that DBS forms micelles in water in a concentration range of 3.0×10^{-4} to 9.5×10^{-3} mol dm^{-3}, while the aggregation number is in the vicinity of 55 to 65. The entropy of mixing of the water and DBS surfactant favours a low number of monomers in each aggregate. As a result the micelles are quite small, with low aggregation numbers [224, 225].

A variety of methods, such as light scattering, sedimentation, small-angle neutron diffraction, fluorescence quenching [178] and conductivity measurements have been used to obtain the CMC and aggregation number [225]. For example, the fluorescence quenching method has been developed by Turro and Yekta [226] as a simple and reliable method to determine the aggregation number. The fluorescence intensity of a micelle-bound probe is monitored as a function of quencher concentration. The mean aggregation number of micelles may be derived from luminescence quenching measurements [227], if static or active sphere quenching of a micellar donor by a micelle associated quencher is dominant [228].

The probe molecule used in this investigation is the ruthenium-bipyridine anion [229], which absorbs blue and emits red light. The lifetime of the luminescence state is much shorter than the lifetime of the average whole micelle. The chloride salt of the ruthenium-bipyridine is soluble in water. This is significant because at concentrations below the CMC the ruthenium-bipyridine anion forms an insoluble compound with the surfactant. However, at higher concentrations (where the micelle formation occurs), the anion is solubilised by the micelle, which quenches the luminescence of the ruthenium-bipyridine if they share the same micelle [202, 224, 225].

1.8 Viologens

Viologens, also known as 1,1'-disubstituted 4,4'- bipyridinium ions, were first reported in 1933 by Michaelis and Hill [230]. They exist in three main oxidation states: dicationic (V^{2+}), cationic radical species (V^{o+}) and neutral species (V^{o}), as depicted in Figure 1.20. Of the three common viologen redox states, the dication is the most stable [231]. The colourless dication can undergo a one-electron reduction generating a radical cation which may be soluble or can form a deposit on the electrode if large substituents are bound to the pyridilium nitrogen [232]. The radicals exhibit a colour which depends on the substituents. Simple alkyl groups, for

example, promote a blue-violet colour, whereas aryl groups generally impart a green hue to the radical cation [231]. When the molecule undergoes a second stage of reduction the radical gains an electron to form a yellow to brown neutral species which is frequently insoluble in aqueous media [232].

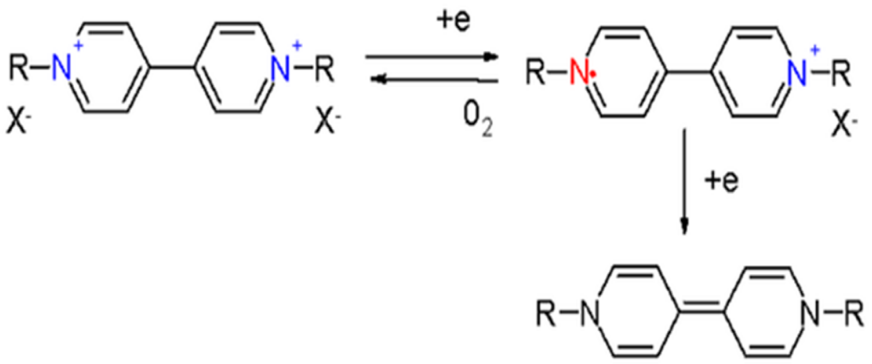

Figure 1.20: Schematic representations of the three oxidation states of the viologen compounds (V^{2+}, V^{0+} and V^{0}).

Viologens can be reduced electrochemically by applying a suitable potential. The 1,1' substituents affect the potential of both reduction steps [17]. In this work three different viologens were investigated: methyl (MV), ethyl (EV) and benzyl (BV) viologen and the respective 1,1'-substituents are summarised in Table 1.1. The methyl viologen is the simplest molecule of this class of compound and it is commonly known as paraquat. It is well known to possess herbicidal activity.

Table 1.1: Summary of the substituents and counter-ions for methyl, ethyl and benzyl viologens.

R = CH_3	X = Cl^-	Methyl viologen dichloride (Paraquat)
R = CH_2CH_3	X = ClO_4^-	Ethyl viologen diperchlorate
R = CH_2Ph	X = Cl^-	Benzyl viologen dichloride

Michaelis and Hill [230] originally investigated the viologens as redox indicators in biological studies. Viologens are now widely studied as electron transfer mediators in enzymatic reactions. For example, Hale *et al.* [233] published results on the efficiency of several water soluble viologens in mediating electron transfer from reduced glucose oxidase to a carbon paste electrode. The advantage of using viologens is that these molecules have sufficiently anodic redox potentials (more positive than that of flavin adenine dinucleotide) to

re-oxidise reduced glucose oxidase. These redox potentials are, however, sufficiently cathodic that glucose sensors based on glucose oxidase and its mediators can operate in a potential range where the oxidation of common interfering species, such as ascorbic acid and uric acid, do not occur. Gomez Moreno and Bes [234] found that the covalent binding of the viologen, N-methyl-N'(aminopropyl)-4,4'-bipyridinium, to the flavoprotein ferredoxin-$NADP^+$ reductase, facilitates the transfer of electrons between the FAD group in the enzyme and oxygen molecules present in the solution. This oxidase activity, which is completely absent in the native protein, indicates that there is an efficient electron transfer between the FAD group in the enzyme and the viologen molecule. Modification of an electrode surface in order to establish an electrical connection with an enzyme is considered a topic of great interest. The redox centre of enzymes, in fact, is usually deeply located within the protein and the protein shell avoids direct electron transfer between the enzymatic active sites and the electrode surface [235]. Cosnier *et al.* [235] constructed a biosensor composed of PPy functionalised with viologens with the ability to shuttle electrons between the electrode and the reactive centre of a nitrate reductase enzyme.

Other successful applications of viologens are as electrochromic materials and nanomaterials [236]. As previously mentioned, viologens can change their optical properties and so can be switched between different colours when exposed to chemical perturbations, giving electrochromism. Electrochromism results from the generation of different visible region electronic absorption bands on switching between redox states [236]. Such a phenomenon occurs in viologens because the radical cations have a delocalised positive charge and hence their colouration arises from an intramolecular electronic transition. In contrast, the dications are transparent since they do not possess any delocalised charge. Suitable choice of nitrogen substituents to attain the appropriate molecular orbital energy levels can, in principle, allow colour choice of the radical cation.

Paraquat is the trade name for N,N'-dimethyl-4,4'-bipyridinium dichloride, one of the most widely used herbicides in the world. It is quick-acting and non-selective, killing green plant tissue on contact [237]. It is also highly toxic. Paraquat was registered for use in 1965 and since that time has been one of the most widely used herbicides for broadleaf weed control. Because of its widespread use, the possibility exists of substantial paraquat contamination of food. Drinking water contamination by paraquat has also been observed. The European Union has banned the use of paraquat since July 2007 but it is still widely used.

As highlighted earlier, the corrosion protection properties of MV, EV and BV were studied at the copper electrode. There are no reports in the literature on the corrosion protection afforded by viologens, however there are some reports which describe the adsorption of viologens at metal surfaces, and these may be relevant to this study. For example, Lee *et al.* [238] have studied the charge transfer properties of self-assembled derivatives of viologens using electrochemical quartz microbalance (EQCM) measurements. The electrochemically induced adsorption of the self-assembled monolayers was achieved and monitored using EQCM. The adsorption of viologens on a highly orientated pyrolytic graphite (HOPG) electrode was monitored using cyclic voltammetry and infrared reflection absorption spectroscopy [238, 239]. It was found that the bipyridine ring planes were adsorbed perpendicular to the HOPG surface, while the alkyl groups were adsorbed parallel to the surface. In another study, Arihara *et al.* [239] monitored the adsorption of heptyl viologen on Au(111) using infrared reflection absorption spectroscopy and concluded that the dication molecule adsorbs in a side-on orientation, but on reduction forms a face-on dimer composed of two monocations.

There have also been some reports on the adsorption of viologens at copper and copper-modified surfaces. Jiang *et al.* [240] have reported the potential-dependent adsorption of heptyl viologen on a Cu(100) surface in a chloride containing electrolyte. In the absence of the viologens, a highly ordered chloride adlayer was observed on the Cu(100) using scanning tunneling microscopy (STM). On injection of the viologen, a highly ordered two dimensional array structure was observed as the dications assembled and adsorbed at the surface. The one electron reduction of the dications caused a phase transition to a stripe-like pattern, while the further reduction produced a more compact stripe phase. Finally, at lower applied potentials, an amorphous phase was observed. However, in the reverse anodic sweep, the reproduction of the ordered stacking phases was achieved on top of the chloride lattice at the Cu(100) surface. Breuer *et al.* [241] also studied the adsorption of dibenzyl and diphenyl viologens at chloride-modified copper. The dibenzyl viologens were adsorbed and stabilised at the chloride-modified copper in the dicationic state. Electrostatic interactions between the anionic chloride layer and the dications were proposed as the main driving force for the formation of the stabilised layer. Again, a stripe-like structure of chains was observed on reduction of the layer. However, the diphenyl viologens could not be stabilised at the chloride-modified surface in a dicationic state. Tsay *et al.* [242] studied the molecular structures obtained on adsorption of dicarboxylated

viologens on Cu(100) in the presence of chloride anions. Again, depending on the oxidation state of the viologen, array-like patterns, stripe patterns, compact stripe patterns, and metastable phases were observed with STM. Hydrogen bonding was considered to be the main factor in achieving the close stacking stripe pattern. Finally, in a paper published by Yuan *et al.* [243] the authors have modified an oxidised copper alloy, Cu-Ni alloy, with viologens to inhibit microbiologically induced corrosion. A 4-(chloromethyl) phenyl trichlorosilane layer was first immobilised onto the oxidised surface. Then, the viologen was coupled to this layer and the terminal pyridine groups were converted to pyridinium groups using benzyl chloride. Good bacterial inhibition efficiency was obtained. In comparison, under the same conditions, the unmodified CuNi alloy was readily susceptible to microbial induced corrosion.

1.9 Introduction to work in this Thesis

Several approaches have been carried out in order to establish corrosion protection coatings for non inert metals, however, much of these publications did not focus on copper.Therefore, the work presented in this thesis illustrates the corrosion protection films synthesised for the easily oxidisible metal copper. The films were based on polypyrrole coatings doped with combinations of tartrate, oxalate and sodium dodecylbenzene sulfonate along with the incorporation of multi-walled carbon nanotubes and viologen films absorbed at the copper surface. The corrosion protection properties of these films were studied using a combination of techniques including cyclic volatmmetry, polarisation curves, Tafel analysis, Open-circuit potential measurements and electrochemical impedance.

As detailed in chapter 3 polypyrrole was successfully deposited at copper from 0.10 mol dm^{-3} oxalate pH 8.0 and tartrate pH 7.0, to generate PPy-Oxalate and PPy-Tartrate films on copper. In chapter 4, further optimisation of the polymer film is achieved with the incorporation of MWCNTs.These were dispersed using the surfactant DBS, and exhibited good corrosion protection properties. In chapter 5 the PPy-DBS polymer coating was investigated to determine if the DBS was the contributing factor for the good corrosion protection displayed by the coatings from the previous chapter. In chapters 6 and 7 a new concept of viologens is introduced.This was an alternative approach in an effort to obtain corrosion protection of the copper surface with out using polymers.There have been no reports published on the

use of viologens for the corrosion protection of copper metal,so it was an obvious approach considering the research group had some knowledge of their chemistry.The electrochemical deposition of benzyl, methyl and ethyl viologen at copper in the presence of 0.10 mol dm^{-3} NaCl supporting electrolyte was studied. The viologens were absorbed at the copper surface and good corrosion protection was achieved.

CHAPTER 2

Experimental

In this chapter the techniques and the different apparatus, used to produce and investigate the properties of an anti-corrosive coating for the non-inert metal copper, are presented and described. Firstly, a description of the instrumentation and cell set-up is provided, along with information on sample preparation, electrolyte compositions and a detailed description of the experimental test procedures used during this research. This is followed by details on the kinetic analysis of electrochemical data and information on corrosion and the analyses of corrosion data.

2.1 Instrumentation and Equipment

The main test procedures used in this study were cyclic voltammetry, potentiostatic measurements, potentiodynamic polarisation, open-circuit potential measurements, electrochemical impedance spectroscopy, ultra-violet visible spectroscopy (UV-Vis) and scanning electron microscopy (SEM) coupled with energy dispersive X-ray analysis (EDX). The electrochemical measurements were carried out using one of three potentiostats; a Solartron (Model SI 1285 or Model SI 1287) both with frequency response analysers (Model SI 1250), or a CH instruments potentiostat (Model CHi 760C). Solution properties such as pH and conductivity were evaluated using an Orion model 720A pH meter and a Jenway 4510 conductivity meter,

respectively. The pH meter was calibrated using buffer solutions, pH 4.0 and pH 7.0 obtained from Lennox Ltd., and a 0.01 mol dm^{-3} KCl from Sigma was employed in the calibration of the conductivity meter. An overview of the main and ancillary equipment used throughout this study is given in Table 2.1. Further details are provided in the relevant sections.

Table 2.1: Analytical equipment and techniques used with model information.

Equipment/technique	**Model**
Electrochemical Measurements	CH Instruments Potentiostat (Model CHi 760C) Solartron (Model SI 1285 or Model SI 1287) Frequency Response Analyser (Model SI 1250)
Spectroscopy Measurements	Varian Cary 50 UV-Vis Spectrometer Cary Eclipse Fluorescence Spectrophotometer
Differential Scanning Calorimetry	Perkin Elmer 2400 Series Analyser/ PYRIS Diamond™ DSC/Pyris 6 DSC
Microwave	Discover CEM 48-72-96
SEM	Hitachi FE-Scanning Electron Microscope / Oxford Instruments Inca X-Act 4.12 Software Package
EDX	Tescan Mira XMU VPFE/51-ADD0009 / Software Package Micro Analysis Suite
Gold Sputter Coater	Emitech K550x / Agar Scientific
Sonicator	Branson 1510
Electronic Balance	Sartorius Models TE612 and TE124S
pH Meter	Orion Model 720A
Conductivity Meter	Jenway 4510
Centrifuge	Merlin Spectra

2.1.1 Electrochemical Cell Set-up

All electrochemical techniques were carried out using a standard three-cell electrode system, as shown in Figure 2.1. This system consists of a working electrode (WE), which was usually a copper metal disc supported inside a Teflon holder. The manufacture of these electrodes is discussed in Section 2.2. A high surface area platinum wire was employed as the counter or auxiliary electrode (CE/AE) to facilitate the movement of electrons to and from the WE. Finally, the reference electrode (REF) was a saturated calomel electrode (SCE). The reference

electrode was serviced regularly by changing the internal filling solution with a saturated solution of super-purum KCl (99.999+%) and by checking the open-circuit potential against an unused SCE. The three electrodes were immersed in the electrolyte solution and were connected to a potentiostat.

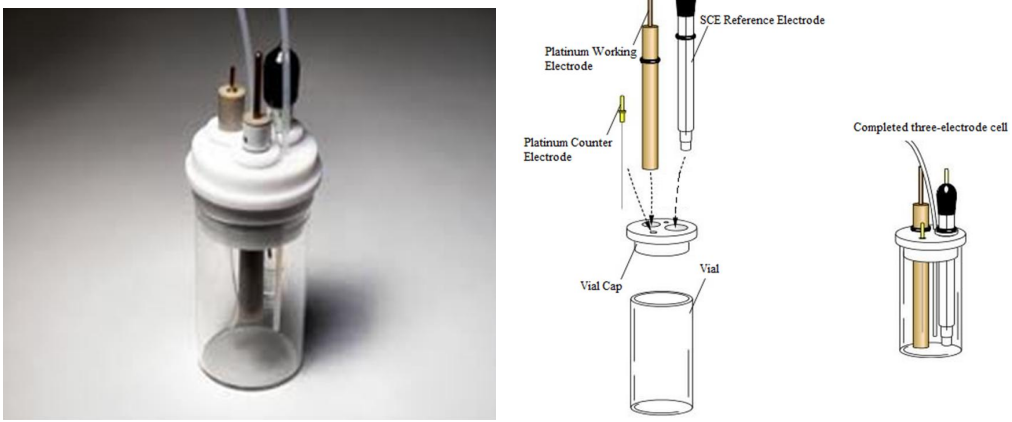

(a) **(b)**

Figure 2.1: A schematic of the three-electrode cell used for electrochemical measurements.

2.1.2 Electrochemical Measurements

All the electrochemical measurements were carried out using a CH instruments potentiostat (Model CHi 760C), with the exception of the electrochemical impedance spectroscopy measurements, Table 2.1. This latter technique was carried out using a Solartron potentiostat (Model SI 1287 or 1285) in conjunction with a Solartron Frequency Response Analyser Model 1255B. Software was used to interface the potentiostat and the cell to the computer, as illustrated in Figure 2.2. The software package for the CH instrument potentiostat was CHi 760C, version 2, and for the Solartron potentiostat, the Zplot for windows 98/NT/2000/XP/vista version 2 was used. From each of these software packages data were transferred and further analysis was carried out. Zview was used to analyse the data from Zplot and Excel for Microsoft Windows was used to analyse the data recorded using the CH instruments potentiostat.

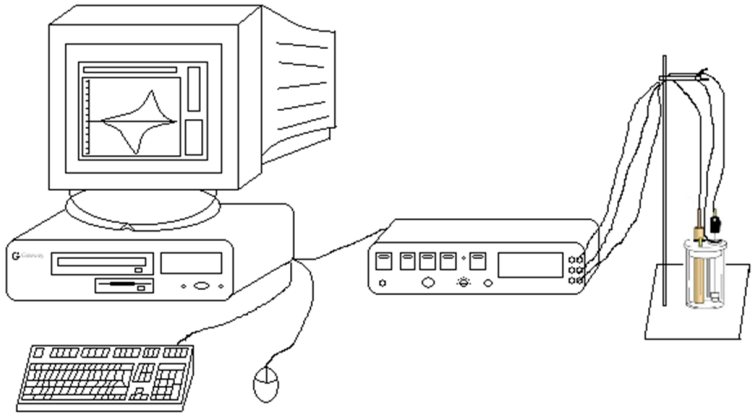

Figure 2.2: A schematic of the experimental setup used to record all electrochemical measurements.

2.2 Preparation of the Working Electrodes

The copper substrates (99.99%) were supplied by Goodfellow or CH instruments. The metals from Goodfellow were supplied in rod form and were cut into lengths of 3 cm. Electrical contact between the electrode and the external circuit was achieved by attaching a copper wire to one end of the rod, holding it in place with a conducting epoxy resin. This wire was then fed through the Teflon holder leaving the substrate exposed at one end. The end of the electrode with the copper wire was sealed with silicone and the end with the exposed substrate was sealed with non-conducting epoxy resin. A diagrammatic representation of the electrode assembly is shown in Figure 2.3.

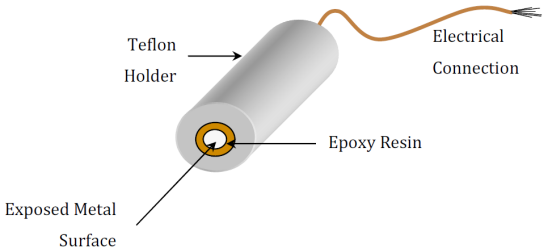

Figure 2.3: Schematic diagram for electrode assembly.

Prior to carrying out each experiment the exposed electrode surface was hand polished using diamond paste to give a smooth even surface and to remove any polymer or excess analyte that may have deposited onto the surface. The paste was a Buehler diamond suspension with particles ranging from 1 to 30 μm. The higher sized diamond particles (15 - 30 μm) were used to remove deposited polymer on the surface followed by the finer, 1 μm sized particles, to give

a polished and smooth electrode surface. The electrodes were rinsed with distilled water and sonicated for about 30 s to remove any diamond particles in between each polish grade. In some cases the polymer was removed from the surface using a Buehler METASERV grinder polisher with Buehler SiC grinding paper (Grit p1200 to p2500) before polishing with the diamond pastes. The electrodes described in Figure 2.3 were used for all experiments except for spectroelectrochemistry experiments, where an indium tin oxide (ITO) was employed, these were purchased from Plasma Quest Ltd. To ensure electrical contact a copper wire was connected to the ITO electrode with a conducting epoxy resin, as shown in Figure 2.4.

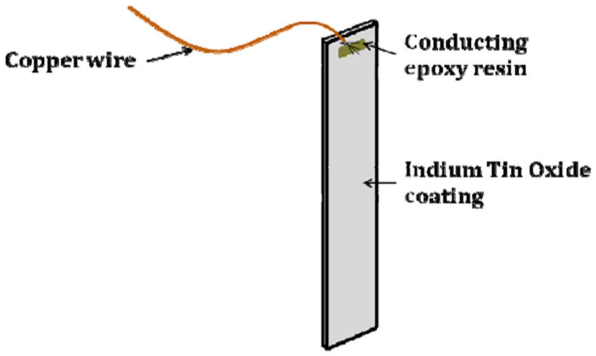

Figure 2.4: Schematic diagram for ITO electrode assembly.

2.3 Chemicals and Solutions

The majority of chemicals for this project were purchased from Sigma Aldrich and were used as received, with the exception of pyrrole, which was distilled and stored in darkness below -20 °C, prior to use. If a given circumstance arose that required a pH change it was adjusted accordingly using an acidic or basic solution. HCl was used to maintain an acidic pH, while NaOH was used to give a basic pH. All electrolytes used for the electropolymerisation process were made up using distilled water. All chemicals, including the most frequently used sodium chloride, sodium oxalate, and sodium potassium tartrate, were analytical grade reagents. Pyrrole monomer was supplied by Aldrich at 98%, the benzyl (BV), ethyl (EV) and methyl (MV) viologens were also supplied by Aldrich and were stored at room temperature. All other solutions used for electrochemical measurements were made from analytical grade reagents and distilled water. Again, where necessary, pH alterations were performed using

either HCl or NaOH to give the required pH. The compositions of all the solutions used are presented in the figure captions or corresponding text of all figures presented. In some cases where difficulties with solubility occurred, the solutions were sonicated until solubility was achieved.

2.4 Polymer Electrosynthesis

All polymers were synthesised by potentiostatic or cyclic voltammetry (CV) techniques, by applying a constant potential to the electrode and then recording the current as a function of time (potentiostatic) or as a function of the sweeping potential (CV). Pyrrole, 0.20 or 0.30 mol dm^{-3}, was dissolved in the desired electrolyte. The supporting electrolyte has the fundamental functions to ensure the conductivity of the solution and to provide doping of the polymer. The electrolytes examined in the present study were dodecylbenzene sulfonate (DBS), sodium potassium tartrate, and sodium oxalate [1, 244]. To dope the polymer with tartrate for instance, pyrrole was dissolved in a 0.10 mol dm^{-3} sodium tartrate solution. The multi-walled carbon nanotubes (MWCNTs) were introduced to establish if they contributed any further enhancement to the polymer coatings and initially the DBS was used to disperse the MWCNTs. A 0.02 mg solution of the MWCNTs was used in conjunction with a 0.05 mol dm^{-3} solution of DBS. This was then combined with pyrrole and used as the electropolymerisation solution [202]. This negatively charged surfactant is sufficiently conductive at 0.05 mol dm^{-3} to allow electropolymerisation. However, in all cases the pH was adjusted to 7.0 with a small quantity of NaOH, in order to promote electropolymerisation. Otherwise the polymer growth was too slow and occurred in patches on the electrode, or no polymerisation occurred at all. To achieve the electropolymerisation of pyrrole, the applied potentials were varied from 0.60 to 0.90 V vs. SCE. It is evident from the Pourbaix diagram of copper (Chapter 1, Section 1.3.1) that a compromise must be achieved between the applied potential and the pH of the solution in order to avoid dissolution of the copper. Potentials higher than 0.9 V vs. SCE were not used as this gives rise to significant dissolution of copper and over-oxidation of the deposited PPy. The thickness of the polymer films was controlled by monitoring the polymerisation time. Further details on the potentials and pH values employed are given in the experimental sections of the relevant chapters.

2.5 Test Procedures and Techniques

The experimental procedures employed in this study are now presented in more detail. In all cases a brief description of the parameters used in the experiment, together with the necessary background information, is provided.

2.5.1 Potentiodynamic Polarisation Measurements

This technique involves varying the potential and monitoring the resultant current flow. This technique is mainly used for polarisation corrosion tests in which the initial potential is the open-circuit potential of the electrode in the desired test environment or some potential below the open-circuit potential [8]. The initial potential was chosen in order to ensure that the polymer coating present on the electrode was not damaged due to the excessively high rates of reduction reactions. For comparison purposes this initial potential was used for all polymer-free electrodes also. Polarisation was then performed in the anodic direction at scan rates of 0.1667 or 1 mV s^{-1} until visible breakdown of the electrode occurred or until a current density of 1 mA cm^{-2} was reached.

2.5.2 Potentiostatic Measurements

Potentiostatic measurements were utilised for a variety of different processes in this study [45]. These tests were carried out by applying a constant potential to the electrode and recording the current density as a function of time, for periods of time from 1000 to 1200 s. The number of data points collected per second determines the resolution. A total of 2000 data points s^{-1} were collected in all experiments. A potentiostatic mode was employed in order to electrodeposit the PPy films doped with the various anions. A constant potential, typically 0.75 V vs SCE, was applied to the working electrode in the polymer-forming electrolyte, initially for a fixed period of time, and then until a desired charge/thickness of the polymer film was reached. This constant potential technique was used to over-oxidise the polymer films by holding the working electrode at a substantially higher potential for a fixed amount of time. Finally, this technique was employed as a pre-treatment step where a low potential was used to "clean" the electrode surface by reducing any unwanted oxides. Again, where necessary, the potentials used are presented in the figure captions, or corresponding text, of all presented data.

Both cyclic voltammetry and potentiostatic techniques are routinely used in growing polymer films. However, in this study it was found that potentiostatic measurements were better for growing the polymers over the cyclic voltammetry method [245]. By employing the potentiostatic mode the polymers formed were smooth and the films were considerably more adherent to the copper electrode, in comparison to the films grown using the cyclic voltammetry methods. The electrodeposition of PPy using a potential step technique gives a well-defined chronoamperometric response, with a rising current-time transient during the initial stage, followed by decay in the current, to a near constant value. These transients have been explained in terms of the nucleation of the polymer at the surface followed by three-dimensional growth. It has also been shown that the initial PPy nodules deposited at the electrode are isolated and randomly dispersed. With continued time, the nodules grow in a three-dimensional manner to give an increasing number of grains on the surface. Depending on the potential applied a large number of nucleation sites can be generated to give a highly adherent polymer film [246].

In contrast, with cyclic voltammetry, the potential is swept across a large window, and the monomer becomes oxidised over a range of potentials to form the polymer. Hernanez-Perrez *et al.* [145] followed, using AFM measurements, the formation of nano-sized PPy nodules and their transformation into larger surface aggregates during cyclic voltammetry measurements. This forms a rough surface and the polymer is less adherent to the electrode as it is being repeatedly oxidised and reduced. Indeed, Hernanez-Perrez *et al.* [145] concluded that the potentiostatic method allows better control over the polymer growth giving a well-defined smooth surface.

2.5.3 Impedance Measurements

Electrochemical impedance spectroscopy (EIS) is a very useful method used to examine multiple factors at the surface of the working electrode [247]. These factors can include the stability, kinetics and double layer capacitance of the working electrode, to name but a few [248, 249, 250]. Impedance measurements involve the application of a small perturbing sinusoidal voltage of 1 to 10 mV, which is superimposed on the fixed baseline potential or versus the open-circuit potential. Any shift that may occur in the phase and amplitude of this sinusoidal voltage will result in an AC current, which is as a result of variations occurring within the electrochemical cell [251].

The various components of the electrochemical cell are the determining factors in the overall impedance of a system. These components can include diffusion, passivating layers, electron-transfer kinetics and the solution resistance. The relative contributions of these components tend to exhibit a variation with frequency, for example, diffusion may dominate at lower frequencies whereas electron-transfer kinetics can dominate at higher frequencies [249, 252]. EIS is extremely useful as it allows measurements to be recorded over a wide frequency range, thus allowing multiple processes with varying time scales to be detected within the same experiment.

EIS results are expressed in two parts, real and imaginary, resulting from the shift in phase that arises as a result of the phase shift that occurs between the applied AC potential and the AC current response on the application of an AC potential to the electrochemical cell. These components are plotted on a vector diagram known as a Complex Plane or Nyquist plot, with the real component (Z') on the x-axis and the imaginary component (Z'') on the y-axis, as depicted in Figure 2.5a.

The experimental data may also be presented in the form of a Bode plot, as illustrated in Figure 2.5b and 2.5c. This displays the total impedance of the system, |Z|, on a logarithmic scale and the phase angle, θ, as a function of the logarithmic of frequency. The total impedance, |Z|, is related to the real and imaginary components through Equation 2.1.

$$|Z| = \sqrt{(Z_{real})^2 + \left(Z_{imag}\right)^2} \tag{2.1}$$

For the purpose of this work, EIS measurements were carried out in order to obtain information on the stability, charge-transfer resistance and capacitance of the polymer films [253]. The exact experimental conditions are described in detail in Chapters 5 and 7. However, in general, the polymer was conditioned for 30 min either at the open-circuit potential (OCP) or at a fixed applied potential, to ensure that a steady state was reached before measurements were performed. This was tested further by recording the impedance data from high to low frequencies, then reversing the sweep and recording the data from low to high frequencies. If no hysteresis was observed it was then concluded that steady-state conditions had been attained. A potential perturbation of 5 mV was used to ensure a pseudo-linear response of the system, while the frequency was varied from 65 kHz to 10 mHz.

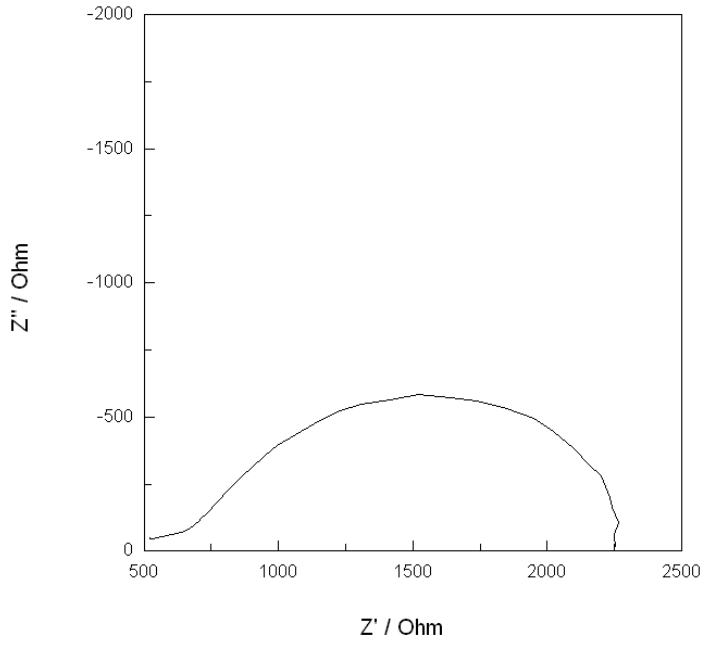

(a)

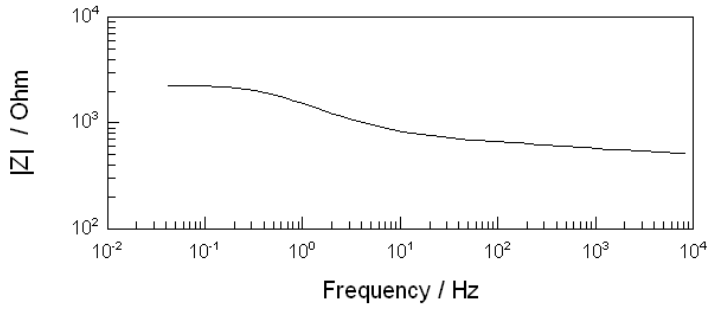

(b)

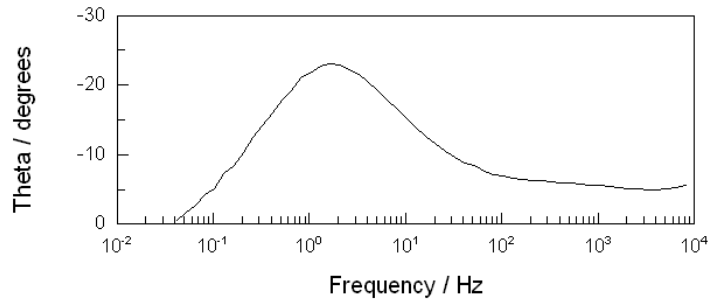

(c)

Figure 2.5: (a) Complex Plane (or Nyquist) plot, (b) Bode plot with impedance plotted as a function of frequency and (c) Bode plot with phase angle plotted as a function of frequency.

The impedance response was modelled using Zview, a data modelling software package that is capable of modelling the data to appropriate equivalent electrical circuits using a non linear least squares fitting routine that considers both the real and the imaginary components of the data. The purpose of fitting the data to these equivalent circuit models is to mimic the actual impedance measurements with an equivalent electrical circuit which consists of resistors, capacitors and constant phase elements. The Zview software is designed to accurately model impedance data, whereby each circuit element in the model is selected to correspond to a real physical component in the electrochemical cell. In this work, estimated initial values were generated and these were used to build an electrical circuit, then the Zview software was used to refine these estimates using an iterative process to select alternative values that best fitted the experimental data.

The main electrical circuit elements used to model data were constant phase elements (CPE) and resistors (R). A resistor has no imaginary component; hence its value is equal to the impedance for the real component. The total resistance value is a combination of the value for the resistance elements in the electrolyte solution (solution resistance, R_S) and the value for the charge transfer resistance (R_{CT}). Constant phase elements (CPE) were used to determine the capacitance and/or the diffusional processes at the interface. In particular, the CPE was used instead of a pure capacitor as this allows for the inhomogeneity of the surface of the electrode to be taken into account [245, 254, 255]. Equation 2.2 defines the impedance of a constant phase element, where ω is the angular frequency (2πf). CPEs are defined using two parameters; a magnitude term (T), where T represents the magnitude of the impedance, and an exponent value (n). The exponent gives information on the physical processes that are occurring within the electrochemical cell; if the exponent value is equal to 1.0, it is correct to assume that the CPE is behaving as an ideal capacitor, however, values of 0.8 and higher are also acceptable capacitance components, which are indicative of a porous surface [1, 256, 257]. On the other hand, an exponent value of 0.5 is consistent with a diffusion process; this coincides with a phase angle of 45° [245, 258].

$$Z = \frac{1}{T\left(\sqrt{-1}\omega\right)^{n}} \tag{2.2}$$

By using various components in series or in parallel it is possible to create an appropriate

equivalent electrical circuit model based on the physical system. Figure 2.6 shows the models that were designed in order to evaluate the data presented in this thesis. When this approach is used, it is very important that each element in the equivalent circuit element corresponds to an actual component of the electrochemical cell; otherwise the equivalent circuit has little or no meaning. For this analysis, the simulated impedance was calculated based on the initial circuit parameters and values. This fit was then compared to the experimental data and the values of the circuit parameters modified. The fit between the experimental and simulated data was re-evaluated. This iterative process was continued until there was a minimum difference between the simulated and experimental data. The percentage errors shown in Table 2.2 give the percentage by which the circuit element can be modified without any loss in fit between the simulated and the experimental data, which, in turn, gives the actual errors in the values of each circuit component. For simple circuits the error was maintained at 2% or lower. If higher errors were achieved, then an alternative circuit was considered. A higher percentage error of 5% was accepted for more complex models that contained a greater number of circuit elements.

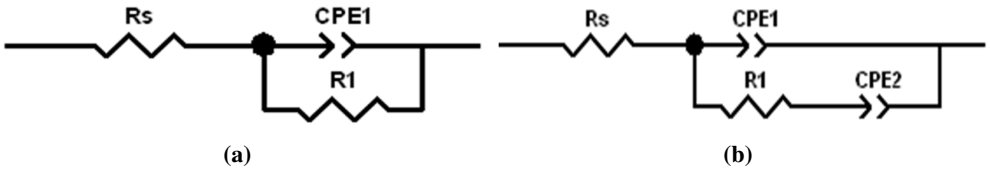

Figure 2.6: Equivalent circuits used to fit impedance data.

Table 2.2: Typical equivalent circuit parameters and the data fitting routine, values and errors used to fit impedance data.

Element	Value	Error	% Error
R_1	171.80	1.59	0.93
$CPE1-T$	5.07×10^{-6}	1.45×10^{-7}	2.87
$CPE1-P$	0.86	0.01	0.52
R_2	17376	905.92	5.21
$CPE2-T$	3.78×10^{-5}	9.72×10^{-7}	2.57
$CPE2-P$	0.57	0.02	3.81

2.5.4 Cyclic Voltammetry

This technique involves a forward sweep by polarisation from a predetermined initial potential to some vertex potential. The potential is then reversed and the back sweep performed by

polarisation from the vertex point to the final potential, which equals the initial potential. This procedure creates a cyclic effect, Figure 2.7. This technique is especially useful in studying the reversibility of a redox couple. For a simple redox couple, the voltammogram exhibits an oxidation wave, with a peak current, and a corresponding reduction wave, centred at a peak potential, as shown in Figure 2.7.

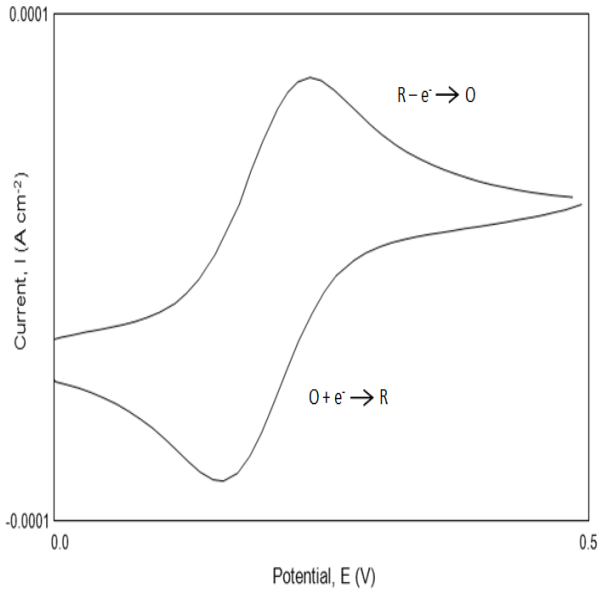

Figure 2.7: Typical current-potential profile for a cyclic voltammogram of a reversible redox species.

This technique was used mainly in the study for the growth of polymer layers and for the study of the electrochemical behaviour of polymer layers in monomer-free solutions [4]. It was also used to generate the BV layers on the copper surface. Different scan rates were used depending on the experimental conditions; however, the most frequent scan rates were 10, 20 or 50 mV s^{-1}. The scan rate used is presented in the figure captions in the results section. Where necessary the charge associated with the resultant peaks was calculated by integrating under the curve. This was regularly performed to give information on the thickness of polymer layers, as the amount of charge passed is proportional to the thickness of the polymer layer due to the conducting properties of the polymer film. Figure 2.8 illustrates an example of a typical cyclic voltammogram. Here arrows indicate the direction of the scan rate while the location of observed oxidation and reduction peaks are indicated by peak 1 and 2, respectively. These are discussed further in subsequent chapters.

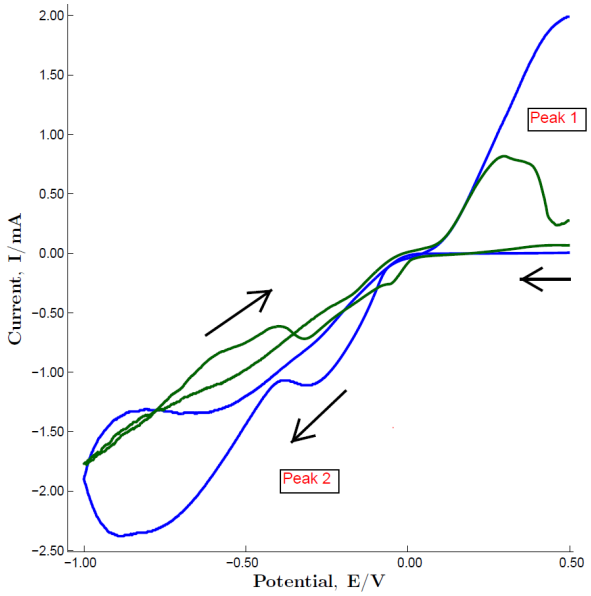

Figure 2.8: Typical cyclic voltammogram indicating the direction of the scan rate and the locations of the oxidation and the reduction peaks, as indicated by peak 1 and 2, respectively.

2.5.5 Open-Circuit Potential Measurements

The open-circuit potential (OCP) is the potential of the working electrode relative to the reference electrode when no potential or current is applied to the cell. It is a relatively simple technique in which the only parameter required apart from the reference potential is time. This technique was mainly used to measure the open-circuit potentials of polymer-coated and viologen-coated copper electrodes and to investigate the corrosion protection properties by monitoring this potential as a function of time [259]. A total of 2000 data points s^{-1} were collected in all experiments.

2.5.6 UV-Vis Spectroscopy and Spectroelectrochemical Measurements

UV-Vis spectroscopy measures the amount of ultraviolet and visible light transmitted or absorbed by a sample placed in the spectrometer. Generally species which absorb in the visible range appear coloured and species which absorb in the UV-Vis region appear colourless. The wavelength at which maximum absorption occurs is known as λ_{max}. At this wavelength which is fixed, the absorbance changes in accordance with the concentration. This relationship is commonly referred to as the Beer-Lambert law, which states that absorbance is proportional to concentration at a fixed wavelength, as shown in Equation 2.3, where A is the absorbance, e is

the molar extinction coefficient, c is the concentration and l is the path length.

$$A = ecl \tag{2.3}$$

A Varian Cary series spectrophotometer was used in all experiments. It consists of a Xenon lamp and has a maximum scan rate of 24000 nm min^{-1}. However, lower scan rates of 300 nm min^{-1} were employed. This method was used to deposit PPy onto ITO electrodes and in the analysis of the copper ion concentration which had leached out into solution. A calibration curve was obtained from standard solutions and this was used to analyse the samples. In all cases a quartz crystal cuvette with a diameter of 1 cm was used and the wavelength was scanned from 300 to 800 nm.

Spectroelectrochemistry measurements [2] were carried out using the Varian Cary UV-Vis spectrometer and a potentiostat twinned together, as illustrated in Figure 2.9. The three electrodes were incorporated into the quartz cuvette. A transparent indium tin oxide (ITO) coated glass served as the working electrode, while the counter electrode was a platinum wire of 1.0 mm in diameter. The references electrode was a silver wire. The lid of the cell was designed to hold the electrodes in place and prevent the path of the UV light from being obstructed. This technique was used to test the protective nature of the polymer coatings. Further details are given in the relevant Chapters.

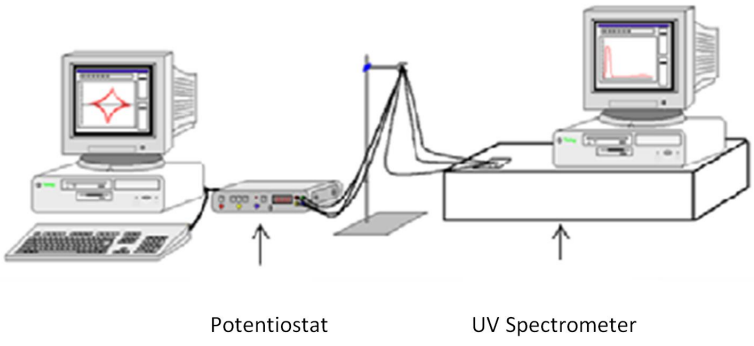

Figure 2.9: Schematic representation of the spectroelectrochemical experimental set-up.

2.5.7 Fluorescence Spectroscopy

The fundamentals of fluorescence spectroscopy focus on the emission of absorbed energy. In contrast to UV-Vis spectroscopy, the detector records light emission as opposed to light

absorbed. The schematic shown in Figure 2.10 illustrates that the light is emitted at right angles to the absorbed light from the sample. The emitted light is then detected, recorded and appears as a spectrum of intensity versus wavelength. The theory of fluorescence is based on the absorption of photons of light, at a particular wavelength. This is known as the excitation wavelength. The absorption of light causes an electronic transition from the lowest vibrational level in the ground state to the lowest vibrational level in the excited state. The lifetime of this excited state is usually very short and then relaxation occurs, which is the process of emission. Emission occurs at a longer wavelength than excitation. The intensity of the emission bands changes linearly with concentration. Also, the intensity of the fluorescence is generally high for compounds containing aromatic functional groups with low-energy $\pi \rightarrow \pi*$ transition levels, along with aliphatic and alicyclic carbonyl structures or highly conjugated double-bond structures. All fluorescent experiments were carried out using a Cary Eclipse fluorescence spectrophotometer and data were recorded using complimentary software, Scan Software Version 1.1. Data were further analysed using Microsoft Excel for Windows. Similar to UV-Vis spectroscopy, the solution sample was placed in a quartz cuvette of path length 1 cm. The instrument was then programmed with a single excitation wavelength and an emission range. These fluorimetric measurements were used to indirectly find the concentration of the critical micelle content of the DBS [224, 228].

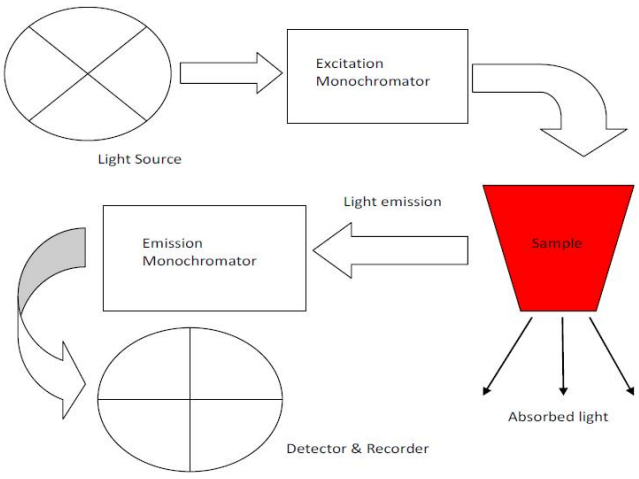

Figure 2.10: Schematic illustration of fluorometer and the method of detection and recording.

2.5.8 Differential Scanning Calorimetry (DSC)

Differential scanning calorimetry (DSC) was used to study the thermal properties and transitions of the polymers. These transitions include the melting interval, decomposition, crystallisation and even the purity of the polymers, as illustrated in Figure 2.11. The apparatus for DSC analysis is shown in Figure 2.12, whereby an aluminium pan containing the polymer is placed in the heating chamber close to an empty pan which acts as a reference. The furnace is set to increase or decrease the temperature at a fixed rate and the arrangement of the aluminium pans ensures that they are both at an identical temperature at all times. The DSC measures the energy that is required to keep both aluminium pans at an identical temperature. Hence the amount of heat absorbed or released by the polymer sample is recorded as the temperature is varied; i.e., during heating or cooling.

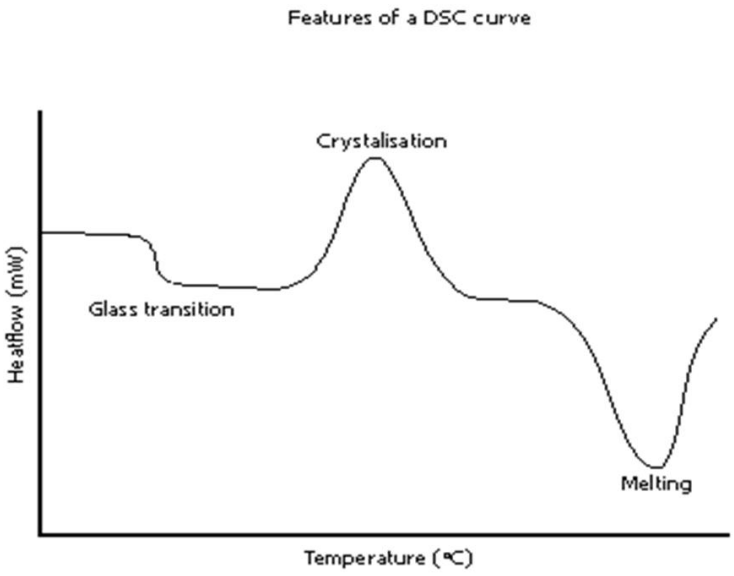

Figure 2.11: Typical features of a DSC curve.

The measured data were recorded as the heat change expressed as heat flow (mW) as a function of the temperature (°C). Approximately 2.0 mg of polymer sample was heated from 25 up to 450 °C, at a constant rate of 10 °C min^{-1}, under an inert atmosphere. The samples were then cooled from 450 back to 25 °C, again at a constant rate of 10 °C min^{-1}, using liquid nitrogen as the cooling agent, and a cyclic pattern was obtained. The instrument used was a Perkin Elmer Pyris 6.0 apparatus and the results were recorded and analysed using Pyris Data Analysis software, this depicts exothermic peaks as well shaped curves and endothermic peaks

as bell shaped curves. This technique was utilised in order to investigate the thermal behaviour of the polymer doped with different dopants.

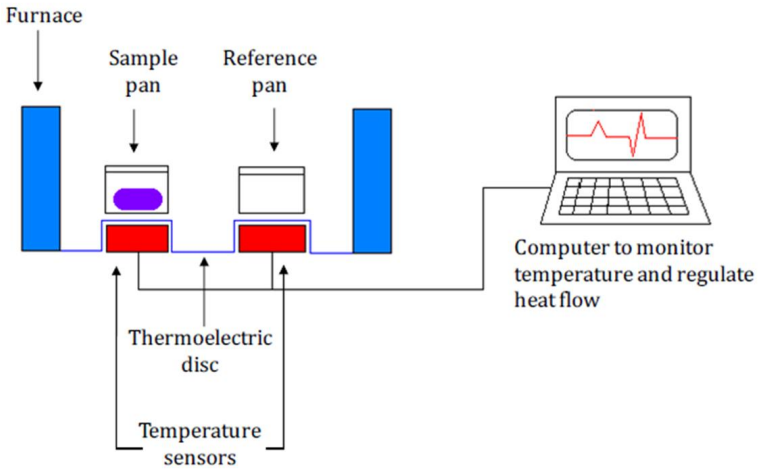

Figure 2.12: Schematic of the differential scanning calorimetry apparatus.

2.5.9 Scanning Electron Microscopy and Energy Dispersive X-ray Analysis

Scanning electron microscopy (SEM) is a method for high-resolution imaging of surfaces and objects [260]. The SEM uses electrons for imaging, much as a light microscope uses visible light. The advantages of SEM over light microscopy include much higher magnification (>100,000X) and greater depth of field up to 100 times that of light microscopy. Electrons are ejected from an electron gun under vacuum. These electrons interact with atoms of the sample and X-rays, backscattered electrons and secondary electrons emitted from the sample are collected by the detector. The SEM is commonly equipped with an energy dispersive X-ray analysis (EDX) system. Qualitative chemical analysis is obtained using this system in conjunction with the SEM. It measures the X-rays generated from the sample when it is bombarded with the electron beam. This X-ray energy is characteristic of the element from which it was emitted, thus EDX analysis is useful in identifying the chemical components of a sample [260].

In this study SEM and EDX analyses were used to obtain information regarding the morphology and chemical components of the polymer films and the BV adsorbed films. All samples were prepared on flat Cu disc electrodes and the samples were dried and sputter coated with a thin gold layer using an Emitech K550x system, before analysis.

2.5.10 Kinetic Analysis

The cyclic voltammetry technique is a very useful tool as mentioned earlier in Section 2.5.4; however, it can also provide information on the kinetics of a system. The voltammogram response at varied scan rates can reveal kinetic information concerning the electrocatalytic process, including diffusion and adsorption effects, and it can also be used to determine the reversible behaviour of a system. For a reversible system, the factors that can influence the behaviour and magnitude of the peak current density can be described by the Randles-Sevcik equation [43], Equation 2.4. Here, i_p is the peak current density (A cm^{-2}), n is the electron stoichiometry, D is the diffusion coefficient (cm^2 s^{-1}), v is the scan rate (V s^{-1}) and C_o is the concentration (mol cm^{-3}). A reversible couple will only be observed when both the oxidation and reduction species are stable and if the electron-transfer occurs at a fast rate.

$$i_p = \left(2.69 \times 10^5\right) n^{3/2} D^{1/2} v^{1/2} C_o \tag{2.4}$$

It can be seen from the Randles-Sevcik equation that the peak current density, i_p, is directly proportional to the concentration of the electroactive species in the system and also to the square root of the scan rate and diffusion coefficient. Therefore, a linear relationship between the current and the square root of the scan rate is indicative that the redox reaction conforms to the Randles-Sevcik equation and hence is governed to some extent by a diffusion-controlled process. As a result, the redox reaction process is considered to be adsorption free. If a plot of the peak current against the square root of the scan rate yields a straight line, the diffusion coefficient can then be determined from the slope of this line when the electron stoichiometry, concentration and area of the electrode are known [39].

When experimental data fit the Randles-Sevcik equation, which correlates with a reversible system, it can then be assumed that the reversible system will follow other patterns also. For example, the forward and reverse peak currents for a reversible system should be equal to unity, i.e., 1.0, Equation 2.5, and be independent of scan rate. The peak separations should comply with Equation 2.6 and the difference in the peak potentials and the half-wave peak potentials should satisfy Equation 2.7. If any of these equations are not satisfied, this means that the electron transfer is not reversible under the conditions of the experiment and that the process is more complex.

$$\frac{i_p^A}{i_p^C} = 1 \tag{2.5}$$

$$\Delta E_p = E_p^A - E_p^C = \frac{59}{n}\, mV \tag{2.6}$$

$$E_p - E_{p/2} = \frac{59}{n}\, mV \tag{2.7}$$

In these equations, i_p^A is the oxidation peak current, i_p^C is the reduction peak current, E_p^A is the peak potential of the oxidation peak, E_p^C is the peak potential of the reduction peak, $E_{p/2}$ is the half-wave potential and n is the number of electrons transferred. If the electron transfer does not take place within the timescale of the experiment, i.e., the rate of electron transfer is too slow, the system can be said to be irreversible. The main characteristic of an irreversible system is the absence of a reverse peak in the cyclic voltammogram. The peak current of an irreversible system can be described by Equation 2.8, where n_α is the number of electrons transferred up to and including the rate-determining step and α_c is the charge-transfer coefficient of the reverse reaction.

$$i_p = (2.99 \times 10^5) n (\alpha_c n_\alpha)^{1/2} C_o D^{1/2} v^{1/2} \tag{2.8}$$

In addition to this, for an irreversible system, although the peak currents may be proportional to the square root of the scan rate, the peak potentials shift by $30/\alpha_c n_\alpha$ mV for each decade change in v. Also, the difference in the peak potentials and the half wave peak potential comply with Equation 2.9.

$$E_p - E_{p/2} = \frac{48}{\alpha_c n_\alpha}\, mV \tag{2.9}$$

When the system is neither totally reversible nor irreversible, a quasi-reversible system exists, Equation 2.10. The kinetics of a quasi-reversible system are not very fast or very slow, but both the forward and reverse reaction make a contribution to the peak current, which increases with the square root of the scan rate, as shown in Equation 2.4. However, at high scan rates where the standard rate constant, k^θ, is slow, the peak current is no longer proportional to

the square root of the scan rate.

$$0.3v^{1/2} \leq k^{\theta} \leq 2 \times 10^{-5} v^{1/2} \tag{2.10}$$

Just as with a totally reversible system, the ratio of the peak oxidation and reduction currents of a quasi-reversible system should equate to unity, provided that α_c and α_A are both equal to 0.5. The anodic and cathodic peaks are separated by more than $59/n$ mV and this separation increases with increasing scan rate, as the peak potential shifts. These characteristics are summarised in Figure 2.13, where the characteristics of reversible and quasi-reversible systems are shown.

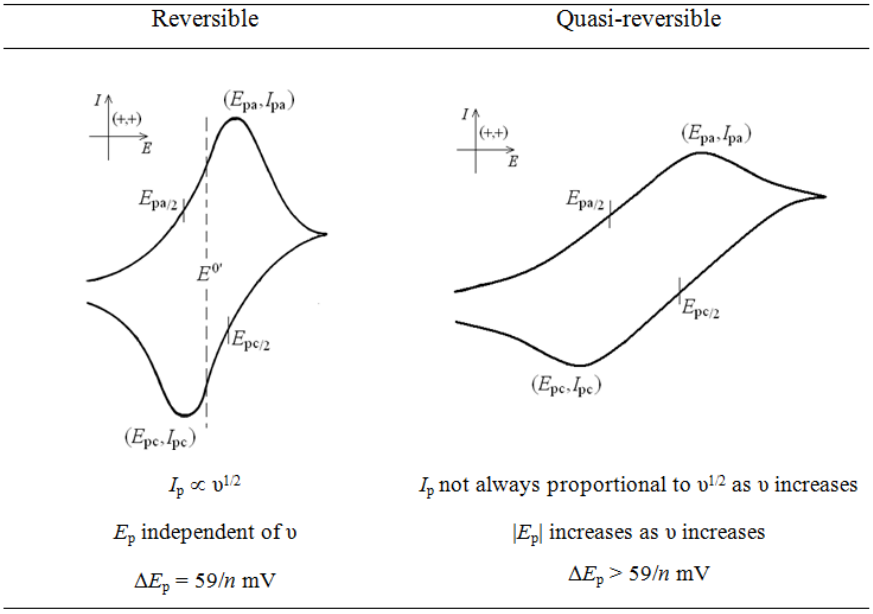

Figure 2.13: Cyclic voltammograms for reversible and quasi-reversible systems.

2.6 Tafel Equation and Kinetics of Corrosion

The rate of corrosion is expressed in terms of a corrosion current, I_{corr}, and the potential adopted during the corrosion process is called the corrosion potential, E_{corr} [261].

The corrosion current, I_{corr}, cannot be measured directly. In many cases, it can be estimated by plotting the applied potential as a function of the logarithm of the measured current. A typical plot of the oxidation reaction is shown in Figure 2.14, where the potential is varied from

values below the corrosion potential, E_{corr}, to values higher than the corrosion potential and the corresponding current is measured. The reduction half reaction adopts a similar trend. The linear regions of the anodic and cathodic branches are then extended and intersected to give the computed corrosion current. In this analysis, the rate of the cathodic process is controlled by the kinetics of the electron transfer reaction at the metal surface, the same applies to the anodic processes. This is generally the case for many corrosion reactions, provided the system is not perturbed too far from E_{corr}. This analysis is based on the Tafel equation. An electrochemical reaction under kinetic control obeys the Tafel equation, Equation 2.11.

$$I = I_0 \exp\left(\frac{2.303\left(E - E^0\right)}{\beta}\right) \tag{2.11}$$

In this equation, I is the current resulting from the reaction, I_0 is the exchange current, E is the electrode potential, E^o is the equilibrium potential, and β is the Tafel constant. In this form Equation 2.11 describes the behaviour of one isolated reaction. However, the Tafel equations for both the anodic and cathodic reactions in a corrosion system can be combined to generate the Butler-Volmer equation, Equation 2.12.

$$I = I_{corr}\left(\exp\left(\frac{2.303(E - E_{corr})}{\beta_a}\right) - \exp\left(\frac{-2.303(E - E_{corr})}{\beta_c}\right)\right) \tag{2.12}$$

Here, I is the measured cell current, I_{corr} is the corrosion current, E is the electrode potential, E_{corr} is the corrosion potential, β_a is the anodic Tafel constant in V/decade and β_c is the cathodic Tafel constant in V/decade.

At E_{corr}, each exponential term equals unity and the cell current is therefore zero. Near E_{corr}, both exponential terms contribute to the overall current. Finally, as the potential is driven further from E_{corr} one exponential term predominates and the other term can be ignored. When this occurs, a plot of the logarithm of the current versus potential becomes linear to give a Tafel plot [262]. In Figure 2.14 the Tafel plot is shown, illustrating the extrapolation, in order to calculate the corrosion current (I_{corr}).

When the corrosion reactions are controlled by kinetics as is frequently observed, the "Tafel lines" are characterised by the slope of the linear part of the polarisation curve and by their intersection when extrapolated to the equilibrium potential. The values of the characteristic constants in the Tafel equation depend on the metal and the environment under consideration.

It is possible to extrapolate the anodic and cathodic linear portions of the polarisation curves to the corrosion potential, E_{corr}. The value of the current at their intersection corresponds to the rate of corrosion I_{corr}, expressed in current density. The values of the exchange current densities for the cathodic and anodic reactions have a profound effect on the corrosion rate [263].

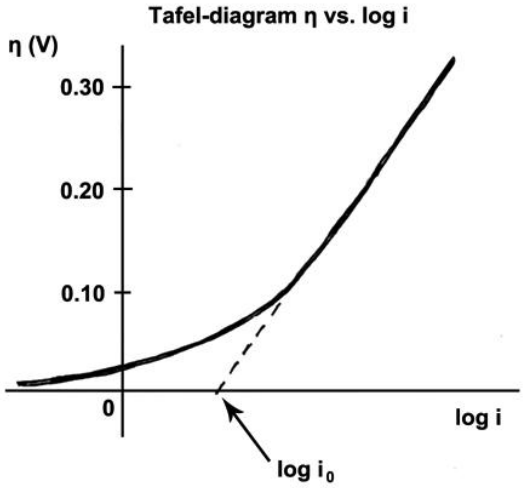

Figure 2.14: A Tafel plot indicating the extrapolation of the corrosion current [39].

In practice, many corrosion systems are kinetically controlled and thus obey Equation 2.12 to give a log current versus potential curve that is linear on both sides of E_{corr}. However, there can be complications, such as; (i) concentration polarisation, where the rate of a reaction is controlled by the rate at which reactants arrive at the metal surface. Often cathodic reactions show concentration polarisation at higher currents, when diffusion of oxygen or hydrogen ions is not fast enough to sustain the kinetically controlled rate; (ii) oxide formation, which may or may not lead to passivation, can alter the surface of the sample. The original surface and the altered surface may have different values for the constants in the Tafel analysis; (iii) preferential dissolution of one alloying component, altering the surface; (iv) a mixed control process where more than one cathodic, or anodic, reaction occurs simultaneously. A common example of mixed control is the simultaneous reduction of oxygen and hydrogen ions.

These complications cause non-linearity in the Tafel plot. The results derived from a Tafel plot that does not have a well-defined linear region should be used with caution. Classic Tafel analysis is performed by extrapolating the linear portions of a log current versus potential plot back to their intersection. The value of either the anodic or the cathodic current at the intersection is I_{corr}. Unfortunately, many real world corrosion systems do not provide a

sufficient linear region to permit accurate extrapolation. Most modern corrosion test software performs a more sophisticated numerical fit to the Butler-Volmer equation [39]. The measured data is fit to Equation 2.12 by adjusting the values of E_{corr}, I_{corr}, β_a, and β_c. The curve fitting method has the advantage that it does not require a fully developed linear portion of the curve.

CHAPTER 3

Synthesis of the Polymer Films on a Copper Substrate

Polypyrrole (PPy), a well-known conducting polymer, has been extensively investigated for several applications, as discussed previously in Chapter 1 [264]. However, one of its more attractive applications is in the development of corrosion protective coatings. The corrosion protective properties of PPy films deposited at stainless steel [24, 265], iron [159, 266] and aluminium [28, 267] are well documented. There are fewer reports on the formation of PPy at copper electrodes, and it is for this reason that copper was selected and chosen in this study [1, 19]. It is well known that copper is easily oxidised and the nature and concentration of the anions used to deposit the polymer will influence the stability of the copper substrate. This, in turn, will influence the rate of electropolymerisation of the monomer, and the nature of the deposited PPy film. Indeed, Annibaldi *et al*. [245] have shown that adherent and homogeneous PPy films were deposited on copper from a salicylate solution. Solutions containing citric acid, sodium acetate and sodium benzoate were used by Sharifirad *et al*. [14] to deposit PPy at copper, while Raso *et al*. [268] have electropolymerised the functionalised monomer, N-methylpyrrole, at copper from an oxalic acid solution, at pH 1.5. However, very high applied potentials, ranging from 1.5 to 2.5 V vs. SCE, were used to deposit these films at copper.

In this chapter results are presented and discussed on the electrodeposition of PPy at copper. Since copper is easily oxidised, different anions, including bromides, chlorides,

sulfates, acetates [5, 269], oxalates [1] and tartrates [244], were considered. The PPy film was successfully deposited at the copper surface at an applied potential of 0.75 V vs. SCE in the presence of oxalates and tartrates to give PPy-Oxalate and PPy-Tartrate films. The chemical structures of these salts are shown in Figure 3.1. It is clear that the anions are sufficiently small and ionised in solution to dope the polymer film. It was found that sodium oxalate solutions [1] adjusted to a pH of 8.0 and sodium potassium tartrate [244] solutions adjusted to a pH of 7.0, provide the optimum conditions for the efficient deposition of adherent PPy films at the copper electrode. In addition, bi-layers, comprising the PPy-Tartrate and the PPy-Oxalate, were successfully formed. It has been reported that the characteristics and properties of the deposited PPy films vary depending on the nature and concentration of the dopant anions, the pH of the solution, the applied potential and electropolymerisation period [269]. Accordingly, the influence of these parameters, including the applied potential, the pH of the solution, and the nature of the dopant anions, on the formation and corrosion protective properties of the PPy films and bi-layers was studied and these results are presented and discussed in this chapter.

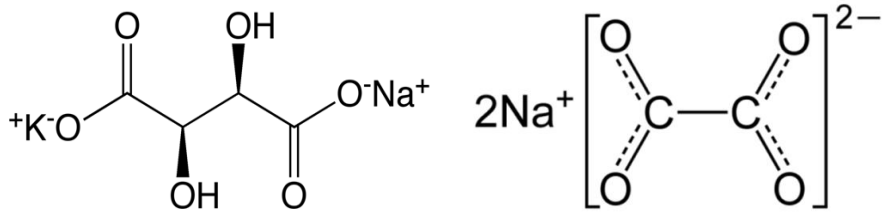

(a) **(b)**

Figure 3.1: Chemical structure of anions: (a) sodium potassium tartrate and (b) sodium oxalate.

In this chapter the procedures and experimental conditions used for the electrochemical synthesis of the polymer films are described. Then, the techniques employed to characterise the polymers are reported and the results obtained are analysed and discussed. Furthermore, all experiments carried out on the polymer films are compared to an uncoated copper electrode and in some instances the polymers were formed at a platinum electrode under similar conditions. Finally, in order to establish the protective nature of these deposited polymer films, corrosion assessment experiments were carried out.

3.1 Experimental

Details on the experimental approach used in the formation and analysis of the PPy films at the copper electrodes are provided in Sections 3.1.1, 3.1.2 and 3.1.3. This includes information on the chemicals, the techniques employed and the equipment used together with the general procedures employed to deposit the polymer films at the copper electrode.

3.1.1 Reagents

The pyrrole monomer (98%) was obtained from Aldrich and was purified by distillation prior to use. It was then stored in the dark at -20 °C between experiments. A 0.20 mol dm^{-3} pyrrole was dissolved in the electrolyte solution for all the electrochemical deposition experiments, unless otherwise stated. The analytical reagents, sodium sulfate (Na_2SO_4), sodium bromide (NaBr), sodium chloride (NaCl), sodium oxalate ($Na_2C_2O_4$), sodium potassium tartrate ($KNaC_4H_4O_6$), D-tartaric and L-tartaric acids ($C_4H_6O_6$), were purchased from Aldrich and used as received. Distilled water was used in all solution preparations. The pH meter was calibrated on a daily basis using buffers (pH 4.0 and pH 7.0) which were purchased from Lennox Ltd.

3.1.2 Electrodes and Instruments

A Cu rod (99.99%, 4 mm in diameter) electrode was used for the deposition of the PPy-Tartrate, PPy-Oxalate and the bi-layer polymer films. The rod was encased in a Teflon holder, as previously described in Chapter 2, Figure 2.3. A flat Cu disc electrode was used for SEM and EDX measurements. The disc and rod electrodes were polished using a 1 μm diamond polish and Buehler micro-cloth and rinsed well with distilled water to ensure a smooth surface finish, as outlined in Chapter 2. A saturated calomel electrode (SCE) was used as the reference electrode and a high surface area platinum wire was employed as the counter electrode.

A CHi 760C potentiostat was used to deposit the PPy films. SEM measurements were performed on a Hitachi FE-scanning electron microscope, with an oxford instruments Inca X-act 4.12 software package. The EDX analyses were carried out using an EDX Model 51-ADD0009 with the software package micro analysis suite. A Carry UV-Vis spectrometer together with the Carry Win software package was used to analyse the polymer films deposited at ITO electrodes. A schematic can be seen in Figure 2.4. These ITO electrodes consist

of indium(III) oxide (In_2O_3) and tin(IV) oxide (SnO_2), with typically 90% In_2O_3 and 10% SnO_2 by weight. Indium tin oxide is one of the most widely used transparent conducting oxides because of its optical properties [270, 271]. The ITO electrodes were connected to the potentiostat using a copper crocodile clip. Differential scanning calorimetry measurements (DSC) were recorded with a Perkin Elmer Pyris 6.0 instrument and FTIR data were recorded with KBr discs, where the sample was compressed in a pressure chamber.

3.1.3 Procedures

The PPy films were formed at potentials from 0.60 to 0.90 V vs. SCE using an electrosynthesis method, which deposited the polymer films at the working electrode [12, 258]. A Cu electrode was used as the working electrode in the majority of cases and in some experiments, for comparison purposes, a platinum electrode (99.99%, 4 mm in diameter) was employed as the substrate. The platinum electrodes were prepared using the procedures described for the Cu electrodes, Section 3.1.2. The polymers were prepared in various electrolyte solutions, at a concentration of 0.10 mol dm^{-3}, containing 0.20 mol dm^{-3} pyrrole. A summary of the various electrolytes, used in an attempt to deposit the PPy films, is given in Table 3.1.

Table 3.1: Various anions, salts or acids used in the formation of PPy films on a copper substrate.

Salt/Anion/Acid	**Concentration /mol dm^{-3}**
Sodium Oxalate	0.10
Sodium Potassium Tartrate	0.10
Sodium Acetate Trihydrate	0.10
Sodium Dihydrogen Phosphate	0.10
Sodium Phosphate Dibasic Heptahydrate	0.10
L-Tartaric Acid	0.10
D-Tartaric Acid	0.10

After electrochemical deposition, the PPy films were characterised using cyclic voltammetry [14]. A three-electrode cell was used for all voltammetry experiments. The protective properties of the PPy films were monitored by cycling in a potential window from -0.50 to 0.90 V vs. SCE, in neutral 0.10 mol dm^{-3} NaCl at scan rates varying from 1 to 100 mV s^{-1}. The pH was adjusted to 7.0 using NaOH. For the SEM and EDX measurements, the polymers were

deposited onto flat Cu disc electrodes at 0.75 V vs. SCE and sputter coated with gold prior to analysis to prevent charging of the polymer film.

3.2 Results and Discussion

3.2.1 Influence of the Nature of the Anions

In order to successfully form a PPy coating at the copper interface a suitable dopant anion is necessary [272, 273]. Due to the low corrosion potential of copper in aqueous media it is readily oxidised and dissolved, as shown in Equation 3.1. The rate of this dissolution reaction increases with increasing applied potential. This is clearly evident from the Pourbaix diagram, presented in Section 1.3.1. Consequently as the potential necessary to oxidise the monomer, which is typically higher than 0.65 V vs. SCE, is reached, significant dissolution of the copper substrate occurs. For this reason the nature of the electrolyte solution and the pH of the solution are important. These were studied in an attempt to minimise the dissolution of the copper substrate [5] and to facilitate the oxidation of the pyrrole monomer and the deposition of an adherent PPy film at the copper substrate.

$$Cu \rightarrow Cu^{2+} + 2e^{-} \tag{3.1}$$

As expected, significant dissolution of the copper was observed in the presence of bromides, sulfates and chloride anions and there was no evidence of electropolymerisation in the presence of these salts. Instead, corrosion products, such as CuCl, and the soluble $CuCl_2^-$ species, or CuBr and $CuBr_n^{n-1}$ species, were formed and deposited at the copper surface [274]. Other salts, such as sodium acetate trihydrate, sodium phosphate dibasic heptahydrate, D-tartaric acid, L-tartaric acid, and sodium dihydrogen phosphate, were considered. The concentration of the salts was fixed at 0.10 mol dm^{-3} and 0.20 mol dm^{-3} pyrrole was added to give the electropolymerisation solutions. A potential of 0.75 V vs. SCE was applied to the copper electrode for a 600 s period. At this applied potential, there was no evidence of polymer growth in the presence of the acetate trihydrate, the phosphate dibasic heptahydrate or the dihydrogen phosphate anions. Instead, the copper electrode was corroded. Evidence of electropolymerisation in the presence of the D- and L-tartaric acid was observed. However, in

some experiments, corrosion of the copper substrate was seen and the reproducibility was poor. However, more promising results were obtained with the tartrate [244] and oxalate salts [1].

A representative current-time transient recorded at 0.75 V vs. SCE in the presence of 0.10 mol dm^{-3} oxalate and 0.20 mol dm^{-3} pyrrole, adjusted to pH 8.0, is shown in Figure 3.2, while similar data recorded in the presence of a neutral 0.10 mol dm^{-3} tartrate solution, containing the pyrrole monomer, are shown in Figure 3.3. This chronoamperometry method, which involves the application of a constant potential, was selected for the formation of the PPy films, as the amount of charge consumed in the electropolymerisation step can be controlled and the experiment terminated once the desired charge is obtained [1, 14, 19, 143]. With this procedure, the thickness of the polymer films can be controlled by the amount of charge passed, hence it is possible to produce uniform polymer films in each experiment. Although cyclic voltammetry is normally used to generate compact conducting polymer films [112], potentiostatic deposition, is well known to yield polymers with consistent and reproducible morphology [12, 112]. The electropolymerisation solution was not stirred as this inhibits electropolymerisation of the monomer at the electrode interface, although oxidation of pyrrole proceeds. Nucleation of the polymer at the electrode interface occurs only when a sufficient concentration of the radical species are formed. Clearly, the concentration of radical cations at the electrode surface is reduced on agitation or stirring of the solution.

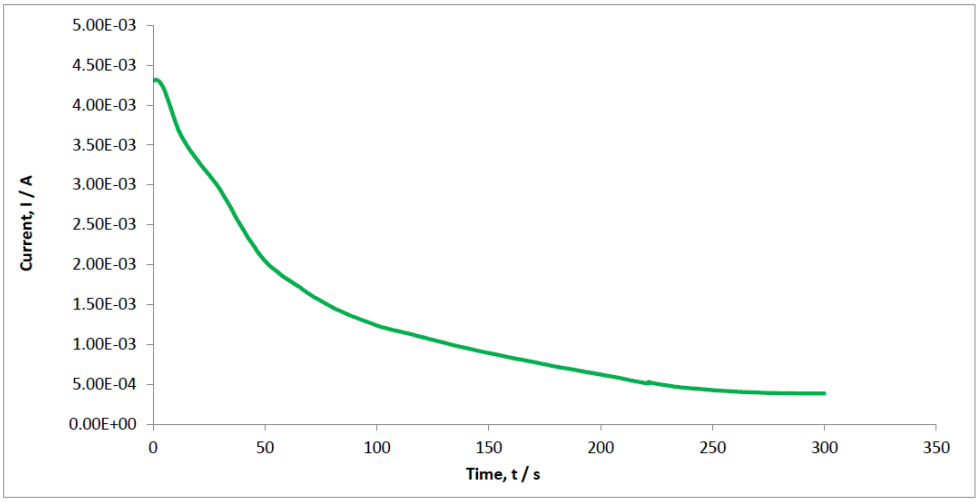

Figure 3.2: Current-time transient recorded for Cu at 0.75 V vs. SCE in a 0.10 mol dm^{-3} oxalate and 0.20 mol dm^{-3} pyrrole at a pH of 8.0.

It is evident from Figures 3.2 and 3.3 that electropolymerisation of the pyrrole monomer occurs in both the near neutral oxalate and tartrate solutions to give PPy films. However, the current-time profiles are somewhat different for the oxalate and tartrate systems. In the case of the oxalate system, there is a sharp increase in the current on application of the potential and this can be attributed to capacitive charging of the electrode. Then, the current decays and the faradaic currents can be attributed to oxidation of the pyrrole monomer and subsequent deposition of the PPy. Dissolution of the copper substrate also contributes to the faradaic current during this period. However, as the PPy is deposited the currents decay and this is clearly evident during the first 100 s of electropolymerisation. There is a further decrease in the current from 100 to 300 s, however, at about 800 s, there is a gradual increase in the current, which is not displayed in Figure 3.2. This may be related to dissolution of the copper substrate or connected to the further deposition of PPy giving a higher surface area and higher currents.

A similar initial increase in the current is observed for the tartrate system. However, once the current decays, there is no further gradual increase in the current over the 600 s time period. Moreover, the currents are higher for the oxalate system, adopting values around 5.0×10^{-4} A at 300 s. On the other hand the current-time transients recorded for copper with the other anions, listed in Table 3.1 were very different and characteristic of copper dissolution, with no evidence of any decay in the current and the deposition of PPy at the copper surface.

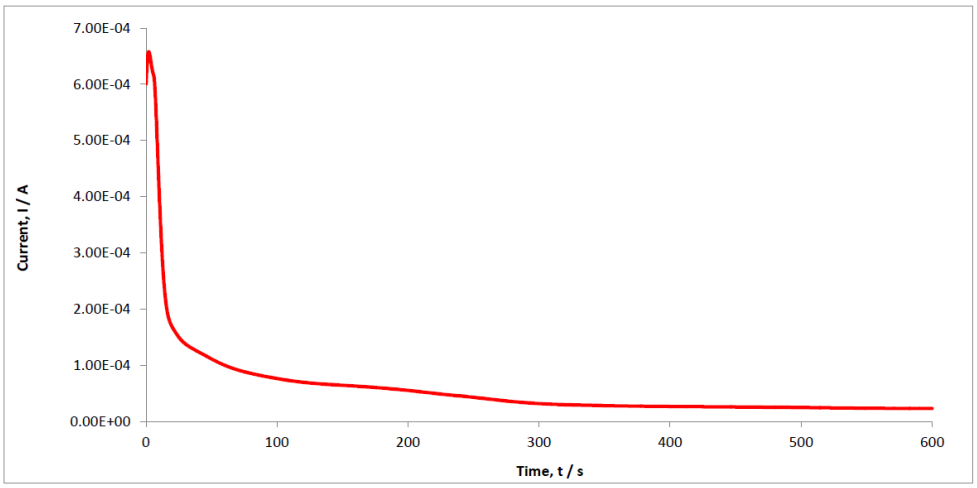

Figure 3.3: Current-time transient recorded for Cu at 0.75 V vs. SCE in 0.10 mol dm^{-3} tartrate and 0.20 mol dm^{-3} pyrrole at a pH of 7.0.

The growth of these polymer films is facilitated by the initial oxidation of the copper in both the oxalate and the tartrate solutions to generate a Cu-oxalate or Cu-tartrate pseudo-passive layer [1]. This layer is sufficiently protective to inhibit further dissolution of the copper and sufficiently conducting to enable electropolymerisation of pyrrole at the copper interface, and the generation of an adherent PPy film, as shown in Figure 3.4 where the surface morphology of the PPy-Tartrate polymer film is presented. Clearly, the polymer film is homogeneous and crack-free despite being relatively thick and dehydrated over an extended period which indicates that the copper-polymer interface is stable [1]. However, the characteristic cauliflower morphology of PPy is not evident and deposition of the PPy appears to take place along polishing lines on the copper surface, as evident from the ridge-like diagonal features [12, 14].

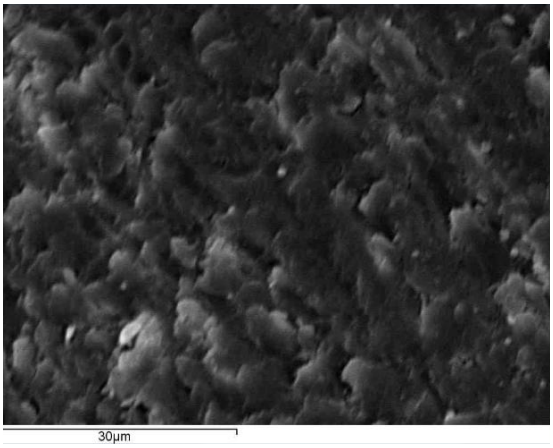

Figure 3.4: SEM micrograph of PPy-Tartrate formed at 0.75 V vs. SCE in a neutral 0.10 mol dm^{-3} tartrate and 0.20 mol dm^{-3} pyrrole solution, the scale bar corresponding to 30 μm.

3.2.2 Parameters Influencing the Formation of PPy-Oxalate and PPy-Tartrate

Once suitable anions were identified, further studies were carried out to optimise the formation of the PPy-Tartrate and PPy-Oxalate polymer films. In this study, the applied potential was varied from 0.60 to 0.90 V vs. SCE [139] and the pH of the solution was varied between pH 4.0 and 10.0 [275]. It was found that the optimum applied potential was between 0.70 and 0.80 V vs. SCE, giving uniform nucleation of the polymer films at the copper interface, and highly adherent polypyrrole films in solutions with 0.10 mol dm^{-3} tartrate or oxalate and 0.20 mol dm^{-3} pyrrole. At potentials below 0.70 V vs. SCE, the rate of electropolymerisation was slow and uniform nucleation of the polymer at the copper surface was not always observed.

Accordingly, the applied potential was fixed at 0.75 V vs. SCE and this potential was used to form the PPy-Tartrate and PPy-Oxalate films, unless otherwise stated.

Next, the pH of the electropolymerisation solution was varied between 4.0 and 10.0 [275]. Again, the concentration of the tartrate and oxalate salts was maintained at 0.10 mol dm^{-3} and the pyrrole concentration was fixed at 0.20 mol dm^{-3}. The PPy-Tartrate and PPy-Oxalate films did not form at pH 4.0 as the dissolution rate of copper was too high. Indeed, this can be easily explained using the Pourbaix diagram of copper [73], Section 1.3.1, where it is clear that at the potential used to deposit the PPy films, 0.75 V vs. SCE, the stable phase at a pH of 4.0 is the oxidised copper cation. Even in the presence of the oxalate and tartrate anions the dissolution rate of copper is too high. Electropolymerisation was observed at pH 10.0, however, the polymer films were not sufficiently adherent and the rate of electropolymerisation was low. Again, this can be explained using the Pourbaix diagram of copper, Section 1.3.1, where it is evident that CuO and Cu_2O are the stable phases at this pH. These oxides are formed at pH 10.0 and the generation of this oxide phase gives poorly adherent polymer films. The rate of electropolymerisation is very low as the oxide films are readily formed at the copper surface. However, high rates of electropolymerisation were observed at pH values of 6.0, 7.0 and 8.0. A smooth black polymer film covering the entire surface of the copper substrate was obtained. The film was homogeneous and adherent and the results were highly reproducible.

Once the experimental conditions were optimised to generate the PPy-Tartrate and PPy-Oxalate films, the polymers were cycled in a neutral 0.10 mol dm^{-3} NaCl solution at 10 mV s^{-1} and the current recorded at 0.40 V vs. SCE was measured. This current is plotted as a function of the cycle number in Figure 3.5 for the uncoated copper, the PPy-Tartrate and the PPy-Oxalate films deposited at copper and, for comparison purposes, the PPy-Tartrate deposited at platinum. The PPy-Tartrate film was deposited at the platinum electrode under conditions similar to that optimised for the copper system. However, regardless of the applied potential or the concentrations of the tartrate or monomer, the PPy-Tartrate could not be formed at the platinum electrode at a pH of 7.0. Instead, the film was formed successfully at 0.75 V vs. SCE in the presence of 0.10 mol dm^{-3} tartrate and 0.20 mol dm^{-3} pyrrole at pH 4.0. It is clear from the data presented in Figure 3.5, that the currents measured for the PPy-Tartrate film deposited at copper and platinum and the PPy-Oxalate film deposited at copper are similar. The currents are low typically varying from 2.0×10^{-4} to 4.0×10^{-4} A and furthermore, the currents remain

constant with increasing cycle number. After 40 cycles, there is little variation in the current. It is also interesting to note that the currents recorded for the PPy-Tartrate deposited at the inert platinum electrode, although somewhat lower, are similar to the data recorded for the polymers deposited at copper. This clearly shows that the PPy-Tartrate and PPy-Oxalate films are stable at pH 7.0 and there is no evidence of dissolution of the underlying copper substrate. On the other hand, the currents recorded for the uncoated copper electrode are considerably higher, of the order of 1.2 mA, and these currents fluctuate with cycle number. This is consistent with the dissolution of copper. It is well known that pure copper is easily oxidised and these relatively high currents are a clear indication of this dissolution reaction [66, 79, 276, 277]. This dissolution gives rise to the formation and deposition of CuCl at the surface of the electrode and the formation of the soluble $CuCl_2^-$ species [67, 278, 279].

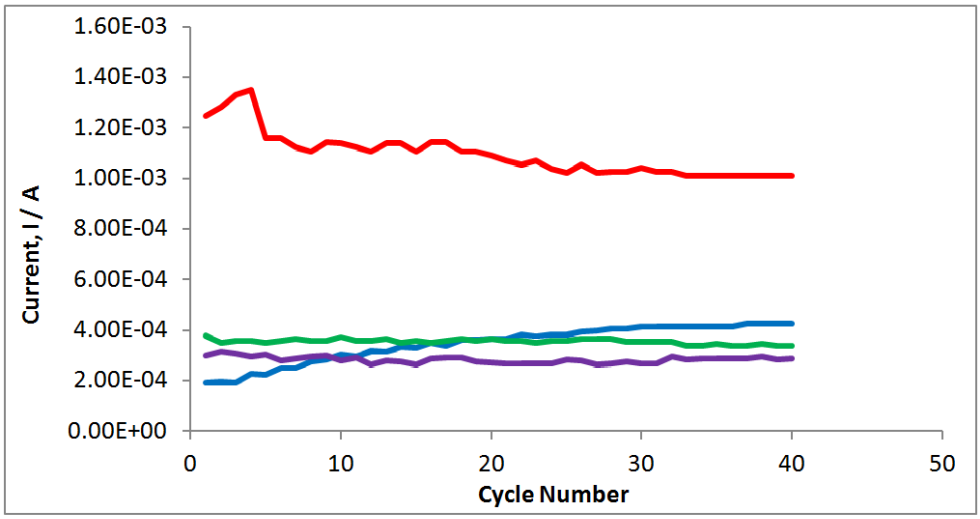

Figure 3.5: Current plotted as a function of cycle number, uncoated Cu (red), PPy-Tartrate (Cu-blue), PPy-Tartrate (Pt-purple) and PPy-Oxalate (Cu-green) cycled at 10 mV s^{-1}, in a 0.10 mol dm^{-3} NaCl solution pH 7.0.

The stability of the PPy-Tartrate film deposited at copper at different pH values ranging from 6.0 to 10.0 is shown in Figure 3.6. At pH 7.0, the current remains low and stable at approximately 2.5×10^{-4} A, indicating very good stability. Somewhat higher currents were observed at pH 6.0, 8.0 and 10.0. As evident, there is a slight increase in the current over the first 5 cycles and then the current remains essentially constant.

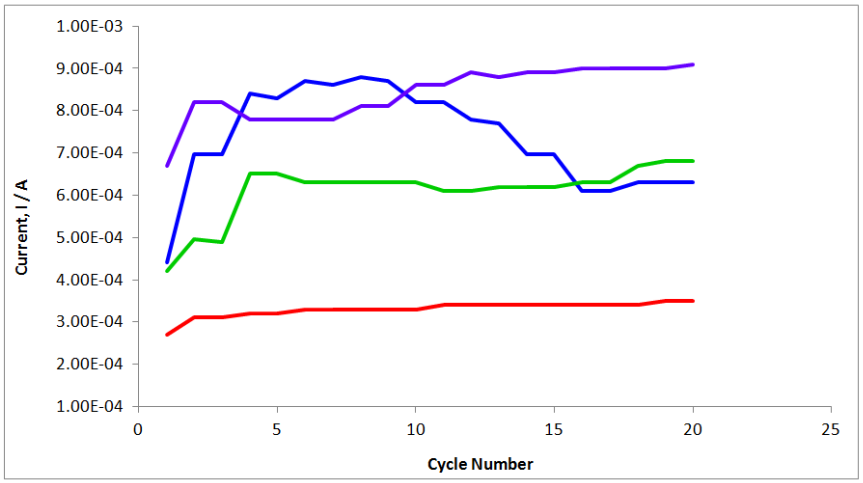

Figure 3.6: Current plotted as a function of cycle number for PPy-Tartrate film cycled at 10 mV s^{-1} in 0.10 mol dm^{-3} NaCl solution adjusted to pH values of pH 6.0 (blue), pH 7.0 (red), pH 8.0 (green) and pH 10.0 (purple).

3.2.3 Influence of the Electropolymerisation Period

In order to determine the effect of the electropolymerisation period on the protective properties of the PPy-Tartrate and PPy-Oxalate films, the electropolymerisation period was varied from 200 to 3600 s to vary the thickness of the deposited PPy films. It is well known that an increase in the electropolymerisation period gives rise to an increase in the film thickness [134]. The PPy-Tartrate and PPy-Oxalate films were deposited at 0.75 V vs. SCE from the near neutral oxalate and tartrate solutions with a fixed concentration of 0.20 mol dm^{-3} pyrrole. The charge consumed during the formation of the PPy-Tartrate and PPy-Oxalate films is plotted as a function of the electropolymerisation period and shown in Figure 3.7. There is a clear increase in the charge with increasing electropolymerisation times for the oxalate system. However, the charge remains essentially constant for the PPy-Tartrate system. This is consistent with the current-time transient shown in Figure 3.3, where the current decays slowly and then remains low at a near constant value for the remaining electropolymerisation period.

The influence of the electropolymerisation period on the properities of the PPy-Tartrate and PPy-Oxalate films is shown in Figure 3.8, where the cyclic voltammograms are compared for the PPy-Tartrate polymer film formed at 0.75 V vs. SCE for periods of 100 and 300 s and the PPy-Oxalate polymer film formed at 0.75 V vs. SCE for periods of 1200 and 3600 s. The voltammograms were recorded at 10 mV s^{-1} in 0.10 mol dm^{-3} NaCl solution at pH 7.0 from -0.50 to 1.0 V vs. SCE.

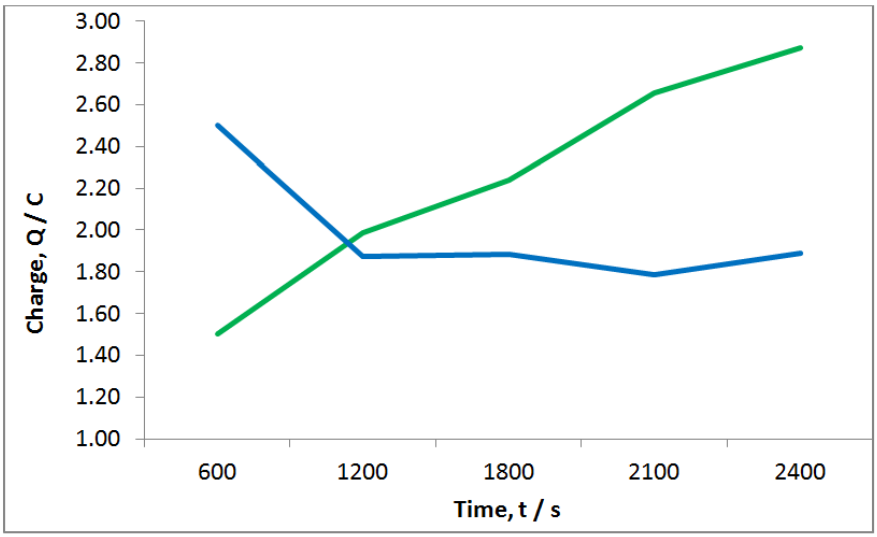

Figure 3.7: Charge plotted as a function of electropolymerisation period: PPy-Tartrate (blue) and PPy-Oxalate (green) polymer films deposited at 0.75 V vs. SCE from 0.10 mol dm^{-3} oxalate or 0.10 mol dm^{-3} tartrate and 0.20 mol dm^{-3} pyrrole.

In the case of the thin PPy-Tartrate polymer films displayed in Figure 3.8a there is little variation in the voltammograms recorded for electropolymerisation periods of 100 and 300 s. The oxidation currents are large and the reduction currents, in the vicinity of -0.20 to -0.50 V vs. SCE, are also significant, indicating that these films are not protective [280, 281]. Instead, dissolution of copper is clearly evident. However, these dissolution reactions are connected with the thickness of the polymer films and as the electropolymerisation period was increased to 1200 s, more protective PPy-Tartrate polymer films were obtained. This can be clearly observed in Figure 3.8b where data are presented for the PPy-Oxalate polymer film formed at the potential of 0.75 V vs. SCE for electropolymerisation periods of 1200 and 3600 s. It is evident that more stable and protective PPy-Oxalate polymer films are formed with the longer electropolymerisation periods. At an electropolymerisation period of 1200 s, dissolution of copper is observed and the reduction region centered at -0.40 V vs. SCE indicates the presence of chloride-containing corrosion products, the reduction of Cu and CuCl containing species that have previously been produced following the oxidation of the Cu metal, similar results are observed for the oxalate based polymer film for both the oxiadation and reduction of the Cu metal. However, more stable and protective polymer films are observed with an electropolymerisation period of 3600 s. There is no evidence of any corrosion products and the currents remain low until potentials higher than 0.45 V vs. SCE are reached.Oxidation

peak was observed for the oxidation of the Cu and the CuCl species at the Cu surface and corresponding reduction peak is due to the Cu and CuCl species being reduced with increased potential. Again, significant dissolution of the copper substrate was observed with the thin PPy-Oxalate polymer films and data similar to that presented in Figure 3.8a were obtained. It is clearly evident that the thickness of both the PPy-Oxalate and PPy-Tartrate polymer films has a significant influence on the protective properties of the coatings formed. Electropolymerisation periods higher than 1200 s are required to generate protective polymer coatings. The results of the influence of electropolymerisation periods forming both thin and thick polymer films can be clearly observed in Figure 3.8. The oxidation peak is no longer evident however, there is still a small reduction peak which indicates that some of the Cu and CuCl species are still being reduced.

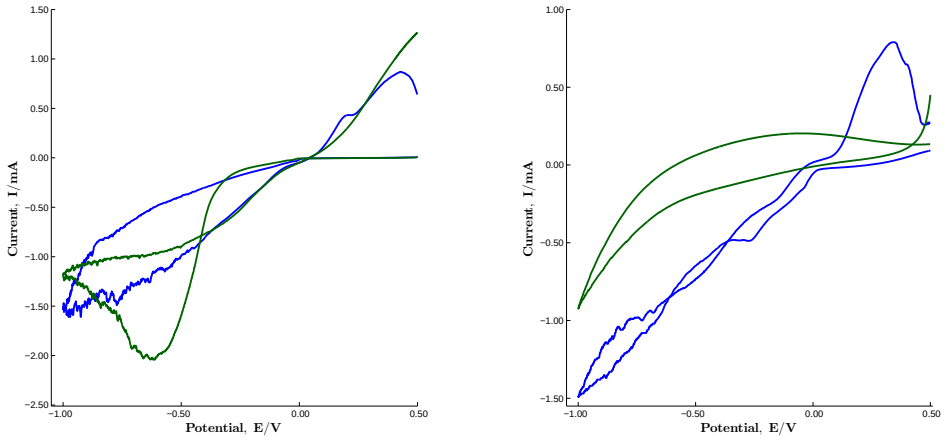

(a) **(b)**

Figure 3.8: Cyclic voltammograms recorded at 10 mV s^{-1} in 0.10 mol dm^{-3} NaCl, at a pH of 7.0 for (a) PPy-Tartrate films formed at 0.75 V vs. SCE for 100 s (green), and 300 s (blue), and (b) PPy-Oxalate films formed at 0.75 V vs. SCE for 1200 s (blue) and 3600 s (green).

3.2.4 Formation of the Bi-Layer Films

Considering the promising results obtained for the PPy-Oxalate and PPy-Tartrate polymer films, this study was extended to the formation of bi-layers comprising the PPy-Oxalate and PPy-Tartrate systems. Again, the polymers were deposited at 0.75 V vs. SCE from near neutral 0.10 mol dm^{-3} tartrate or oxalate solutions with 0.20 mol dm^{-3} pyrrole. It was possible to generate the PPy-Oxalate film at the PPy-Tartrate modified copper electrode and

equally possible to deposit the PPy-Tartrate layer at the PPy-Oxalate modified copper. Similar results were obtained regardless of which layer was initially deposited, and the significant parameter was the electropolymerisation period, as detailed in Section 3.2.3. Again, very good reproducibility was observed on formation of the bi-layers. The total electropolymerisation period was varied from 100 to 7200 s. The high stability and protective properties of the bi-layer is evident from the data presented in Figure 3.9, where the voltammograms recorded in 0.10 mol dm^{-3} NaCl, at pH 7.0, for the bi-layer deposited at copper and platinum are compared. In this case, the bi-layer was deposited at 0.75 V vs. SCE for 3600 s. The bi-layer was formed in the near neutral 0.10 mol dm^{-3} oxalate or tartrate solutions at the copper electrode, however the solution was acidified to pH 4.0 to facilitate the deposition of the PPy-Tartrate and PPy-Oxalate layers at the platinum surface. Very low currents are observed for the bi-layer deposited at platinum, and although these currents are higher for the bi-layer modified copper electrode, it is clearly evident that the bi-layer deposited at the copper electrode is stable and highly protective.

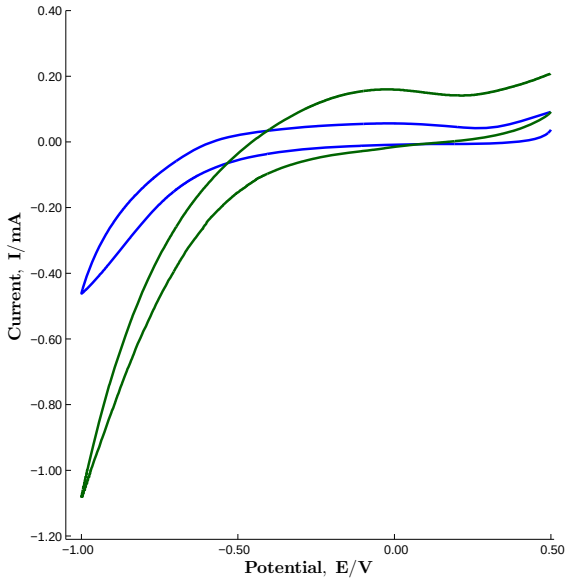

Figure 3.9: Cyclic voltammograms recorded at 10 mV s^{-1} in 0.10 mol dm^{-3} NaCl at a pH of 7.0 for the PPy-Oxalate/PPy-Tartrate bi-layer film formed at the Cu substrate (green) and the Pt substrate (blue), the bi-layer film was formed at 0.75 V vs. SCE for a total period of 3600 s.

However, at the higher electropolymerisation periods, the bi-layers polymer films were less adherent, and as outlined in Section 3.2.3, thin bi-layers polymer films were not sufficiently

protective and dissolution of the underlying pure copper substrate was observed. The optimum electropolymerisation period was found between 1200 and 3600 s. In the case of the polymer film formed for a total electropolymerisation period of 1200 s, the initial PPy-Oxalate layer was deposited at 0.75 V vs. SCE for 600 s, and then the outer PPy-Tartrate layer was formed at 0.75 V vs. SCE for an additional 600 s period to generate the bi-layer film. Once formed, the bi-layers were cycled in 0.10 mol dm^{-3} NaCl, adjusted to pH 7.0 at 10 mV s^{-1}, as shown in Figure 3.10a. Again, it is clear that the thickness of the polymer bi-layer has a significant effect on the protective properties of the film [134]. Breakdown of the bi-layer film is observed at about 0.20 V vs. SCE for an electropolymersiation period of 400 s and the breakdown potential increases only slightly with higher electropolymerisation periods of 600 and 900 s. Moreover, a clear reduction wave, corresponding to the chloride-containing corrosion products, CuCl, is evident at the shorter electropolymerisation periods of 400 and 600 s. However, as shown in Figure 3.10b, highly protective properties are seen on increasing the electropolymerisation period to 1200 s. In this case, there is no evidence of the reduction wave and the oxidation currents are considerably lower than the currents measured for the uncoated copper electrode. The oxidation of Cu metal to Cu (II) is observed clearly in 3.10b, this is then followed by the reduction of Cu(II) to Cu (I) and Cu metal.

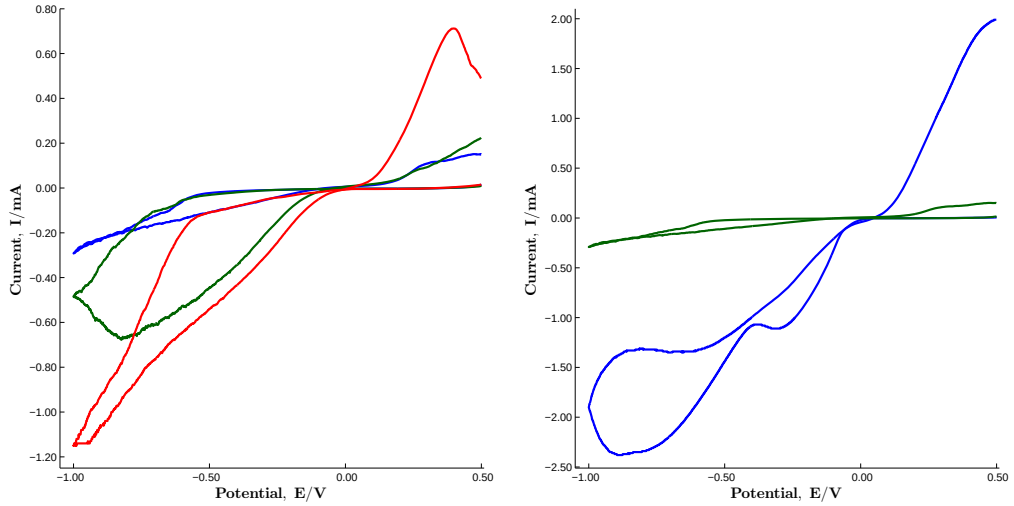

(a) **(b)**

Figure 3.10: Cyclic voltammograms recorded at 10 mV s^{-1} in 0.10 mol dm^{-3} NaCl, at a pH of 7.0 for (a) PPy-Oxalate/PPy-Tartrate bi-layer film formed at 0.75 V vs. SCE for a total period of 400 s (red), 600 s (green) and 900 s (blue), and (b) uncoated Cu (blue) and PPy-Oxalate/PPy-Tartrate bi-layer film (green) formed at 0.75 V vs. SCE for a total period of 1200s.

It is clear from a comparison of the data presented in Figure 3.10 for the bi-layer and in Figure 3.8 for the PPy-Tartrate and PPy-Oxalate polymer films that the bi-layer is more stable and exhibits very good corrosion protection properties.

3.3 Assessment of the Corrosion Performance of the Polymer Films

The corrosion protection properties of the PPy-Oxalate, PPy-Tartrate and the PPy-Oxalate/PPy-Tartrate bi-layer films were assessed and studied using cyclic voltammetry [169] and open-circuit potential measurements [245].

3.3.1 Cyclic Voltammetry and Breakdown Potentials

In order to determine the protective nature of the polymer films, cyclic voltammograms were recorded in 0.10 mol dm^{-3} NaCl [4, 282], adjusted to pH 7.0 with NaOH. The voltammograms were recorded at 10 mV s^{-1} cycling between -0.50 and 1.00 V vs. SCE. Typical voltammograms are shown in Figure 3.11 for the PPy-Tartrate and PPy-Oxalate films. In both cases, the films were formed for a 1200 s period at 0.75 V vs. SCE in the near neutral oxalate or tartrate solutions. The data recorded for copper is also presented for comparison purposes. Dissolution of copper is observed at 0.05 V vs. SCE and the current then increases to give a broad peak at about 0.10 to 0.20 V vs. SCE. This broad peak has been explained in terms of the dissolution of copper and the formation of chloride-containing corrosion species [64, 283], such as CuCl, hydroxy-containing chloride species [280, 282, 284] and the soluble $CuCl_2^-$ species [39]. Although not shown, the current reaches a maximum value between 0.60 to 0.80 V vs. SCE. This indicates significant dissolution of the copper and the generation of Cu(II) species at these higher potentials. Indeed there is some variation in the voltammograms recorded for the uncoated copper, which is evident from a comparison of Figure 3.11a and 3.11b. This is consistent with the formation of corrosion products and oxides, such as CuOH, CuCl and CuO, with the current increasing as the copper is dissolved and decaying as the surface is protected with the corrosion products [32, 284]. On the reverse cycle there is a slight drop in the current, as the corrosion products are deposited at the surface but dissolution continues as this corrosion product layer is well known to be porous [285]. A clear reduction wave is observed at about

-0.60 V vs. SCE. This reduction wave can be attributed to the chloride-containing corrosion products, such as CuCl and other hydroxy-containing chloride products, which are generated at the copper surface, during the oxidation and dissolution reactions [278].

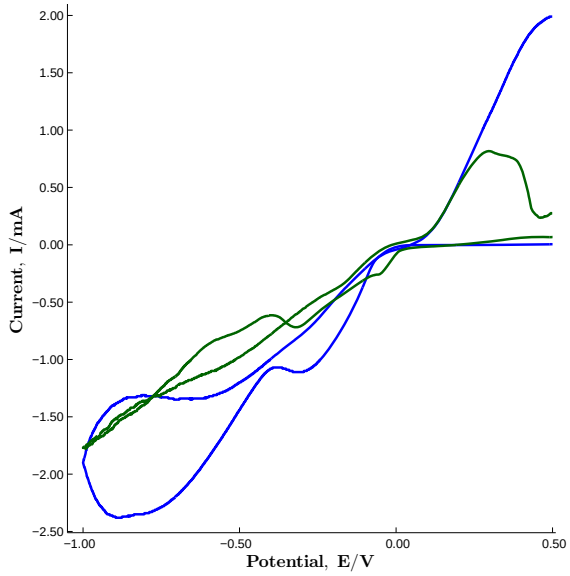

(a)

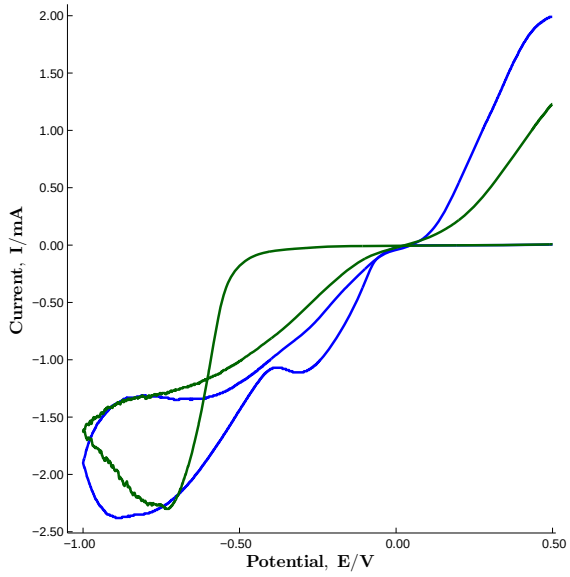

(b)

Figure 3.11: Cyclic voltammograms recorded at 10 mV s^{-1} in 0.10 mol dm^{-3} NaCl, at a pH of 7.0 for (a) uncoated Cu (blue) and PPy-Oxalate (green) formed at 0.75 V vs. SCE for 1200 s and (b) uncoated Cu (blue) and PPy-Tartrate (green) formed at 0.75 V vs. SCE for a total period of 1200 s.

It is evident that both polymer films inhibit the dissolution of copper, to some extent, when compared to the uncoated copper. The oxidation currents are slightly lower and there is a significant variation in the reduction peak centered at -0.60 V vs. SCE, both PPy-Oxalate and PPy-Tartrate films give rise to similar low peak currents. However, there is still evidence for the dissolution of the copper substrate. The PPy-Tartrate and PPy-Oxalate films were immersed in the 0.10 mol dm^{-3} NaCl solution for a 12 h period and then the voltammograms were recorded. Again, data similar to that presented in Figure 3.11 were obtained, but with a slight increase in the measured currents.

The corrosion protection properties of the PPy-Tartrate and PPy-Oxalate films were improved by increasing the electropolymerisation period. This is clearly shown in Figure 3.12a, where the breakdown potentials, E_B, are plotted as a function of the electropolymerisation period for the PPy-Oxalate and the PPy-Tartrate films, while the integrated charges associated with the reduction peak, centred at about -0.60 V vs. SCE, are shown for the PPy-Oxalate and PPy-Tartrate films in Figure 3.12b. In all cases, the polymer films were deposited from the near neutral oxalate or tartrate solutions at 0.75 V vs. SCE and the electropolymerisation period was varied from 600 to 3600 s. The voltammograms were recorded at 10 mV s^{-1} in 0.10 mol dm^{-3} NaCl solution at pH 7.0. The breakdown potentials, E_B, were measured at 0.50 mA. There is a clear increase in the breakdown potentials for the PPy-Oxalate film as the electropolymerisation period is increased. This is consistent with the data presented in Figure 3.7, which show that an increase in the electropolymerisation period gives rise to polymer films with a higher thickness. Indeed, the breakdown potentials are close to -0.03 V vs. SCE for an electropolymerisation period of 600 s, but then increase to 0.30 V vs. SCE as the polymers are formed for 3600 s.

The breakdown potentials of the PPy-Tartrate vary little with the increasing electropolymerisation periods. Again, this is consistent with the data presented in Figure 3.7, where the charge appears to be independent of the electropolymerisation period. These data show that the PPy-Tartrate films are somewhat more protective than the PPy-Oxalate polymer films. This is also evident from the data presented in Figure 3.12b, where it is clear that the charges associated with the reduction waves, corresponding to the corrosion products, mainly CuCl, are lower with the PPy-Tartrate films. Even with increasing electropolymerisation periods and the deposition of thicker PPy-Oxalate films, the charges computed for the PPy-Tartrate are lower indicating a more protective polymer coating.

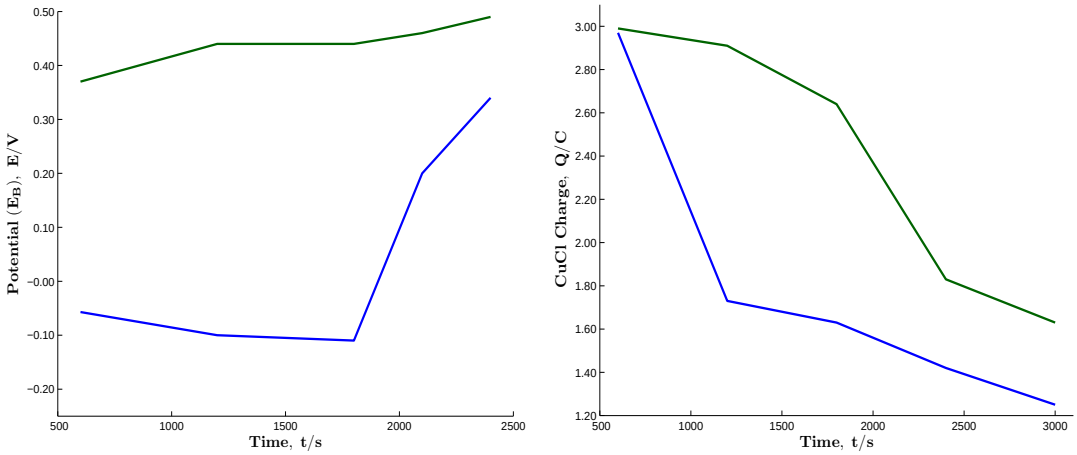

(a) **(b)**

Figure 3.12: (a) Breakdown potential, E_B, plotted as a function of the electropolymerisation period for the PPy-Oxalate (blue) and the PPy-Tartrate (green) films formed at 0.75 V vs. SCE and (b) charge corresponding to the reduction wave at -0.60 V vs. SCE for the PPy-Oxalate (green) and the PPy-Tartrate (blue) polymer films.

Although the corrosion protection properties of the PPy-Oxalate, and to a lesser extent the PPy-Tartrate films, can be increased with a corresponding increase in the electropolymerisation periods, the best corrosion protection properties were observed with the bi-layer. This is shown clearly in Figure 3.13, where voltammograms are shown for the bi-layer deposited at copper and platinum, and compared with the voltammograms recorded for the uncoated copper. Again, the voltammograms were recorded in 0.10 mol dm^{-3} NaCl at 10 mV s^{-1}. The bi-layer was deposited for a total time of 1200 s, and accordingly, these data can be compared directly with the voltammograms presented in Figure 3.11. Again, dissolution of the uncoated copper is clearly evident. However, excellent corrosion protection properties are observed with the bi-layer. The currents remain low throughout the entire electrochemical window and there is no evidence for the CuCl reduction wave, which is seen with the uncoated copper and to a lesser extent, with the PPy-Tartrate and PPy-Oxalate modified copper electrodes, Figure 3.11. Indeed, the voltammograms recorded for the bi-layer deposited at copper and platinum are similar, but with slightly higher currents recorded for the bi-layer deposited at copper. When these data are compared with the voltammograms presented in Figure 3.11, it is clear that the bi-layer, deposited for 1200 s has significantly better corrosion protection properties than either the PPy-Oxalate or the PPy-Tartrate films.

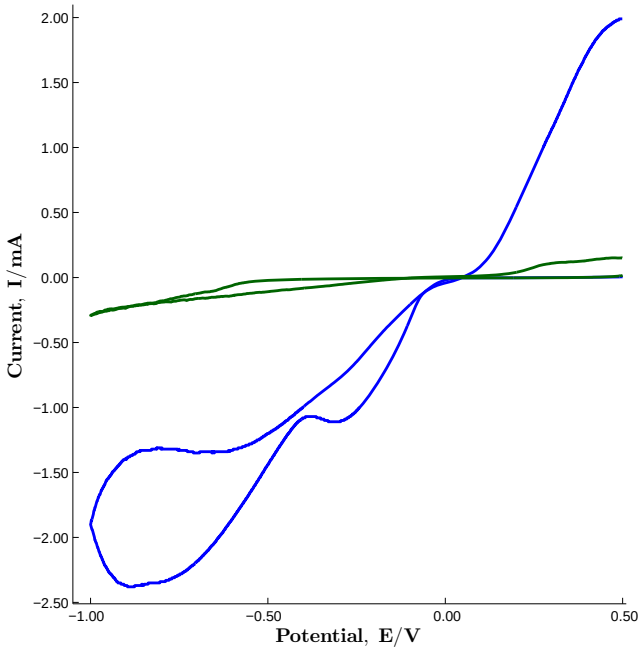

(a)

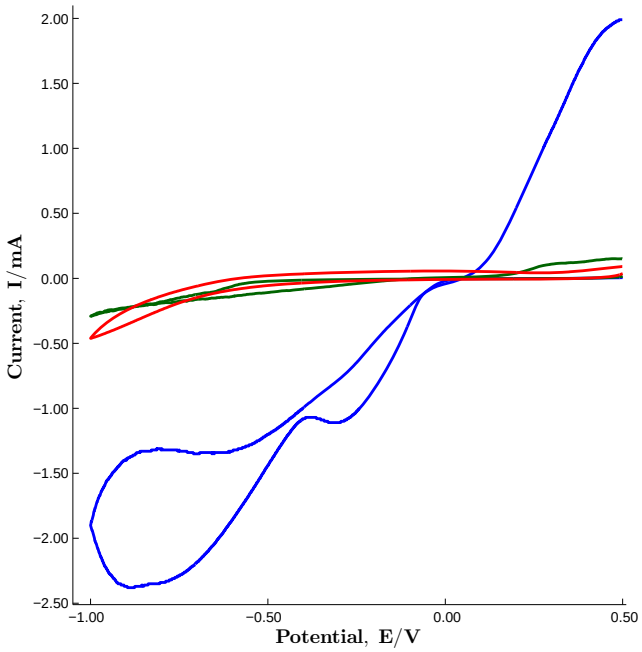

(b)

Figure 3.13: Cyclic voltammograms recorded at 10 mV s^{-1} in 0.10 mol dm^{-3} NaCl, at pH 7.0 for (a) uncoated Cu (blue) and PPy-Oxalate/PPy-Tartrate bi-layer (green) film formed at 0.75 V vs. SCE for 1200 s and (b) uncoated Cu (blue) and PPy-Oxalate/PPy-Tartrate bi-layer (red) film formed at 0.75 V vs. SCE for 1200 s at Cu substrate and PPy-Oxalate/PPy-Tartrate bi-layer film formed at 0.75 V vs. SCE for 1200 s at Pt substrate (green).

3.3.2 Open-Circuit Potential Measurements

In order to investigate the corrosion protection properties further and to compare the protective properties of the bi-layer and the PPy-Oxalate and PPy-Tartrate polymer films, immersion experiments were performed and the potential adopted was recorded as a function of time in the aggressive chloride-containing solutions [245, 259]. The open-circuit potential, or corrosion potential, is a mixed potential and it depends on the rate of the anodic and the cathodic half reactions. By recording the open-circuit potential as a function of the immersion time, the protective properties of the films can be assessed by the extent to which the potential adopted by the polymer coated electrodes differ from the potential adopted by the uncoated copper electrode. Moreover, the corrosion protective period can be determined by the time required for the open-circuit potential of the polymer-modified electrode to decay to the values adopted by the uncoated electrode. The evolution of the corrosion, or open-circuit potential, was monitored as a function of time in 0.10 mol dm^{-3} NaCl solutions adjusted to pH 7.0.

The PPy-Tartrate, PPy-Oxalate and PPy-Oxalate/PPy-Tartrate bi-layer films were deposited from near neutral solutions of 0.10 mol dm^{-3} tartrate or oxalate and 0.20 mol dm^{-3} pyrrole at 0.75 V vs. SCE for 1200 s. The polymer modified electrodes and uncoated copper were immersed in the chloride solution and the open-circuit potential was measured initially for a period of 3600 s. The electrodes were then removed and stored in a sealed container with a fresh chloride solution and left overnight and this procedure was repeated over a 30 day period.

Representative results are presented in Figures 3.14, 3.15, 3.16 and 3.17. In Figure 3.14, the open-circuit potentials adopted by the PPy-Tartrate, PPy-Oxalate, PPy-Oxalate/PPy-Tartrate bi-layer and uncoated copper are compared after a 12 day immersion period. The potential adopted by the uncoated copper is approximately -0.15 V vs. SCE and there is little variation in this potential over the 3600 s period. The open-circuit potentials adopted by the three polymer systems are approximately 0.02 V vs. SCE for the PPy-Oxalate, 0.05 V vs. SCE for the PPy-Tartrate and 0.07 V vs. SCE for the bi-layer. These potentials are constant over the 3600 s measurement period and there is no evidence of any decay in the potential to the values adopted by the uncoated copper electrode [245]. This indicates very good stability after a 12-day immersion period. Indeed, the evolution of the open-circuit potential is shown clearly in Figures 3.15, 3.16 and 3.17, where the open-circuit potentials are shown following 1 day and

12 day immersion periods for the PPy-Oxalate and PPy-Tartrate systems and 1 day and 20 day immersion periods for the bi-layer. There is very little variation in the open-circuit potentials recorded for the PPy-Tartrate modified copper on comparing the data recorded after day 1 and day 12. A similar result is obtained with the bi-layer. However, there is some decay in the open-circuit potential adopted by the PPy-Oxalate modified copper. Indeed, on further immersion the open-circuit potential of the PPy-Oxalate modified copper decayed to the value adopted by the uncoated copper. This was observed following an immersion period of approximately 15 days and this indicates that the corrosion protection properties of the PPy-Oxalate film are lost following a 15 day immersion period in 0.10 mol dm^{-3} NaCl. A similar effect was observed with the PPy-Tartrate and the corrosion-protection properties were lost after approximately 16 days. However, the bi-layer was stable for periods exceeding 30 days, indicating very good corrosion protection properties over an extended period in an aggressive chloride-containing solution [1, 286].

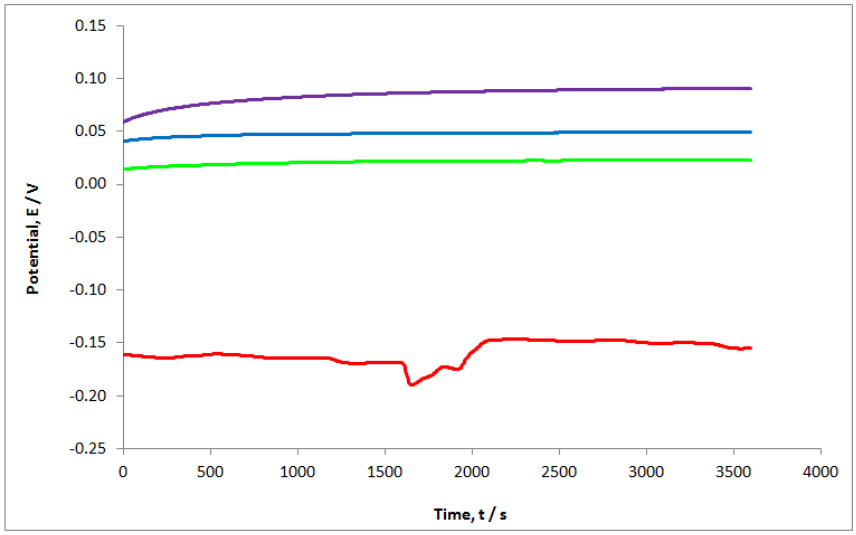

Figure 3.14: OCP recorded in 0.10 mol dm^{-3} NaCl solution at a pH of 7.0 for uncoated Cu (red), the bi-layer polymer film (purple), PPy-Tartrate (Blue) and PPy-Oxalate (green) recorded on day 12.

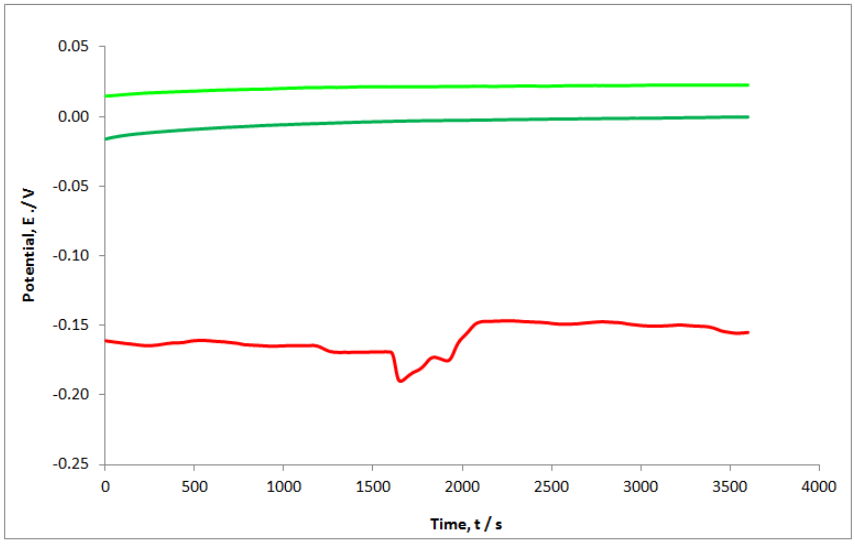

Figure 3.15: OCP recorded in 0.10 mol dm^{-3} NaCl solution at a pH of 7.0 for uncoated Cu (red) and PPy-Oxalate day 1 (light green) and day 12 (dark green).

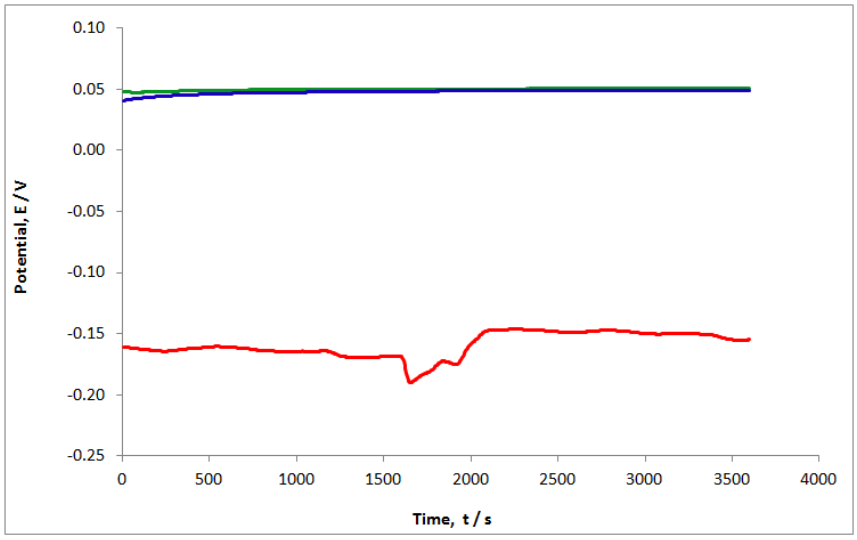

Figure 3.16: OCP recorded in 0.10 mol dm^{-3} NaCl solution at a pH of 7.0 for uncoated Cu (red) and PPy-Tartrate day 1 (blue) and day 12 (green).

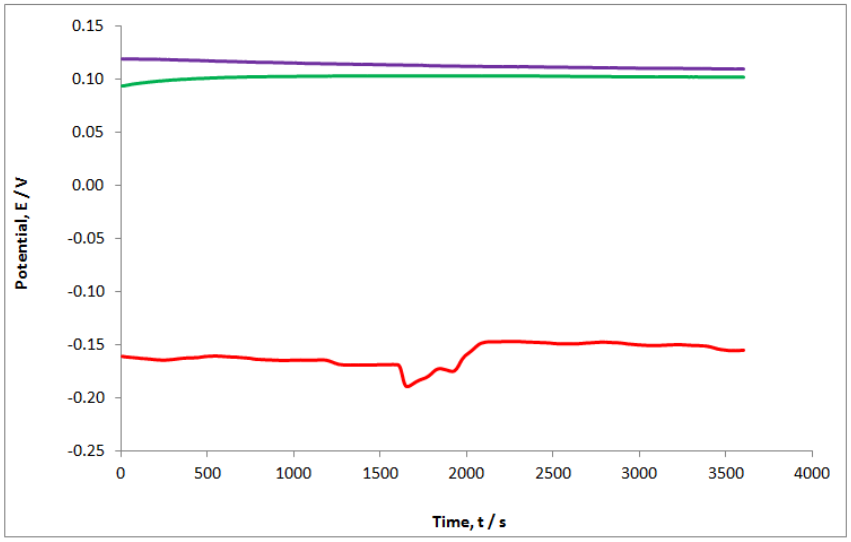

Figure 3.17: OCP recorded in 0.10 mol dm^{-3} NaCl solution at a pH of 7.0 for uncoated Cu (red) and bi-layer day 1 (purple) and day 20 (green).

3.3.3 Analysis of the Polymer Films using Spectroscopy

The PPy-Tartrate, PPy-Oxalate and PPy-Oxalate/PPy-Tartrate bi-layers were studied using DSC, FTIR and UV-Vis spectroscopy in an attempt to observe some differences between the bi-layer and the individual polymer layers that may explain the variations in the protective properties of the coatings. FTIR spectra were recorded for the three polymer systems and the oxalate and tartrate salts [287]. The OH, CH and C=O stretching vibrations of the tartrate salt were seen between 1400 and 3600 cm^{-1} [287]. For the oxalate salt, the C=O stretching vibrations were also observed [287], however the FTIR spectra recorded for the three polymer systems were similar. The spectra gave distinct and prominent peaks at 1585 cm^{-1}, which may be assigned to the C=C ring stretching, at 1494 cm^{-1} corresponding to the C-N stretching mode, and at 1159 cm^{-1} for the C-H plane deformation [288]. However, no significant difference was seen for the spectra recorded with the bi-layer. Likewise, the DSC data were similar for all three polymer systems. Again, there was no clear difference between the DSC thermograms recorded for the bi-layer and the individual PPy-Oxalate and PPy-Tartrate polymer films, there was no evidence of the polymers breaking down.

In order to record the UV-Vis spectra of the polymers, they were deposited onto ITO electrodes [131, 289]. A three-electrode cell was used and the polymers were deposited at 0.75 V vs. SCE, however the ITO was employed as the working electrode. The adherence

of the polymers to the ITO electrodes was poor when longer electropolymerisation periods were employed and accordingly the electropolymerisation periods were only varied from 100 to 1200 s. The UV-Vis spectra were recorded from 300 to 750 nm.

Some small differences were observed in the UV-Vis spectra of the three polymer systems. A peak with a λ_{max} at 333 nm was observed with the PPy-Oxalate film and as the electropolymerisation period was increased at the ITO electrode this peak was observed at approximately 347 nm. The maximum absorption, λ_{max}, was recorded at 349 nm for the PPy-Tartrate film, while the PPy-Oxalate/PPy-Tartrate bi-layer showed a λ_{max} at approximately 344 nm. These data are presented in Figure 3.18, where the λ_{max} is shown as a function of the electropolymerisation period. There is little variation in the λ_{max} for the bi-layer and the PPy-Tartrate polymer systems. Absorption bands near 350 nm have previously been reported for PPy and these bands are generally associated with the neutral form of the polymer, while absorption bands between 600 to 800 nm are attributed to the oxidised PPy films [290, 291]. Absorption was also observed between 600 to 750 nm for the three polymer films, indicating that these films are oxidised, or at least partially oxidised. However, it is evident from Figure 3.18 that there is little variation between the three polymer systems.

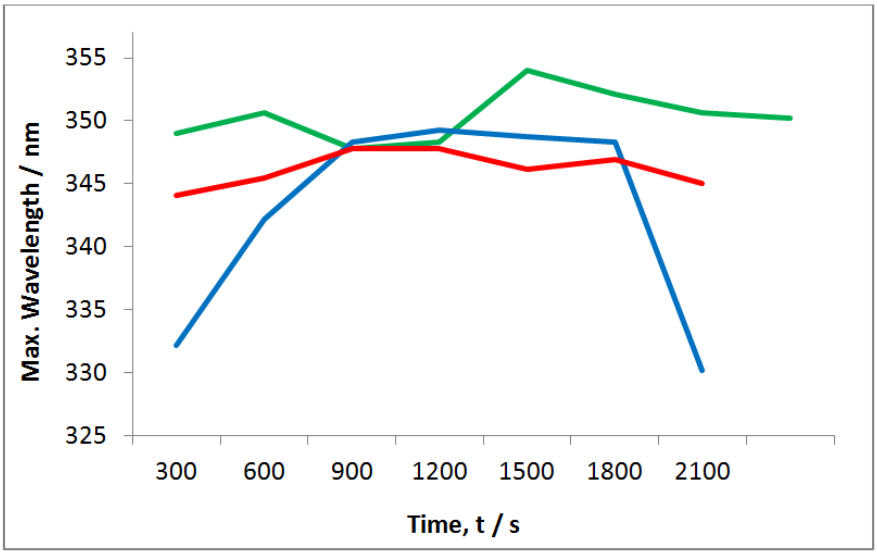

Figure 3.18: Maximum wavelength, λ_{max}, recorded as a function of the electropolymerisation period for the bi-layer film (red), PPy-Oxalate polymer film (blue) and PPy-Tartrate polymer film (green) deposited at ITO electrodes at 0.75 V vs. SCE for 1200 s and then recorded in 0.10 mol dm^{-3} NaCl at a pH of 7.0.

In Figure 3.19 the absorbance recorded at 345 nm is plotted as a function of the electropolymerisation period for the bi-layer film. The absorbance increases with an increase in the electropolymerisation period and this is consistent with the formation of increasing amounts of the polymer at the ITO electrode. Although not shown here, the rate of electropolymerisation was somewhat higher for the PPy-Oxalate and PPy-Tartrate films, this is perhaps due to the fact that the oxalate grows at a faster rate under specific conditions at the copper interface. However, these small differences do not account for the enhanced corrosion protection properties observed with the PPy-Oxalate/PPy-Tartrate bi-layers.

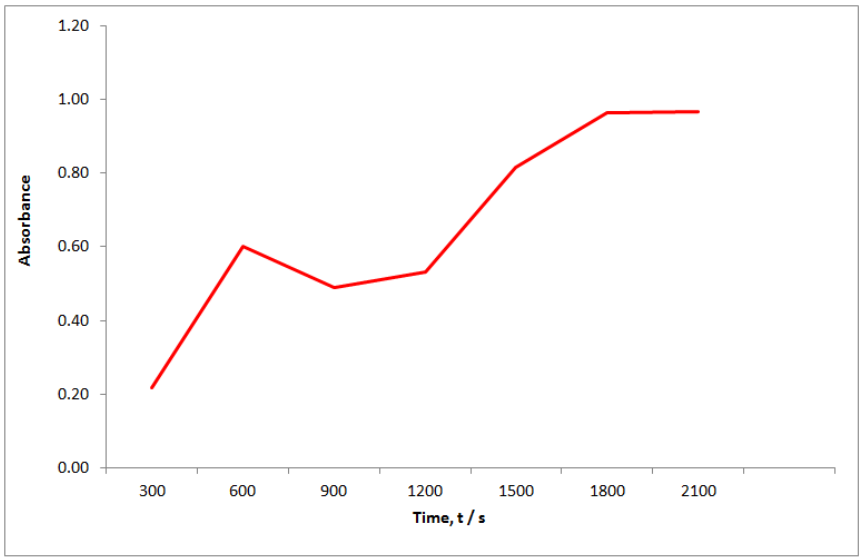

Figure 3.19: Absorbance recorded at 345 nm for the PPy-Oxalate/PPy-Tartrate bi-layer plotted as a function of the electropolymerisation time.

3.4 Summary of Results

The results presented in this chapter show that PPy films can be deposited at copper from a 0.10 mol dm^{-3} oxalate solution at a pH of 8.0 and a 0.10 mol dm^{-3} tartrate solution at pH 7.0 to generate PPy-Tartrate and PPy-Oxalate films on copper. Highly adherent polymer films were formed using these optimised conditions. SEM micrographs confirmed that the polymers were homogeneous, defect and crack-free. It was also possible to deposit the PPy-Tartrate film at pH values of 6.0 and 8.0. In addition, bi-layers comprising PPy-Tartrate/PPy-Oxalate and PPy-Oxalate/PPy-Tartrate were successfully formed at the copper surface. The PPy-Tartrate and PPy-Oxalate films were also deposited at platinum, however a more acidic pH was required to

deposit these films and adherent and homogeneous polymer films were only formed at pH 4.0 in the presence of either the oxalate or tartrate anions.

The electropolymerisation period was varied from 200 to 3600 s to give polymer films with different thickness. The breakdown potential of the PPy-Tartrate film was approximately 0.45 V vs. SCE and this remained essentially independent of the electropolymerisation period. However, more protective PPy-Oxalate films were formed with electropolymerisation periods between 2400 and 3600 s. The bi-layer coating was also more protective with increasing electropolymerisation periods. On comparing the corrosion protection properties of the PPy-Tartrate, PPy-Oxalate and the bi-layer, it is clear that the bi-layer provides the more corrosion protective coatings. Higher breakdown potentials were observed with the bi-layer. Furthermore, the open-circuit potential recorded for the bi-layer remained constant at about 0.10 V vs. SCE for a 30 day period in a neutral 0.10 mol dm^{-3} NaCl solution. Slightly lower open-circuit potentials were recorded for the PPy-Tartrate, at 0.05 V vs. SCE, and the PPy-Oxalate film, at -0.02 V vs. SCE, but again the open-circuit potential remained essentially constant over a 12 day period. However, at longer immersion times, the open-circuit potentials decayed to the values adopted by the uncoated copper electrode, indicating a loss in the protective properties of the films. However, this loss in corrosion protection was not observed with the PPy-Oxalate/PPy-Tartrate bi-layer.

CHAPTER 4

Incorporation of MWCNT into the Polymer Matrix

PPy has been extensively studied [132, 292], as discussed previously in Chapter 1 and Chapter 3. As shown in Chapter 3, PPy films doped with oxalate and tartrate can be formed from near neutral solutions to give PPy-Tartrate [244, 287] and PPy-Oxalate polymer films [1, 287]. Furthermore, a bi-layer polymer film [163], comprising PPy-Oxalate/PPy-Tartrate, with very good corrosion protection properties was successfully formed. In an attempt to increase further the corrosion protection properties of these polymer films, multi-walled carbon nanotubes (MWCNT) were incorporated into the polymer films [15].

In recent years there has been considerable interest in nano-structured carbon materials, in particular carbon nanotubes [200]. Single-walled carbon nanotubes (SWCNT) consist of single layers of graphite rolled into perfect cylinders with a diameter usually in the range of 0.70 to 2.00 nm, whereas multi-walled carbon nanotubes consist of sets of concentric cylindrical shells, each of which resembles a SWCNT. Carbon nanotubes exhibit unique mechanical properties, with a tensile strength greater than that of steel but with only one sixth the weight of steel. They also have unique electronic, thermal and magnetic properties. The properties and applications of carbon nanotubes have been well reviewed in the literature and several reviews with an electrochemical emphasis have been published [195, 293]. However, the modification of carbon nanotubes has recently been the focus of much research, primarily to improve the

dispersion of the carbon nanotubes in various solvent systems [217, 223, 294].

In this chapter results are presented and discussed on the incorporation of multi-walled carbon nanotubes into PPy films. The carbon nanotubes were evenly dispersed in solution with dodecylbenzene sulfonate (DBS) [21, 218]. The experimental conditions were optimised to give stable and well dispersed solutions of the carbon nanotubes in DBS [294]. The PPy films were then deposited from the dispersed carbon nanotubes in DBS on the addition of pyrrole, to give PPy-DBSCNT films at copper, or the PPy-DBSCNT film was formed at PPy-Tartrate or PPy-Oxalate to give PPy-Tartrate/PPy-DBSCNT and PPy-Oxalate/PPy-DBSCNT bi-layers and multi-layers. Once formed and characterised the corrosion protection properties of PPy-Tartrate/PPy-DBSCNT and PPy-Oxalate/PPy-DBSCNT were assessed using a combination of polarisation plots, open-circuit potential measurements and Tafel analysis [40]. In all cases the protective properties of the coatings were compared to the uncoated copper electrode. To the best of our knowledge there have been no reports on the formation of these PPy-based films.

4.1 Experimental Approach

Details on the experimental approach used in the formation and analysis of the PPy films at the copper electrodes are provided in Sections 4.1.1, 4.1.2 and 4.1.3. This includes information on the chemicals, the techniques and equipment used and the general procedures employed to deposit the polymer films. In Section 4.1.4 details on the procedures employed in the dispersion of the multi-walled carbon nanotubes (MWCNT) are provided.

4.1.1 Reagents

The pyrrole monomer (98%) was obtained from Aldrich and was purified by distillation prior to use. It was then stored in the dark at -20 °C between experiments. Unless otherwise stated, 0.30 mol dm^{-3} pyrrole was dissolved in the electrolyte solution for all the electropolymerisation experiments. The analytical reagents, copper sulfate ($CuSO_4$), sodium hydroxide (NaOH), sodium chloride (NaCl) sodium oxalate ($Na_2C_2O_4$) sodium potassium tartrate ($KNaC_4H_4O_6$), bathocuproine ($C_{26}H_{20}N$) (2,9-dimethyl-4,7-diphenyl-1,10-phenanthroline), dodecylbenzene sulfonate (DBS) ($C_{12}H_{25}C_6H_4SO_3Na$), nitric acid (HNO_3), hydrogen peroxide (20% solution) and sulfuric acid (H_2SO_4), were purchased from Aldrich and used as received. Multi-walled

carbon nanotubes, MWCNT, were also obtained from Aldrich. Distilled water was used in all solution preparations. The pH meter was calibrated on a daily basis using buffers (pH 4.0 and pH 7.0) which were purchased from Lennox Ltd.

4.1.2 Electrodes and Instruments

A Cu rod (99.99%, 4 mm in diameter) electrode was used for the deposition of polymer films. The rod was encased in a Teflon holder, as previously described in Chapter 2, Figure 2.3. A flat Cu disc electrode was used for SEM and EDX measurements. The disc and rod electrodes were polished using a 1 μm diamond polish and Buehler micro-cloth and rinsed well with distilled water to ensure a smooth surface finish, as outlined in Chapter 2. A saturated calomel electrode (SCE) was used as the reference electrode and a high surface area platinum wire was employed as the counter electrode.

A CHi 760C potentiostat was used to deposit the PPy films, while potentiodynamic polarisation measurements were carried out with a Solartron potentiostat (Model SI 1285 or 1287), using the software package Corrware for Windows. A Carry Win UV-Vis spectrometer was used with the Carry Win software package for UV-Vis measurements, while the fluorescence study was carried out with a Cary Eclipse fluorescence spectrophotometer. The conductivity measurements were carried out using a Jenway 4510 conductivity meter, while an Orion 720A pH meter, calibrated daily with buffers at pH 4.0 and 7.0, was used for all pH measurements. Once polished the electrodes were sonicated in a Branson 1510 sonicator to ensure the removal of any residues from the polishing. SEM measurements were performed on a Hitachi FE-scanning electron microscope, with an Oxford instruments Inca X-act 4.12 software package. The EDX analyses were carried out using an EDX Model 51-ADD0009 with the software package Micro Analysis Suite. A Discover CEM 48-72-96 microwave was used to purify the carbon nanotubes and a Merlin Spectra centrifuge was used to separate the purified carbon nanotubes from the chemical solution employed in the microwave-assisted purification step [295].

4.1.3 Procedures

The synthesis of the PPy films was carried out using an electrosynthesis method, in which the polymer films were deposited at the working electrode [18, 286]. Polymers were prepared

in various electrolyte solutions at 0.75 V vs. SCE containing 0.30 mol dm^{-3} pyrrole, unless otherwise stated. This concentration of pyrrole is higher than that used in Chapter 3, where a 0.20 mol dm^{-3} pyrrole-containing solution was employed in the formation of the PPy-Tartrate and PPy-Oxalate polymer films. However, these higher concentrations were required to form the PPy films in the MWCNT-containing solutions. In general, the polymer films were deposited from neutral 0.10 mol dm^{-3} tartrate or 0.10 mol dm^{-3} oxalate solutions, with 0.30 mol dm^{-3} pyrrole, to give PPy-Tartrate and PPy-Oxalate films. Then, further electropolymerisation was carried out in 0.30 mol dm^{-3} pyrrole, 0.05 mol dm^{-3} DBS and 0.02 mg of MWCNT, with the MWCNT suspended and dispersed in the 0.05 mol dm^{-3} solution of DBS, to give PPy-Tartrate/PPy-DBSCNT or PPy-Oxalate/PPy-DBSCNT bi-layers. Multi-layers [157, 296] of alternating PPy-Tartrate and PPy-DBSCNT and multi-layers of alternating PPy-Oxalate and PPy-DBSCNT were also formed at the copper electrodes. In addition, PPy-Tartrate/DBSCNT and PPy-Oxalate/DBSCNT multi-layers were formed by adsorbing the MWCNT dispersed in 0.05 mol dm^{-3} DBS onto the polymer films.

After electrochemical deposition, the PPy films were characterised using cyclic voltammetry, by cycling in a potential window from -0.50 to 1.00 V vs. SCE, at different scan rates from 100 mV s^{-1} to 1 mV s^{-1} in a 0.10 mol dm^{-3} NaCl solution at a pH of 7.0. Polarisation curves were recorded in a neutral 0.10 mol dm^{-3} NaCl solution at 1 mV s^{-1} and 0.1667 mV s^{-1} from 200 mV below to 200 mV above the corrosion potential or until significant dissolution of the copper was observed. A scratch in the coating was made and the polarisation data were compared to a freshly deposited polymer coating. Again, these measurements were performed in 0.10 mol dm^{-3} NaCl at 0.1667 mV s^{-1}. Tafel analysis was used to estimate the corrosion potential, E_{corr} and the corrosion current, I_{corr}. For SEM and EDX characterisation, the polymer films were synthesised onto a Cu disc electrode. The samples were sputter coated with gold prior to SEM analysis. A spectrophotometric analysis using the bathocuproine reagent was employed to monitor the concentration of dissolved copper. A quartz crystal cuvette with a diameter of 1 cm was used and the absorbance was recorded at the λ_{max} of 480 nm.

4.1.4 Dispersion of the MWCNT in Solution

The ability to control the dispersion of carbon nanotubes is critical in most applications. Carbon nanotubes tend to agglomerate in solution, and it is difficult to separate the individual

nanotubes [216, 297]. The need for cost-effective methods to readily disperse single-walled and multi-walled carbon nanotubes (SWCNT and MWCNT) has motivated numerous researchers to investigate the dispersion of nanotubes in a variety of different solvent systems.

Initially, 0.02 mg of MWCNT was added to a 0.10 mol dm^{-3} tartrate solution containing 0.30 mol dm^{-3} pyrrole. Then, the electrochemical cell was set up and a potential of 0.75 V vs. SCE was applied in an attempt to form the polymer at copper. Electropolymerisation was observed, however when the surface morphology was inspected using SEM, it was clear that very poor dispersion of the nanotubes was achieved. Typical SEM micrographs are shown in Figure 4.1. There is clear evidence of large agglomerations of the nanotubes on the surface, indicating very poor dispersion. The polymer films were then formed with continuous stirring of the MWCNT-containing electropolymerisation solution, but again agglomerations of the nanotubes were evident on the surface.

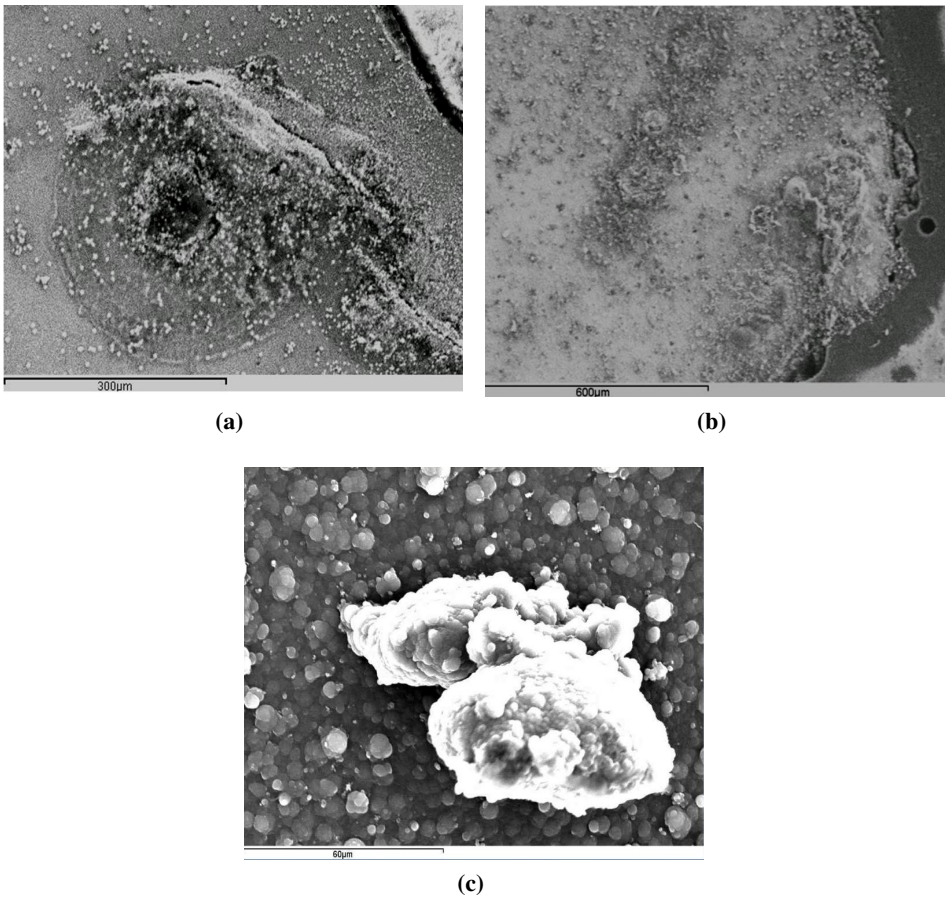

(a) **(b)**

(c)

Figure 4.1: SEM micrographs recorded of PPy films formed in 0.10 mol dm^{-3} tartrate, 0.30 mol dm^{-3} pyrrole and 0.02 mg MWCNT (a) the scale bar corresponds to 300 μm, (b) the scale bar corresponds to 600 μm and (c) the scale bar corresponds to 60 μm.

In an attempt to combat these agglomerations a microwave purification method [295] was employed. The microwave-assisted purification of MWCNT was carried out in a closed vessel at 180 °C in the presence of 20% hydrogen peroxide for a 30-min period. A comparison of the purification efficiencies of hydrogen peroxide and nitric acid was carried out and it was concluded, using a gravimetric method, that the hydrogen peroxide is sufficient for the purification of the nanotubes at a temperature of 180 °C for 30 min. Following this, the vessel was removed and the nanotubes were separated from the remaining solution in a centrifuge for 10 min. The nanotubes were then washed with distilled H_2O and centrifuged for a further 10 min. This process was repeated for a total period of 60 min. The now purified nanotubes were added to the electropolymerisation solution, 0.10 mol dm^{-3} tartrate and 0.30 mol dm^{-3} pyrrole, and the solution was also stirred during electropolymerisation. The polypyrrole film was deposited at 0.75 V vs. SCE and the surface was analysed using SEM. Although there was a more notable and even dispersion of the nanotubes on the surface, nanotube agglomerations were also clearly evident, giving unsatisfactory results.

The dispersion of the nanotubes was then investigated using surfactants [216, 223]. Indeed, several reports show efficient dispersion of the nanotubes in solutions containing surfactants [199, 222]. Moreover, it has been demonstrated that surfactants have the ability to break up the nanotube bundles and stabilise the individual nanotubes. Islam and co-workers [298] showed that sodium dodecylbenzene sulfonate (DBS) is an effective surfactant for the dispersion of carbon nanotubes. However, parameters such as pH, surfactant and nanotube concentrations, and sonication time have a significant influence on the stability of the dispersions. During the sonication period mechanical energy is provided to overcome the weak van der Waals interactions in nanotube bundles [216], while the surfactant adsorbs at the surface of the nanotube walls [217]. According to Grossiord *et al.* [299] the colloidal stability of the dispersion of the nanotubes with adsorbed surfactants is guaranteed by electrostatic and steric repulsion. The organisation of these surfactants has been extensively investigated [216, 217, 218] with three main arrangements [202, 207, 208, 215]: structure less random adsorption on the nanotube walls without any preferential arrangements of the head or tail [300], hemi-micellar adsorption on the nanotube surface [298], and encapsulation of the nanotubes in a cylindrical surfactant micelle [301]. The majority of the experimental and theoretical evidence supports the hemi-micelle configuration [202, 216, 218].

The MWCNT sample (0.02 mg) was dispersed in 25 ml of 0.05 mol dm^{-3} DBS in the presence of 0.30 mol dm^{-3} pyrrole and the solution was then sonicated for 60 min, to give a black homogeneous mixture. At this point there was no evidence of any nanotube agglomerates in the solution. Indeed, the solution was stable for considerable periods of time, exceeding several hours. This solution was then used as the electropolymerisation electrolyte and the PPy film was formed at 0.75 V vs. SCE at copper with continuous stirring of the solution during the electropolymerisation period. The morphology of the resulting polymer is shown in Figure 4.2, and in this case there is no evidence of any significant agglomerations of the carbon nanotubes.

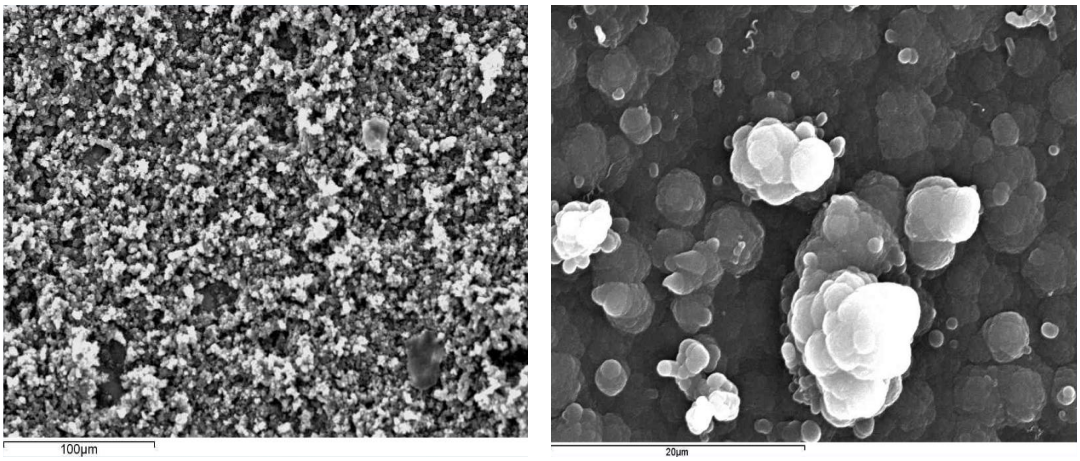

(a) **(b)**

Figure 4.2: SEM micrographs recorded of PPy films formed in 0.10 mol dm^{-3} pyrrole and 0.20 mg MWCNT dispersed in 0.05 mol dm^{-3} DBS and sonicated for 60 min (a) the scale bar corresponds to 100 μm, (b) the scale bar corresponds to 20 μm.

4.2 Results and Discussion

4.2.1 CMC of DBS

Given that DBS was successfully used to disperse the carbon nanotubes, studies were carried out to determine the critical micelle concentration, CMC, of DBS [209]. As detailed earlier in Chapter 1, surfactants are amphiphilic containing both polar, usually an ionic head group, and a long-chain hydrocarbon tail. In polar solvents, such as water, this dual character of the amphiphile leads to self-association and the surfactant molecules arrange into organised molecular assemblies, known as micelles [177]. Accordingly, the critical micelle concentration (CMC) corresponds to the concentration above which any added surfactant will have a high

probability to form micellar aggregates [204, 212]. Above the CMC it can be noted that micelles and monomers are in equilibrium. Not all monomers are organised into micellar aggregates. The monomer-micelle equilibrium can be written using Equation 4.1, where n represents the number of monomer units in solution that give rise to the formation of the micelle, S represents the surfactant and S_n is a micelle formed from the surfactant monomers [209].

$$nS \leftrightarrow S_n \tag{4.1}$$

The equilibrium is then given by Equation 4.2, where K_m is the micellar equilibrium constant, $[S]$ represents the surfactant concentration, $[S_n]$ indicates the micellar concentration of the surfactant and n is the number of monomers in the micelles, also known as the aggregation number [302]. Generally, N is used to represent the aggregation number.

$$K_m = \frac{S_n}{S^n} \tag{4.2}$$

This equation clearly shows that on further addition of surfactant molecules, this leads to a higher concentration of micelles. However, there is no increase in the size of the existing micelles [225, 227]. The aggregation number, N, is based on the assumption that a micelle is constructed of a definite number of surfactants. The value of N depends on temperature, nature of surfactant and concentration of electrolytes in the aqueous solution [204, 227]. It is also important to note that temperature has a significant influence on the value of the CMC [210, 211].

The CMC of the surfactant was estimated using conductivity measurements and fluorescence spectroscopy [227, 303]. In the case of the conductivity measurements, the conductivity meter was first calibrated using a 0.01 mol dm^{-3} KCl solution at 25 °C. Two different experiments were carried out. In the first experiment, the conductivity of DBS was measured in distilled water and in the second experiment the conductivity of DBS was measured with an added salt. For each experiment a 15 ml volume of solution was taken and the conductivity was measured with each addition of DBS. Upon each addition the conductivity meter was allowed to equilibrate for approximately 1 min. As temperature has a significant influence on the value of the CMC, the temperature was maintained constant at 25 °C. In Figure 4.3 a typical conductivity measurement is shown, where the conductivity is plotted as a function of

the DBS concentration. Two linear regions are clearly observed. The linear region at low DBS concentrations, less than 7×10^{-3} mol dm^{-3}, is associated with an increase in conductivity of the solution with the addition of the DBS. At these low concentrations no micelles are formed and the conductivity is due to the counter ions (Na^+) and the DBS anions, (DBS^-), Equation 4.3. As further additions of DBS are made, there is a notable linear increase in the conductivity as the Na^+ and the DBS^- remain independent of each other [304]. The slope of this linear plot is 26900 μS mol^{-1} dm^{-3}.

$$k_{Total} = kNa^+ + kDBS^- \tag{4.3}$$

However, above the CMC further additions of DBS result in the formation of micelles and as more DBS is added this gives rise to an increase in the micelle concentration. The ionic mobility of the micelle is very different to the mobility of the DBS. Even though there is an increase in the conductivity in a linear manner, the rate of increase is considerably slower giving rise to a lower slope of 6350 μS mol^{-1} dm^3. The intersection of these two linear segments gives an estimation of the CMC. Using this approach the critical micelle concentration was calculated to be 6.8×10^{-3} mol dm^{-3}. This value is in good agreement with literature values for the CMC of DBS in water. These literature values range from 3.0×10^{-3} to 9.0×10^{-3} mol dm^{-3} [305]. When a fixed concentration of 0.05 mol dm^{-3} NaCl was added to the distilled water the CMC was measured at a much lower concentration of 3.7×10^{-3} mol dm^{-3} DBS, compared with the CMC value of 6.8×10^{-3} mol dm^{-3} in distilled water. This clearly shows that the addition of chloride anions reduces the CMC [304].

A more recognised method of measuring the CMC is using fluorescence spectroscopy. For the purpose of these experiments it is assumed that a micelle is comprised of a definite number of surfactant molecules, which is termed the aggregation or mean aggregation number (N). It is important to understand that the value of N is dependent on temperature, the nature of the surfactant and on the concentration of the electrolytes in aqueous solution [225].

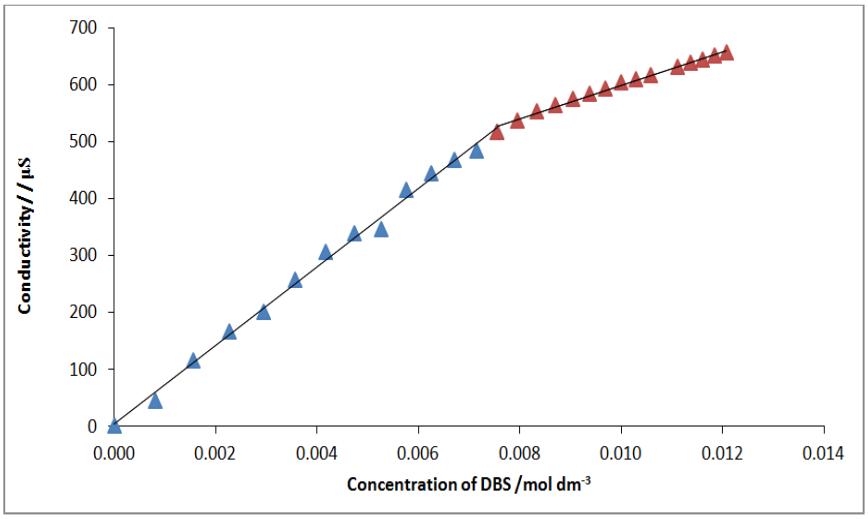

Figure 4.3: Conductivity plotted as a function of the DBS concentration in water at 25 °C.

For the experiments carried out with a fixed surfactant concentration, an aqueous solution was considered where the bulk concentration of DBS was maintained constant, at a concentration higher than the CMC. Taking into consideration that the DBS is present as either a monomeric unit or is part of a micelle that contains N monomers, the concentration of the micelles (M) can be expressed using Equation 4.4.

$$[M] = \frac{[DBS] - CMC}{N} \tag{4.4}$$

In reality, however, this is not a static system as micelles and monomers are in equilibrium. Hence, in Equation 4.4, N is representative of the mean aggregation number and M represents the average micelle concentration. Since the CMC can be obtained experimentally, the value of N can be obtained if the average micelle concentration of the solution is known.

This information can easily be found indirectly through fluorescence measurements. However, this investigation is based on various assumptions. The first one is that not all micelles have a probe molecule, and so the luminescence intensity of the solution is proportional to the fraction of micelles that contain a probe. The second is that the micelles are either empty or associated with a single probe molecule. The solution contains more micelles that probe molecules. With respect to the fixed quencher concentration it is important to note that a quencher prevents the luminescence of the probe after it absorbs light. It is assumed that the quencher is not solvated in the aqueous solution; it is associated with micelles only.

For a bulk quencher concentration the ratio of luminescence intensity, I, to the solution with no quencher (constant probe concentration), I_0, is equal to the fraction of micelles that contain probes and no quencher molecule, Equation 4.5.

$$\frac{I}{I_0} = \exp\left(-\frac{[Q]}{[M]}\right) \tag{4.5}$$

Equation 4.5 relates the measured parameters to the fraction of quencher occupied micelles. When this equation is rearranged and by substituting the expression obtained for $[M]$, Equation 4.4, into Equation 4.5, then Equation 4.6 is obtained.

$$\ln\left(\frac{I}{I_0}\right) = \frac{[Q]N}{[DBS] - CMC} \tag{4.6}$$

When the surfactant concentration ($[DBS]$) was maintained constant (fixed surfactant concentration) and $[Q]$ was varied, a linear least squares plot was obtained and this was used to compute N. A typical plot is shown in Figure 4.4. By varying the DBS concentration and ensuring $[Q]$ was fixed, (fixed quencher concentration) both N and the CMC values were obtained from a fit of the data to Equation 4.6. Using this approach the CMC was computed as 8.1×10^{-3} mol dm^{-3} and the mean aggregation number, N, was estimated as 52.7. These CMC values are in good agreement with the conductivity measurements and in good agreement with literature reports [305]. Given that the CMC values are approximately 6.0×10^{-3} mol dm^{-3} at 25 °C, it is clear that the DBS solutions used to disperse the MWCNT at a concentration of 0.05 mol dm^{-3} will contain micelles, with a dynamic equilibrium between the monomer and micelle, Equation 4.1. However, this concentration appeared to give the best dispersion of the MWCNT.

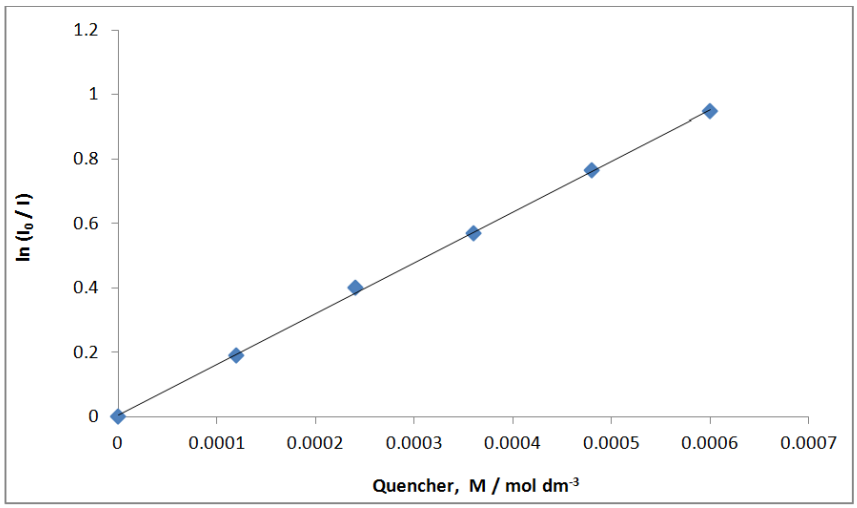

Figure 4.4: Plot of the logarithm of I_0/I as a function of the quencher concentration with a fixed concentration of 0.05 mol dm^{-3} DBS in water.

4.2.2 Formation of the PPy-DBSCNT Polymer Films

Once the uniform dispersion of the carbon nanotubes was achieved in the DBS solution and this dispersion was found to be stable, initial attempts were made to directly electropolymerise the monomer in the dispersion at the copper electrode. Although this proved successful, and the PPy-DBSCNT polymer film was formed, the adherence of the polymer film was poor. The electropolymerisation period was varied from 100 to 3600 s and the applied potential was varied from 0.60 V to 0.90 V vs. SCE. However, there was no improvement in the adherence of the polymer film to the copper substrate.

In an attempt to increase the adherence of the polymer film, a PPy-Tartrate film was initially formed at the copper electrode and then the PPy-DBSCNT polymer film was deposited as an outer layer. The initial PPy-Tartrate polymer film was deposited from 0.30 mol dm^{-3} pyrrole in 0.10 mol dm^{-3} tartrate anion at pH 7.0. A potential of 0.75 V vs. SCE was applied for times ranging from 100 to 3600 s, as detailed in Chapter 3. Once this initial layer was in place it was then possible to deposit the PPy-DBSCNT film.

The ratio of MWCNT to DBS was varied according to the ratios used in the literature [223] and the optimum concentrations were identified as 0.02 mg of MWCNT to 0.05 mol dm^{-3} DBS. The MWCNT-containing pyrrole solution, with a pyrrole concentration of 0.30 mol dm^{-3}, was sonicated for 1800 to 3600 s and the solution was agitated during the formation of the PPy-DBSCNT to ensure uniform dispersion of the MWCNT [220, 221, 222]. Again, the PPy-

DBSCNT was formed at a fixed potential of 0.75 V vs. SCE. The major advantage of this fixed potential method is that the potential and the time can be varied to alter the polymer thickness, with the longer electropolymerisation periods giving thicker polymer films and higher applied potentials giving higher rates of electropolymerisation and accordingly thicker polymer films. Although the tartrate solution was not stirred as this inhibits electropolymerisation at the electrode interface, the MWCNT-containing electropolymerisation solution was stirred to ensure uniform dispersion of the nanotubes [216].

Typical current-time plots recorded for the deposition of the PPy-Tartrate and the PPy-DBSCNT to generate the PPy-Tartrate/PPy-DBSCNT polymer film are shown in Figure 4.5. The oxidation current, which represents the rate of polymer growth, is plotted as a function of the time. The data recorded for the PPy-Tartrate film are typical of the data recorded during electropolymerisation. On application of the potential to the electrode there is an initial charging current, which arises from the charging of the double layer [42]. This charging current decays rapidly, being governed by the R_sC time constant, which, in turn, is related to the size of the electrode and the conductivity of the solution, where C is the double layer capacitance and R_s is the solution resistance. Other factors that might contribute to the current during this initial period are the oxidation of pyrrole to form oligomeric species and possibly the dissolution of copper. However, as the polymer is deposited at the copper substrate, the current decays indicating that the polymer inhibits any dissolution of the underlying copper substrate. As the concentration of pyrrole used in all these experiments, which is 0.30 mol dm^{-3}, is high this promotes a very fast initiation step for the electropolymerisation reaction. Accordingly, the PPy-Tartrate film is formed rapidly and this inhibits any further dissolution of the copper.

A very different current-time plot is recorded for the growth of the PPy-DBSCNT films. This polymer was formed at the PPy-Tartrate modified copper, with the polymer deposited for 600 s, as shown in Figure 4.5. Again, a potential of 0.75 V vs. SCE was applied to the PPy-Tartrate modified copper. Initially the current is low, but then the current increases over a 200 s period to give nearly constant currents reaching about 0.25 mA. This indicates a high and constant rate of electropolymerisation. These data show that the initial PPy-Tartrate film is sufficiently conducting to facilitate the electropolymerisation of pyrrole in the MWCNT and DBS solution. Indeed, it was possible to generate multi-layers by depositing an initial PPy-Tartrate film at 0.75 V vs. SCE for 300 s, followed by the PPy-DBSCNT film for an additional

300 s, then a third layer of PPy-Tartrate was deposited at 0.75 V vs. SCE for a 300 s period and a final layer of PPy-DBSCNT was formed to give four layers of polymer, alternating between PPy-Tartrate and PPy-DBSCNT. This clearly shows that the films are sufficiently conducting to facilitate the deposition of further layers of polymer.

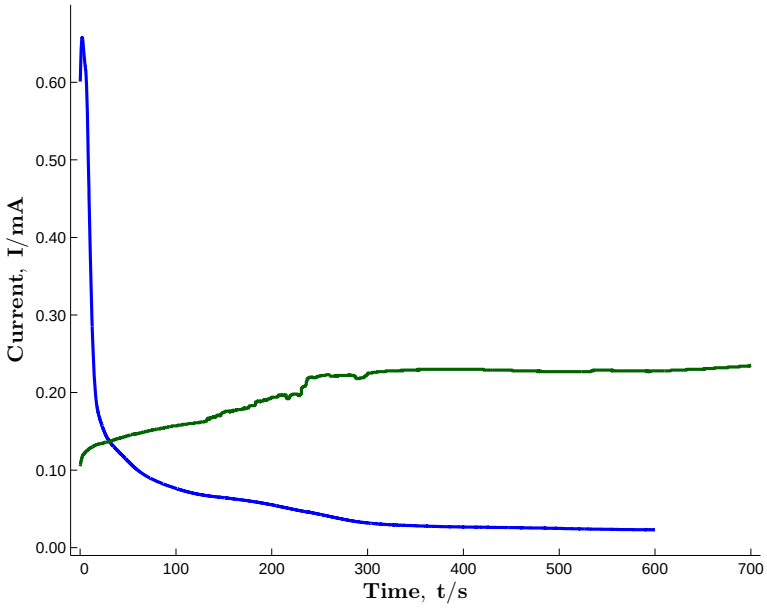

Figure 4.5: Current-time transient recorded at 0.75 V vs. SCE for Cu in a 0.10 mol dm^{-3} tartrate and 0.30 mol dm^{-3} pyrrole to generate PPy-Tartrate (blue) and for PPy-Tartrate in 0.05 mol dm^{-3} DBS with 0.02 mg CNT and 0.30 mol dm^{-3} pyrrole to generate PPy-DBSCNT at the PPy-Tartrate film (green) .

These bi-layers and multi-layers were thoroughly washed to remove any monomer or MWCNT from the surface and the surface morphology was investigated using SEM. Representative SEM micrographs are shown in Figure 4.6 for the PPy-Tartrate/PPy-DBSCNT bi-layer and the PPy-Tartrate. The surface morphologies of both films are different. The EDX spectra showed a lower intensity Cu signal for the PPy-Tartrate/PPy-DBSCNT, indicating a thicker polymer film. This is consistent with the relatively high currents recorded during electropolymerisation, Figure 4.5. There is no evidence of any cauliflower structures, which are typically observed with PPy [1] with simple dopants, such as chloride anions. Indeed, this morphology is very different to that obtained on depositing the PPy film in a DBS solution, but in the absence of MWCNT, where the characteristic cauliflower morphology is seen. However, it is clear that the films are homogeneous and crack-free and it appears that the growth of the polymer is influenced by the structure of the copper substrate, with the appearance of ridge-like

diagonal features. Similar surface morphologies were obtained with the multi-layers, but the influence of the underlying copper appeared to exert less influence with increasing layers.

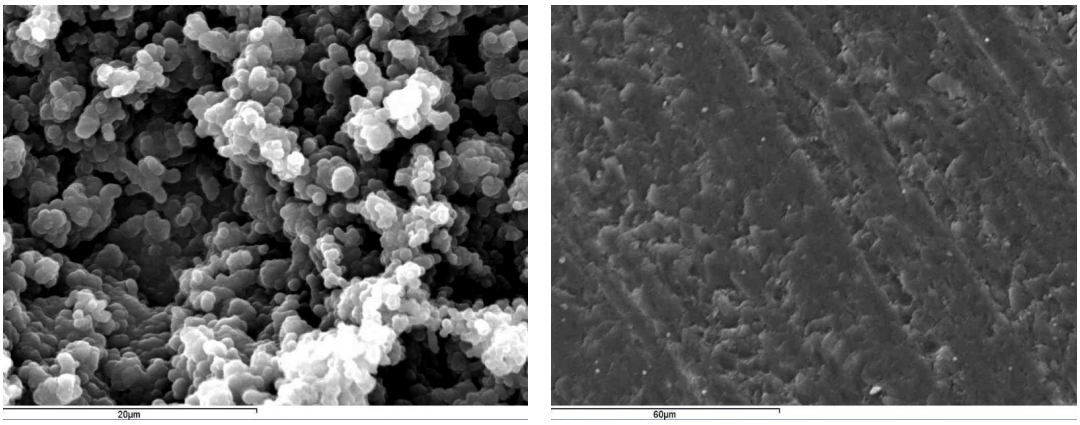

(a) **(b)**

Figure 4.6: SEM micrographs recorded for (a) PPy-Tartrate/PPy-DBSCNT film formed at 0.75 V vs. SCE, where the scale bar corresponds to 20 μm and (b) the PPy-Tartrate film formed at 0.75 V vs. SCE at Cu, where the scale bar corresponds to 60 μm, both films were formed as detailed in Figure 4.5.

A similar study was carried out with the oxalate system. In this case, the initial PPy-Oxalate films were formed at the copper electrode at 0.75 V vs. SCE from a near neutral 0.10 mol dm^{-3} oxalate solution [19], with 0.30 mol dm^{-3} pyrrole as detailed in Chapter 3. The PPy-DBSCNT film was then formed at the PPy-Oxalate layer and again bi-layers and multi-layers were formed by alternating the PPy-Oxalate and PPy-DBSCNT layers, a schematic is illustrated in Figure 4.7 showing the typical formation of the various bi/multi layers of polymer. The combination of polymer layers formed is summarised in Table 4.1. In this case, the PPy-Oxalate/DBSCNT and PPy-Tartrate/DBSCNT correspond to the adsorption of the multi-walled carbon nanotubes dispersed in DBS at the initial PPy-Oxalate or PPy-Tartrate polymer layers.

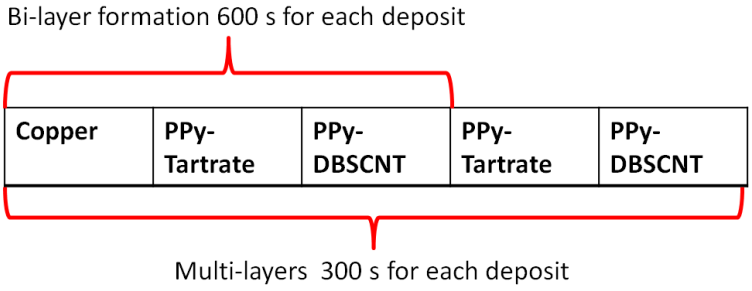

Figure 4.7: Schematic showing the composition of bi-layers (600 s for each layer) and multi-layers formed (300 s for each layer).

Table 4.1: Combinations of Polymer Systems Investigated.

Combinations of Polymer Systems	**Layers**
PPy-Tartrate/PPy-DBSCNT	Multi-layer
PPy-Tartrate/DBSCNT	Multi-layer
PPy-Tartrate/PPy-DBSCNT	Bi-layer
PPy-Oxalate/DBSCNT	Multi-layer
PPy-Oxalate/PPy-DBSCNT	Multi-layer
PPu-Oxalate/PPy-DBSCNT	Bi-layer
PPy-DBSCNT	Direct Polymerisation

Both the pH of the solution and applied potential appeared to influence the formation of the polymer films, listed in Table 4.1. The optimum conditions required to deposit the PPy-Oxalate and PPy-Tartrate, are detailed in Chapter 3, and involve an applied potential of 0.75 V vs. SCE and near neutral solutions. The influence of the applied potential on the formation of the PPy-DBSCNT film at the PPy-Tartrate and PPy-Oxalate and pure copper was studied and the potential was varied from 0.60 to 0.90 V vs. SCE. There was no evidence of formation of the PPy-DBSCNT film at 0.60 V vs. SCE. However, at this applied potential the rate of electropolymerisation is very low [139]. Indeed, the currents recorded were low, indicating very inefficient deposition of the polymer film. Again, the optimum applied potential was observed at 0.75 V vs. SCE, in good agreement with the results obtained with the PPy-Oxalate and PPy-Tartrate polymer films, Chapter 3. The adherence properties of the PPy-DBSCNT polymer film were dependent on the pH of the electropolymerisation solution. The formation of adherent PPy-DBSCNT films was not observed at pH values of 5.0 or 6.0 or at higher pH values of 8.0, 9.0 and 10.0. Using a simple sellotape test, the PPy-DBSCNT layers were easily removed. However, highly adherent PPy-DBSCNT layers were deposited at a pH of 7.0 in the presence of 0.05 mol dm^{-3} DBS, 0.02 mg of MWCNT and 0.30 mol dm^{-3} pyrrole. This optimum pH is similar to that observed for the formation of the PPy-Tartrate and PPy-Oxalate films, as shown in Chapter 3. Furthermore, as shown in Section 3.2.2, Chapter 3, the PPy-Tartrate film is considerably more stable at a pH of 7.0 than at pH values of 6.0, 8.0 and 10.0. It appears that the stability of the initial polymer layer influences the adhesion of the outer PPy-DBSCNT film.

The electropolymerisation period was also varied and the optimum polymer systems were identified as a multi-layer and a bi-layer. This multi-layer system involved the deposition of

an initial PPy-Tartrate polymer film at the copper electrode at 0.75 V vs. SCE for 300 s, followed by the PPy-DBSCNT deposited at 0.75 V vs. SCE for an additional 300 s period. During this step the solution was continuously stirred. Then a further layer of PPy-Tartrate was formed at 0.75 V vs. SCE for another 300 s period and finally the PPy-DBSCNT film was formed again for a 300 s, or instead the final step was achieved by adsorbing the carbon nanotubes on the polymer layers from a DBS solution containing MWCNT. The stability of the PPy-Tartrate/PPy-DBSCNT bi-layer was also excellent and this bi-layer was deposited with an initial PPy-Tartrate film formed at 0.75 V vs. SCE for 600 s and then the PPy-DBSCNT layer formed at 0.75 V vs. SCE for an additional 600 s. The optimum electropolymerisation periods were identified as 600 s for each layer in the bi-layer polymer systems, and 300 s for each layer in the case of the multi-layer polymer system.

However, in the oxalate system it was found that a longer electropolymerisation time was necessary, 900 s for each layer in the multi-layer polymer film was necessary to produce a polymer film with properties similar and comparable to the tartrate multi-layer coatings. This suggests that the oxalate polymer layer is less stable than the tartrate polymer system. This is in good agreement with the results presented in Chapter 3.

4.3 Analysis of Corrosion Performance of the Polymer Coatings

The corrosion protection properties of the polymer-modified copper electrodes were studied using a combination of electrochemical techniques, including cyclic voltammetry, open-circuit potential measurements, potentiodynamic polarisation plots and Tafel analysis. In addition, a spectrophotometric analysis was used to monitor the copper ion concentration. As the tartrate system appeared to give the more stable multi-layers and bi-layer the corrosion assessment studies were mainly focussed on this more promising system.

4.3.1 Spectrophotometric Determination of the Copper Ion Concentrations

In order to determine the concentration of copper dissolved from the polymer modified copper electrodes, a spectrophotometric method [306] involving the bathocuproine chelating agent, Figure 4.8, was used [306, 307]. This chelating agent forms an orange-coloured complex in the presence of copper ions, as shown in Figure 4.9. It has been used in experiments where redox

regulation of cell function is studied in human smooth muscle cells, where the bathocuproine is employed as a chelator of Cu^{2+} ions [308]. In this study, the bathocuproine method was used to determine the concentration of dissolved copper from the polymer-modified copper electrodes. A calibration curve was generated by recording the absorbance of the solutions at 480 nm [306]. The solutions were prepared and the absorbance was recorded following 1 min. The absorbance was measured again after 15 min and 24 h periods. Identical absorbance values were recorded indicating very good stability.

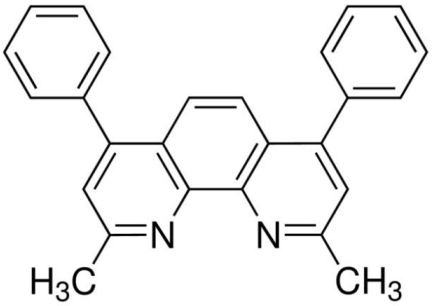

Figure 4.8: Chemical structure of the chleating bathocuproine ($C_{26}H_{20}N_2$) agent.

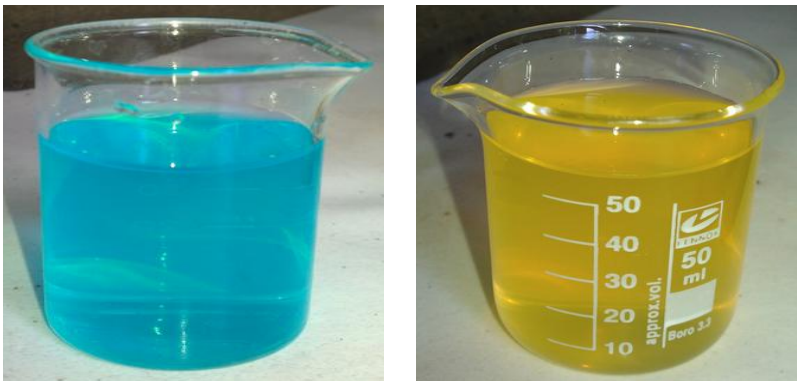

(a) **(b)**

Figure 4.9: (a) $CuSO_4$ solution and (b) $CuSO_4$ solution on addition of the chelating bathocuproine agent.

In Figure 4.10, a typical calibration curve is shown for the solutions prepared in distilled water. Excellent linearity is observed with a correlation coefficient, R^2, of 0.9985 and a slope of 171.19 mol^{-1} dm^3. It has been reported that chloride anions can participate in the bathocuproine reaction [306], as detailed in Equation 4.7. Therefore, calibration curves were recorded in the presence of chloride anions, at a relatively high concentration of 0.20 mol dm^{-3}, and a representative calibration curve is presented in Figure 4.11. Again, excellent linearity

is observed with R^2 equal to 0.9993, however the slope of the calibration curve is different with a slope of 256.14 mol^{-1} dm^3. This clearly indicates that the formation of the complex and the corresponding absorbance values are influenced by the presence of chloride anions. Therefore, care was taken to record the calibration curves in the presence of chloride anions, and furthermore, at the concentration of chloride used in the corrosion assessment experiments.

$$CuCl_n^{(n-1)} + (bathocuproine) \rightarrow Cu(bathocuproine)Cl + (n-1)Cl^- \tag{4.7}$$

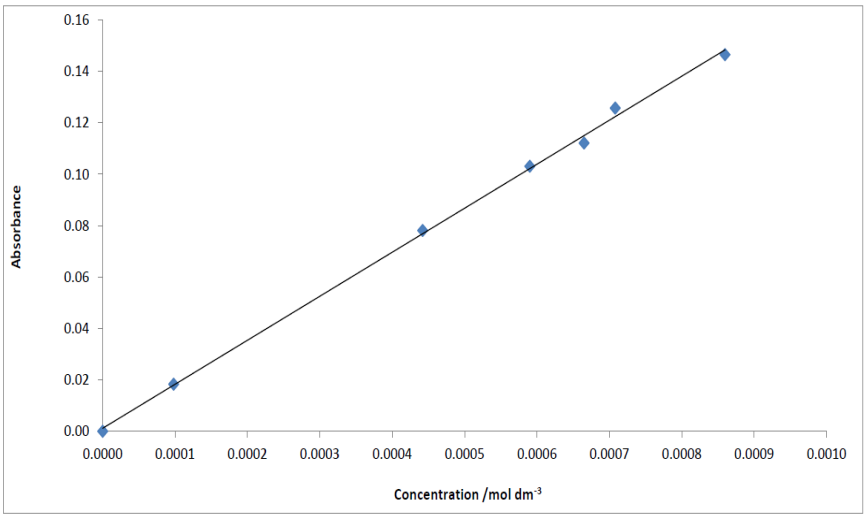

Figure 4.10: Calibration curve recorded in distilled water with the absorbance plotted as a function of the concentration of $CuSO_4$.

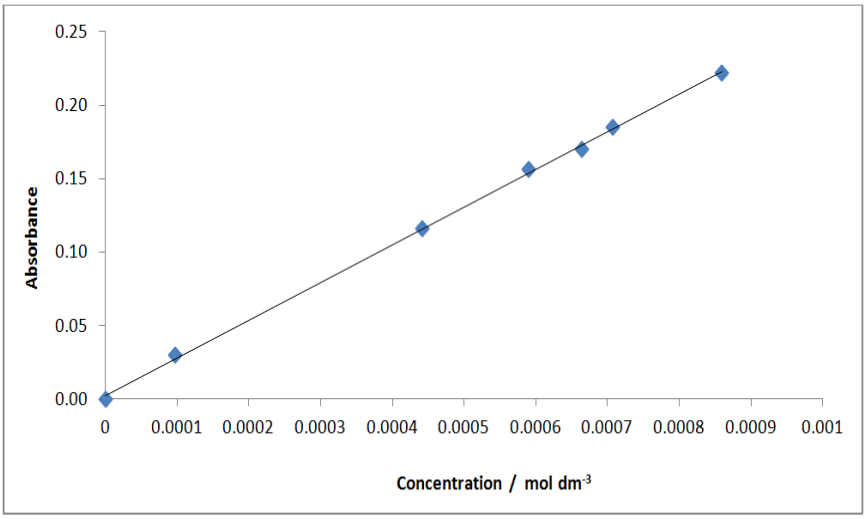

Figure 4.11: Calibration curve recorded in 0.20 mol dm^{-3} NaCl with the absorbance plotted as a function of the concentration of $CuSO_4$.

The uncoated copper, the PPy-Tartrate and the PPy-Tartrate/PPy-DBSCNT and PPy-Tartrate/DBSCNT multi-layers were immersed in 0.10 mol dm^{-3} NaCl for a 2-day period and then the solutions were analysed by adding the bathocuproine reagent from a stock solution and the absorbance was recorded at 480 nm. The concentration was calculated using the slope of the calibration curve recorded in 0.10 mol dm^{-3} NaCl. These data are summarised in Table 4.2. Here it is evident that the PPy-Tartrate/PPy-DBSCNT multi-layer provides the best corrosion protection properties, with the lowest concentration of dissolved copper. However, these concentrations are influenced by the deposition of copper-containing corrosion products at the uncoated copper electrode. In the presence of chloride anions, CuCl, is deposited at the surface, and while this may have very poor corrosion protection properties, the porous nature of the film may limit the true concentration of copper released into the solution, giving solution concentrations that are lower than the true rate of dissolution. These corrosion products are not observed with the polymer-coated copper electrodes and the concentrations of dissolved copper are a more realistic measure of the corrosion rate and the protective properties of the coatings.

Table 4.2: Concentration of dissolved Cu ions (n = 6) from Cu and the polymer-modified Cu following a 2-day immersion period in 0.10 mol dm^{-3} NaCl at a pH of 7.0.

System	**Concentration /mmol dm^{-3}**
Uncoated Cu	4.65 ± 0.15
PPy-Tartrate	1.93 ± 0.17
PPy-Tartrate/PPy-DBSCNT (Multi-layer)	1.60 ± 0.10
PPy-Tartrate/DBSCNT (Multi-layer)	2.13 ± 0.14

4.3.2 Cyclic Voltammetry

The protective properties of the PPy-Tartrate/PPy-DBSCNT and the PPy-Oxalate/PPy-DBSCNT multi-layers were studied using cyclic voltammetry. The voltammograms were recorded in 0.10 mol dm^{-3} NaCl [6], adjusted to a pH of 7.0 with a few drops of NaOH. Data were recorded at scan rates from 1 to 100 mV s^{-1} and the potential was cycled from -0.50 V to 1.0 V vs. SCE. The multi-layers were deposited for a total period of 1200 s, with the initial PPy-Tartrate or PPy-Oxalate films deposited at 0.75 V vs. SCE for 300 s. This was followed by the PPy-DBSCNT layers for 300 s and then additional layers of PPy-Tartrate or PPy-Oxalate for 300 s

and finally PPy-DBSCNT for 300 s, as detailed in Section 4.2.2.

In Figure 4.12 representative voltammograms recorded at 1 mV s^{-1} are shown for the PPy-Tartrate/PPy-DBSCNT multi-layer and the uncoated copper, while similar data recorded with the PPy-Oxalate/PPy-DBSCNT multi-layer system are shown in Figure 4.13. There is a significant difference between the voltammograms recorded for the PPy-Tartrate/PPy-DBSCNT modified copper and the uncoated copper electrodes, as shown in Figure 4.12. The protective properties of the polymer-coated copper are clearly evident with very low currents and no indications of the dissolution of the copper substrate. The current begins to increase at about 0.80 V vs. SCE and this indicates breakdown of the polymer film and the dissolution of copper. However, the currents recorded at 1.0 V vs. SCE are considerably lower that the values recorded for the uncoated copper electrode, which suggests that the coating limits the dissolution of copper even after the breakdown event. Indeed, there was no evidence of any changes in the surface morphology, indicating excellent stability in the aggressive chloride-containing solution.

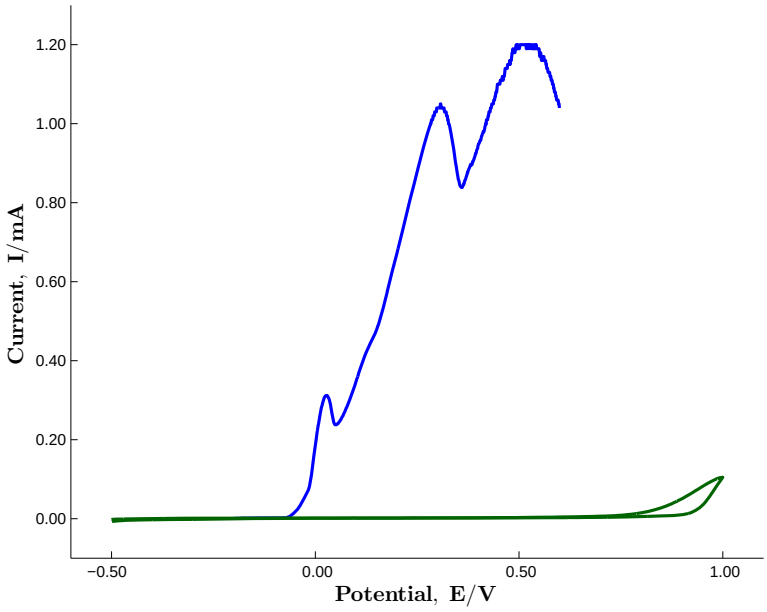

Figure 4.12: Cyclic voltammograms recorded at 1 mV s^{-1} in 0.10 mol dm^{-3} NaCl at a pH of 7.0 for the PPy-Tartrate/PPy-DBSCNT multi-layer film (green) deposited at Cu compared to the uncoated Cu (blue).

On the other hand, significant dissolution of the uncoated copper electrode is seen, in good agreement with the data shown in Chapter 3, Section 3.3.1. The initial dissolution of the copper electrode [8] is observed at about -0.10 V vs. SCE and then the current increases to

give a broad peak at about 0.20 V vs. SCE with a peak current of approximately 1.00 mA. This indicates considerable dissolution and the formation of chloride-containing corrosion products, such as CuCl and the soluble $CuCl_2^-$ species. As these corrosion products are precipitated at the copper surface, there is a rapid decrease in the current. However, these corrosion products, mainly CuCl and hydroxy-containing copper-chloride species, are porous and with higher applied potentials dissolution, and a corresponding increase in the current, is observed.

The voltammograms recorded for the PPy-Oxalate/PPy-DBSCNT and the PPy-Tartrate/PPy-DBSCNT multi-layers are compared in Figure 4.13. Again, these data were recorded at a scan rate of 1 mV s^{-1}. The voltammograms recorded for the two multi-layer systems are very different. Very good protective properties are observed with the PPy-Tartrate/PPy-DBSCNT multi-layer, however breakdown of the PPy-Oxalate/PPy-DBSCNT is seen at about 0.30 V vs. SCE indicating the onset of the dissolution of the copper substrate. There is a further increase in the current with an increase of the potential to give a current of approximately 5.00 mA at 1.0 V vs. SCE. Indeed, at this potential the currents recorded for the PPy-Oxalate/PPy-DBSCNT modified copper and the uncoated copper are similar. These data clearly show that the PPy-Oxalate/PPy-DBSCNT multi-layer has relatively poor corrosion protection properties. However, as detailed earlier in Section 4.2.2, the corrosion protection properties of the PPy-Oxalate/PPy-DBSCNT multi-layer can be improved by increasing the electropolymerisation period to 900 s for each polymer layer.

These data are in good agreement with the results obtained in Chapter 3, where it was shown that the corrosion protection properties afforded by the PPy-Oxalate polymer film were poor, particularly at short electropolymerisation periods. Indeed, the breakdown potential was close to 0.01 V vs. SCE for electropolymerisation periods of 600 s to 1200 s. The breakdown potential recorded for the PPy-Oxalate/PPy-DBSCNT multi-layer deposited for a total period of 1200 s is significantly higher at about 0.30 V vs. SCE, indicating that the PPy-DBSCNT polymer film plays a significant role in the corrosion protection of the underlying copper. This is also evident with the tartrate system. The breakdown potentials recorded for the PPy-Tartrate polymer film are approximately 0.45 to 0.50 V vs. SCE, for electropolymerisation periods from 600 to 3600 s, Section 3.3.1, Chapter 3. A significant increase in the breakdown potential, to values higher than 0.80 V vs. SCE, is observed with the deposition of the PPy-DBSCNT layer. Again, this highlights the significant role of the PPy-DBSCNT layer.

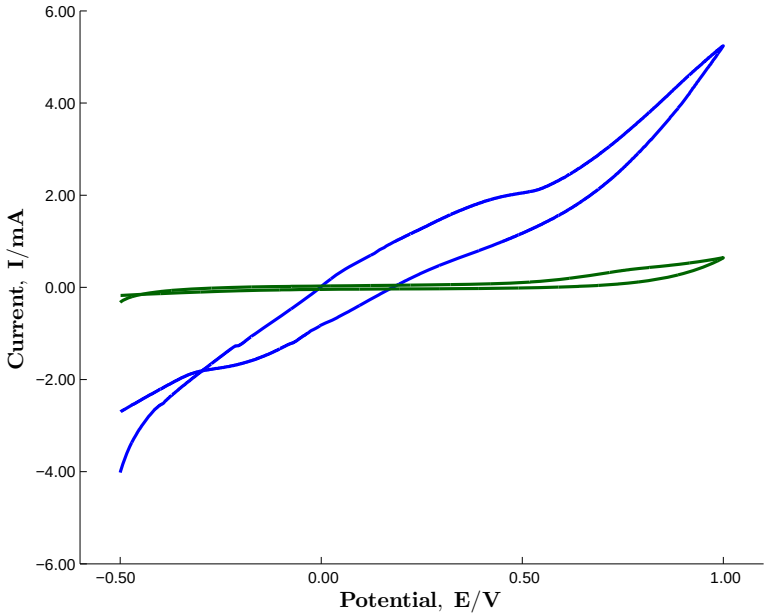

Figure 4.13: Cyclic voltammograms recorded at 1 mV s^{-1} in 0.10 mol dm^{-3} NaCl at a pH of 7.0 for the PPy-Tartrate/PPy-DBSCNT multi-layer (green) and the PPy-Oxalate/PPy-DBSCNT multi-layer films deposited at Cu (blue).

The influence of the scan rate is shown in Figure 4.14, where the cyclic voltammograms recorded for the PPy-Tartrate/PPy-DBSCNT multi-layer in neutral 0.10 mol dm^{-3} NaCl at scan rates of 100 mV s^{-1} and 10 mV s^{-1} are compared. It is evident that the scan rate has a significant influence on the measured currents, with higher currents recorded at the higher scan rate. It is unlikely that these higher currents are connected with the dissolution of the underlying copper substrate, as excellent corrosion protection properties were observed at 1 mV s^{-1}, Figure 4.12. This increase in the current can be rationalised in terms of the size of the diffusion layer, where an increase in the size of the diffusion layer is observed at lower scan rates. As the current is proportional to the flux across the diffusion layer, the magnitude of the current will vary with the scan rate and increase at higher scan rates [43]. This hypothesis was tested by depositing the PPy-Tartrate/PPy-DBSCNT multi-layers at two inert substrates, platinum and glassy carbon, and then the voltammograms were recorded at different scan rates. As detailed in Chapter 3, the tartrate solution was acidified to a pH of 4.0 to facilitate the formation of the PPy-Tartrate film at platinum. Otherwise, the electropolymerisation conditions were similar, with an initial layer of PPy-Tartrate deposited for 300 s at 0.75 V vs. SCE, followed by a layer of PPy-DBSCNT for 300 s at 0.75 V vs. SCE. Then, additional layers of PPy-Tartrate and PPy-DBSCNT were formed to give a total electropolymerisation period of 1200 s. These data are presented in

Figure 4.15 where the influence of the copper, platinum and glassy carbon substrates is shown. The voltammograms were recorded at 100 mV s^{-1} as higher currents were observed at this scan rate for the copper system, Figure 4.14.

Although not shown in the figure, an increase in the currents was observed with an increase in the scan rate, in agreement with several literature reports [309]. However, it is clear from Figure 4.15 that the nature of the substrate has an added influence on the measured currents. Very low currents are observed with the platinum substrate, as shown in Figure 4.15b. Somewhat higher currents are observed with the glassy carbon substrate, Figure 4.15a, particularly at potentials higher than 0.80 V vs. SCE, indicating that the currents observed with the copper system may be connected with the multi-layer polymer film. Nevertheless, higher currents are observed with the copper system. Again, it is unlikely that these higher currents are connected with dissolution of the copper substrate and the variations in the currents may be connected to the thickness of the multi-layer polymer films at the different substrates.

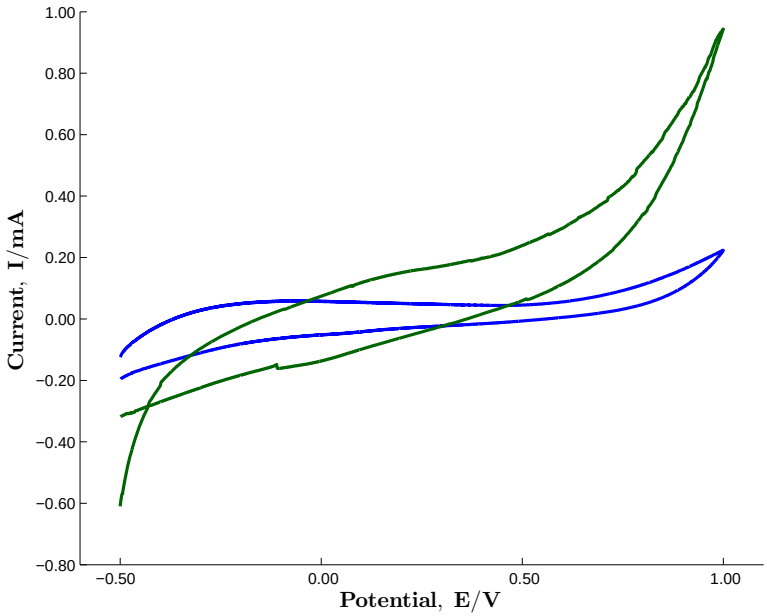

Figure 4.14: Cyclic voltammograms recorded in 0.10 mol dm^{-3} NaCl at a pH of 7.0 for the PPy-Tartrate/PPy-DBSCNT multi-layer films deposited at Cu cycled at 100 mV s^{-1} (green) and 10 mV s^{-1} (blue).

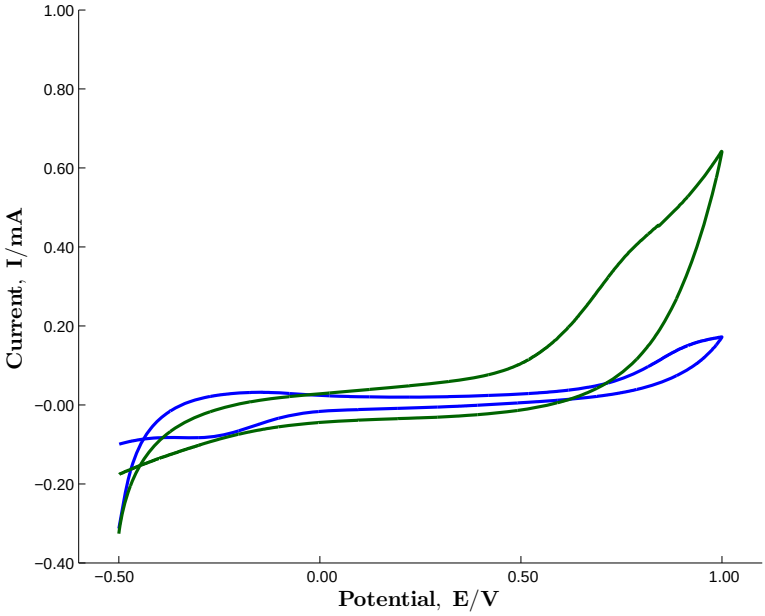

(a)

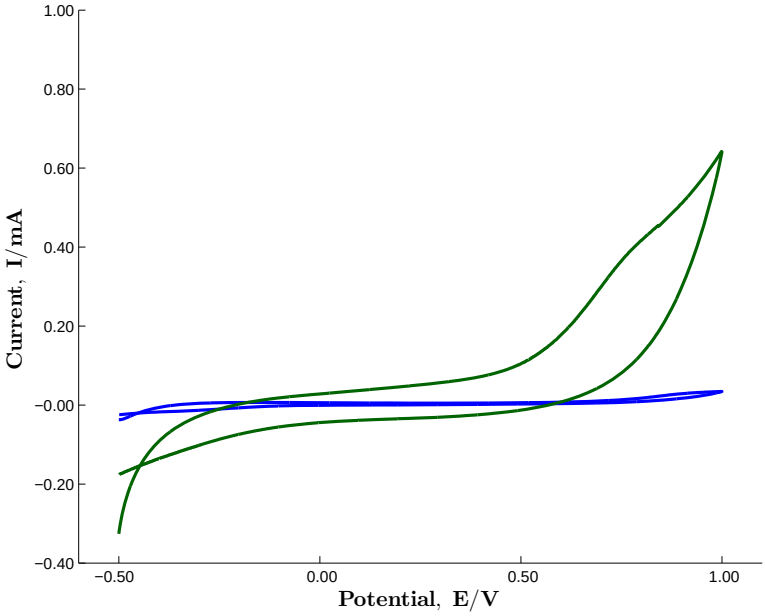

(b)

Figure 4.15: Cyclic voltammograms recorded at 100 mV s^{-1} in 0.10 mol dm^{-3} NaCl at a pH of 7.0 for the PPy-Tartrate/PPy-DBSCNT multi-layer films deposited on (a) Cu (green) and GC (blue) and (b) Cu (green) and Pt (blue).

4.3.3 Open-Circuit Potential Measurements

As previously shown in Chapter 3, the open-circuit potential (OCP), which is also frequently termed the corrosion potential, E_{corr}, is a mixed potential adopted in the absence of any polarisation and corresponds to the potential at which there is no current flow. At this point the rate of the oxidation half and reduction half reactions are equal. A negative shift in the open-circuit potential is observed when anodic dissolution occurs. Consequently, the measurement of the open-circuit potential is often the first step in assessing the corrosion susceptibility of a material or the protective properties of a coating [259].

The open-circuit potentials were recorded for the PPy-Tartrate/PPy-DBSCNT and PPy-Oxalate/PPy-DBSCNT multi-layers in a neutral 0.10 mol dm^{-3} NaCl solution [259], as detailed in Section 3.3.2, Chapter 3. The polymer films were formed for a total period of 1200 s, with the initial PPy-Tartrate or PPy-Oxalate films deposited at 0.75 V vs. SCE for 300 s, followed by the PPy-DBSCNT layers for 300 s. Then, additional layers of PPy-Tartrate or PPy-Oxalate for 300 s and finally the outer PPy-DBSCNT layers were deposited for 300 s, as detailed in Section 4.2.2. The open-circuit potentials were monitored over a 30-day period, with measurements on a daily basis. Once the open-circuit potential measurements were made, the polymer-modified copper electrodes were placed in a fresh 0.10 mol dm^{-3} NaCl solution and the container was sealed and left until the measurements were made on the following day. This was repeated over a 30-day period. Typical data are shown in Figure 4.16 for the PPy-Tartrate/PPy-DBSCNT and PPy-Oxalate/PPy-DBSCNT multi-layers following immersion for a 1 and 15 day period. The open-circuit potential is recorded over a 3600 s period. For comparison purposes, the open-circuit potential recorded for the uncoated copper is presented. There is a clear variation between the open-circuit potentials adopted by the polymer-modified copper electrodes and the uncoated copper. The open-circuit potential adopted by the uncoated copper is about -0.15 V vs. SCE, while higher open-circuit potentials, at approximately -0.01 to 0.05 V vs. SCE, are observed with the polymer modified copper electrodes. The open-circuit potentials are clearly constant and there is no evidence of any significant decay in the potential over this 3600 s period. This indicates very good stability.

However, it is evident that the open-circuit potential of the oxalate based polymer film decays with increasing immersion periods, as shown from a comparison of the data recorded

on day 1 and day 15, Figure 4.16b. Following an immersion period of approximately 20 days, the open-circuit potential decays to values adopted by the uncoated copper electrode, indicating a loss in the corrosion protective properties [259]. In comparison, the tartrate-based polymer continues to adopt a much higher and constant open-circuit potential over the 30 day test period. Although the potential drops slightly, with continued immersion, it remains considerably higher than the value adopted by the uncoated copper, indicating very good long-term corrosion protection of the underlying copper. These data are consistent with the voltammetry measurements presented in Section 4.3.2 and clearly show that the PPy-Tartrate/PPy-DBSCNT provides the best corrosion protection properties.

The open-circuit potentials of the PPy-Oxalate/DBSCNT and the PPy-Tartrate/DBSCNT multi-layer polymer films are displayed in Figure 4.17a and 4.17b, respectively. These films were deposited at a potential of 0.75 V vs. SCE for 300 s for each consecutive layer, with a combined time of 1200 s. A constant potential of 0.75 V vs. SCE for 300 s was used to adsorb the DBSCNT layer onto the base PPy-Tartrate layer, instead of the conventional electropolymerisation using a fixed potential in the presence of pyrrole. Again, it can be clearly seen that the open-circuit potential adopted by the oxalate system is lower than that measured for the corresponding tartrate system. Moreover, the open-circuit potential decays over the first 1300 s, to reach values of approximately -0.05 V vs. SCE after 2000 s. This potential is still higher than the open-circuit potential of the uncoated copper, -0.15 V vs. SCE, however, the decay in the open-circuit potential indicates some loss in the protective properties of the PPy-Oxalate/DBSCNT multi-layers. The open-circuit potential adopted by the PPy-Tartrate/DBSCNT multi-layer remains more constant and the potential only varies from 0.03 to 0.02 V vs. SCE during the initial 300 s period. The open-circuit potential remains constant at about 0.02 V vs. SCE for the remaining 4000 s period, Figure 4.17a. This indicates good stability. Indeed, the open-circuit potential varied little with increasing immersion periods and there was no evidence of decay in the open-circuit potential following the 30 day immersion period.

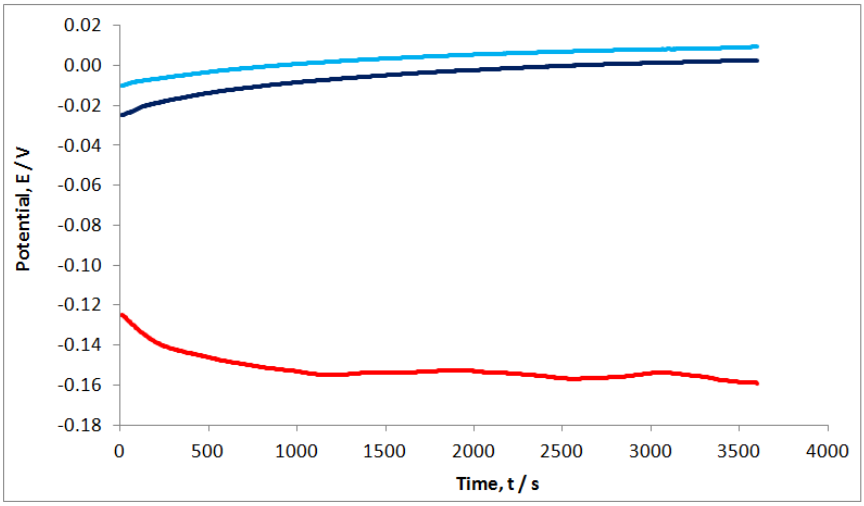

(a)

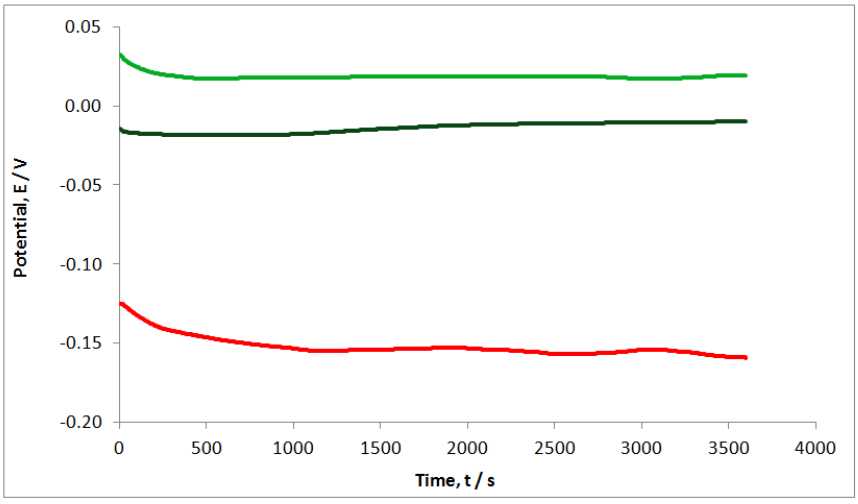

(b)

Figure 4.16: OCP recorded in 0.10 mol dm^{-3} NaCl solution at a pH of 7.0 for (a) uncoated Cu (red) and the PPy-Tartrate/PPy-DBSCNT multi-layer modified Cu following immersion periods of 1 day (light blue) and 15 day (dark blue) and (b) uncoated Cu and the PPy-Oxalate/PPy-DBSCNT multi-layer modified Cu following immersion periods of 1 day (light green) and 15 day (dark green).

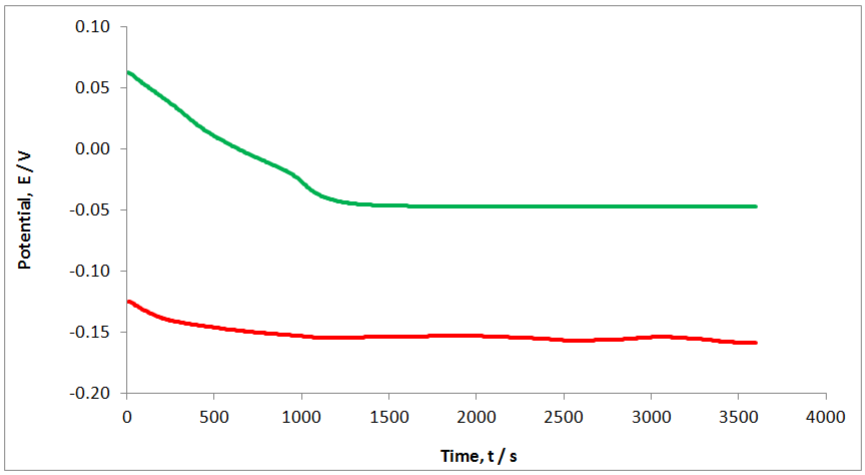

(a)

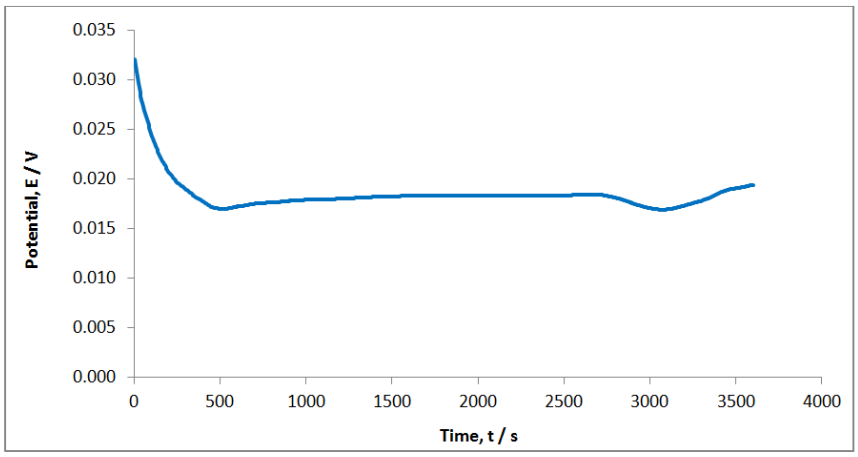

(b)

Figure 4.17: OCP recorded in 0.10 mol dm^{-3} NaCl solution at a pH of 7.0 for (a) uncoated Cu (red) and the PPy-Oxalate/DBSCNT multi-layer modified Cu (green) and (b) PPy-Tartrate/DBSCNT multi-layer modified Cu (blue).

4.3.4 Polarisation Curves and Tafel Analysis

It is well established in the literature that potentiodynamic polarisation curves are valuable in monitoring the corrosion protection properties of a coating or film [310, 311, 312]. In order to further demonstrate the protective nature of the tartrate-based polymer system, polarisation plots were recorded in a neutral 0.10 mol dm^{-3} NaCl solution at 0.1667 mV s^{-1} from 200 mV below to about 200 mV above the corrosion potential, or until significant dissolution of the copper was observed. The PPy-Tartrate/PPy-DBSCNT and the PPy-Tartrate/DBSCNT multi-layers were deposited at 0.75 V vs. SCE for a total period of 1200 s, with 300 s for each consecutive layer, as detailed in Section 4.2.2. Typical polarisation curves are shown in Figure 4.18, where the data recorded for the uncoated copper are compared to the data recorded for the PPy-Tartrate/PPy-DBSCNT multi-layer in Figure 4.18a. Similar plots are shown for uncoated copper and the PPy-Tartrate/DBSCNT multi-layer in Figure 4.18b. These data were recorded at a scan rate of 0.1667 mV s^{-1}.

Dissolution of copper is clearly evident for the uncoated copper. The corrosion potential is observed at about -0.120 V vs. SCE and there is a significant increase in the current at slightly higher applied potentials. There is no evidence of any passive region. This is consistent with the dissolution of copper and the formation of copper and chloride-containing corrosion products [285, 313]. These corrosion products include the insoluble CuCl and the soluble $CuCl_2^-$ species that are well known to limit the mass transport, as these species are removed from the electrode surface to the bulk solution [39]. A clear passive region is evident with the polymer-coated copper electrodes [165], indicating that the dissolution of copper and the generation of the corrosion products are inhibited. The corrosion potential of the PPy-Tartrate/PPy-DBSCNT is approximately -0.065 V vs. SCE, some 100 mV more positive than that recorded for the uncoated copper. The corrosion potential of the PPy-Tartrate/DBSCNT is about -0.035 V vs. SCE, giving a difference of 110 mV compared with the uncoated copper. It appears that the corrosion protection properties of the multi-layers arise from two effects. Firstly, the tartrate-based passivation layer deposited during the formation of the PPy-Tartrate protects and passivates the copper electrode. Secondly, the outer polymer layer acts as a barrier and prevents the depassivating ions, such as chlorides and dissolved oxygen, from penetrating through the multi-layers [286].

It is evident from the data presented in Figure 4.18 that the corrosion potentials are somewhat different to the open-circuit potentials presented in Figures 4.16 and 4.17. However, this is connected with the fact that the electrodes were polarised some 200 mV below the corrosion potential at a relatively slow scan rate of 0.1667 mV s^{-1}. Indeed, when the copper and polymer-modified copper electrodes were immersed in the chloride-containing solutions and scanned from the corrosion potential, at 0.1667 mV s^{-1}, the corrosion potentials were identical to that recorded in Section 4.3.3. It is also evident from the polarisation curves that the reduction currents are considerably higher for the polymer-modified copper electrodes. This effect was not observed with the cyclic voltammetry experiments, as shown in Section 4.3.2. It appears to be related to the slow scan rate. The oxygen reduction reaction is the predominant reduction half-reaction at a near neutral pH, with Equation 4.8 describing the reduction of dissolved oxygen in neutral or alkaline media. Equation 4.9 gives the reduction reaction for more acidic media. Other potential reduction reactions are the reduction of H^+, Equation 4.10.

$$O_2 + 2H_2O + 4e^- \rightarrow 4OH^- \tag{4.8}$$

$$O_2 + 4H^+ + 4e^- \rightarrow 2H_2O \tag{4.9}$$

$$2H^+ + 2e^- \rightarrow H_2 \tag{4.10}$$

It appears that one or more of these reduction reactions occur at the polymer-modified copper electrodes at this slow scan rate, to account for the higher reduction reactions, which are clearly evident in Figure 4.18.

A scratch test was carried out by using a sharp object to damage the PPy-Tartrate/PPy-DBSCNT and the PPy-Tartrate/DBSCNT multi-layers and expose the copper substrate. The polarisation behaviour of the scratched multi-layer coatings was then compared to the freshly deposited multi-layer polymer films and representative polarisation curves are shown in Figure 4.19. It is clearly evident that the data recorded for the scratched multi-layer polymer coatings are somewhat different, with a higher current density. This indicates dissolution of the copper substrate and a clear anodic peak is observed at about 0.02 V vs. SCE, indicating significant dissolution of the copper substrate [282].

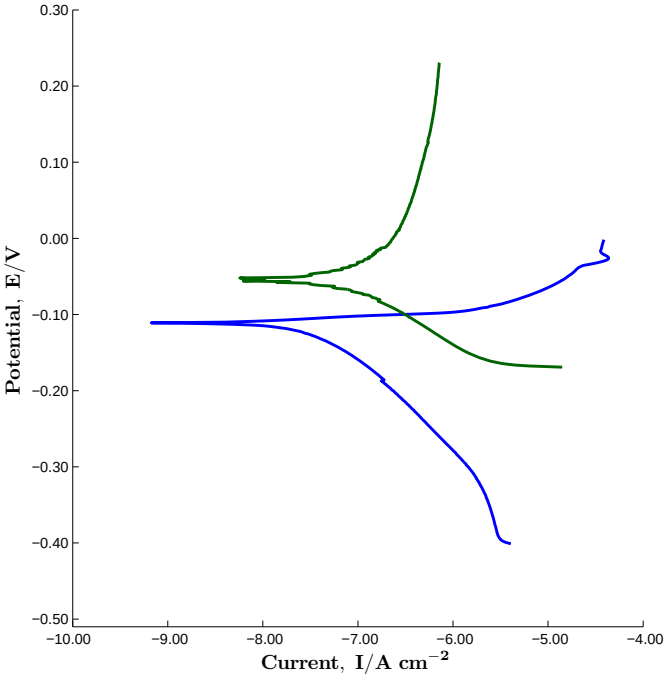

(a)

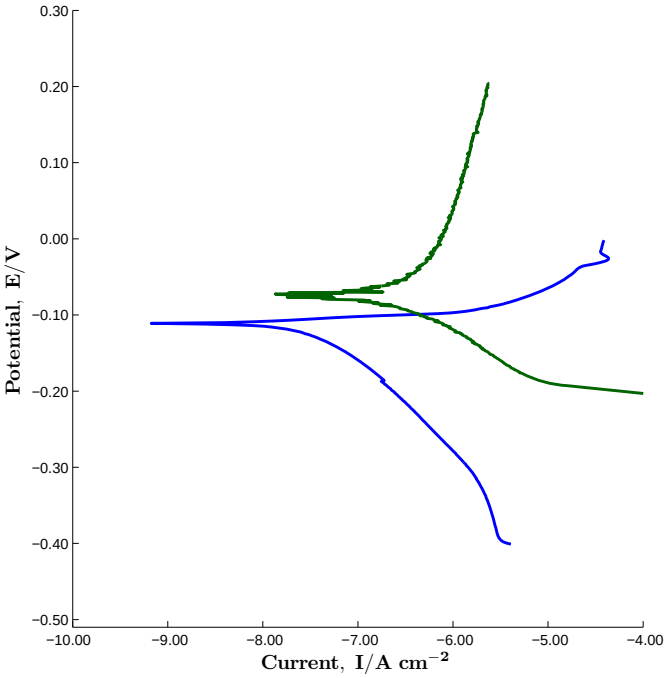

(b)

Figure 4.18: Polarisation curves recorded at 0.1667 mV s^{-1} in 0.10 mol dm^{-3} NaCl at a pH of 7.0 for (a) uncoated Cu (blue) and PPy-Tartrate/PPy-DBSCNT multi-layer deposited at Cu (green) and (b) uncoated Cu (blue) and PPy-Tartrate/DBSCNT multi-layer deposited at Cu (green).

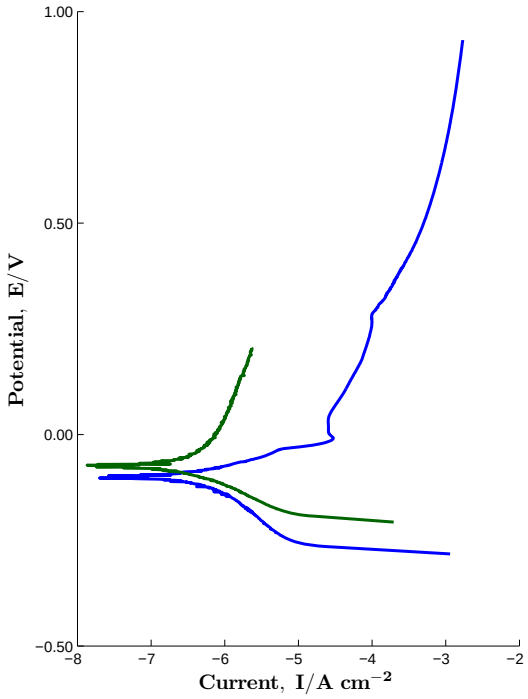

(a)

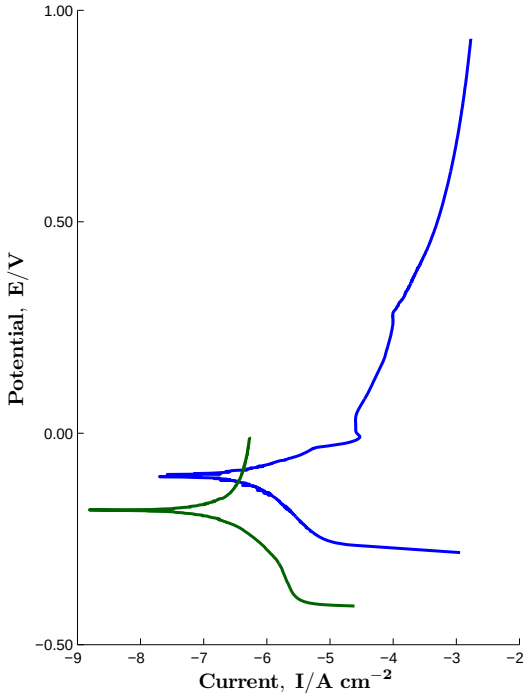

(b)

Figure 4.19: Polarisation curves recorded at 0.1667 mV s^{-1} in 0.10 mol dm^{-3} NaCl at a pH of 7.0 for (a) PPy-Tartrate/DBSCNT multi-layer (green) and scratched PPy-Tartrate/DBSCNT multi-layer (blue) and (b) PPy-Tartrate/PPy-DBSCNT multi-layer (green) and scratched PPy-Tartrate/PPy-DBSCNT multi-layer (blue).

It is also evident from Figure 4.19 that there is a considerable shift in the corrosion potential. This is consistent with the significant increase in the anodic current, where the current is increased from approximately 1.0×10^{-6} A cm^{-2} to 1.0×10^{-4} A cm^{-2}. These data are similar to the results obtained by Al-Hinai and co-workers [7], who observed a significant increase in the current on forming a scratch in the surface. A current increase of several orders of magnitude was obtained, similar to that observed in Figure 4.19. Indeed, the corrosion potential was shifted to more negative potentials, as observed for the PPy-Tartrate/DBSCNT and the PPy-Tartrate/PPy-DBSCNT multi-layers. These data clearly show that the multi-layer is no longer highly protective when copper is exposed through a scratch [314] in the multi-layer coating.

A Tafel analysis was carried out in an attempt to estimate the corrosion current, I_{corr}, for the PPy-Tartrate/PPy-DBSCNT and PPy-Tartrate/DBSCNT multi-layers. For comparison purposes, a similar analysis was performed with the uncoated copper and PPy-Tartrate films. As detailed in Section 4.3.3, the corrosion potential, E_{corr}, is a mixed potential and under these conditions the rate of the anodic half-reaction is equal to the rate of the cathodic half-reaction. As the displacement from the corrosion potential, E_{corr}, is increased beyond 10 mV, a logarithmic relationship between the potential and the current is observed, to give the Tafel equation, Equation 4.11. This equation can be expressed in the simpler form, given in Equation 4.12.

$$E - E_r = \frac{2.303RT}{\alpha F} \log I_0 - \frac{2.303RT}{\alpha F} \log I \tag{4.11}$$

$$E - E_r = a + b \log I \tag{4.12}$$

The term I_0 is the exchange current density, the term $E - E_r$ is the overpotential and the constant, b, which is equal to the slope, $\frac{\partial E}{\partial \log I}$ of the polarisation curve, is termed the Tafel slope. In Tafel plots the potential, E, is plotted as a function of the logarithm of the current density, $\log I$, and provided the corrosion reactions are controlled by activation polarisation, as is frequently observed, linear plots are obtained [315]. It is possible to extrapolate the anodic and cathodic linear portions of the polarisation curves to the corrosion potential E_{corr}, and the magnitude of the current at this intersection gives the corrosion current, I_{corr}, which is a direct measure of the rate of corrosion. In general, reliable data are only obtained if a linear

relationship is maintained for at least one decade (where the current increases by a factor of 10). In addition, this analysis is strictly only applicable to activation controlled corrosion processes. It is well known that the dissolution of copper in chloride-containing solutions is under mixed activation and diffusion control [8, 165, 280] and this may complicate the analysis leading to less reliable Tafel slopes.

Polarisation curves were recorded at a scan rate of 0.1667 mV s^{-1} in an attempt to reduce the current contribution from the PPy [1, 258] and these data were used in the Tafel analysis. The computed corrosion potential, E_{corr}, corrosion current, I_{corr}, and Tafel slopes, b_a and b_c, are summarised in Table 4.3. The Tafel slopes obtained for copper are in relatively good agreement with the data obtained by Mansfeld *et al.* [310] for copper in chloride solutions. The corrosion current, I_{corr}, is lower than the value of 2.0 μA cm^{-2} reported by Mansfeld and co-workers [310], however, this is probably connected to variations in the pH of the chloride-containing solutions. It is clear that higher I_{corr} values are computed for the uncoated and PPy-Tartrate modified copper, while relatively low I_{corr} values are seen with the Tartrate/PPy-DBSCNT and PPy-Tartrate/DBSCNT multi-layers. This is in good agreement with the spectrophotometric data presented in Section 4.3.1, the voltammetry data presented in Section 4.3.2 and the open-circuit potential data shown in Section 4.3.3.

Table 4.3: Tafel analysis for uncoated Cu and the polymer-modified Cu electrodes in 0.1 mol dm^{-3} NaCl, at a pH of 7.0.

System	b_a mV $decade^{-1}$	b_c mV $decade^{-1}$	E_{corr} V vs. SCE	I_{corr} μA cm^{-2}
Uncoated Cu	68	95	-0.120	0.29
PPy-Tartrate/PPy-DBSCNT	41	74	-0.065	0.05
PPy-Tartrate/DBSCNT	57	76	-0.035	0.05
PPy-Tartrate	90	50	-0.077	2.00

4.4 Summary of Results

The coatings formed in this chapter are novel, exhibiting good corrosion protection properities. These coatings involved the successful incorporation of multi-walled carbon nanotubes into PPy films to generate a number of bi-layers and multi-layers, comprising PPy-Tartrate and PPy-DBSCNT or PPy-Oxalate and PPy-DBSCNT. There has been no previous literature reports on this combination of polymer coating. A stable and well dispersed solution of the carbon nanotubes was obtained using DBS. It was found that the ratio of the concentration of DBS to the mass of MWCNT was critical in forming this stable and highly dispersed solution, in good agreement with literature reports [298]. Stable and homogeneous dispersions were obtained using a 3:1 ratio of 0.05 mol dm^{-3} DBS and 0.02 mg of MWCNT. The critical micelle concentration (CMC) was measured as 6.8×10^{-3} mol dm^{-3} using conductivity and fluorescence measurements, indicating that the MWCNT and DBS solution contains both the DBS monomer and micelles.

The bi-layers were successfully formed with the formation of an initial PPy-Tartrate or PPy-Oxalate film at copper from near neutral 0.10 mol dm^{-3} oxalate or 0.10 mol dm^{-3} tartrate solutions with 0.30 mol dm^{-3} pyrrole at 0.75 V vs. SCE for 300 s. Then, the PPy-DBSCNT film was deposited at 0.75 V vs. SCE from the MWCNT and DBS solution with 0.30 mol dm^{-3} pyrrole for an additional 300 s period. Multi-layers were formed with alternating layers of PPy-Tartrate or PPy-Oxalate and PPy-DBSCNT formed for 300 s to give a total electropolymerisation period of 1200 s. Four consecutive layers were deposited to give the multi-layers. The PPy-Tartrate/DBSCNT and PPy-Oxalate/DBSCNT films were formed slightly different. The PPy-Tartrate or PPy-Oxalate modified electrodes were placed in the MWCNT-containing DBS solution and a fixed potential was applied and the MWCNT layer was adsorbed at the surface.

The corrosion protection properties of the polymer coatings PPy-Tartrate/PPy-DBSCNT, PPy-Tartrate/DBSCNT, PPy-Oxalate/PPy-DBSCNT and PPy-Oxalate/DBSCNT multi-layers were assessed using a spectrophotometric determination of the dissolved copper concentration, open-circuit potential measurements, anodic polarisation plots and cyclic voltammetry. Excellent corrosion protection properties were observed with the tartrate-based system, with the PPy-Tartrate/PPy-DBSCNT and PPy-Tartrate/DBSCNT multi-layers providing similar corrosion

protection. Breakdown of the polymer films was only observed at approximately 0.80 V vs. SCE, while the open-circuit potential measurements illustrate long-term corrosion protection properties exceeding 30 days. The spectrophotometric analysis was consistent with these measurements, showing low concentrations of dissolved copper and very good corrosion protection properties. However, lower breakdown potentials were recorded with the oxalate-based system and the corrosion protection properties were lost following a 15-day immersion period in 0.10 mol dm^{-3} NaCl. To demonstrate the overall corrosion capabilities of the tartrate-based polymers a scratch in the polymer film was made to expose the copper substrate. Dissolution of copper was observed giving higher currents, indicating a loss in the corrosion protection properties of the films. However, it is clear that the tartrate-based polymer system exhibits very good corrosion protection for the copper substrate, giving stable and highly adherent PPy films. This coinsides with the protection of the copper metal obtained from these coatings. The polypyrole forms adherent polymer coatings at the copper surface which is detailed in the previous chapter 3. The incorporation of the MWCNTs dispersed in DBS enhances the protection properities of the coating to a greater extent than observed in Chapter 3.

CHAPTER 5

Synthesis and Analysis of the DBS Polymer Film

In the following chapter, the results of an investigation into the formation and protective nature of a PPy bi-layer are presented and discussed. This bi-layer consists of an initial layer of PPy with tartrate as the dopant and an outer layer of PPy formed in the presence of dodecylbenzene sulfonate (DBS), to give PPy-Tartrate/PPy-DBS. The structure of the DBS is considerably larger and is shown in Figure 5.1a. Nevertheless, it contains sulfur which is easily detected in the polymer film using energy dispersive X-Ray analysis (EDX). It is clear that the tartrate is sufficiently small with a negative charge to give an ideal dopant, Figure 5.1b.

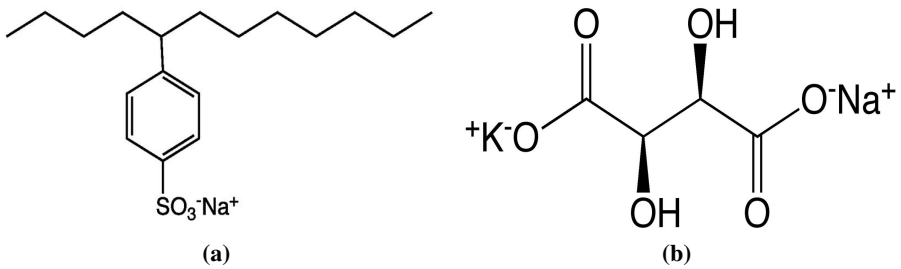

Figure 5.1: Chemical structures of anions (a) sodium dodecylbenzene sulfonate (DBS) and (b) sodium potassium tartrate.

This bi-layer structure with PPy-DBS as the outer layer was selected for further study as the MWCNT coating developed and discussed in Chapter 4, PPy-Tartrate/PPy-DBSCNT, has very good corrosion protection properties. However, as DBS was used to disperse the MWCNTs, it

was difficult to determine if the DBS or MWCNT was responsible for the corrosion protection observed. Indeed, when the MWCNTs were removed from the electropolymerisation solution and the protective properties of PPy-Tartrate/PPy-DBS and PPy-Tartrate/PPy-DBSCNT were compared very similar results were obtained, as shown in Figure 5.2. These data were recorded in a neutral 0.10 mol dm^{-3} NaCl solution at 1 mV s^{-1}, and it is clear that the two polymer films have similar breakdown potentials and very good corrosion protection properties, making it difficult to differentiate between the two polymer films and the role of the MWCNTs.

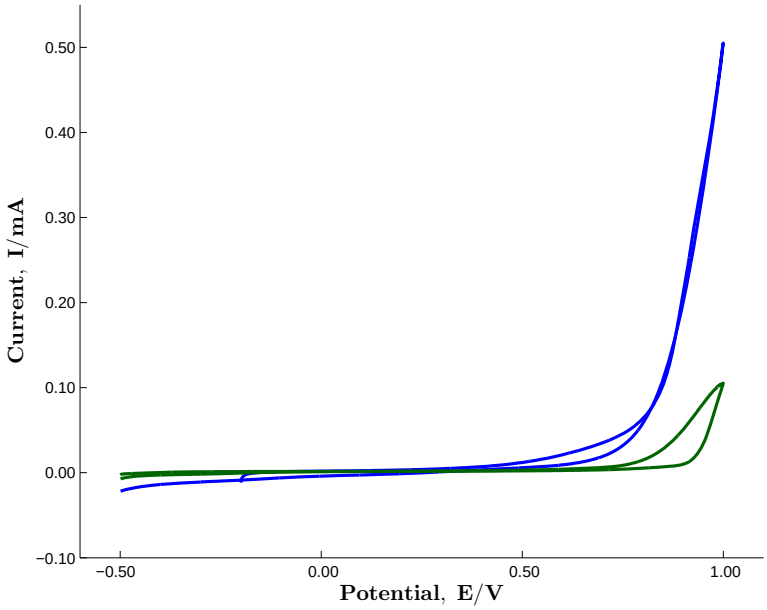

Figure 5.2: Cyclic voltammograms recorded at 1 mV s^{-1} in 0.10 mol dm^{-3} NaCl at a pH of 7.0 for the PPy-Tartrate/PPy-DBS (green) and PPy-Tartrate/PPy-DBSCNT (blue).

Accordingly, in this chapter, a more in-depth study on the development and analysis of the PPy-Tartrate/PPy-DBS polymer coating is carried out. The concentration of DBS, the applied potential, and the electropolymerisation period were varied to obtain the optimum experimental conditions to deposit the PPy-Tartrate/PPy-DBS films at copper. Then, the corrosion protection properties of the coating were assessed using open-circuit potential (OCP) measurements, polarisation plots, Tafel analysis and electrochemical impedance spectroscopy (EIS).

5.1 Experimental

Details on the experimental approach used in the formation and analysis of the PPy-Tartrate/PPy-DBS films at the copper electrodes are provided in Sections 5.1.1, 5.1.2 and 5.1.3.

This includes information on the chemicals, the techniques and equipment used and the general procedures employed to deposit the polymer films.

5.1.1 Reagents

Pyrrole monomer (98%) was obtained from Aldrich and was purified by distillation prior to use. It was then stored in the dark at -20 °C between experiments, for a maximum period of five days. The analytical reagents, sodium chloride (NaCl), dodecylbenzene sulfonate (DBS) ($C_{12}H_{25}C_6H_4SO_3Na$), sodium potassium tartrate ($KNaC_4H_4O_6$), hydrochloric acid (HCl) and sodium hydroxide (NaOH) were purchased from Aldrich and used as received. The pH meter was calibrated on a daily basis, with buffers specifically for the calibration of the pH meter (pH 4.0 and pH 7.0) which were purchased from Lennox Ltd.

5.1.2 Electrodes and Instruments

A Cu rod (99.99%, 4 mm in diameter) electrode was used for the deposition of PPy-Tartrate/PPy-DBS. The rod was encased in a Teflon holder, as previously described in Chapter 2, Figure 2.3. A flat Cu disc electrode was used for SEM and EDX measurements. The disc and rod electrodes were polished using a 1 μm diamond polish and Buehler micro-cloth and rinsed well with distilled water to ensure a smooth surface finish, as outlined in Chapter 2. A saturated calomel electrode (SCE) was used as the reference electrode and a high surface area platinum wire was employed as the counter electrode. A CHi 760C potentiostat was used to deposit the PPy films, while potentiodynamic polarisation measurements were carried out with a Solartron potentiostat (Model SI 1285 or 1287), using the software package Corrware for Windows. Electrochemical impedance spectroscopy (EIS) measurements were recorded using a Solartron Model SI 1285 or Model SI 1287 potentiostat coupled with a frequency response analyser, Model SI 1250. A potential perturbation of 10 mV was used to ensure a pseudo-linear response of the system, while the frequency was varied from 65 kHz to 10 mHz. SEM measurements were performed on a Hitachi FE-scanning electron microscope, with an Oxford instruments Inca X-act 4.12 software package. The EDX analyses were carried out using an EDX Model 51-ADD0009 with the software package Micro Analysis Suite.

5.1.3 Procedures

The PPy-Tartrate/PPy-DBS coating was formed by depositing an initial layer of PPy doped with tartrate. Then, the PPy film doped with DBS was formed to give a bi-layer structure. The PPy-Tartrate film was deposited at 0.75 V vs. SCE from an aqueous solution of 0.10 mol dm^{-3} sodium potassium tartrate and 0.30 mol dm^{-3} pyrrole adjusted to a pH of 7.0, using a few drops of concentrated NaOH. The electropolymerisation period was fixed at 600 s. The PPy-DBS films were deposited at 0.75 V vs. SCE from a neutral aqueous solution containing 0.050 mol dm^{-3} DBS and 0.30 mol dm^{-3} pyrrole, unless otherwise stated. Distilled water was used in the preparation of all solutions and all measurements were made at room temperature. In some experiments the concentration of DBS was varied from 0.001 to 0.090 mol dm^{-3}, while the applied potential was varied from 0.65 to 0.90 V vs. SCE and the electropolymerisation period was varied between 100 and 1200 s. In an attempt to deposit PPy-DBS directly at the copper electrode, the pH was varied between 5.0 and 9.0 and applied potentials from 0.60 to 0.90 V vs. SCE were used.

After electrochemical deposition, the PPy films were characterised using cyclic voltammetry, by cycling in a potential window from -0.50 to 1.00 V vs. SCE, at 1 mV s^{-1} in 0.10 mol dm^{-3} NaCl at pH 7.0. A scratch in the PPy-Tartrate/PPy-DBS coating was made using a sharp surface and the corrosion protection properties were compared to a freshly deposited polymer coating. For SEM and EDX characterisation, the polymer films were synthesised onto a Cu disc electrode. Unless otherwise stated, the samples were sputter coated with gold prior to SEM analysis. Electrochemical impedance spectroscopy measurements were carried out in 0.10 mol dm^{-3} NaCl, at pH 7.0 using a sinusoidal excitation voltage of 10 mV. The impedance of the bi-layer film and uncoated copper was recorded at various applied potentials.

5.2 Results and Discussion

5.2.1 Formation of the Bi-layer Polymer Films

The polymers were deposited at a constant applied potential of 0.75 V vs. SCE. The main advantage of this potentiostatic technique is that the applied potential can be varied to control the rate of electropolymerisation, while variations in the electropolymerisation period give

rise to polymer films of different thickness. Although cyclic voltammetry is normally used to generate compact conducting polymer films [112], potentiostatic deposition, is well known to yield polymers with consistent and reproducible morphologies [112, 245]. The tartrate doped PPy, PPy-Tartrate, was deposited from 0.30 mol dm^{-3} pyrrole and 0.10 mol dm^{-3} tartrate, at pH 7.0. The solution was not stirred as this inhibits electropolymerisation at the electrode interface, although oxidation of pyrrole proceeds. Nucleation of the polymer at the electrode occurs only when the length of the oligomer chain surpasses the solubility limit and deposits on the electrode surface [316]. Thus solution stirring would disperse the radical species into the bulk solution, inhibiting the electropolymerisation reactions.

The current-time plots recorded on application of 0.75 V vs. SCE to the copper electrode in the pyrrole and tartrate-containing solution are shown in Figure 5.3. The growth profile is typical for the electropolymerisation of pyrrole in a simple dopant solution and reasonably good reproducibility is observed, as shown from a comparison of the plots. Although not clearly evident in the current-time plots presented in Figure 5.3, on application of the potential to the electrode there is an initial charging current, which arises from the charging of the double layer. This charging current decays rapidly, being governed by the R_sC time constant, which, in turn, is related to the size of the electrode and the conductivity of the solution, where C is the double layer capacitance and R_s is the solution resistance [41]. Other factors that might contribute to the current during the initial milliseconds are the oxidation of pyrrole to form oligomeric species, which are still soluble and/or adsorption of pyrrole at the electrode interface [317, 318]. It is also likely that dissolution of copper occurs during this early period to contribute to the current [6]. However, once the polymer begins to nucleate at the surface, the dissolution of the copper substrate is inhibited and the current decays to lower values in the region of 1.0×10^{-4} A. No further increase in the current is observed, indicating that the deposited polymer prevents the dissolution of the copper substrate. The concentration of pyrrole used in all these experiments, which is 0.30 mol dm^{-3}, is sufficiently high to promote a fast initiation step for the polymerisation reaction. Accordingly the dissolution of copper is limited.

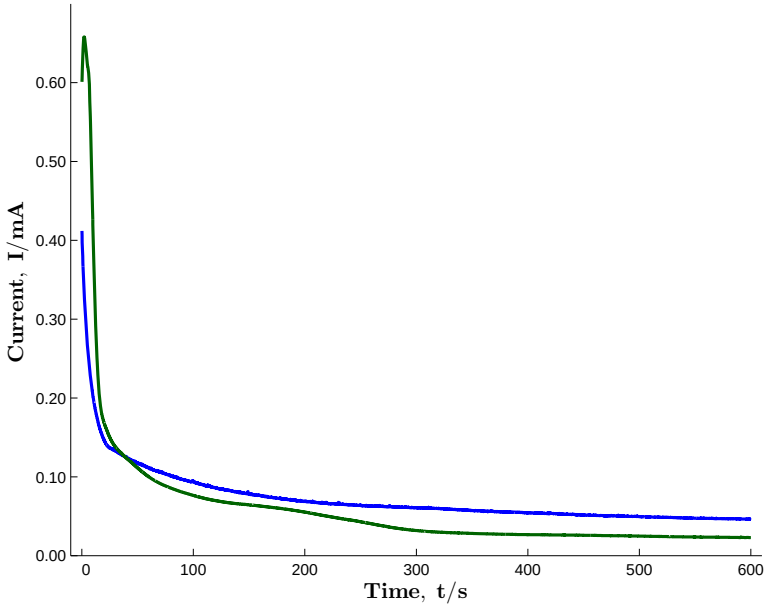

Figure 5.3: Current-time transient recorded for Cu polarised at 0.75 V vs. SCE in 0.30 mol dm^{-3} pyrrole and 0.10 mol dm^{-3} tartrate at a pH of 7.0 (blue and green).

The protective properties of the deposited polymer can be seen by comparing the current-time plots in Figure 5.3 with the data recorded in the absence of the pyrrole monomer, Figure 5.4. The current-time plot depicted in Figure 5.4 was recorded on polarising copper in 0.10 mol dm^{-3} tartrate at pH 7.0 at 0.75 V vs. SCE. There is a noticeable difference in the current-time transients recorded in the absence and presence of pyrrole and it is clear that the PPy-Tartrate polymer coating is stable and reasonably protective. At pH 7.0, oxides, such as Cu_2O, CuOH and CuO, are formed [32, 278, 285]. It is well known that the composition and stability of the passive film is pH dependent [32], and in solutions of pH 6.0 to 9.0, the oxide films (Cu_2O and CuO) become more protective. Indeed, Strehblow *et al.* [278] documented that Cu forms passivating layers in alkaline solutions. Therefore, at pH 7.0, and in the presence of tartrates, the rate of copper dissolution is significantly lower than that observed in more acidic solutions and in the presence of chloride anions [8, 51, 86, 282]. The tartrate ion has been used as a complexing agent in the electrodeposition of copper, giving high quality electrodeposits [244]. At pH 7.0, the ion exists as $C_4H_4O_6^{2-}$ as the pKa value is 3.77 for the equilibrium shown in Equation 5.1.

$$C_4H_5O_6^{1-} \rightarrow C_4H_4O_6^{2-} + H^+ \tag{5.1}$$

Ballesteros *et al.* [244] have carried out a thermodynamic analysis of the copper(II)-tartrate chloride system and have shown that as the pH increases, there is a higher tendency for the formation of hydroxyl tartrate containing complex species, Equation 5.2.

$$Cu^{2+} + 2OH^{-} + 2C_4H_4O_6^{2-} \rightarrow Cu(C_4H_4O_6)_2(OH)_2^{4-} \tag{5.2}$$

Indeed at pH 7.0, this complex is the predominate species and as the copper is dissolved and the Cu^{2+} ion concentration increases, the hydroxyl-tartrate complex is formed and this will limit the dissolution of copper. This is consistent with the data presented in Figures 5.3 and 5.4.

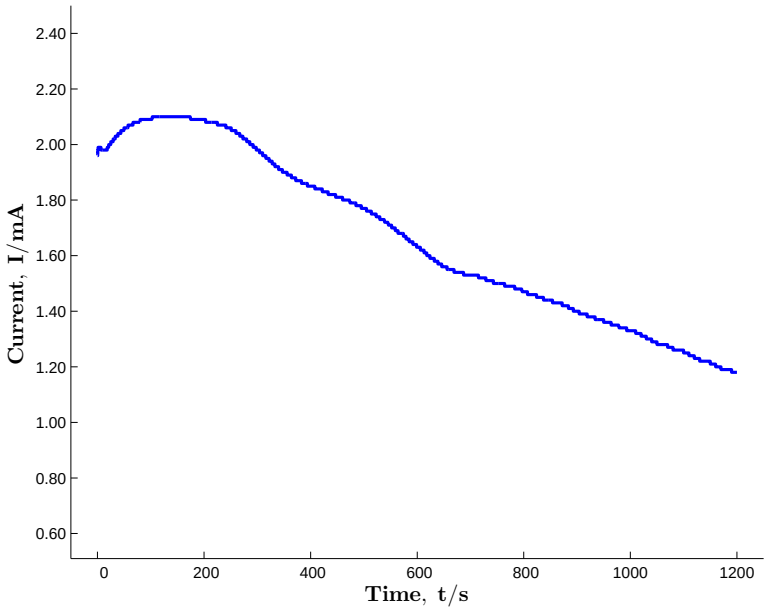

Figure 5.4: Current-time transient recorded for Cu polarised at 0.75 V vs. SCE in 0.10 mol dm^{-3} NaCl at a pH of 7.0.

The deposition of the PPy-DBS polymer film at the PPy-Tartrate modified copper to generate the bi-layer was carried out in a 0.050 mol dm^{-3} solution of DBS with 0.30 mol dm^{-3} pyrrole at 0.75 V vs. SCE. A representative current-time plot, is shown in Figure 5.5. From this plot is it obvious that the growth of the PPy-DBS film adopts a different shape in comparison to that of the tartrate-doped PPy film, Figure 5.3. However, this is probably connected to the electropolymerisation of pyrrole at the PPy-Tartrate interface. Indeed, the growth of the PPy-DBS polymer adopted a slightly different profile from experiment to experiment. However, similar characteristics and currents were recorded in all experiments. As the polymer is

deposited on top of the PPy-Tartrate base, the current is initially low, but then increases from about 200 s, indicating that the resistance of the PPy-Tartrate is sufficiently low to facilitate the electropolymerisation of the monomer and the formation of further layers of PPy. The current continues to increase. This is probably connected to the further deposition of PPy giving a higher surface area and higher currents. These rising currents may also be due to dissolution of the copper substrate, however significant dissolution was not observed. Indeed, given the corrosion protection properties of this bi-layer, as shown in Figure 5.2, it is unlikely that significant dissolution of the copper substrate occurs on deposition of the PPy-DBS film.

It is clear from the data presented in Figure 5.5 that the currents measured during the formation of PPy-DBS are lower compared to the values recorded with the tartrate system, Figure 5.3. It appears that the rate of electropolymerisation is slower in the presence of DBS. This may be related to binding of the DBS to the polymer layer already present (PPy-Tartrate), as DBS has surfactant-like properties. Alternatively it may be connected to the slower rate of diffusion of the large DBS species to the electrode surface.

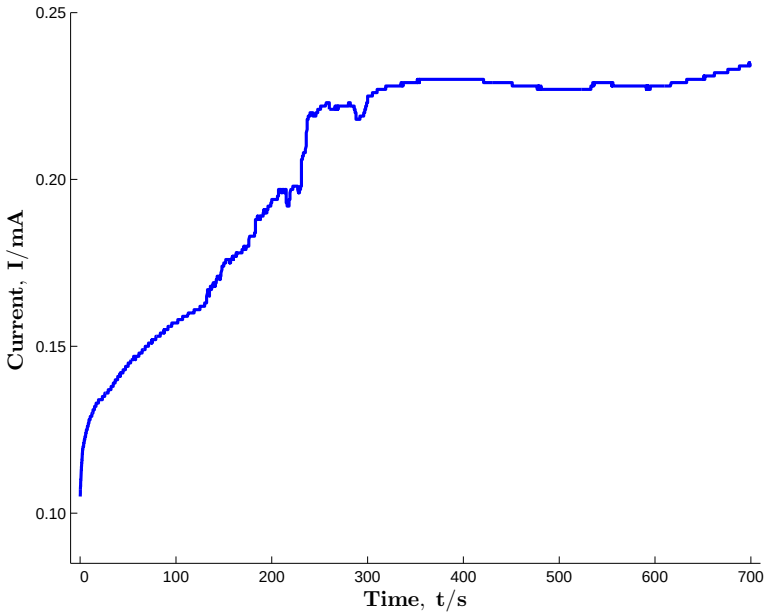

Figure 5.5: Current-time transient recorded at 0.75 V vs. SCE in 0.050 mol dm^{-3} DBS and 0.30 mol dm^{-3} pyrrole at PPy-Tartrate-modified Cu.

Once the PPy-Tartrate/PPy-DBS films were formed, the polymers were cycled in 0.10 mol dm^{-3} NaCl at pH 7.0 at 1 mV s^{-1}, as detailed in Figure 5.2. A typical voltammogram for the uncoated copper is shown in Figure 5.6. Dissolution of copper is observed at about -0.05 V

vs. SCE. The current continues to increase to reach a maximum value of 0.30 mA at about 0.04 V vs. SCE and then decays to give a relatively broad peak. This peak has been explained in terms of the dissolution of copper and the formation of chloride-containing species, such as CuCl and the soluble $CuCl_2^-$ species [282, 319, 320, 321]. As the CuCl complex species are formed and deposited at the surface [280, 322], the current decays [165], but then increases to reach high values in the vicinity of 1.1 mA cm^{-2}. This indicates significant dissolution of the copper and the generation of Cu(II) species at the higher potentials. Indeed, there is a noticeable fluctuation in the current from 0.20 to 0.60 V vs. SCE and this is consistent with the formation of corrosion products and oxides, CuOH, CuCl and CuO [32, 278, 285], with the current increasing as the copper is dissolved and decaying as the surface is protected with the corrosion products. Ingelgem *et al.* [285] showed, from the analysis of the composition of the corrosion product layers, that the corrosion product layer is porous and consists of both copper oxides and chlorides, with higher concentrations of chloride in the outermost layer. Different compositions, with higher concentrations of chlorides and lower levels of Cu_2O, were found at sites of localised corrosion, indicating different rates of dissolution.

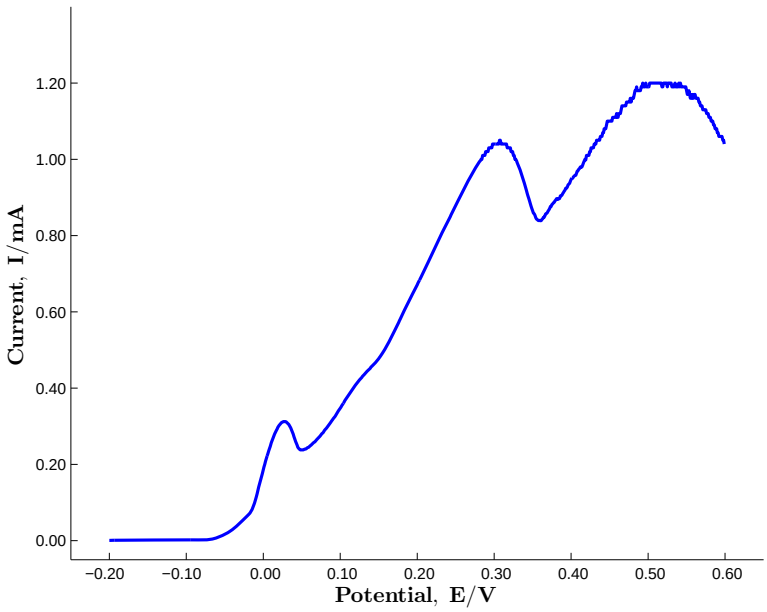

Figure 5.6: Cyclic voltammogram recorded at 1 mV s^{-1} in 0.10 mol dm^{-3} NaCl, at a pH of 7.0, for Cu.

The protective properties of the PPy-Tartrate/PPy-DBS bi-layer film and the PPy-Tartrate film are shown and compared in Figure 5.7. The PPy-Tartrate was deposited from 0.30 mol dm^{-3} pyrrole at 0.75 V vs. SCE for 600 s, while the PPy-Tartrate/PPy-DBS bi-layer was formed on depositing PPy-DBS onto the PPy-Tartrate layer in 0.30 mol dm^{-3} pyrrole and 0.050 mol dm^{-3} DBS at 0.70 V vs. SCE for an additional 600 s. Very good corrosion protection properties are observed with the PPy-Tartrate/PPy-DBS film, in agreement with the data presented in Figure 5.2. Breakdown of the film occurs at approximately 0.80 V vs. SCE. However, the protective properties of the PPy-Tartrate film are somewhat different. Clearly, the PPy-Tartrate polymer film is not as stable as the PPy-Tartrate/PPy-DBS bi-layers. The dissolution of the copper substrate is visible at potentials of about 0.10 V vs. SCE. The current continues to increase at higher potentials, but it is clear from a comparison of Figures 5.6 and 5.7 that the currents are significantly lower than those recorded for the uncoated copper. This indicates that while the PPy-Tartrate film has a relatively low breakdown potential, significant dissolution of the copper is not observed.

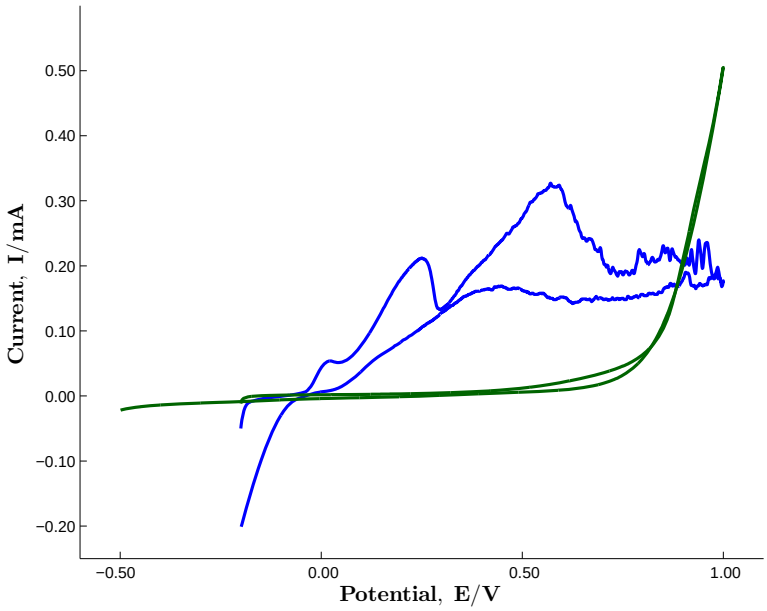

Figure 5.7: Cyclic voltammograms recorded at 1 mV s^{-1} in 0.10 mol dm^{-3} NaCl, at a pH of 7.0, for PPy-Tartrate (blue) and PPy-Tartrate/PPy-DBS (green), where the PPy-DBS was formed at 0.70 V vs. SCE for 600 s.

The PPy-Tartrate film was formed for an additional 600 s to increase the film thickness and although the data are not shown, more protective PPy-Tartrate films were obtained. In this case, the PPy-Tartrate films remained stable until potentials in the vicinity of 0.50 V vs. SCE

were applied. However, it is clear that the formation of the additional PPy-DBS layer, to give the bi-layers, gives rise to a significant increase in the corrosion protection properties of the polymer. It is clear from a comparison of Figure 5.6 with the data presented in Figures 5.2 and 5.7 that the PPy-Tartrate/PPy-DBS bi-layer is highly protective and limits the dissolution reactions of copper and the build-up of corrosion products at the copper surface.

These cyclic voltammetry tests were also used to ensure that the electrochemical technique and solution compositions employed in the formation of the bi-layer gave consistent and reproducibility films. While the level of reproducibility was generally high, some variations were obtained. Representative data are shown in Figure 5.8 and it is clearly evident that a different voltammogram indicating very poor reproducibility is obtained in Figure 5.8a. In this case, the bi-layer was formed under identical conditions, with the initial PPy-Tartrate film deposited at 0.75 V vs. SCE for 600 s, followed by the PPy-DBS film at 0.90 V vs. SCE for 300 s. However, a highly protective film is obtained in one experiment, while dissolution of copper is evident at potentials higher than 0.05 V vs. SCE in the second experiment, giving very poor corrosion protection properties.

In an attempt to increase the reproducibility of the bi-layer, variations in the solution temperature, from 15 to 25 °C, the pyrrole concentration, from 0.10 to 0.40 mol dm^{-3}, the electropolymerisation period, from 300 to 1200 s, the applied potential, from 0.65 to 0.90 V vs. SCE, and the pH of the solution, from pH values of 6.0 to 8.0, were made during the formation of the bi-layer. However, data similar to that shown in Figure 5.8a were recorded. Furthermore, the purity of the water was considered and the solutions were prepared in distilled and de-ionised water. However, no significant improvement in the reproducibility was obtained. Finally, excellent reproducibility was achieved on preparing new solutions for each experiment. Typical plots, which were recorded when new solutions were prepared for each polymer film, are shown in Figure 5.8b. In this case, highly reproducible voltammograms are obtained and in all cases the bi-layer shows very good corrosion protection properties, with breakdown of the film and dissolution of the copper substrate observed at about 0.80 V vs. SCE. Consequently, new solutions were prepared for all subsequent experiments and the data presented correspond to freshly prepared solutions.

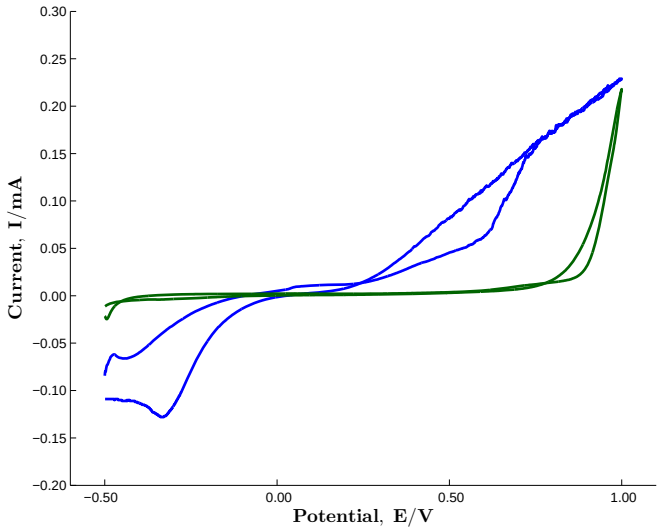

(a)

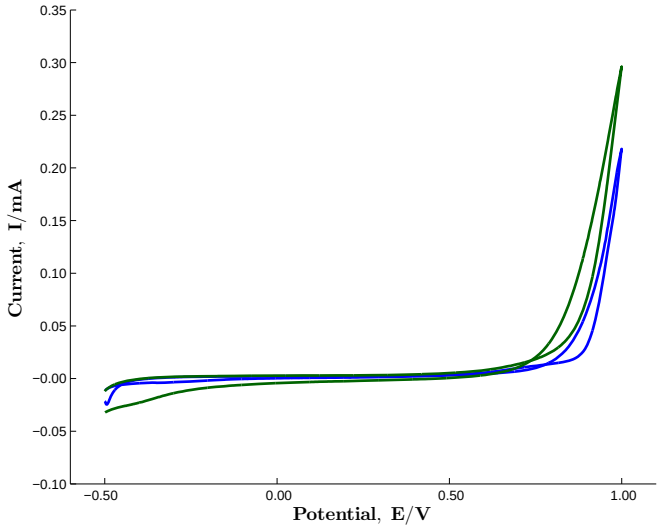

(b)

Figure 5.8: Cyclic voltammograms recorded at 1 mV s^{-1} in 0.10 mol dm^{-3} NaCl, at a pH of 7.0, for PPy-Tartrate/PPy-DBS formed at 0.75 V vs. SCE for a total period of 600 s and PPy-DBS deposited at 0.90 V vs. SCE for 300 s (a) aged solutions (green) compared to a fresh solution (blue) and (b) freshly prepared solutions (green) and (blue).

5.2.2 Influence of the Applied Potential and Electropolymerisation Time

The influence of the applied potential and the electropolymerisation period on the corrosion protection properties of the PPy bi-layer was studied. It is well known that the applied potential has a significant influence on the rate of electropolymerisation [139, 144] and that longer electropolymerisation periods give rise to polymer films with increasing thickness [132]. Electropolymerisation proceeds faster at higher applied potentials although the resistance of the films may increase due to over-oxidation of the polymer backbone [139, 323]. Lewis and co-workers [324] showed that over-oxidation of PPy begins at 0.65 vs. SCE, at pH 6.0, but becomes more significant at potentials higher than 0.80 V vs. SCE.

The PPy-Tartrate film was deposited at 0.75 V vs. SCE for 600 s, while the PPy-DBS film was formed at potentials varying from 0.60 to 0.90 V vs. SCE and for time periods ranging from 100 to 1200 s. EDX spectra recorded for the bi-layer polymer film deposited at 0.70 and 0.90 V vs. SCE are compared in Figure 5.9. These data were recorded after several washings of the bi-layer to remove any adsorbed DBS from the surface. It is clearly evident, from the intense sulfur signal that DBS has indeed been incorporated within the PPy bi-layer. The influence of the applied potential is also clearly evident. The ratio of the sulfur to copper signal is considerably higher for the bi-layer formed at 0.90 V vs. SCE. This is consistent with the formation of a thicker polymer film at 0.90 V vs. SCE. The PPy-Tartrate/PPy-DBS bi-layer formed at 0.70 V vs. SCE is sufficiently thin to observe X-Rays from the copper substrate, however the higher rate of electropolymerisation at 0.90 V vs. SCE gives a sufficiently thick PPy-DBS layer and the X-Rays from the copper substrate are no longer detected. It is also clear from these EDX spectra, in particular the spectrum presented in Figure 5.9b, that there is little evidence for dissolved copper ions within the polymer matrix. Although, the PPy-Tartrate film was polarised at 0.90 V vs. SCE to deposit the PPy-DBS layer, there is no evidence to support the dissolution of copper and the generation of copper ions which are dispersed throughout the polymer matrix.

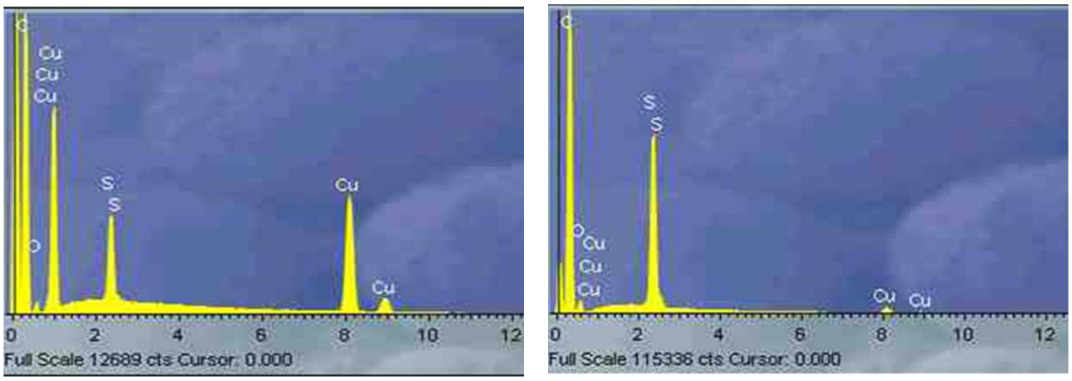

(a) **(b)**

Figure 5.9: (a) EDX spectrum of PPy-Tartrate/PPy-DBS with the PPy-DBS layer formed at 0.70 V vs. SCE and (b) EDX spectrum of PPy-Tartrate/PPy-DBS with the PPy-DBS layer formed at 0.90 V vs. SCE.

The influence of the electropolymerisation period is summarised in Figures 5.10 and 5.11. In these experiments the PPy-Tartrate layer was deposited at 0.75 V vs. SCE and the PPy-DBS film was formed at 0.70 or 0.90 V vs. SCE for different time periods, ranging from 100 to 1200 s. The data presented in Figure 5.10 show that there is little difference in the protective properties of the bi-layer, when the PPy-DBS layer is deposited at 0.75 V vs. SCE for 700 or 800 s. Although not shown, similar voltammograms were recorded for electropolymerisation periods from 300 to 1000 s, which indicated that this was the optimum electropolymerisation period. Indeed, when the PPy-DBS film was deposited for 100 or 200 s, dissolution of the copper substrate was observed, while somewhat less protective bi-layer films were formed with times greater than 1000 s, as shown in Figure 5.10. A similar trend was observed at 0.90 V vs. SCE, Figure 5.11. In this case, highly protective bi-layer films were obtained at 300 and 400 s, with breakdown potentials higher than 0.80 V vs. SCE. However, when the electropolymerisation period was increased to 500 s, breakdown of the bi-layer film was observed at about 0.40 V vs. SCE. This shows that the optimum electropolymerisation period at 0.90 V vs. SCE is between 300 and 400 s.

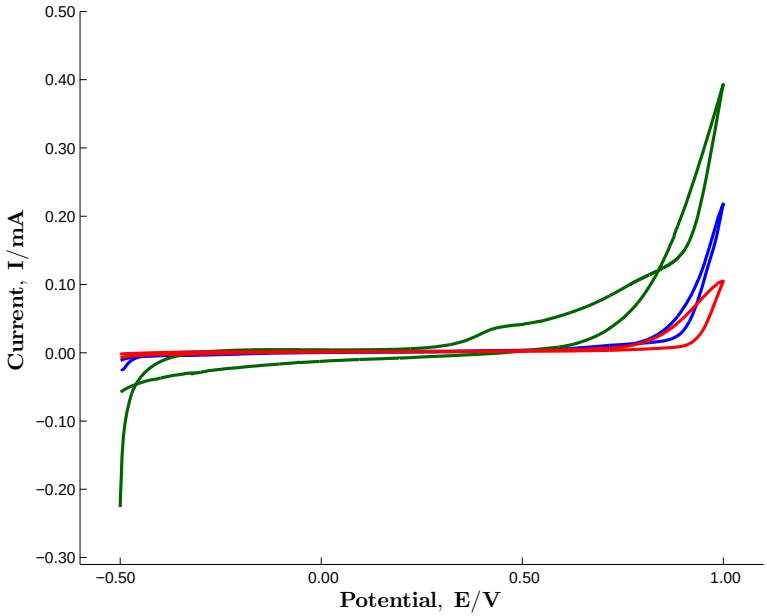

Figure 5.10: Cyclic voltammograms recorded at 1 mV s^{-1} in 0.10 mol dm^{-3} NaCl, at a pH of 7.0, for PPy-Tartrate/PPy-DBS, the PPy-Tartrate was formed at 0.75 V vs. SCE for 600 s and the PPy-DBS was deposited at 0.70 V vs. SCE for 700 s (red), 800 s (blue) and 1200 s (green).

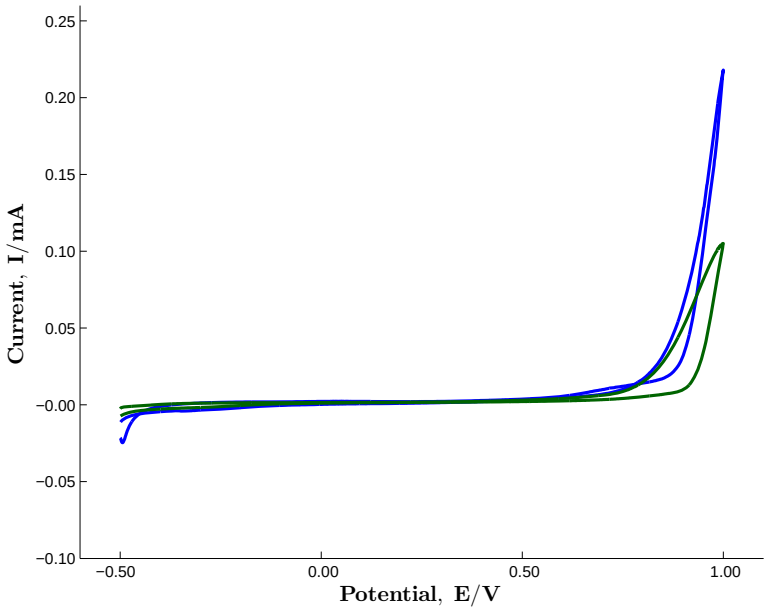

Figure 5.11: Cyclic voltammograms recorded at 1 mV s^{-1} in 0.10 mol dm^{-3} NaCl, at a pH of 7.0, for PPy-Tartrate/PPy-DBS, the PPy-Tartrate was formed at 0.75 V vs. SCE for 600 s and the PPy-DBS was deposited at 0.90 V vs. SCE for 300 s (green) and 400 s (blue).

5.2.3 Influence of the Concentration of DBS

The influence of the concentration of the DBS on the formation and protective properties of the PPy-Tartrate/PPy-DBS bi-layer was studied by varying the concentration of the DBS in the electropolymerisation solution [325]. The PPy-Tartrate film was deposited in 0.10 mol dm^{-3} tartrate at 0.75 V vs. SCE for 600 s, and then the PPy-DBS film was formed at 0.70 V vs. SCE for 600 s in solutions containing DBS at concentrations ranging from 0.001 to 0.090 mol dm^{-3}. The bi-layered PPy films were then cycled in 0.10 mol dm^{-3} NaCl and the results are shown in Figure 5.12. The concentration of DBS appears to have a clear influence on the protective properties of the bi-layer, with the DBS concentration at 0.050 mol dm^{-3} giving the more protective film, as shown in Figure 5.12a and Figure 5.12b. In all cases, the bi-layer inhibits the dissolution of the copper substrate, but the breakdown potentials depend on the concentration of DBS, with breakdown of the film observed at about 0.35 V vs. SCE, with 0.009 mol dm^{-3} DBS, indicating poor corrosion protection properties. There is a significant increase in the breakdown potential as the concentration of the DBS is increased, to give more protective films. However, at relatively high concentrations, of 0.090 mol dm^{-3}, slightly lower breakdown potentials are measured compared to that recorded with 0.050 mol dm^{-3} DBS. It is clear that formation of the PPy-DBS film in 0.050 mol dm^{-3} DBS gives the best corrosion protection properties.

It is also evident from the cyclic voltammograms presented in Figure 5.12 that the magnitude of the reduction currents, measured about -0.05 to -0.50 V vs. SCE, depends on the concentration of DBS in the electropolymerisation solution. Lower reduction currents are measured at the higher DBS concentrations, indicating that the DBS inhibits the cathodic reduction reactions. This is in good agreement with previous literature reports. For example, Kellou-Kerkouche *et al*. [326] have shown that DBS blocks the cathodic sites, and this gives rise to the suppression of the hydrogen evolution reaction. It is well known that the inhibition efficiency increases with increasing surfactant concentration until it reaches a maximum at the critical micelle concentration, CMC [201, 207, 327]. However, Kellou-Kerkouche *et al.* [326] reported that high inhibitor efficiency was obtained at concentrations above the CMC. This is in good agreement with previous reports in the literature [328].

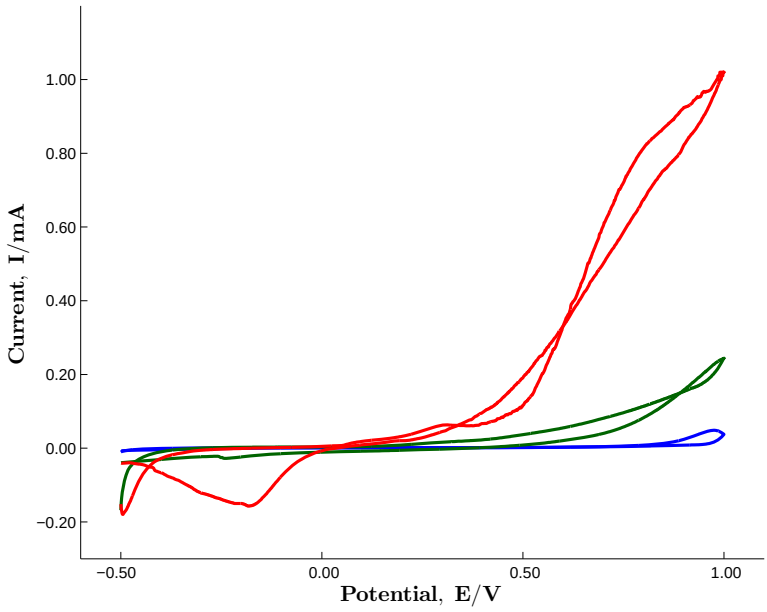

(a)

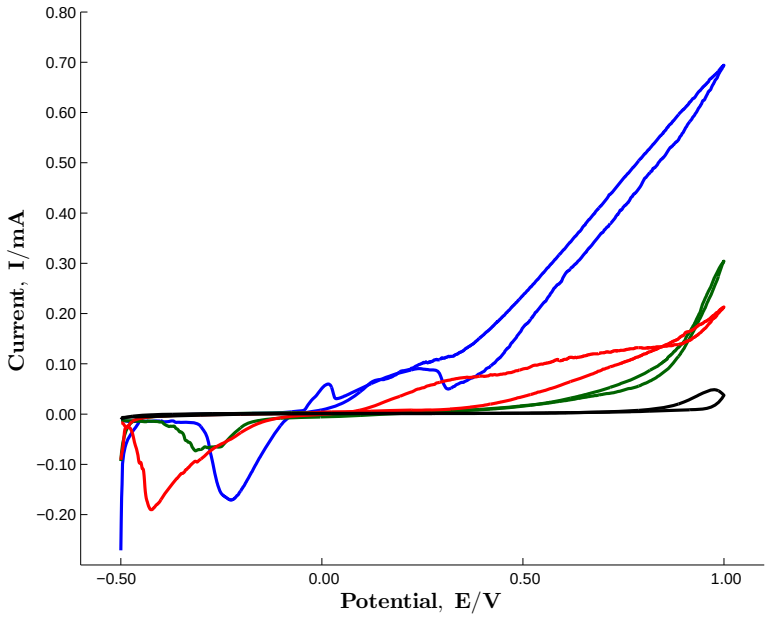

(b)

Figure 5.12: Cyclic voltammograms recorded at 10 mV s^{-1} in 0.10 mol dm^{-3} NaCl, at a pH of 7.0 for PPy-Tartrate/PPy-DBS, the PPy-Tartrate was formed at 0.75 V vs. SCE for 600 s and the PPy-DBS was deposited at 0.75 V vs. SCE in the presence of (a) 0.010 (red), 0.050 (blue) and 0.090 (green) mol dm^{-3} DBS, (b) 0.005 (blue), 0.009 (green), 0.001 (red) and 0.050 (black) mol dm^{-3} DBS.

5.2.4 Morphology of the PPy-Tartrate/PPy-DBS Bi-layer

The morphology of the PPy-Tartrate/PPy-DBS films formed with different concentrations of DBS was studied using scanning electron microscopy (SEM). The films were prepared and washed carefully to remove any adsorbed DBS or monomer from the surface, then dried under a stream of air. A thin gold layer was sputter deposited onto the films to minimise charging, while the EDX spectra were recorded in the absence of the sputtered gold film. The PPy-Tartrate layer was deposited at 0.75 V vs. SCE from 0.10 mol dm^{-3} tartrate for 600 s, and then the PPy-DBS layer was formed at 0.75 V vs. SCE for 600 s in the presence of DBS at concentrations varying from 0.001 to 0.090 mol dm^{-3}. The SEM micrographs are presented in Figures 5.13 for the PPy-DBS film prepared in 0.005 mol dm^{-3} DBS, while micrographs recorded under similar conditions but with different DBS concentrations are presented in Figure 5.14, Figure 5.15, Figure 5.18, Figure 5.19 and Figure 5.20.

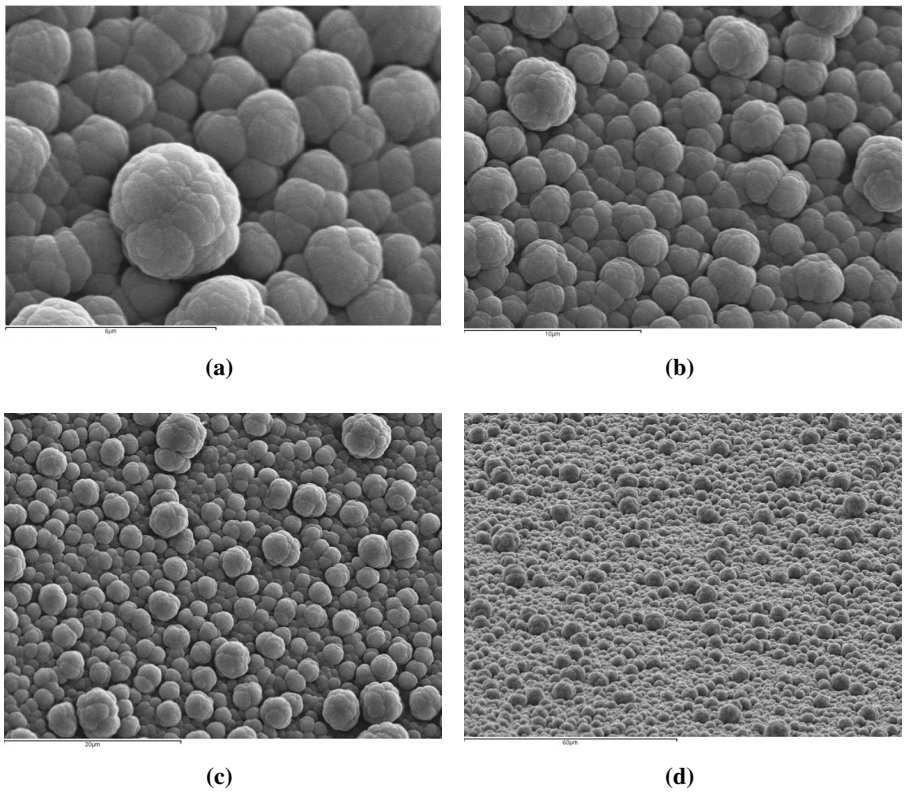

(a) **(b)**

(c) **(d)**

Figure 5.13: SEM micrographs recorded for the PPy-Tartrate/PPy-DBS film, where the PPy-DBS layer was formed at 0.75 V vs. SCE for 600 s in 0.005 mol dm^{-3} DBS, (a) scale bar corresponds to 10 μm, (b) scale bar corresponds to 6 μm, (c) the scale bar corresponds to 20 μm and (d) the scale bar corresponds to 60 μm.

The micrographs presented in Figure 5.13, show that a homogeneous and adherent polymer film is deposited with 0.005 mol dm^{-3} DBS. The morphology is similar to that of PPy doped with simple anionic dopants, such as Cl^-, giving the typical cauliflower morphology [145, 245]. The size of the cauliflower structures varies somewhat with the larger structures reaching diameters of about 3.1 μm, while the smaller structures are approximately 1.5 to 2.0 μm in diameter. EDX spectra were recorded and spectra similar to that depicted in Figure 5.9 were obtained, confirming the presence of DBS within the polymer bi-layer. The % weight distributions of copper, sulfur and oxygen were found to be approximately 12.0, 5.1 and 5.8%, respectively, clearly showing that the DBS is incorporated within the PPy-DBS layer.

The surface morphology of the bi-layer film when the PPy-DBS film was formed in 0.009 mol dm^{-3} DBS is depicted in Figure 5.14, while similar data recorded with a 0.090 mol dm^{-3} DBS solution are presented in Figure 5.15. Again, the cauliflower morphology is evident. However, the size and diameter of the cauliflower structures are significantly larger at the higher DBS concentration. At a DBS concentration of 0.090 mol dm^{-3}, the diameters vary from 9 to 12 μm, but again a uniform film is formed across the entire electrode, as shown from the micrograph at lower magnification, Figure 5.15b. The cauliflower structures with a diameter of about 2 μm, which is similar to that seen in Figure 5.13 were obtained with 0.009 mol dm^{-3} DBS.

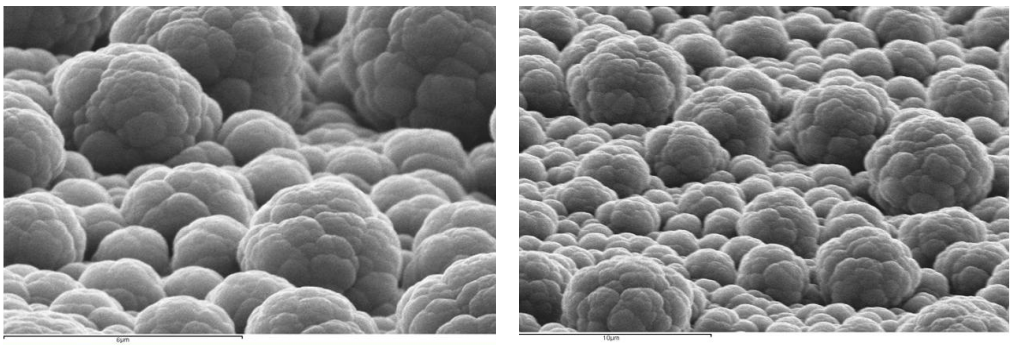

(a) **(b)**

Figure 5.14: SEM micrographs recorded for the PPy-Tartrate/PPy-DBS film, where the PPy-DBS layer was formed at 0.75 V vs. SCE for 600 s in 0.009 mol dm^{-3} DBS, (a) scale bar corresponds to 6 μm, (b) scale bar corresponds 10 μm.

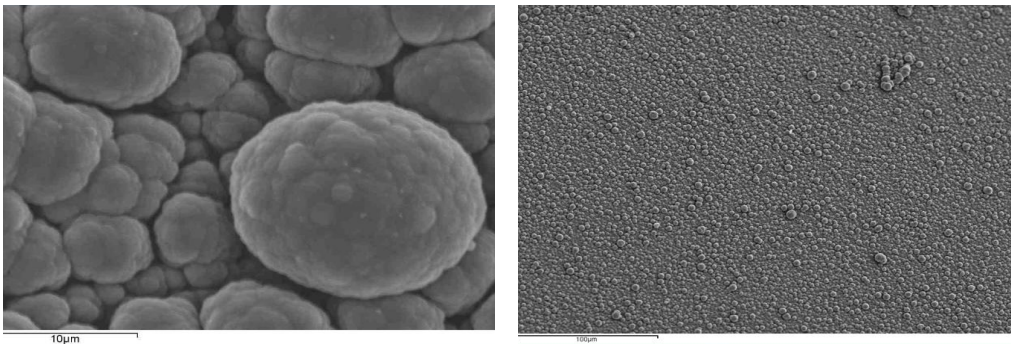

(a) **(b)**

Figure 5.15: SEM micrographs recorded for the PPy-Tartrate/PPy-DBS film, where the PPy-DBS layer was formed at 0.75 V vs. SCE for 600 s in 0.090 mol dm^{-3} DBS, (a) scale bar corresponds to 10 μm, (b) scale bar corresponds to 100 μm.

Again, EDX spectra were recorded for the PPy-DBS film, formed in the presence of 0.009 mol dm^{-3} DBS, and again, sulfur was clearly evident in the spectra. The % weight distributions of copper, sulfur and oxygen were found to be approximately 6.1, 4.9 and 6.8%, respectively, clearly showing that the DBS is incorporated within the PPy-DBS layer. These ratios are similar to those found with the lower DBS concentration of 0.005 mol dm^{-3}, indicating little variation in the composition of the film from 0.005 to 0.009 mol dm^{-3} DBS.

In Figure 5.16, data are presented for the PPy-DBS film deposited from 0.009 mol dm^{-3} DBS, where the distribution of copper, sulfur and oxygen are shown across the area highlighted in Figure 5.16a. In this figure the darker areas represent lower levels of the element, while higher concentrations of the element are indicated by the lightly coloured segments. The mapping profile for copper shows that more copper is detected at the base of the cauliflower structures, while the darker middle region, where the cauliflower structures are seen, give a lower count for copper. This indicates slight variations in the thickness of the bi-layer film. The oxygen signal shows a similar trend, with lower levels of oxygen at the base of the cauliflower structure. Interestingly, the sulfur appears to be uniformly dispersed across the mapping area, indicating that the DBS is incorporated with the PPy-DBS film in a uniform manner. Similar data were recorded for the 0.005 and 0.090 mol dm^{-3} DBS concentrations, giving high levels and uniform distributions of sulfur across the surface.

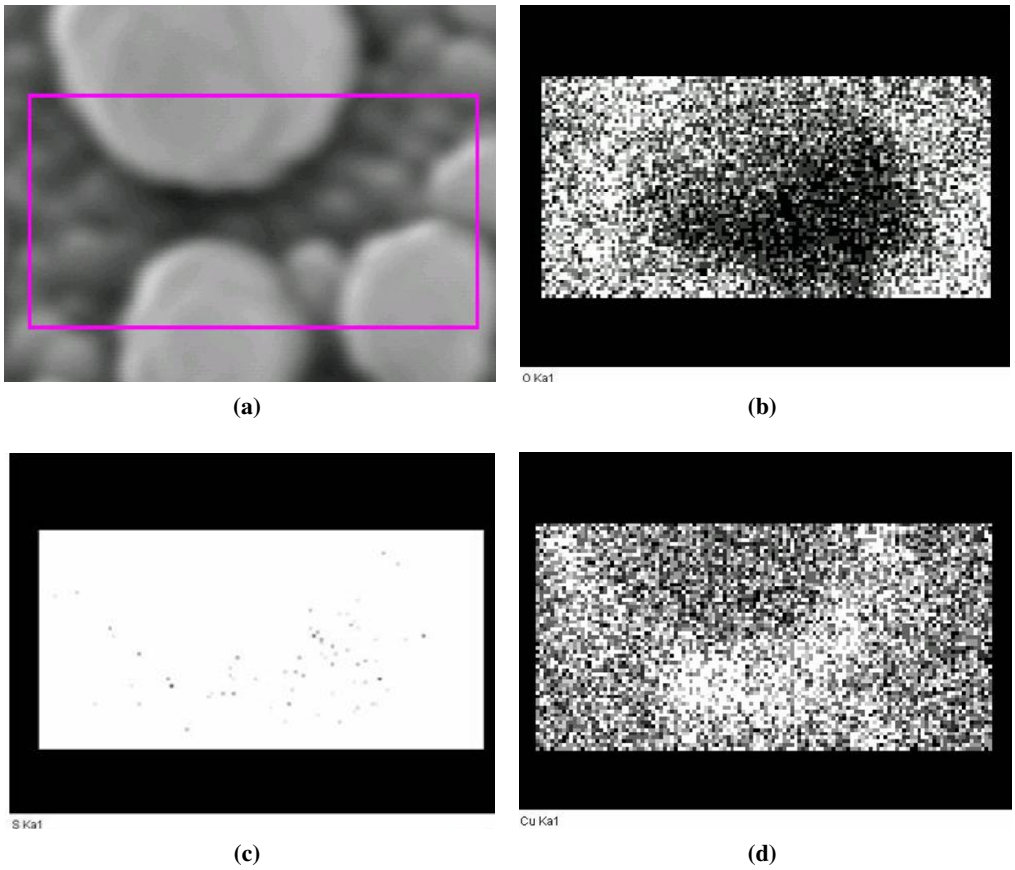

Figure 5.16: Analysis of the PPy-Tartrate/PPy-DBS film, where the PPy-DBS layer was formed at 0.75 V vs. SCE for 600 s in 0.009 mol dm^{-3} DBS (a) area selected for mapping, (b) distribution of Cu, (c) distribution of sulfur and (d) distribution of oxygen, where the white coloured segments indicate the presence of the element.

The EDX spectrum presented in Figure 5.17 corresponds to the surface morphology of the bi-layer formed in the presence of 0.010 mol dm^{-3} DBS shown in Figure 5.18. The morphology of the film is shown in Figure 5.18a and Figure 5.18b and again the cauliflower morphology is evident [26, 245]. The surface appears homogeneous, crack and defect free [1] and the entire surface is covered with structures that resemble cauliflower which vary in size [26]. The diameter of the cauliflower structures is approximately 1 to 3 μm, which is similar to that recorded at the lower DBS concentrations, observed in Figure 5.13, and considerably smaller than the diameters obtained at 0.090 mol dm^{-3} DBS, Figure 5.15. In Figure 5.18c and Figure 5.18d cross sections are shown and these were used to give an approximate film thickness. Using this approach the thickness of the bi-layer was found to range from 1.8 to 3.0 μm.

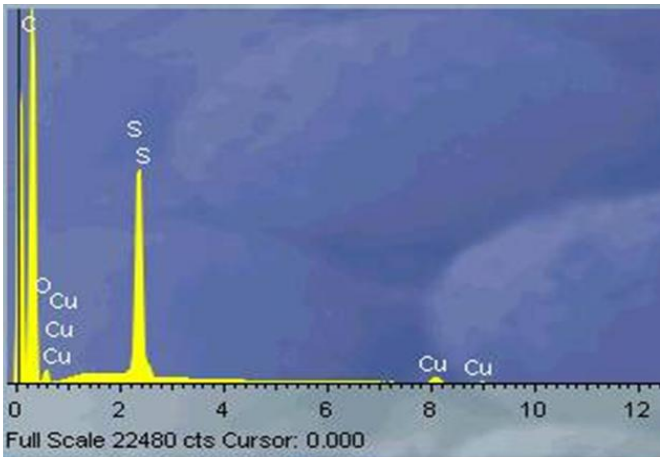

Figure 5.17: EDX spectrum recorded of PPy-Tartrate/PPy-DBS bi-layer, where the PPy-DBS layer was formed at 0.75 V vs. SCE for 600 s in 0.010 mol dm^{-3} DBS.

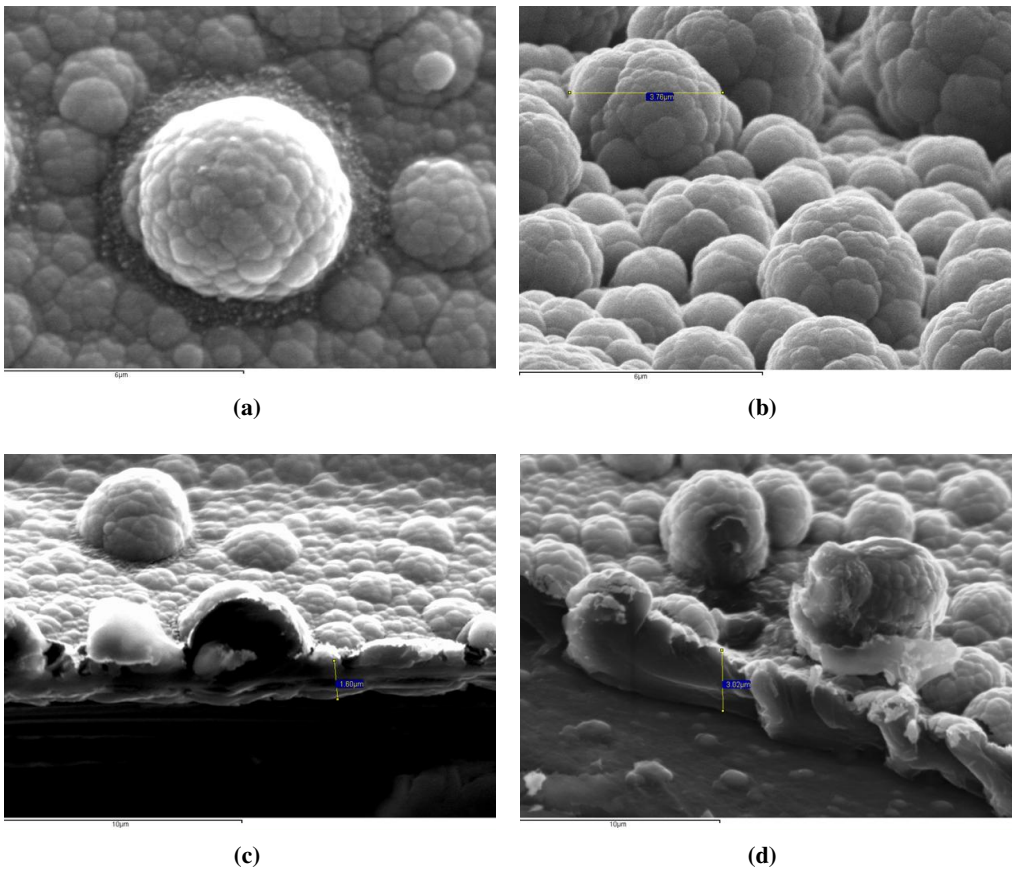

(a) **(b)**

(c) **(d)**

Figure 5.18: SEM micrographs recorded for the PPy-Tartrate/PPy-DBS film, where the PPy-DBS layer was formed at 0.75 V vs. SCE for 600 s in 0.010 mol dm^{-3} DBS, (a) scale bar corresponds to 10 μm, (b) the scale bar corresponds to 6 μm, (c) and (d) cross-sectional areas for determination of polymer thickness.

The EDX spectrum recorded for PPy-Tartrate/PPy-DBS formed in a solution containing 0.010 mol dm^{-3} DBS is shown in Figure 5.17. This is similar to the spectra recorded in Figure 5.9, where the PPy-DBS film was deposited from a 0.050 mol dm^{-3} DBS-containing solution. The intensity of the copper is low indicating that the bi-layer is sufficiently thick to block the X-rays from the copper substrate. The presence of the sulfur clearly shows that the DBS is incorporated within the PPy-DBS layer, while the oxygen signal can be attributed to the tartrate and DBS. The carbon peak is possibly due to the PPy and the long carbon chain of the DBS.

The surface morphology of the PPy-Tartrate/PPy-DBS with the PPy-DBS film formed in the presence of 0.001 mol dm^{-3} DBS is shown in Figure 5.19. It can be clearly seen that the surface morphology of the PPy-DBS film is very different. The morphology no longer resembles that of the typical cauliflower morphology of PPy, but instead adopts oval type structures which appear to have voids. Although there are still a few cauliflower structures at this low concentration of DBS, the oval structures are in abundance. As shown in Figure 5.19, the diameter of an oval structure is measured and found to be 2.7 μm in length, indicating relatively large structures.

Although the surface morphology is very different at this low concentration of DBS, the polymer surface is homogeneous, crack and defect free. EDX spectra were recorded, and although not shown here, the sulfur signal was much lower in intensity than that observed in Figure 5.17, while a higher copper count was measured. This indicates that the PPy-DBS films are thin and have a lower amount of DBS incorporated within the PPy-DBS film at this low DBS concentration. Indeed, the % weight distributions of copper, sulfur and oxygen were found to be approximately 30.0, 1.2 and 3.1%, respectively, clearly showing the PPy-DBS film formed with 0.001 mol dm^{-3} is very different to the films formed at the higher concentrations.

The SEM micrographs recorded for the PPy-Tartrate/PPy-DBS bi-layer formed in the presence of 0.050 mol dm^{-3} DBS are presented in Figure 5.20. Again, the characteristic cauliflower morphology is seen at this higher DBS concentration. The diameter of the cauliflower structures is approximately 8 to 12 μm, which is very similar to the diameters calculated for the PPy-DBS film formed in the presence of 0.090 mol dm^{-3} DBS, Figure 5.15. Indeed, it is evident from the micrographs presented in Figures 5.13, 5.14, 5.15, 5.18, 5.19 and 5.20 for the different DBS concentrations that the size and diameter of the cauliflower

structures increase with increasing concentrations of DBS, with the highest diameters observed at 0.090 mol dm^{-3} DBS. Uniform and homogeneous films are formed with DBS concentrations ranging from 0.005 to 0.090 mol dm^{-3} DBS, however the PPy-DBS films formed in the presence of 0.050 mol dm^{-3} DBS, which are shown in Figure 5.20, provide the best corrosion protection, as highlighted in Figure 5.12. This may be related to the size of the cauliflower structures and the compact film structure which is evident in Figure 5.20.

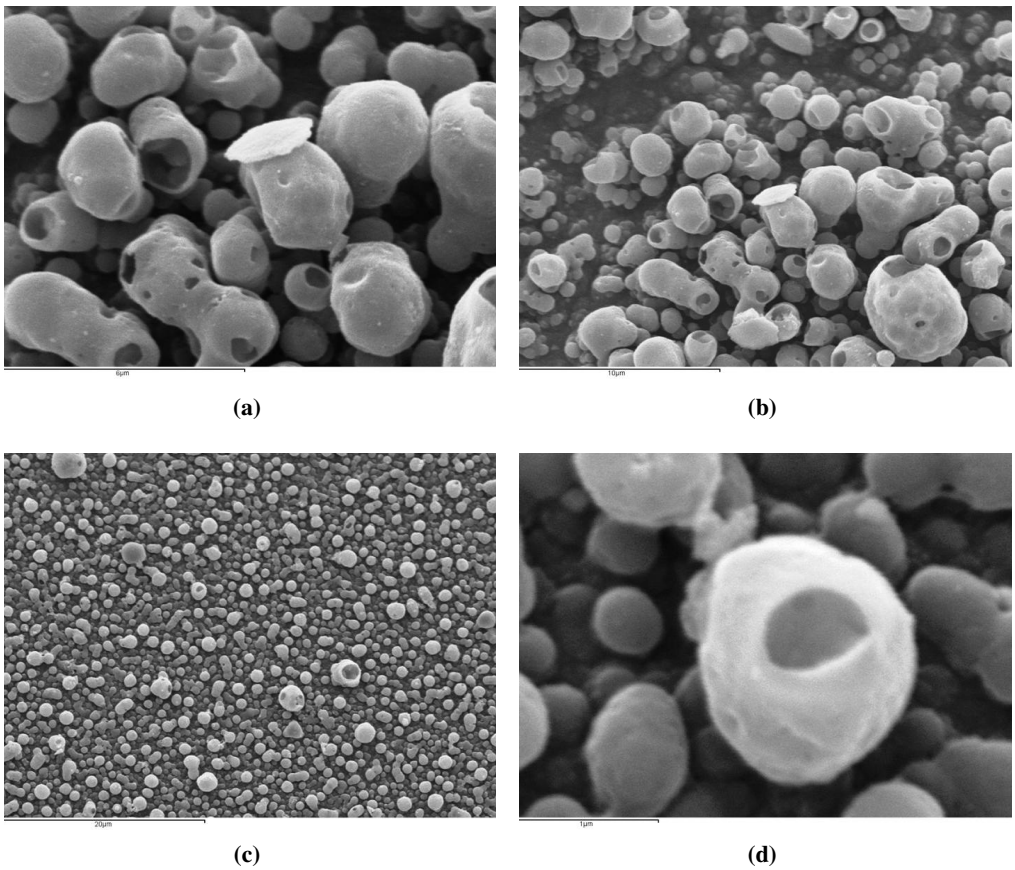

Figure 5.19: SEM micrographs recorded for the PPy-Tartrate/PPy-DBS film, where the PPy-DBS layer was formed at 0.75 V vs. SCE for 600 s in 0.001 mol dm^{-3} DBS, (a) scale bar corresponds to 6 μm, (b) the scale bar corresponds to 10 μm, (c) the scale bar corresponds to 20 μm and (d) the scale bar corresponds to 1 μm.

It is clear from the EDX analyses presented in Figure 5.9 and Figure 5.17 that the DBS is incorporated into the polymer films to balance the charge on the polymer chain. It appears that the large amphiphilic DBS anion is trapped inside the polymer matrix. As the DBS is large and bulky it is not lost during the reduction of the polymer. Instead, reduction of the polymer is accompanied by the ingress of Na^+ cations from the NaCl electrolyte.

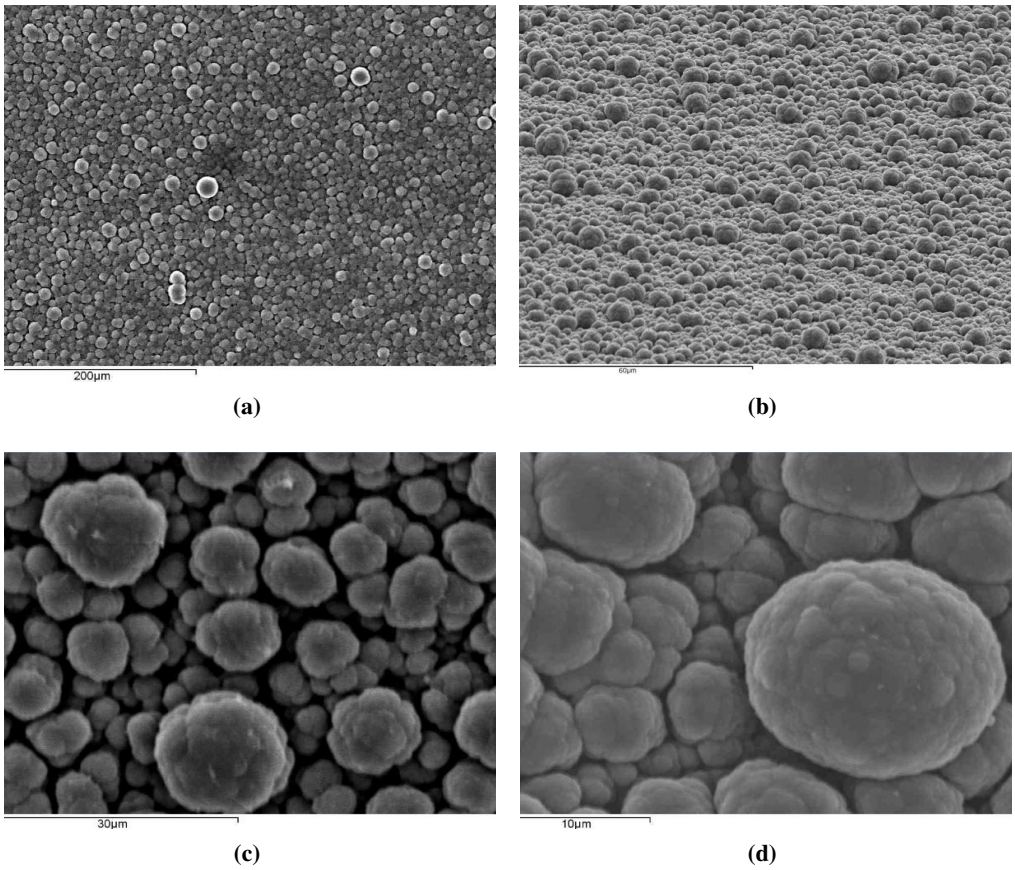

Figure 5.20: SEM micrographs recorded for the PPy-Tartrate/PPy-DBS film, where the PPy-DBS layer was formed at 0.75 V vs. SCE for 600 s in 0.050 mol dm^{-3} DBS, (a) scale bar corresponds to 200 μm, (b) the scale bar corresponds to 60 μm, (c) the scale bar corresponds to 30 μm and (d) the scale bar corresponds to 10 μm.

5.2.5 Preliminary Investigation into the Direct Formation of PPy-DBS at the Copper Interface

It is evident from the results presented that the PPy-DBS films can be deposited onto an initial layer of PPy-Tartrate and that the applied potential, electropolymerisation period and the concentration of DBS in the electropolymerisation solution influence the corrosion protective properties of this bi-layer. To the best of our knowledge, there are no publications on the direct electropolymerisation of pyrrole in the presence of DBS to generate a PPy-DBS polymer at copper. Wang *et al.* [16] have described attempts, but concluded that the formation of PPy-DBS at copper was unsuccessful using electrochemical methods. Instead, the PPy films doped with DBS were prepared on an under layer of PPy doped with oxalate.

Initially, the electropolymerisation of pyrrole at 0.75 V vs. SCE in the presence of 0.050

mol dm^{-3} DBS, at a pH of 7.0 was attempted. Although these experimental conditions were successful in forming the PPy-DBS film at the initial layer of PPy-Tartrate, only the dissolution of copper was observed and there was no evidence of any polymer formation at the copper electrode. The applied potential was lowered in an attempt to reduce the rate of dissolution of the copper substrate, but again there was no evidence of any polymer formation. In order to establish if the pH of the solution had any significant influence, a pH study was carried out [65, 275, 329, 330]. The pH of the DBS solution was varied from 5.0 to 9.0, and the DBS concentration was maintained at 0.050 mol dm^{-3}, while the monomer concentration was fixed at 0.30 mol dm^{-3} pyrrole. Highly adherent PPy-DBS films were observed at a pH of 6.0. Dissolution of the copper was observed at pH values lower than 6.0, and although the copper appeared passive at higher pH values, close to 9.0, poor reproducibility was obtained and in some cases the entire copper surface was not covered with the polymer film.

Typical current-time plots recorded for copper polarised at potentials ranging from 0.60 to 0.90 V vs. SCE in 0.05 mol dm^{-3} DBS and 0.30 mol dm^{-3} pyrrole at a pH of 6.0 are shown in Figure 5.21. These current-time transients are very different to that recorded on the electropolymerisation of pyrrole in the presence of the tartrate anion at a pH of 7.0, Figure 5.3. The current remains high for a significant time period, which appears to depend on the applied potential. For example, the current only decays after about 200 s at an applied potential of 0.60 V vs. SCE. This may be connected to the slow rate of electropolymerisation at this applied potential. This active period is reduced at higher applied potentials, and at 0.80 V vs. SCE, the current decays after approximately 100 s. It is also evident from Figure 5.21 that the near constant currents recorded following this active period increase with increasing potential. This trend may be due to increasing rates of electropolymerisation and the deposition of larger amounts of the conducting PPy-DBS film to give a higher surface area, however it may also be related to increasing rates of copper dissolution at the higher applied potentials. Indeed, at an applied potential of 0.90 V vs. SCE an unusual growth profile is evident. There is a gradual increase in the current after about 400 s and this may be related to the dissolution of copper and the breakdown of the polymer film.

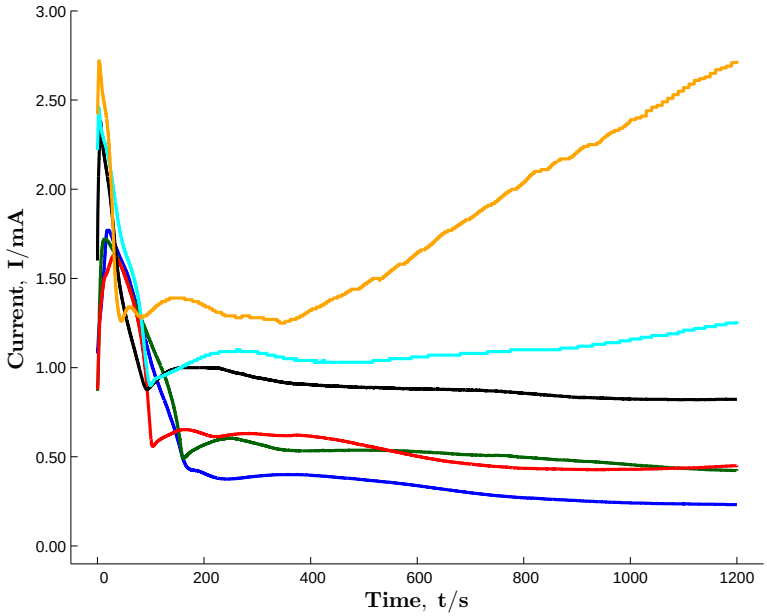

Figure 5.21: Current-time transients recorded for Cu in 0.050 mol dm^{-3} DBS, 0.30 mol dm^{-3} pyrrole, at a pH of 6.0 at 0.60 (blue), 0.65 (green), 0.70 (red), 0.75 (black), 0.80 (light blue) and 0.90 (orange) V vs. SCE.

Nevertheless, very good reproducibility was obtained and nearly identical current-time transients were recorded at 0.90 V vs. SCE, which suggests that the current-time profile may not be connected with breakdown of the film and the dissolution of copper. Indeed, when pure copper was polarised in the absence of the pyrrole monomer, the current remained high during the entire 1200 s period, which shows that the deposited PPy-DBS film inhibits, at least to some extent, the dissolution of the copper. EDX spectra were recorded for the PPy-DBS film formed at 0.90 V vs. SCE and data similar to that shown in Figure 5.17, were obtained, with an intense sulfur peak and little evidence for the presence of copper. This indicates that the PPy-DBS film is sufficiently thick to block the underlying copper from the electron beam. Moreover, there was no evidence of copper-containing corrosion products within the PPy-DBS. Similar data were recorded for the PPy-DBS films formed at the lower applied potentials. The intensity of the sulfur and copper peaks varied with the applied potential, with the intensity of the copper peak decreasing with increasing applied potentials and the intensity of the sulfur peak increasing gradually with increasing applied potential. This is consistent with the higher rates of electropolymerisation and the deposition of thicker PPy-DBS films at the higher applied potentials. In all cases, highly adherent and homogeneous polymer films were obtained.

Further evidence to support this analysis was obtained on cycling the PPy-DBS films

formed at 0.90 V vs. SCE for 1200 s from -0.50 to 1.0 V vs. SCE in 0.10 mol dm^{-3} NaCl at a pH of 7.0. A representative voltammogram is shown in Figure 5.22. This voltammogram is similar to that shown in Figure 5.2, the currents remain low and there is no evidence of any copper dissolution until the PPy-DBS coated copper is polarised to potentials higher than about 0.70 V vs. SCE. These data are consistent with the formation of an adherent and protective PPy-DBS film and there is no evidence to support the dissolution of copper and the formation of copper-containing corrosion products during the formation of the PPy-DBS films at copper.

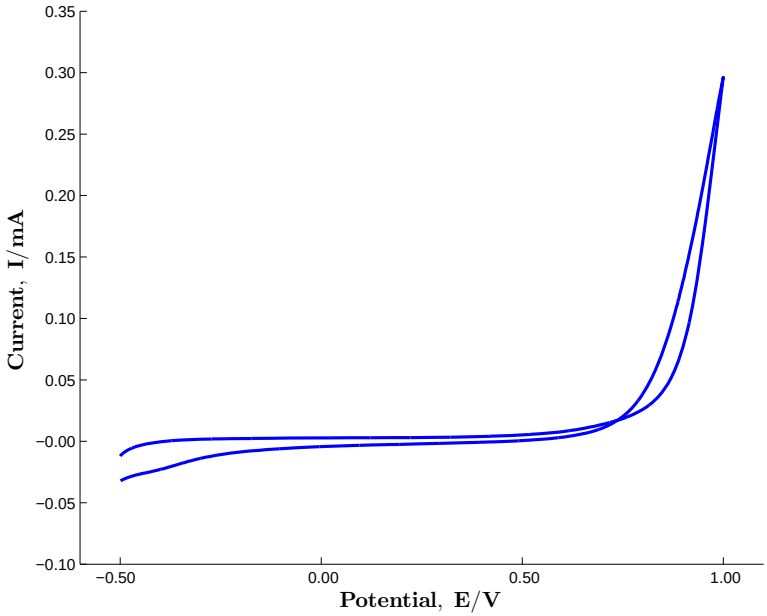

Figure 5.22: Cyclic voltammogram recorded at 1 mV s^{-1} in 0.10 mol dm^{-3} NaCl, at a pH of 7.0, for PPy-DBS formed on Cu at 0.90 V vs. SCE for 1200 s in 0.05 mol dm^{-3} DBS and 0.30 mol dm^{-3} pyrrole.

The corrosion protection properties of the PPy-DBS film deposited at copper and the PPy-Tartrate/PPy-DBS bi-layer formed at copper are compared in Figure 5.23. Adherent and stable films were formed in both cases. The voltammograms were recorded in 0.10 mol dm^{-3} NaCl at 1 mV s^{-1}. Good corrosion protection is observed with both polymer films, however the PPy-Tartrate/PPy-DBS bi-layer gives the best corrosion protection properties with a breakdown potential higher than 0.85 V vs. SCE. In the case of the PPy-DBS film, the currents remain low which suggests that the film protects the copper substrate up to relatively high potentials of about 0.70 to 0.80 V vs. SCE. At this point breakdown of the PPy-DBS film is observed and the polymer is no longer protective and significant dissolution of the copper substrate occurs. It can be clearly observed that although the direct formation of the PPy-DBS polymer can be

achieved at copper, the bi-layer film of PPy-Tartrate/PPy-DBS exhibits the more significant corrosion protection properties.

The data presented in Figure 5.21, Figure 5.22 and Figure 5.23 clearly show that the PPy-DBS film can indeed be formed at copper. However, the successful formation of the film is connected with the pH of the solution, the monomer and DBS concentrations and to a lesser extent, the applied potential. The EDX analyses showed the presence of the DBS within the polymer matrix. This is consistent with the trapping of the DBS within the polymer matrix. DBS is an amphiphilic anion with a polar end that will balance the positively charged oxidised polymer backbone and a hydrophobic chain that is compatible with the neutral polymer matrix. Although not shown, the morphology of the PPy-DBS was similar to that presented in Figure 5.18 and Figure 5.20, with the characteristic cauliflower morphology [26, 245].

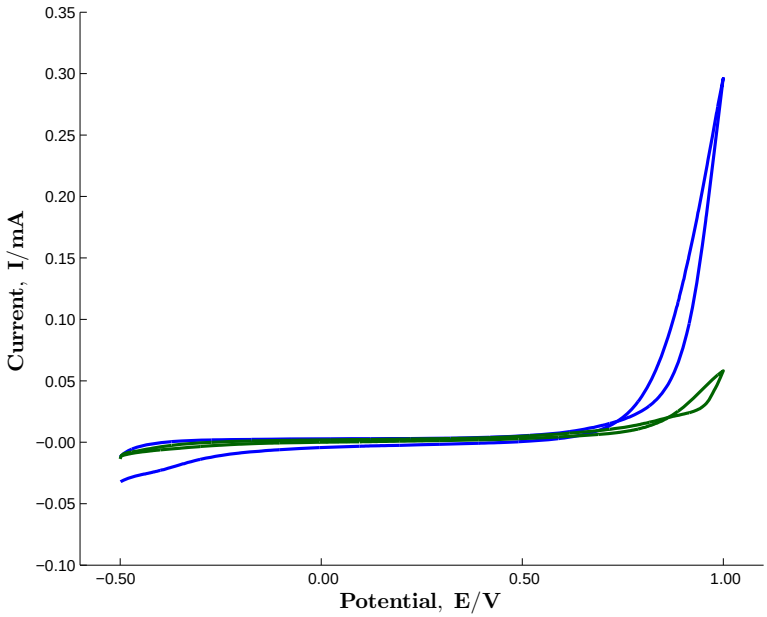

Figure 5.23: Cyclic voltammogram recorded at 1 mV s^{-1} in 0.10 mol dm^{-3} NaCl, at a pH of 7.0, for PPy-Tartrate/PPy-DBS (bi-layer green) formed directly on Cu at 0.90 V vs. SCE for 1200 s in 0.05 mol dm^{-3} DBS and 0.30 mol dm^{-3} pyrrole (PPy-DBS blue).

Wang *et al.* [16] concluded that it was difficult to deposit PPy-DBS at copper. Electropolymerisation was attempted from a 0.10 mol dm^{-3} pyrrole and 0.10 mol dm^{-3} DBS solution. However, dissolution of copper was observed. Indeed, currents as high as 80 mA cm^{-2} were observed in the DBS-containing solution, indicating that passive films could not be formed in the DBS solution. However, Wang *et al.* [16] make no reference to the pH of the solutions or considered variations in the pyrrole and DBS concentrations, or the

ratio of these concentrations. Indeed, it has been reported that the pyrrole monomers are preferentially dissolved into the DBS micellar assembly as a consequence of their hydrophobic nature [325]. Accordingly, the monomers are transported, included in the core of the micelles, to the electrode surface and this will have a significant influence on the rate of electropolymerisation. However, given the concentrations of the monomer used in this study, 0.30 mol dm^{-3} pyrrole, the concentration of free monomers is sufficiently high to give efficient rates of electropolymerisation. This is somewhat different to the concentrations used by Wang *et al.* [16] in their attempts to deposit PPy-DBS at copper.

Han and Shi [296] have reported the formation of a tri-layer conducting polymer composite film, PPy/polythiophene/PPy, comprising PPy doped with perchlorate and PPy layers doped by DBS, PPy-DBS. The PPy-DBS polymer film was deposited first at a stainless steel anode from an aqueous solution of 0.10 mol dm^{-3} pyrrole and 0.10 mol dm^{-3} DBS, with the pH adjusted to between 3.0 and 4.0. Paisal *et al.* [325] generated PPy-DBS films at platinum by scanning the potential between -0.90 and 0.80 V vs. SCE at 20 mV s^{-1} in an aqueous solution containing 0.10 mol dm^{-3} pyrrole and various concentrations of DBS ranging from 0.30 to 0.25 mol dm^{-3}. Careem *et al.* [331] deposited PPy-DBS polymer films at platinum wire in a solution containing 0.050 mol dm^{-3} pyrrole and 0.05 mol dm^{-3} DBS. These reports show that PPy-DBS polymer films can indeed be formed with careful selection of the experimental conditions. However, the deposition of the PPy-DBS film at copper, which is prone to oxidation and dissolution, is more challenging.

As the corrosion protection properties of the PPy-DBS film deposited directly at the copper surface were somewhat less than the bi-layered, PPy-Tartrate/PPy-DBS film, only the more promising bi-layer polymer film was selected for further study. The corrosion protection properties of this bi-layer, formed using the optimum conditions, are presented and discussed in Section 5.3.

5.3 Assessment of the Corrosion Performance of the Polymer Coatings

The corrosion protection properties of the PPy-Tartrate/PPy-DBS bi-layer were assessed and studied using a combination of potentiodynamic polarisation plots, scratch tests, open-circuit

potential measurements, Tafel analysis and electrochemical impedance spectroscopy.

5.3.1 Potentiodynamic Polarisation Measurements

Potentiodynamic polarisation curves are valuable in rapidly identifying the corrosion protection properties of any coating or film [312, 332, 333, 334]. In order to investigate the corrosion protection properties of the PPy-Tartrate/PPy-DBS bi-layer formed at copper, anodic polarisation data were recorded at a pH of 7.0 in a 0.10 mol dm^{-3} NaCl solution [8, 39, 280, 335, 336, 337]. These data were recorded by polarising the electrode from -0.50 V vs. SCE in the anodic direction at a scan rate of 0.1667 mV s^{-1}. Shown in Figure 5.24 are the polarisation data recorded for the PPy-Tartrate/PPy-DBS polymer-modified copper electrodes and the uncoated copper electrode. Evident in the trace for the uncoated copper is the dissolution of copper, this is characteristic of copper in chloride environments due to the formation of corrosion products, such as CuCl, on the surface. These corrosion products offer some protection but this is limited, as the potential is increased further dissolution is observed. These plots depicted for pure copper are consistent with dissolution of copper, with corrosion potentials close to -100 mV vs. SCE and high anodic currents, exceeding 1 mA cm^{-2}, are observed at potentials higher than -50 mV vs. SCE. These data are in good agreement with the analysis carried out by Kear *et al.* [338] who investigated the literature dealing with the electrochemical corrosion characteristics of unalloyed copper in aqueous chloride media. It was shown that at potentials close to the corrosion potential the anodic reaction is under mixed charge transfer and mass transport controlling kinetics, where the mass transport limiting step is the rate of movement of a cuprous chloride complex, $CuCl_2^-$, away from the electrode surface and into the bulk electrolyte. The cathodic reaction is dominated by the comparatively irreversible reduction of oxygen via either a two- or four-electron exchange reaction which remains under complete charge transfer control at potentials close to the corrosion potential. At the corrosion (mixed) potential the anodic reaction is under mixed control, while oxygen reduction is under pure charge transfer control and, as such, the corrosion rate is dependent on mass transport conditions. It was also shown that the corrosion of copper in aqueous chloride media is made complicated by the formation of surface films and these generally act to reduce the rate of both the anodic and cathodic charge transfer processes.

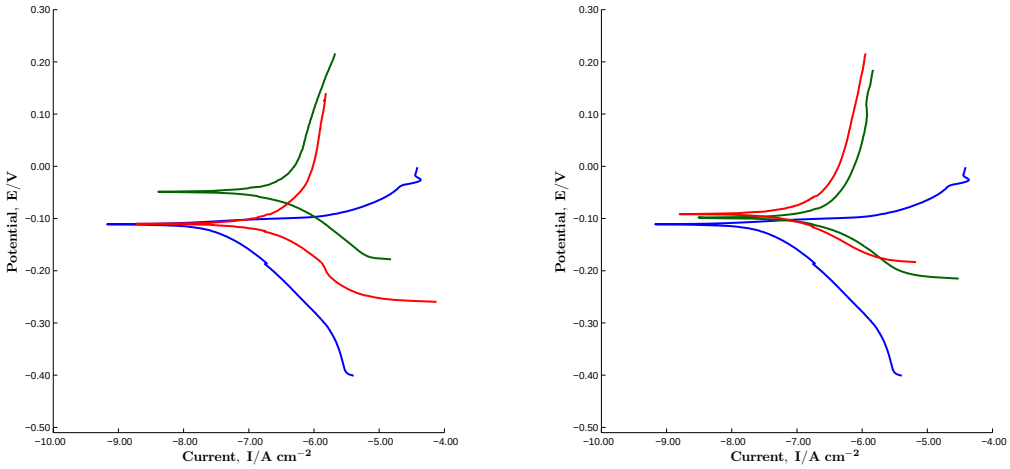

(a) **(b)**

Figure 5.24: Potentiodynamic polarisation plots recorded at 0.1667 mV s^{-1} in pH 7.0, 0.10 mol dm^{-3} NaCl for the uncoated Cu (blue), (a) PPy-Tartrate/PPy-DBS bi-layer with the PPy-Tartrate/PPy-DBS formed at 0.90 V vs. SCE for 300 s (red) and formed at 0.70 V vs. SCE for 700 s (green) and (b) PPy-Tartrate/PPy-DBS bi-layer with the PPy-DBS film formed at 0.70 V vs. SCE for 800 s (green) and formed at 0.90 V vs. SCE for 400 s (red).

The behaviour of the polymer coated copper electrodes is significantly different. It is obvious that the polymer film inhibits the dissolution of copper. Although the reduction half reaction is apparent the oxidation of the metal does not occur until high potential values are reached. The corrosion potential is higher than that observed with the uncoated copper, and occurs at approximately -0.05 V vs. SCE. Although it is not evident in these plots, the breakdown of the polymer film is only observed at potentials in the vicinity of 0.80 V vs. SCE. There is very little difference in the protective properties of the PPy-Tartrate/PPy-DBS films depicted in Figure 5.24. Formation of the PPy-DBS layer at 0.70 V, 0.75 V and 0.90 V vs. SCE, for times ranging from 300 to 700 s has little influence on the protective properties of the bi-layer. In Figure 5.25 the polarisation plots recorded for PPy-Tartrate/PPy-DBS, pure copper and PPy-Tartrate are compared. Higher currents are measured for the PPy-Tartrate film. This is consistent with the data presented in Figure 5.7, which show that the PPy-Tartrate film is less protective that the bi-layer.

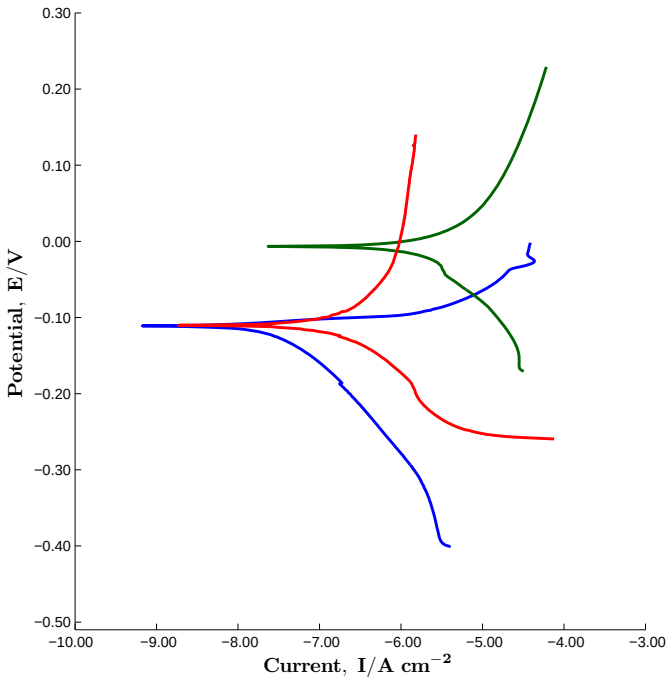

Figure 5.25: Potentiodynamic polarisation plots recorded at 0.1667 mV s^{-1} in pH 7.0, 0.10 mol dm^{-3} NaCl for the uncoated Cu (blue), the PPy-Tartrate/PPy-DBS film where the PPy-DBS layer was formed at 0.70 V vs. SCE for 700 s (red) and the PPy-Tartrate polymer film deposited at 0.75 V vs. SCE for 1200 s (green).

5.3.1.1 Scratch Test Analysis

In order to establish further the stability of the bi-layer polymer film a scratch test was carried out [7, 339]. A small scratch was made in the surface of the bi-layer polymer coating at copper using a sharp object. The polarisation behaviour of the scratched bi-layer coating was then compared to a freshly deposited bi-layer polymer and the results of this study are presented in Figure 5.26 and Figure 5.27. It is clear that the bi-layer polymer film without the scratch is stable and protects the underlying copper from dissolution. This is clearly evident in Figure 5.27, where the potential is increased to values of 1.00 V vs. SCE. However, the data recorded for the scratched bi-layer polymer coating is somewhat different. The polymer film with the scratch has a higher current density and a clear anodic peak is observed at about 0.0 V vs. SCE indicating dissolution of the copper substrate. There is also a shift in the corrosion potential to lower values, which are more typical of the uncoated copper electrode, Figures 5.24 and 5.25. In addition, the breakdown potential for the scratched coating is considerably lower, as shown in Figure 5.27. Indeed, the breakdown potential is about 0.10 V vs. SCE, and at

higher applied potentials dissolution of the copper substrate is observed. These data clearly show that the bi-layer is no longer highly protective when copper is exposed through a scratch in the coating.

Al-Hinai and Osseo-Asare [7] observed similar results on performing scratch tests in the presence of benzotriazole, BTA. Potentiodynamic polarisation curves were recorded for both the scratched and unscratched electrodes and a clear increase in the current, by several orders of magnitude, was observed with the scratched electrode. In addition, the open-circuit potential (OCP) was shifted to more negative potentials, which is consistent with the large increase in anodic current. The negative shift in OCP observed on the scratched electrodes was accompanied by an increase in the corrosion current. This was contrary to the trends observed for the unscratched metal, where the OCP shifts to more positive values and the corrosion current decreases with increasing BTA concentration.

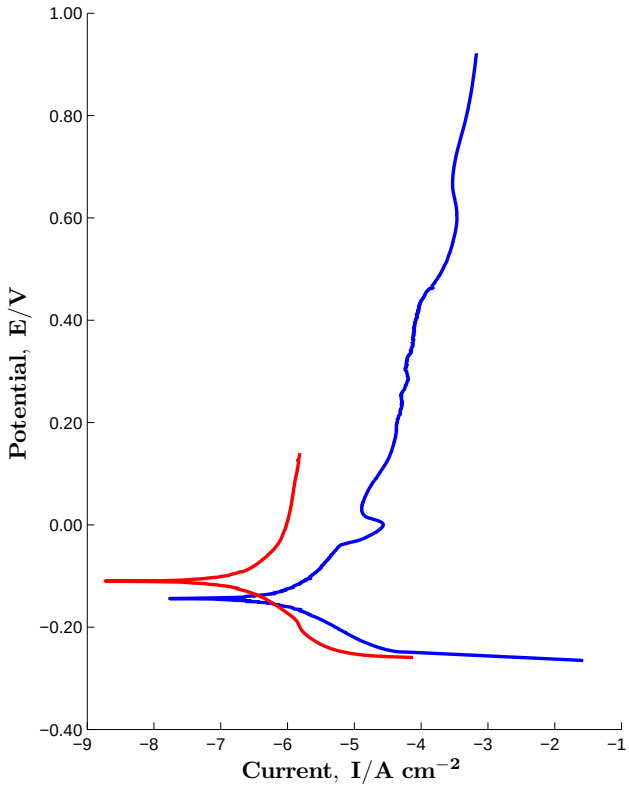

Figure 5.26: Potentiodynamic polarisation plots recorded at 0.1667 mV s^{-1} in pH 7.0, 0.10 mol dm^{-3} NaCl, for the PPy-Tartrate/PPy-DBS film where the PPy-DBS layer was formed at 0.90 V vs. SCE for 300 s, the unscratched bi-layer (red) and the scratched bi-layer (blue).

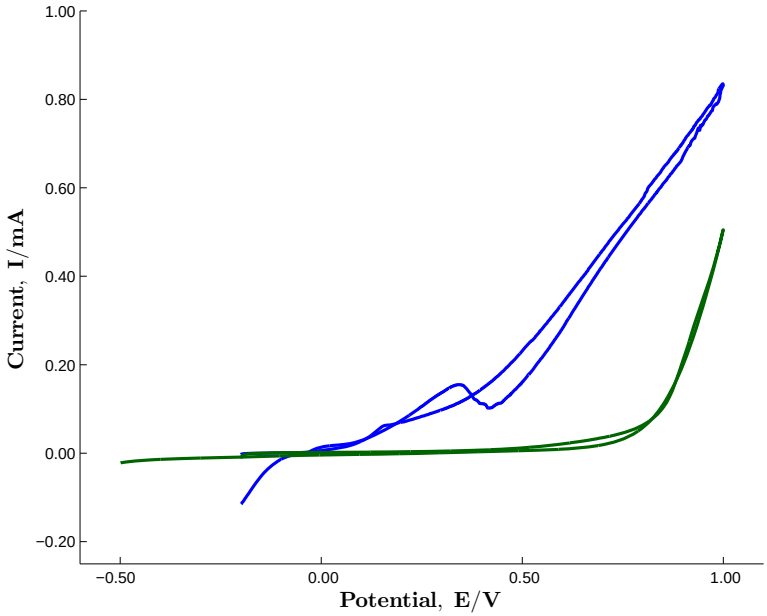

Figure 5.27: Cyclic voltammograms recorded at 0.1667 mV s^{-1} in pH 7.0, 0.10 mol dm^{-3} NaCl for the PPy-Tartrate/PPy-DBS film where the PPy-DBS layer was formed at 0.90 V vs. SCE for 300 s, the unscratched bi-layer (green) and the scratched bi-layer (blue).

5.3.2 Tafel Analysis

A corroding metal in solution adopts a mixed potential, the corrosion potential, E_{corr}, such that the rate of the anodic reaction of the metal dissolution is equal to the rate of the cathodic reaction of hydrogen and/or oxygen reduction. If the potential of the corroding metal is displaced slightly from the corrosion potential, then the potential E is initially a linear function of the current density, I. This linear relationship holds for a potential displacement of about 10 mV. The slope of the linear polarisation curve, dE/dI, is termed the polarisation resistance, Rp [261, 262, 310]. The polarisation resistance is inversely proportional to the rate of corrosion expressed as the equivalent corrosion current density, I_{corr}, Equation 5.3.

$$I_{corr} = B/R_p \tag{5.3}$$

Measurements of the polarisation resistance provide a valuable means of rapidly determining the instantaneous rate of corrosion and the value of the constant B can be determined from weight loss measurements or electrochemical data [309, 310].

As the displacement from the corrosion potential is increased beyond 10 mV, the polarisation curve increasingly deviates from the linear relationship between the potential

and current until a region is reached when the potential exhibits a linear dependence on the logarithm of current density. This behaviour is characteristic of the occurrence of a single electrochemical reaction on the metal surface, either the oxidation half reaction, or the reduction half reaction and the current is related to the overpotential, Equation 5.4. Then, the relationship between the observed potential, E, and current density, I, is given by the Tafel equation, Equation 5.4. This equation can be expressed in the simpler form, as shown in Equation 5.5.

$$E - E_r = \frac{2.303RT}{\alpha F} \log I_0 - \frac{2.303RT}{\alpha F} \log I \tag{5.4}$$

$$E - E_r = a + b \log I \tag{5.5}$$

The term I_0 is the exchange current density, the term $E - E_r$ is the overpotential and the constant, b, which is equal to the slope, $dE/d \log I$ of the polarisation curve, is termed the Tafel slope. In Tafel plots the potential, E, is plotted as a function of the logarithm of the current density, $\log I$, and provided the corrosion reactions are controlled by activation polarisation, as is frequently observed, linear plots are obtained. The Tafel lines are characterised by the slope of the linear region of the polarisation curve. These slopes depend on the nature of the metal and the environment under consideration. It is possible to extrapolate the anodic and cathodic linear portions of the polarisation curves to the corrosion potential, E_{corr}, and the magnitude of the current at this intersection is termed the corrosion current, I_{corr}, which is a direct measure of the rate of corrosion. However, it should be pointed out that this analysis is strictly only applicable to activation controlled corrosion processes. It is well known that the dissolution of copper in chloride-containing solutions is under mixed activation and diffusion control and this may limit the usefulness of this approach [280, 282].

From the data presented in Figures 5.24 and 5.25 it can be clearly seen that the Tafel analysis can be applied to the reduction half reactions for the polymer-modified copper and the uncoated copper electrodes. However, there is no obvious oxidation half reaction for the PPy-Tartrate/PPy-DBS modified copper system, making it difficult to accurately determine the Tafel slope, b_a. In contrast, the uncoated copper and the PPy-Tartrate modified copper adopt a typical Tafel plot. The computed corrosion potential, E_{corr}, corrosion current, I_{corr}, and Tafel slopes, b_a and b_c, are summarised in Table 5.1. The Tafel slopes obtained for copper are in relatively good agreement with the data obtained by Mansfeld and Kus [340] for copper in

chloride solutions, where b_a was calculated as 58 mV and b_c as 107 mV. The corrosion current, I_{corr}, is somewhat lower than the value of 2.0 μA cm^{-2} reported by Mansfeld and Kus, however, this is probably connected with the neutral chloride-containing solution. On comparing the different systems in Table 5.1, it is clear that higher I_{corr} values are computed for the uncoated and PPy-Tartrate modified copper, while relatively low I_{corr} values are seen with the bi-layer modified copper. This is consistent with the good corrosion protection properties afforded by this bi-layer polymer film.

Table 5.1: Tafel analysis for uncoated Cu and the polymer-modified Cu electrodes in 0.10 mol dm^{-3} NaCl, at a pH of 7.0.

System	b_a mV decade^{-1}	b_c mV decade^{-1}	E_{corr} V vs. SCE	I_{corr} μA cm^{-2}
Uncoated Cu	68	95	-0.10	0.29
PPy-Tartrate/PPy-DBS (0.75 V vs. SCE for 600 s)	-	91	-0.05	0.13
PPy-Tartrate/PPy-DBS (0.90 V vs. SCE for 300 s)	-	57	-0.05	0.19
PPy-Tartrate/PPy-DBS (0.80 V vs. SCE for 800 s)	-	49	-0.05	0.14
PPy-Tartrate (0.75 V vs. SCE for 1200 s)	91	48	-0.08	2.00

5.3.3 Open-Circuit Potential (OCP) Measurements

In order to investigate the corrosion protection properties further and the stability of the polymer-modified copper, immersion experiments were performed and the potential adopted was recorded as a function of time in the aggressive chloride-containing solution. As detailed in Section 5.3.2, the corrosion potential is a mixed potential and it depends on the rate of the anodic and the cathodic half reactions. The evolution of the corrosion, or open-circuit potential, was monitored as a function of time in 0.10 mol dm^{-3} NaCl solutions adjusted to a pH of 7.0. The PPy-Tartrate/PPy-DBS films were deposited with the initial PPy-Tartrate layer formed at 0.75 V vs. SCE for 600 s and then the PPy-DBS films were deposited at either 0.70 V vs. SCE for 700 or 800 s or at 0.90 V vs. SCE for 300 or 400 s. This corresponds to the optimum conditions at each potential, Section 5.2.2. The polymer-modified electrodes and uncoated copper were immersed in the chloride solution and the open-circuit potential was measured

initially for a period of 3600 s. The electrodes were then removed and stored in a sealed container with a fresh chloride solution and left overnight. The open-circuit potentials were then recorded on the following day. Representative results are presented in Figures 5.28, 5.29 and 5.30.

In Figure 5.28 the open-circuit potential is shown as a function of time for the PPy-Tartrate/PPy-DBS film, where the PPy-DBS layer was formed at 0.75 V vs. SCE for 600 s. Similar data are presented in Figure 5.29 for the PPy-DBS film deposited at 0.90 V vs. SCE for 300 s, while the data presented in Figure 5.30 were recorded for the PPy-DBS formed at 0.70 V vs. SCE for 700 s. In all cases, the polymer-modified copper adopts a higher open-circuit potential compared to the uncoated copper in the chloride-containing solutions. The open-circuit potential of the polymer-modified electrodes reach a near steady-state potential, that is always more noble that the potential recorded for the uncoated copper. There is little variation in this potential from day 1 to day 2, indicating good stability of the bi-layer modified copper. Similar open-circuit potentials are adopted by the different bi-layer films, Figure 5.28, Figure 5.29 and Figure 5.30, indicating that the protective properties are similar when the PPy-DBS layer is formed at 0.90 V vs. SCE for a short period of time, 300 s, or at the lower potentials of 0.70 and 0.75 V vs. SCE for a longer period, typically 600 to 700 s.

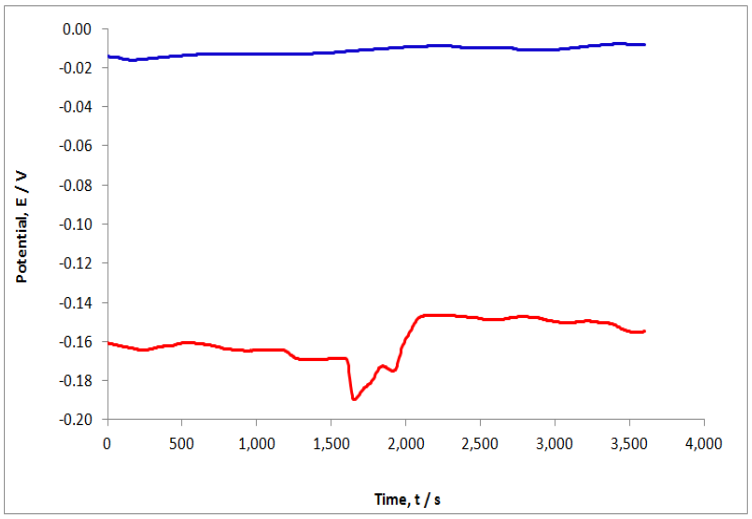

Figure 5.28: OCP recorded in 0.10 mol dm^{-3} NaCl solution at a pH of 7.0 for uncoated Cu (red) and PPy-Tartrate/PPy-DBS (blue) where the PPy-DBS layer was formed at 0.75 V vs. SCE for 600 s.

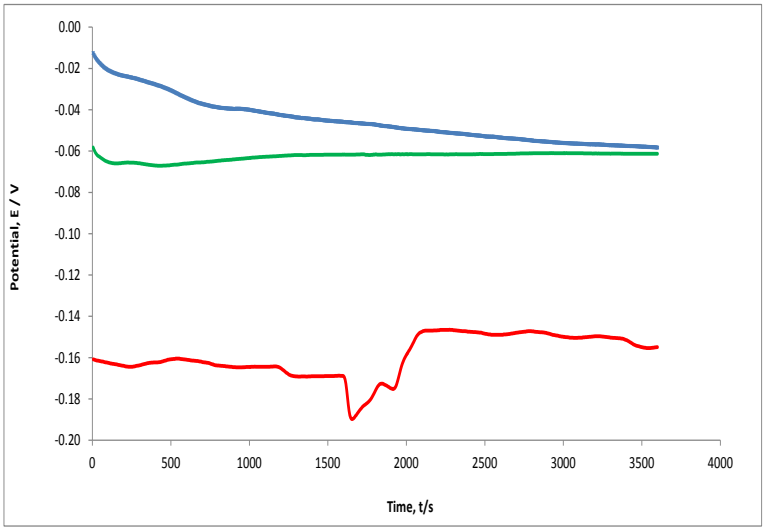

Figure 5.29: OCP recorded in 0.10 mol dm^{-3} NaCl solution at a pH of 7.0 for uncoated Cu (red) and PPy-Tartrate/PPy-DBS where the PPy-DBS layer was formed at 0.90 V vs. SCE for 300 s, day 1 (blue) and day 2 (green).

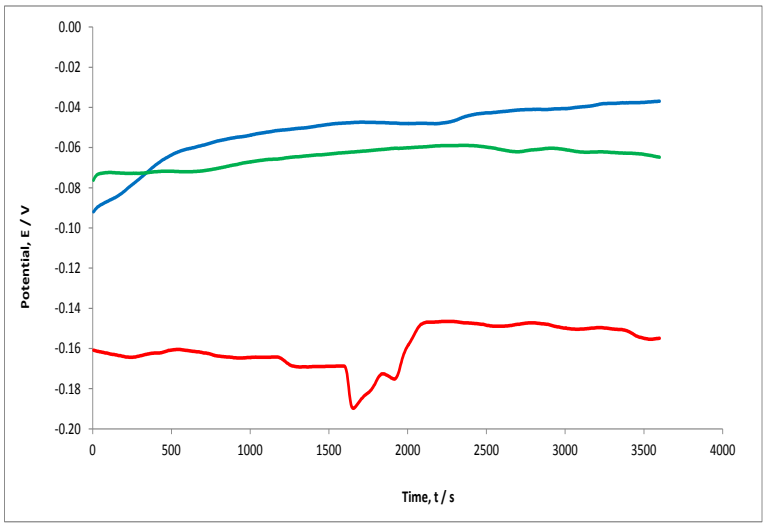

Figure 5.30: OCP recorded in 0.10 mol dm^{-3} NaCl solution at a pH of 7.0 for uncoated Cu (red) and PPy-Tartrate/PPy-DBS where the PPy-DBS layer was formed at 0.70 V vs. SCE for 700 s, day 1 (blue) and day 2 (green).

The open-circuit potentials of the polymer-modified electrodes were monitored over a period of 15 h and there was no evidence of any decay in the potential to the values adopted by the uncoated copper electrode. This indicates very good stability over extended periods of time. If indeed the open-circuit potentials of the polymer-modified copper electrodes did eventually reach the open-circuit potential of the pure copper then this would indicate a loss in the protective properties of the polymer films. It is clear from the data presented that there is no evidence of any substantial loss in the corrosion protection properties of the PPy coatings. The polymer coatings provide ample protection over a long period of time with no sufficient evidence of breakdown of the polymer films. Indeed, this is in good agreement with the Tafel analysis, Table 5.1 and the polarisation data, Figures 5.24 and Figure 5.25.

5.3.4 Electrochemical Impedance Spectroscopy (EIS)

Electrochemical impedance spectroscopy was employed to monitor the corrosion protection properties of the PPy-Tartrate/PPy-DBS polymer coating, as this technique provides detailed information on the protective properties of coatings [16, 341, 342, 343]. The impedance response was recorded as a function of the immersion period, to study the stability and any loss in the protective properties of the bi-layer coatings [249]. Similar data were recorded for the uncoated copper and these data were used as a comparison in this investigation. The data were recorded following different immersion times and at different applied potentials and then the data were fitted to equivalent circuits, as detailed in Chapter 2.

The electrochemical impedance data were recorded for the uncoated copper and the PPy-Tartrate/PPy-DBS bi-layers in an aggressive chloride solution, 0.10 mol dm^{-3} adjusted to a pH of 7.0. Representative plots are shown in Figure 5.31 for the uncoated copper which was polarised at -0.20 V vs. SCE. The modulus of the impedance, Z, and the phase angle presented as a function of the frequency give the Bode plot, while the imaginary and real components of the impedance are plotted to give the complex plane. The impedance response of uncoated Cu and the impedance response for the PPy-Tartrate/PPy-DBS bi-layer deposited at the copper electrode are shown in Figures 5.31 and 5.32. Again, these data were recorded at a fixed potential of -0.20 V vs. SCE.

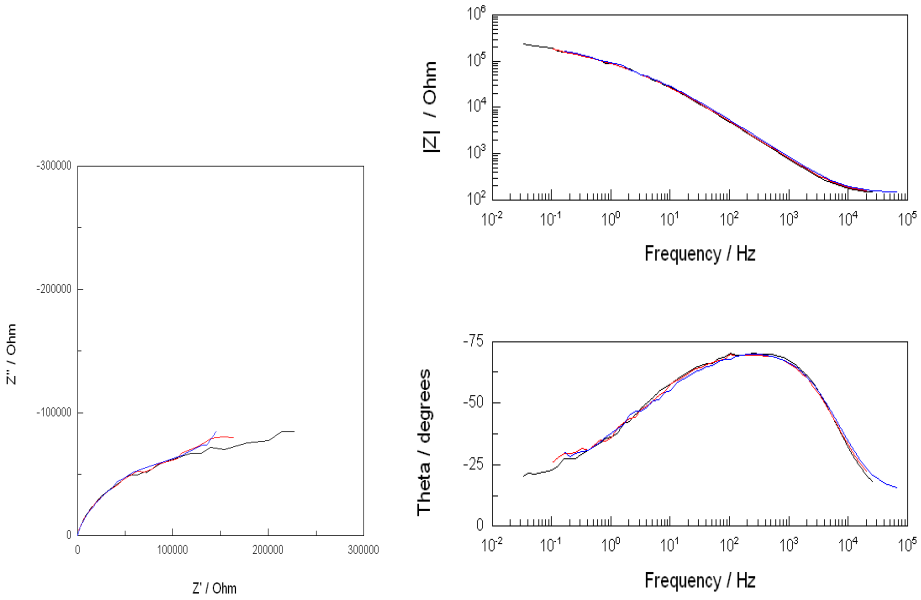

(a) **(b)**

Figure 5.31: (a) Complex plane and (b) Bode plot recorded in 0.10 mol dm^{-3} NaCl at pH 7.0 for uncoated Cu polarised at -0.20 V vs. SCE, experimental data recorded at 135 min (blue), 165 min (red) and 200 min (black).

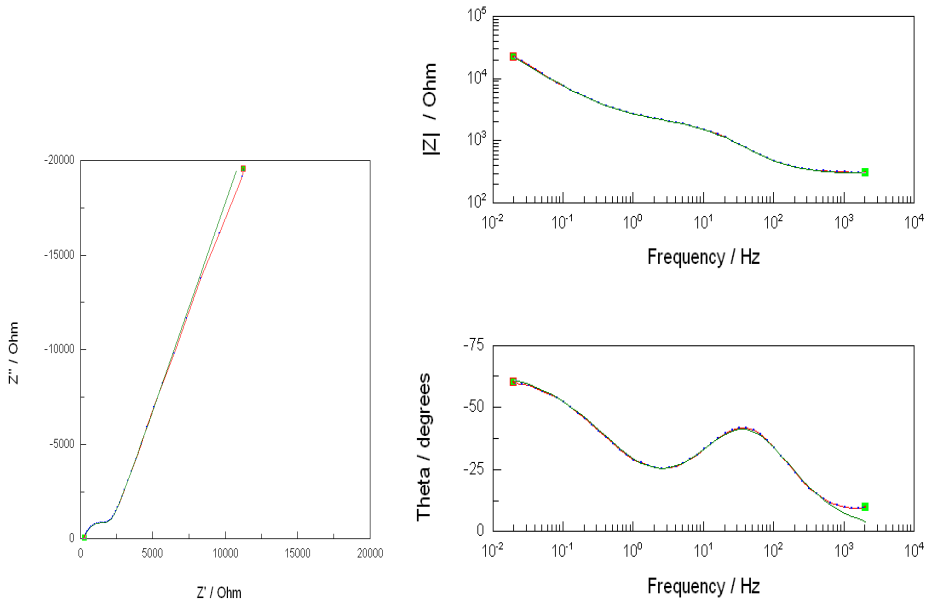

(a) **(b)**

Figure 5.32: (a) Complex plane and (b) Bode plot recorded in 0.10 mol dm^{-3} NaCl for PPy-Tartrate/PPy-DBS (PPy-DBS layer formed at 0.70 V vs. SCE for 800 s) polarised at -0.20 V vs. SCE, experimental (red) and simulated fitted traces (green).

These impedance data were fitted to the equivalent circuit depicted in Figure 5.33 using a non-linear least squares fitting minimisation method, as detailed in Chapter 2. In this circuit, R_s represents the solution resistance, R_1 represents the charge-transfer resistance, while CPE_1 and CPE_2 are constant phase elements. Excellent agreement between the experimental and the simulated data was obtained as shown in Figure 5.32, where the experimental data are compared to the simulated traces. Constant phase elements were used, rather than pure capacitors, to determine the capacitance of the interface and also to model the diffusional processes [256]. Excellent agreement between the experimental data and the theoretical fitted data was obtained when these frequency-dependent constant phase elements (CPE) were used, as opposed to ideal capacitors or Warburg elements. Constant phase elements (CPE) take into account the inhomogeneity of the surface of the electrode [252]. The impedance of a constant phase element, Z_{CPE} is defined in Equation 5.6. Here, j is the imaginary number, ω is the angular frequency and the fractional exponent, n, represents a phase shift that is a measure of surface inhomogeneity, with, n, having values between 0.0 and 1.0 [256, 344].

$$Z_{CPE} = \frac{1}{Q(j\omega)^n} \tag{5.6}$$

When the exponent is zero, n = 0.0, the CPE describes an ideal resistor and when the exponent is unity, n = 1.0, the CPE is equivalent to an ideal capacitor, while an exponent of 0.5, n = 0.5, corresponds to homogeneous semi-infinite diffusion and in this case the CPE represents a Warburg diffusion term. The higher exponent values, n >0.95, point to a relatively high degree of surface homogeneity, while lower values, 0.85<n <0.95, indicate poor surface homogeneity, consistent with a porous surface [245, 341].

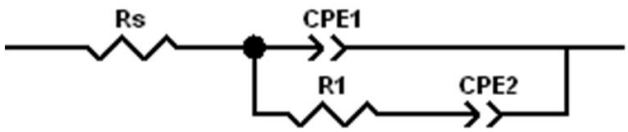

Figure 5.33: Equivalent circuit used in the fitting of the experimental data.

The three traces shown in Figure 5.31 correspond to different polarisation periods of 135, 165 and 200 min, and this highlights the stability of the copper as a function of the polarisation period at -0.20 V vs. SCE. Although there is some variation in the impedance response, the

fitted parameters were similar, indicating that the uncoated copper is stable at -0.20 V vs. SCE. Indeed, this is evident from the cyclic voltammograms presented in Figure 5.11. The n value for the constant-phase element, CPE_1, was close to 1.0, indicating that this component is a near ideal capacitor and represents the capacitance associated with the double layer. An electrical double layer exists at the interface between an electrode and its surrounding electrolyte. This double layer is formed as ions from the solution are attracted to the electrode surface. Charges at the electrode are separated from the charges of these ions over a very small distance. The capacitance was calculated as 5 μF cm^{-2}, which is typical of double layer capacitance values recorded in chloride-containing electrolytes [256, 345]. The CPE_1 values remain relatively constant as a function of the polarisation period. The CPE_2 has an n value close to 0.5, which represents a diffusional term. This is consistent with the fact that the chloride-containing layers are somewhat porous allowing diffusion to the underlying substrate. The uncoated copper metal is clearly stable at this potential. Moreover, the impedance is relatively high of the order of 10^5 Ω cm^2 at 0.01 Hz, Figure 5.31. However, once the applied potential was increased to more positive potentials, dissolution of the copper was observed.

The impedance response of the PPy-Tartrate/PPy-DBS polymer coating is displayed in Figure 5.32. This bi-layer was deposited with an initial PPy-Tartrate layer at 0.75 V vs. SCE for 600 s, followed by the PPy-DBS layer at 0.70 V vs. SCE for 800 s. A semi-circle is evident at high frequency, followed by a straight line portion in the low frequency region. The semi-circle can be attributed to the charge transfer resistance and the double layer capacitance [277, 322]. The intercept of the semi-circle with the real axis gives the charge transfer resistance value. The low frequency linear portion is generally believed to be attributed to diffusion [14, 322]. These data were fitted to the equivalent circuit shown in Figure 5.33. The capacitance term, CPE_1, has a value of the order of 100 μF cm^{-2}, and again this can be equated with the double layer capacitance. The exponent value, n, remains around 0.75 throughout the polarisation period. Considering that a value of 1 for n constitutes an ideal capacitor, then it can be concluded that there is some dispersion in the capacitance. This is consistent with the fact that the polymer has a porous structure. It has been previously reported that at the beginning of the polymer deposition process a very dense polymer is formed, but with subsequent polymer chain growth, as in this study, loosely packed porous structures are produced, [1, 173, 286]. The CPE_2 parameter has a much higher capacitance value, approximately 30 mF cm^{-2}. These

high capacitance values have been documented in previous works and are normally associated with the conducting and charging of the PPy film [346, 347]. In this case the exponent, n, was calculated as 0.95, indicating that the polymer film has a high capacitance. The bi-layer appeared to remain stable in the chloride-containing solution and the R and CPE terms remained essentially constant independent of the polarisation period.

The impedance response of the PPy-Tartrate/PPy-DBS film polarised at 0.40 V is shown in Figures 5.34 and 5.35, while the date recorded at 0.60 V vs. SCE in a neutral 0.10 mol dm^{-3} NaCl are presented in Figure 5.36. The data presented in Figure 5.34, show the experimental and simulated traces, which were recorded following a 40 min polarisation period at 0.40 V vs. SCE, while the data presented in Figure 5.35 were recorded following a 200 min polarisation period, again at 0.40 V vs. SCE. These data were fitted to the equivalent circuit depicted in Figure 5.33. There is an increase in the impedance of the bi-layer on continued polarisation at 0.40 V vs. SCE. This is a clear indication that the bi-layer polymer coating is indeed protecting the copper substrate from corrosion. This is in good agreement with the OCP data, Figures 5.28, 5.29 and 5.30, the Tafel analysis, Table 5.1, and the polarisation plots, Figures 5.24 and 5.25, recorded in the chloride-containing solutions. There appears to be a diffusional term in both cases. However, this appears to become less prominent as the polarisation time is increased, thus indicating that the polymer film is densely packed and provides good corrosion protection to the underlying copper substrate.

The impedance data recorded at 0.60 V vs. SCE at 103, 134 and 165 min are very different and it is clear that continued polarisation at 0.60 V vs. SCE gives rise to a modification of the PPy-Tartrate/PPy-DBS bi-layer. The impedance is reduced with continued polarisation and this is shown more clearly on plotting the impedance recorded at 0.01 Hz as a function of the polarisation period for the bi-layers polarised at 0.20 V and 0.60 V vs. SCE.

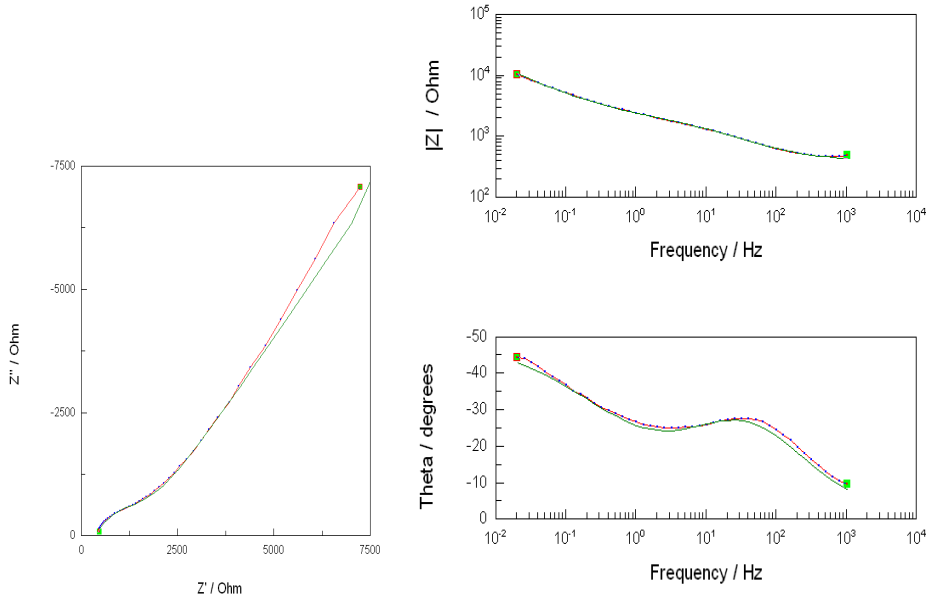

(a) **(b)**

Figure 5.34: (a) Complex plane and (b) Bode plot recorded in 0.10 mol dm^{-3} NaCl for PPy-Tartrate/PPy-DBS (PPy-DBS layer formed at 0.70 V vs. SCE for 800 s) polarised at 0.40 V vs. SCE, experimental (red) and simulated fitted traces (green).

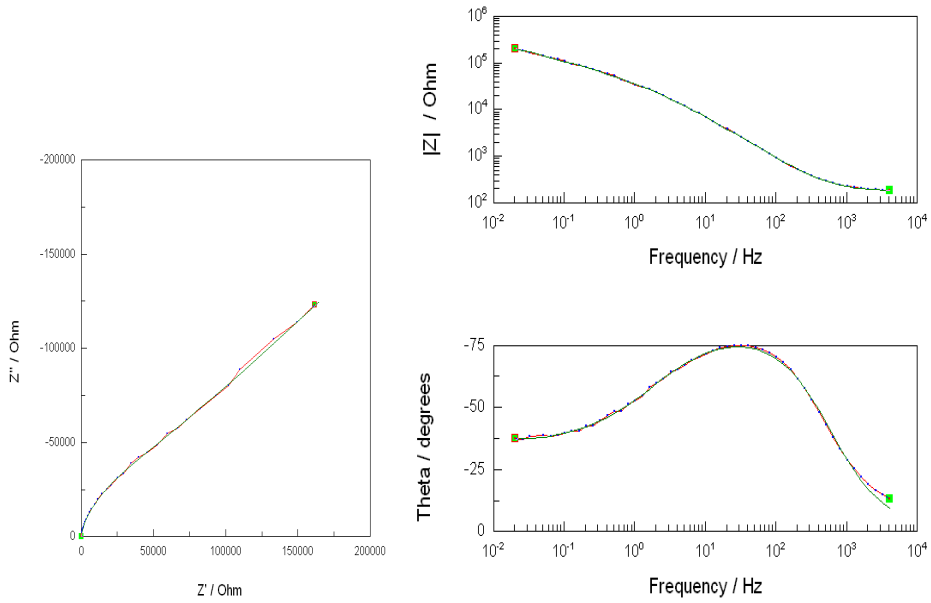

(a) **(b)**

Figure 5.35: (a) Complex plane and (b) Bode plot recorded in 0.10 mol dm^{-3} NaCl for PPy-Tartrate/PPy-DBS (PPy-DBS layer formed at 0.70 V vs. SCE for 800 s) polarised at 0.40 V vs. SCE, experimental (red) and simulated fitted traces (green). Data recorded following 200 min.

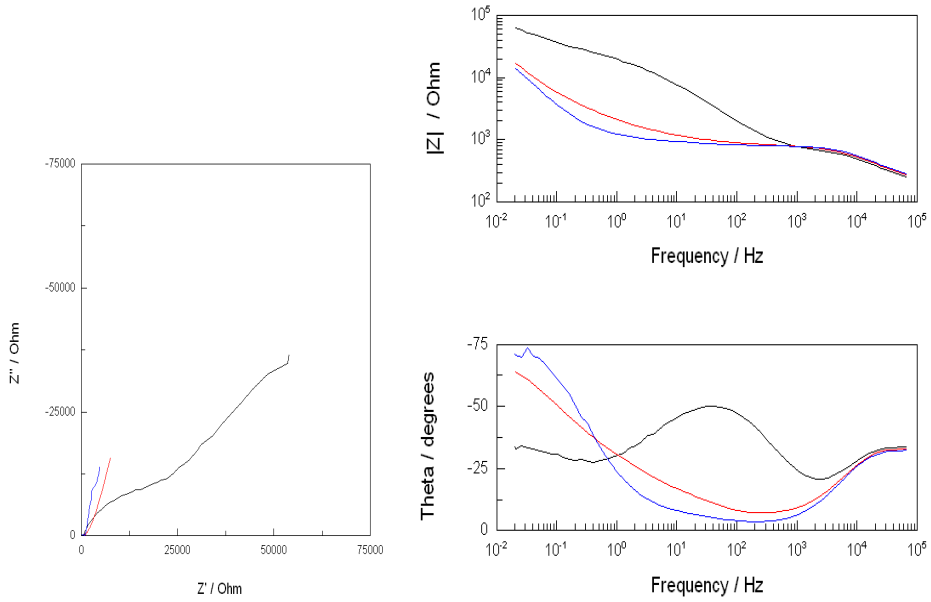

Figure 5.36: (a) Complex plane and (b) Bode plot recorded in 0.10 mol dm^{-3} NaCl for PPy-Tartrate/PPy-DBS (PPy-DBS layer formed at 0.90 V vs. SCE for 300 s) polarised at 0.60 V vs. SCE, data recorded following 103 min (black), 134 min (red) and 165 min (blue).

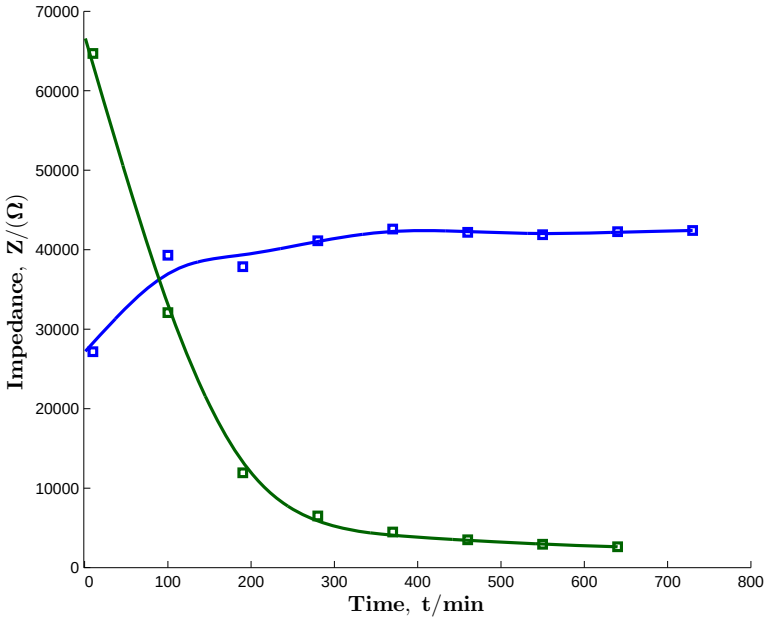

Figure 5.37: Impedance (Z/Ω) plotted as a function of time for the PPy-Tartrate/PPy-DBS bi-layer film, where the PPy-DBS layer was deposited at 0.90 V vs. SCE for 300 s, held at 0.20 V vs. SCE (blue) and held at 0.60 V vs. SCE (green).

It is clear from Figures 5.36 and 5.37 that the PPy-Tartrate/PPy-DBS film is not at steady-state conditions as the impedance varies with time. In Figure 5.37 breakdown of the polymer film is clearly evident at 0.60 V vs. SCE, when compared to the polymer film polarised at the lower applied potential of 0.20 V vs. SCE. In this case, the impedance remains essentially constant indicating very good stability over an extended polarisation period in a harsh chloride-containing solution. Nevertheless, as the potential is further increased to 0.60 V vs. SCE for the same extended time period the polymer film is no longer able to maintain this stability and there is a significant drop in the impedance, indicating breakdown of the polymer at these high applied potentials. Nevertheless, very good stability is seen at -0.20 and 0.40 V vs. SCE, Figures 5.31, 5.32, 5.34 and 5.35 and furthermore, as shown earlier in the Tafel analysis, Section 5.3.2, OCP measurements, Section 5.3.3, and polarisation data, Section 5.3.1, this bi-layer provides very good corrosion protection properties.

5.4 Summary of Results

The results presented in this chapter show that the PPy-Tartrate/PPy-DBS bi-layer can be readily formed at copper. The initial PPy-Tartrate layer was formed at 0.75 V vs. SCE for 600 s in 0.30 mol dm^{-3} pyrrole and 0.10 mol dm^{-3} tartrate. The PPy-DBS was then deposited at the PPy-Tartrate film at 0.75 V vs. SCE for an additional 600 s from 0.30 mol dm^{-3} pyrrole and 0.050 mol dm^{-3} DBS at pH of 7.0, to give the bi-layered film. The resultant polymer layer is black in colour indicating that the PPy is generated in its stable oxidised state. Freshly prepared solutions were used to deposit the PPy bi-layer, giving very good reproducibility. EDX analyses confirmed that the DBS was incorporated within the PPy-DBS layer.

The influence of the applied potential and deposition times on the formation of the outer PPy-DBS film was studied and it was shown that highly adherent and corrosion protective films were deposited at 0.70 V vs. SCE for time periods ranging from 300 to 1000 s and at 0.90 V vs. SCE for times between 300 and 400 s. At lower growth times the polymer was not sufficiently thick to protect the copper substrate and at longer growth times the polymers formed were less stable. The concentration of DBS was varied from 0.001 to 0.090 mol dm^{-3} and adherent bi-layers were formed regardless of the concentration, within this range. However, a DBS concentration of 0.050 mol dm^{-3} gave the best corrosion protection properties and as shown

from SEM analysis of the surface morphology, a compact PPy-DBS was deposited at this concentration. The cauliflower morphology was observed at the higher DBS concentrations, however, when the concentration of DBS was reduced to 0.001 mol dm^{-3}, oval-like structures were observed at the surface and the rate of electropolymerisation was reduced, giving thinner PPy-DBS layers.

The direct electopolymerisation of pyrrole in the DBS-containing solution to generate the PPy-DBS film at the copper was successful at a pH of 6.0 in a 0.30 mol dm^{-3} pyrrole and 0.050 mol dm^{-3} DBS solution. Homogeneous, adherent and stable PPy-DBS films were formed directly at the copper substrate at applied potentials from 0.60 V to 0.90 V vs. SCE. Although these PPy-DBS films showed good corrosion protection properties, somewhat more protective properties were observed with the PPy-Tartrate/PPy-DBS bi-layers.

The corrosion protective properties of the PPy-Tartrate/PPy-DBS bi-layers were assessed and studied using a combination of cyclic voltammetry, polarisation curves, Tafel analysis, open-circuit potential measurements and electrochemical impedance spectroscopy. The bi-layer adopted a more positive open-circuit potential compared to the open-circuit potential of the uncoated copper. In addition, the open-circuit potential was stable and constant and did not decay to the potentials of the uncoated copper, indicating high stability and good corrosion protection properties. Using cyclic voltammetry and anodic polarisation plots, breakdown of the bi-layer was only observed at potentials higher than 0.85 V vs. SCE, highlighting the stability and excellent corrosion protection properties of the bi-layer. Using Tafel analysis the corrosion current for the bi-layer protected copper was estimated at 0.15 μA cm^{-2} in a neutral 0.10 mol dm^{-3} NaCl solution. Good stability of the bi-layer was also observed in the electrochemical impedance spectroscopy study. The impedance data were recorded at potentials from -0.20 to 0.60 V vs. SCE. However, breakdown of the bi-layer coating was observed at 0.60 V vs. SCE and this potential is somewhat lower than that observed in the voltammetry measurements. However, this is probably connected with the extended polarisation periods, at 0.60 V vs. SCE, in the chloride-containing electrolyte.

In conclusion, it appears from the results obtained that the PPy-DBS film is the key factor in the formation of a highly protective bi-layer polymer. Indeed, the corrosion protection properties of the PPy-Tartrate layer were significantly lower, with breakdown of the polymer film at potentials from 0.20 to 0.50 V vs. SCE.

CHAPTER 6

Synthesis of Viologen Films at the Copper Interface

In this chapter, an alternative approach to the previously discussed polymer coatings was considered.Since viologens had been used in the past within the research group there was some existing knowledge on their electrochemistry. However, there has been no previous reports of viologens being using as corrosion protection films for the metal copper, therefore this chapter details the results on the corrosion protection properties of methyl viologen (MV), ethyl viologen (EV) and benzyl viologen (BV) which are presented and discussed. There is however, some literature on the binding of viologens to the copper metal [348], so this was useful to understand the chemical interactions taking place in order to obtain the corrosion protection films at the copper surface.

Most corrosion inhibition involving viologens deals with anti-microbial corrosion. For example, Yuan *et al.* [243] reported that viologens are effective in inhibiting microbiology-induced corrosion, which is very prevalent in the maritime industry. The surface of an oxidised CuNi alloy was modified, due to the successful build up of the viologen to give inhibition of the bacterial growth. In a later study, Yuan *et al.* [265] modified the surface of stainless steel by covalent coupling of the viologen moieties to the tertiary amino groups of P(DMAEMA) (2-diamino) ethyl methacrylate brushes on the stainless steel. Enhanced anti-bacterial and anti-corrosion capabilities against the bacteria, desulfovibrio desulfuricans, were

revealed using anti-bacterial assays and electrochemical studies in anaerobic seawater. With the inherent advantages of the high corrosion resistance of stainless steel and the good anti-bacterial and anti-corrosion capabilities of the viologen-quaternised P(DMAEMA) brushes, the functionalised stainless steel is potentially useful in harsh seawater environments and for desalination plants.

As described in more detail, in Section 1.8, viologen molecules exist in nature in the stable form of dications [241]. When an appropriate potential is applied, they undergo electron transfer reactions by two consecutive one-electron reduction reactions, as highlighted in Figure 6.1, leading firstly to the generation of a radical species followed by the formation of a neutral compound [17]. Viologens have been adsorbed onto metal surfaces, particularly copper, but this generally involves the deposition of an anionic chloride layer at the surface. The electrostatic attraction between the partially solvated viologen dications and the anionic chloride layer is discussed as the main driving force for the viologen stabilisation on the electrode surface. The laterally ordered V^{2+} monolayer is hydrophilic with at least four water molecules for each viologen present within this cationic organic film. The chloride anions are specifically adsorbed, and in direct contact with the metallic copper surface underneath the organic layer [241]. The interfacial behaviour becomes even more complex when reactants and/or products of the electron transfer process are adsorbed on the anion-modified electrodes. Provided the anions retain to a large extent their negative charge upon specific adsorption, the subsequent adsorption of cationic reactants from the electrolyte onto the electrode surface will be facilitated through electrostatic attraction, thus, giving rise to the formation of "paired" anion-cation layers [349, 350] which remain stable even during an electron transfer reaction with the bulk solution species. Such an anion-cation layering effect has recently been reported for the adsorption and subsequent reaction of redox-active viologens, (1,1'-disubstituted-4,4'-bipyridinium molecules) on a chloride modified Cu (100) electrode surface [17, 241, 349, 351].

The anodic dissolution of copper in alkaline solutions has attracted a great deal of attention due to its relevance to the understanding of the corrosion mechanisms of copper [352, 353]. The subject has been studied using galvanic techniques, however cyclic voltammetry has been widely used to characterise the oxidation process [354]. The formation of weak passivating layers on copper in aqueous media, especially in alkaline solutions, has been observed and this

has attracted considerable attention in corrosion research [278, 355]. Electrochemical studies present conflicting views about the nature and composition of surface oxides especially in relation to the initial oxidation processes. However, it is generally accepted that the lowest oxidation state, Cu_2O, or a Cu(I) hydroxide, CuOH layer, forms initially at the bare copper anode [356, 357]. This has a significant influence on the corrosion processes. However, these films do not offer long-term protection of the copper metal from corrosion and alternative films or coatings are needed.

Based on previous research on the corrosion protection of copper metal, most studies involve the formation of polymers in various electrolytes at the surface interface [185, 358]. Accordingly, this study focuses on an alternative method to combat the dissolution of copper into solution. In this case, three viologens, MV, EV and BV, were deposited at copper and their corrosion protection properties were assessed. The viologens are depicted in Figure 6.2, showing the BV, EV and MV groups and the counter anions. As discussed earlier viologen-modified copper electrodes have been previously used in microbiological influenced corrosion [243]. However, there has been no focus on atmospheric corrosion or the development of coatings for the corrosion protection of copper using viologens. The development of a cheap and environmentally acceptable corrosion protection film for copper would be a significant step.

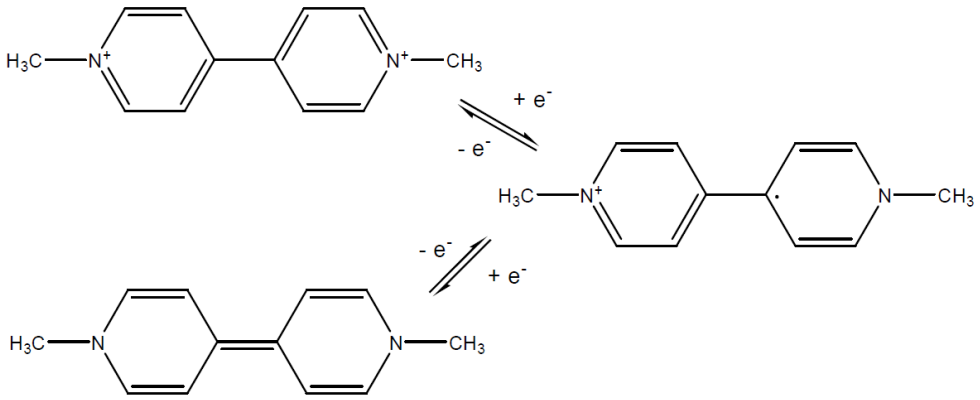

Figure 6.1: Scheme representing the first and second reduction for viologen compounds.

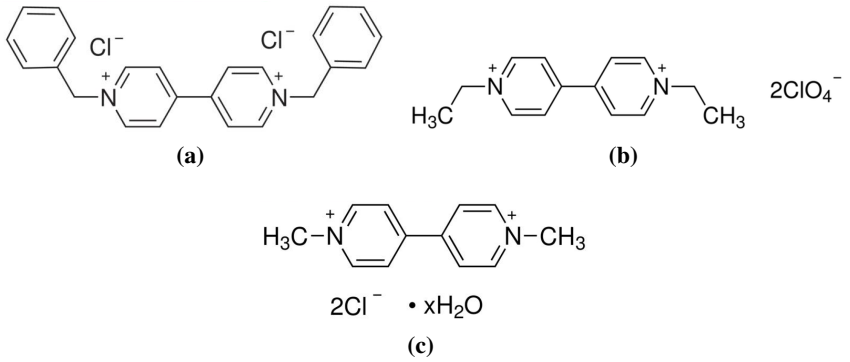

Figure 6.2: Chemical structures of the viologens investigated in this study (a) benzyl viologen ($C_{24}H_{22}Cl_2N_2$), (b) ethyl viologen ($C_{14}H_{18}Cl_2N_2O_8$) and (c) methyl viologen ($C_{12}H_{14}Cl_2N_2. \times H_2O$)

In this chapter, results are presented and discussed on the deposition of the viologens in the presence of chloride anions at the copper surface. This was achieved using a simple one-step electrochemical synthesis using cyclic voltammetry. Surface analytical techniques were used to obtain information on the morphology and composition of the films. The BV film appeared to offer the best corrosion protection and the deposition of this viologen at the copper surface was further explored to optimise the deposition and stability of the layer. The corrosion protection properties of this layer were compared to the well known benzotriazole (BTA) inhibitor [83].

6.1 Experimental

The experimental approach used in the formation of the viologen films at the copper electrode and the techniques employed in the analysis of the films are provided in Section 6.1.1, Section 6.1.2 and Section 6.1.3.

6.1.1 Reagents

The viologens, benzyl viologen dichloride (97%), ethyl viologen diperchlorate (98%) and methyl viologen dichloride hydrate (98%) were obtained from Aldrich and stored at room temperature. Unless otherwise stated, a 2.0×10^{-3} or 5.0×10^{-3} mol dm^{-3} solution of the viologen was prepared in a 0.10 mol dm^{-3} NaCl solution, using distilled water. All the viologen-containing solutions were purged with nitrogen to remove any traces of dissolved oxygen, before and during the experiments. Other analytical reagents included benzotriazole (BTA), sodium hydroxide (NaOH) and hydrochloric acid (HCl). These were purchased from

Aldrich and used as received. Buffers used to calibrate the pH meter, at pH 4.0 and pH 7.0, were purchased from Lennox Ltd.

6.1.2 Electrodes and Instruments

The electrochemical deposition of the viologens was carried out using a CHi 760C potentiostat. All measurements were made at room temperature. For the cyclic voltammetry experiments a copper rod (4 mm diameter) electrode encased in a Teflon holder, previously described in Chapter 2, Figure 2.3, was used with an exposed surface area of 0.1257 cm^2. The rod electrodes were polished using a 1 μm diamond polish and Buehler micro-cloth, sonicated to remove any polishing residue using a Branson 1510 sonicator and rinsed well with distilled water to give a smooth surface finish, as outlined in Chapter 2. A saturated calomel electrode, (SCE), was used as the reference electrode and a high surface area platinum wire was employed as the counter electrode. An Orion 720A pH meter, calibrated daily using both pH 4.0 and pH 7.0 buffers, was used in all pH measurements. Scanning electron micrographs were obtained using a Hitachi FE-scanning electron microscope, with an Oxford instruments Inca X-act 4.12 software package, and EDX analysis was carried out using an EDX Model 51-ADD0009 with the software package Micro Analysis Suite, while a Emitech K550x was used to sputter thin films of gold onto the samples for SEM analysis.

6.1.3 Procedures

The viologens were deposited at copper from a 0.10 mol dm^{-3} NaCl supporting electrolyte and the viologen concentration was 2.0×10^{-3} or 5.0×10^{-3} mol dm^{-3}, unless otherwise stated. The solution was adjusted to pH 3.0, using a few drops of concentrated HCl. This facilitated the deposition of a viologen-Cl-Cu film, as the chloride is the only anion present, in the case of the MV and BV. The EV diperchlorate salt was used. However, the chloride concentration is in large excess compared with the ethyl viologen diperchlorate. The chloride anion is incorporated into the viologen film to balance the charge and give a stable viologen-Cl complex at the copper interface. The viologen-Cl-Cu film was deposited by cycling the copper in the viologen-containing chloride electrolyte from -0.20 to 1.00 V vs. SCE at 1 mV s^{-1} for the desired number of cycles. The influence of the pH of the viologen-containing solution was studied by varying the pH of the 0.10 mol dm^{-3} NaCl solution with the added viologen from a

pH of 2.0 to 9.0. The pH was adjusted using concentrated HCl or NaOH, ensuring that no other anions were added to the electrolyte. The chloride concentration was varied from 1.25×10^{-3} to 0.30 mol dm^{-3} and the pH was maintained at a value of 3.0, while the concentration of the viologens was varied from 1.0×10^{-4} to 5.0×10^{-3} mol dm^{-3} in a 0.10 mol dm^{-3} NaCl solution at a pH of 3.0. Electrochemical studies were also carried out using BTA as a corrosion inhibitor. The BTA (2.0×10^{-3} mol dm^{-3}) was added to the 0.10 mol dm^{-3} NaCl solution and the pH of the solution was varied between 2.0 to 9.0 using HCl or NaOH. Then the copper was cycled from -0.20 to 1.00 V vs. SCE at 1 mV s^{-1} in the BTA-containing solution and the results were compared to the viologen systems.

After electrochemical deposition, the viologen films were characterised using cyclic voltammetry by cycling in a potential window from -0.20 to 1.00 V vs. SCE. Scanning electron microscopy (SEM) was used to study the morphology of the deposited films, while energy dispersive X-Ray analysis (EDX) was employed to identify the chemical components of the films. In both cases, flat disc electrodes were used and when necessary, the samples were sputter coated with a thin gold layer prior to the SEM measurements.

6.2 Results and Discussion

Results are presented and discussed on the formation of the MV, EV and BV films at the copper surface. The factors that influence the formation of these films are highlighted, while the corrosion protection properties of the films are compared to the well-known corrosion inhibitor BTA.

6.2.1 Formation of the Viologen Films

Initially the viologen films were formed on the copper surface using cyclic voltammetry. This technique appeared to produce uniform films of the viologens on the copper surface. In Figure 6.3a the cyclic voltammogram recorded at 1 mV s^{-1} for 2.0×10^{-3} mol dm^{-3} BV dissolved in 0.10 mol dm^{-3} NaCl is presented. As detailed in Section 6.1.3, the solution was maintained at a pH of 3.0, and the voltammograms were recorded from an initial potential of -0.20 V vs. SCE to a final potential of 1.00 V vs. SCE. The corresponding charge-potential plot is depicted in Figure 6.3b.

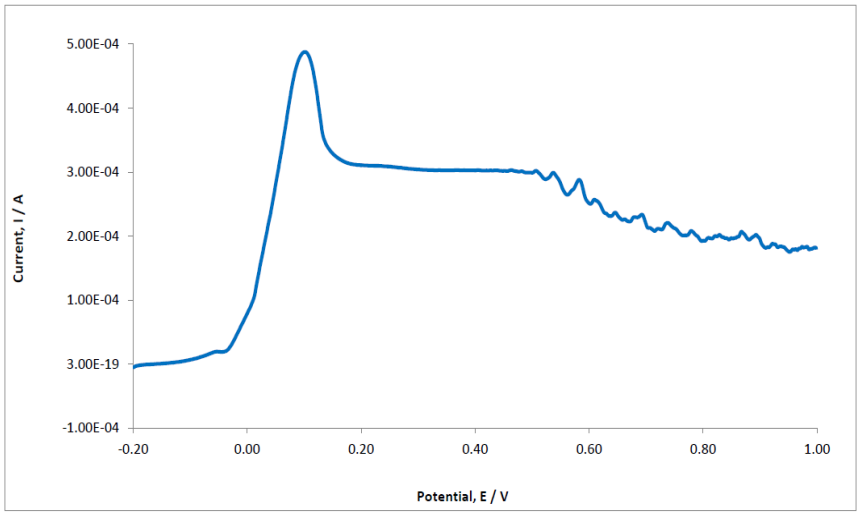

(a)

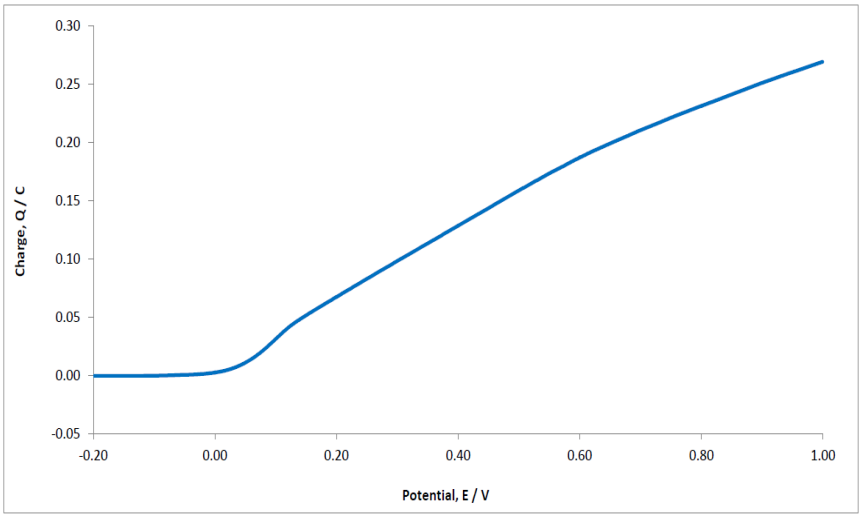

(b)

Figure 6.3: Current plotted as a function of increasing applied potential and (b) charge plotted as a function of potential for Cu cycled at 1 mV s^{-1} in 0.10 mol dm^{-3} NaCl, 2.0×10^{-3} mol dm^{-3} BV, at a pH of 3.0.

At -0.20 V vs. SCE, the currents are low, indicating little dissolution of the copper at this potential. This is not surprising given the Pourbaix diagram of copper, Section 1.3, Chapter 1. However, as the potential is increased to about 0.05 V vs. SCE, the onset of copper dissolution is observed. The current continues to increase to reach a maximum value of 0.50 mA at about 0.10 V vs. SCE and then decays rapidly to give a pseudo-passive region. These highly active conditions are maintained for a short period and indicate active dissolution of the copper. Indeed, this peak has been explained in terms of the dissolution of copper and the nucleation

of copper oxides, hydroxides and chloride-containing species, such as CuCl and the soluble $CuCl_2^-$ species [283, 359]. According to Kear *et al* [338] the rate of dissolution is usually governed by mixed charge transfer and mass transport. As the potential is increased further the current decays to give a pseudo-passive region, with a current of approximately 0.3 mA. This indicates the formation of a pseudo-passive film on the copper electrode, following the initial dissolution of copper. The pseudo-passive region extends from about 0.20 to 0.60 V vs. SCE and then a more gradual decay in the current is seen. Very good reproducibility was observed and nearly identical peak potentials, peak currents and a pseudo-passive range were obtained in all experiments.

The charge-potential plot presented in Figure 6.3b again shows very good stability of the copper from -0.20 to 0.05 V vs. SCE. Then the charge increases with increasing potential to give three linear regions. The first extends from about 0.05 to 0.15 V vs. SCE and this corresponds to the active dissolution of copper. The next linear segment is related to the formation of the pseudo-passive film and the final segment, with a slightly lower slope, is consistent with the final more gradual decay in the current as the copper is cycled from approximately 0.60 to 1.00 V vs. SCE.

In Figure 6.4 the voltammograms recorded for copper cycled in the absence and presence of the BV are compared. Again, the pH was adjusted to a pH of 3.0. A considerable difference in the two plots is evident, highlighting the protective properties of the BV films. In the absence of the viologen, the initial dissolution of copper occurs to give a peak centered at about 0.03 V vs. SCE, while this initial dissolution appears to be inhibited in the presence of the viologen, with the peak current at 0.10 V vs. SCE. As the CuCl complex species are formed and deposited at the surface, the current decays, but then increases to reach high values in the vicinity of 1.0 mA cm^{-2} in the absence of the viologen. This indicates that while the initial copper-chloride deposit offers some corrosion protection, this is limited and dissolution of the copper predominates, generating Cu(II) species at the higher potential. It is clear that significant dissolution and corrosion of the copper occurs. Indeed, the currents measured from 0.25 to 0.60 V vs. SCE are dominated by deposited corrosion products and the periodic removal of these deposits, and poor reproducibility was obtained in this potential window.

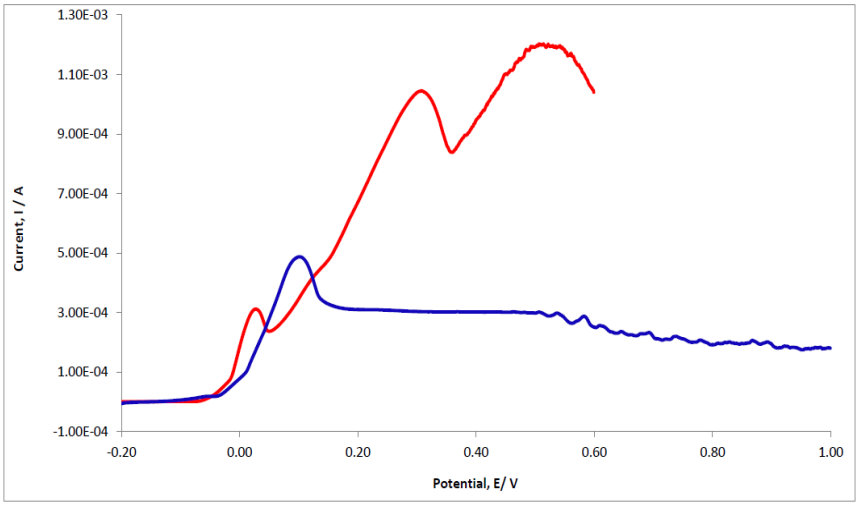

Figure 6.4: Current plotted as a function of increasing applied potential for Cu cycled at 1 mV s^{-1} in 0.10 mol dm^{-3} NaCl at a pH of 3.0, in the presence (blue) and absence (red) of 2.0×10^{-3} mol dm^{-3} BV.

Similar data were recorded for the MV and EV and representative plots are shown in Figure 6.5. Again dissolution of copper is observed from about 0.05 to 0.20 V vs. SCE. The peak current is similar to that recorded in the BV-containing solution, indicating a similar dissolution rate of the copper. However, the peaks occur at slightly different peak potentials and are closer to the peak potentials observed for copper in the absence of the viologen, Figure 6.4. The current decays rapidly to reach values in the vicinity of 0.05 mA and then increases slightly to give a pseudo-passive film, with a current of 0.20 mA for the MV and approximately 0.30 mA for the EV. This second broad peak, extending from 0.10 to 0.20 V vs. SCE, indicates further dissolution of copper. In the case of the MV solution a stable pseudo-passive region is formed and this remains stable as the copper is polarised at 1 mV s^{-1} to potentials in the vicinity of 1.00 V vs. SCE. Again, this highlights that the films are stable and protective. However, for the EV, the current increases gradually, from about 0.30 to 1.00 V vs. SCE, indicating that these EV films are not as protective as the MV or BV films. Again, when these data are compared to that presented in Figure 6.4, it is clear that there is no evidence to support the formation of a pseudo-passive film in the absence of the viologens. This pseudo-passive layer is only formed when the viologens are added to the chloride-containing electrolyte.

These results are consistent with the early adsorption of chloride anions at the copper electrode followed by the viologens to give a protective viologen-containing film. The

adsorption of anions from the supporting electrolyte can alter the electronic properties of the surface and as a consequence the charge distribution at the surface-electrolyte interface [39, 41]. Although the initial adsorbed chloride layer is not protective in the case of copper, it gives rise to the anionic conditions that favour the formation of the viologen films. It is well known that viologens can form well ordered thin films on metal surfaces, normally consisting of π-stacking formations [241]. It is clear from Figures 6.3, 6.4 and 6.5 that these films are protective. In particular, the BV and MV-containing films afford very good corrosion protection to the copper substrate.

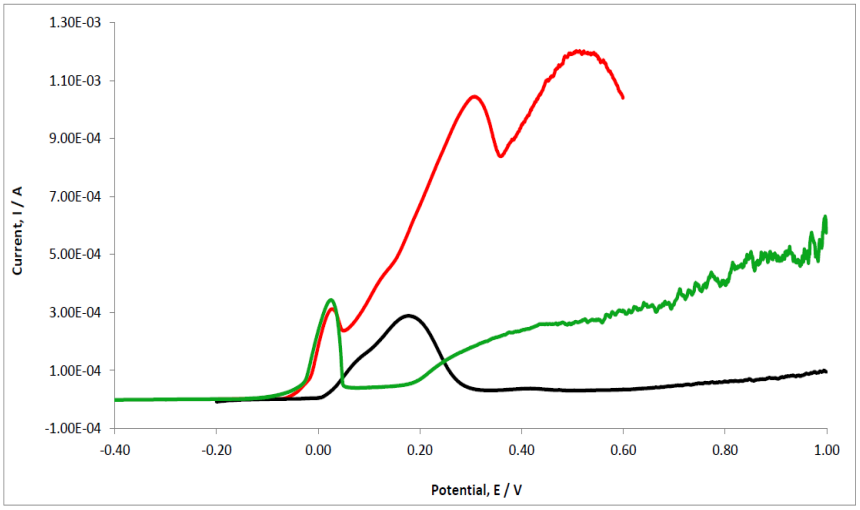

Figure 6.5: Current plotted as a function of increasing applied potential for Cu (red) cycled at 1 mV s^{-1} in 0.10 mol dm^{-3} NaCl at a pH of 3.0, in the presence of 2.0 $\times$ 10^{-3} mol dm^{-3} MV (black) and 2.0 $\times$ 10^{-3} mol dm^{-3} EV (green).

6.2.2 Influence of the Concentration of the Viologens

Another aspect that was investigated was the influence of the viologen concentration on the formation of the viologen film at the copper surface. Here, the concentration of the viologens was altered in order to determine if an optimum concentration existed that would provide good corrosion protection for the copper metal. The concentration of the viologens was varied from 1.0 $\times$ 10^{-4} to 5.0 $\times$ 10^{-3} mol dm^{-3}. Again, the copper was cycled in the viologen-containing solution adjusted to a pH of 3.0 at a scan rate of 1 mV s^{-1}.

The data recorded for the higher viologen concentrations, 2.0 $\times$ 10^{-3} and 3.0 $\times$ 10^{-3} mol dm^{-3} are summarised in Figure 6.6. Data are presented for the BV and EV. In the case of the

EV, the concentration appears to have some influence, with more stable pseudo-passive films formed at the higher concentration. This is clearly evident in Figure 6.6b, where the charge is plotted as a function of the applied potential. In this case, there is very little difference between the plots until potentials higher than 0.40 V vs. SCE are reached. Then it is clear that the charge is lower at the higher concentration. Although, there is evidence of copper dissolution at the lower concentration, it is clear that better stability is observed with the higher concentration. Accordingly, the EV films are equally as protective as the MV and BV, but a higher concentration of the EV is required in forming the film. The concentration of the BV appears to have little influence. The charge is essentially independent of the BV concentration. Although not shown in the figure, the data recorded for the 5.0×10^{-3} mol dm^{-3} BV solution were similar to that presented at the lower concentrations. Similar results were obtained when the concentration of the viologen was reduced, as highlighted in Figure 6.7. Here data are presented for the MV, EV and BV systems at a concentration of 4.0×10^{-4} mol dm^{-3} in Figure 6.7a and 6.7b, while the plots shown in Figure 6.7c and 6.7d were recorded with EV and BV at concentrations of 1.0×10^{-4} and 3.0×10^{-4} mol dm^{-3}.

As shown in Figure 6.7a the plot recorded for the BV is similar to that presented in Figure 6.3a. Indeed, the plots shown in Figure 6.7c and 6.7d, where the BV concentration is 1.0×10^{-4} mol dm^{-3} are similar, indicating that the BV films can be successfully formed using relatively low concentrations of the viologen. Moreover, these films are stable and highly protective giving stable pseudo-passive films and low charges. Similar results were observed with the MV. The plot depicted in Figure 6.7a, where the concentration of the MV is reduced to 4.0×10^{-4} mol dm^{-3} exhibits equally good stability. Indeed, this is particularly evident in the charge plot, where a near linear increase in the charge is observed to extend from 0.30 to 1.00 V vs. SCE, indicating no evidence for the dissolution of the underlying copper substrate. However, very different results are obtained with the EV. When the concentration of the EV was reduced to 4.0×10^{-4} mol dm^{-3} significant dissolution of the copper was observed. This is clearly evident in the increasing currents measured from 0.50 to 1.00 V vs. SCE. Indeed, a rapid increase in the charge is seen, Figure 6.7b. Even higher rates of dissolution are observed when the EV concentration is reduced further, as highlighted in Figure 6.7d.

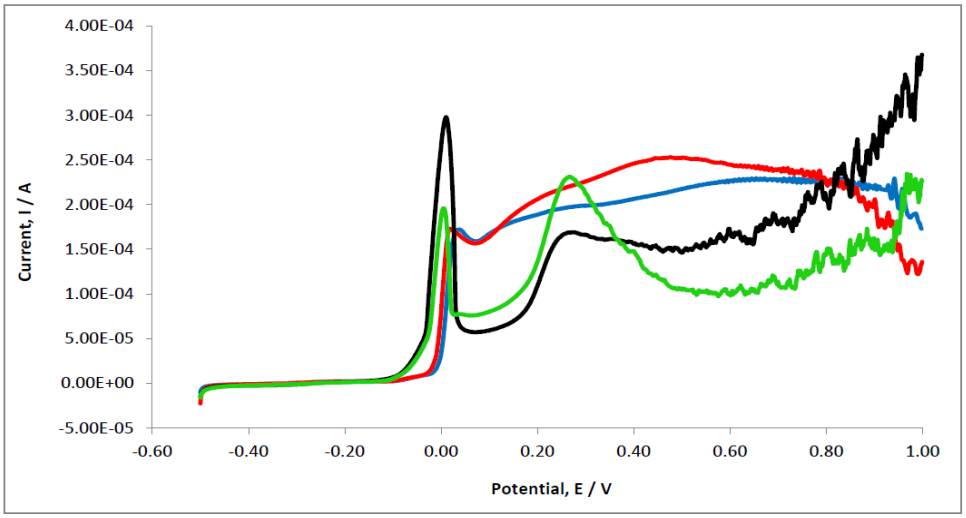

(a)

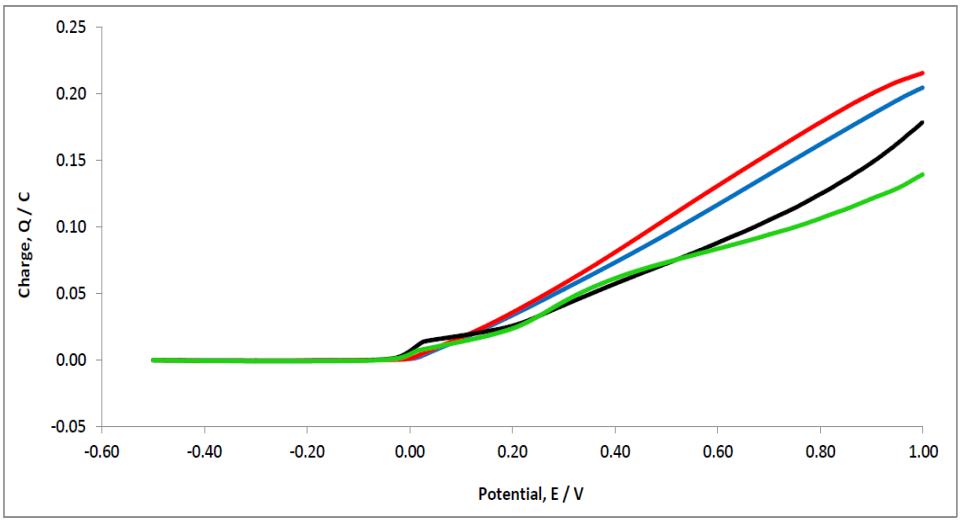

(b)

Figure 6.6: (a) Current plotted as a function of increasing applied potential and (b) charge plotted as a function of applied potential for Cu cycled at 1 mV s^{-1} in 0.10 mol dm^{-3} NaCl at a pH of 3.0 with the addition of BV and EV at a concentration of 2.0×10^{-3} (BV-blue, EV-black) and 3.0×10^{-3} mol dm^{-3} (BV-red, EV-green).

Again, these data show that the concentration of the MV and BV, has relatively little influence on the formation and stability of the films, however protective and stable EV films can only be formed at concentrations higher than 5.0×10^{-3} mol dm^{-3}. This is interesting as there is little difference in the MV and EV, as shown in Figure 6.2, except for a slight difference in the length of the alkyl chain. However, it has been shown by Min *et al.* [348], in studying the effects of alkyl chain length on the structure of the viologens formed on a Cu(100) surface, that the final structure is highly dependent on the length of the alkyl chain.

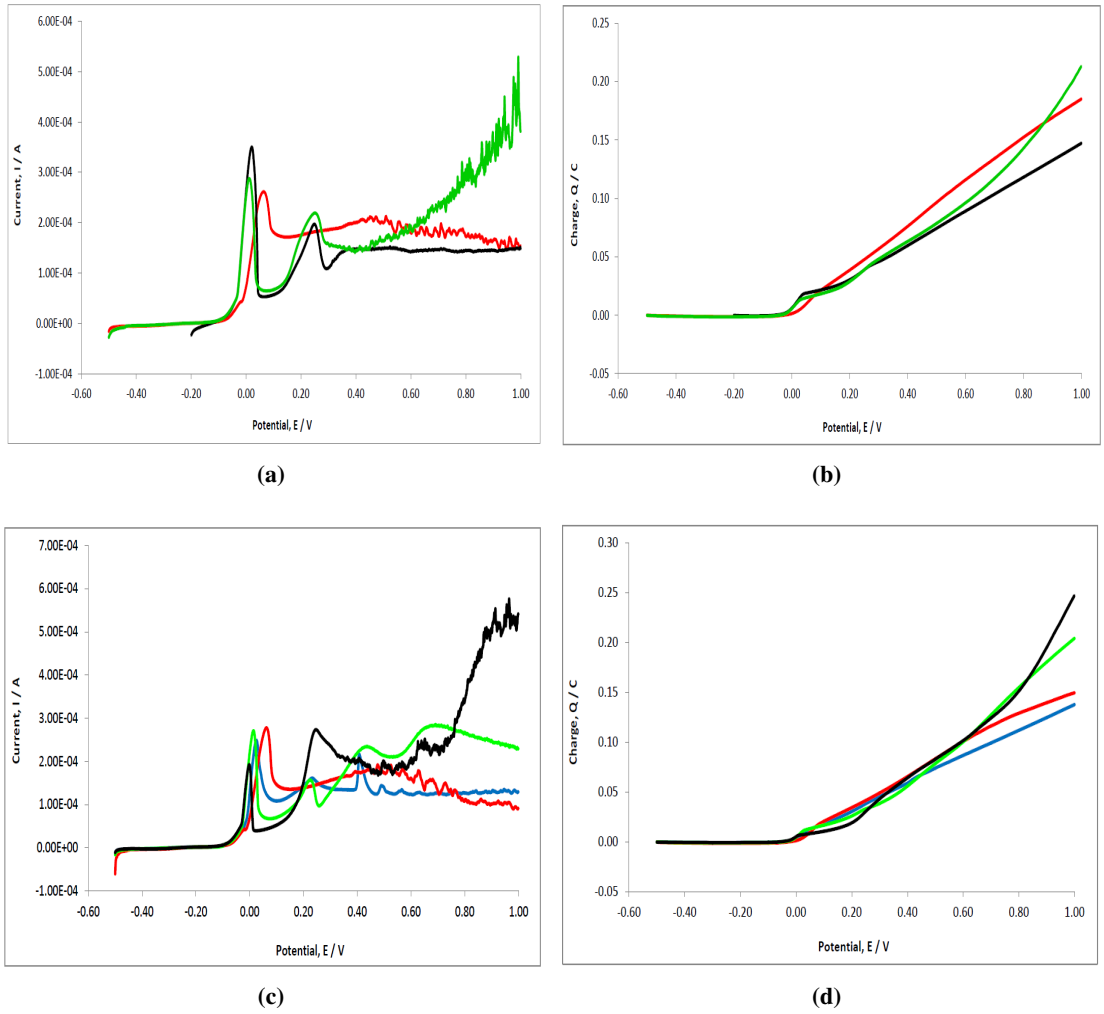

Figure 6.7: (a) Current plotted as a function of increasing applied potential and (b) charge plotted as a function of applied potential for Cu cycled in 4.0×10^{-4} mol dm^{-3} MV (black), EV (green) and BV (red), (c) current plotted as a function of applied potential and (d) charge plotted as a function of applied potential for Cu cycled in 1.0×10^{-4} and 3×10^{-4} mol dm^{-3} EV (green and black) or BV (blue and red) in 0.10 mol dm^{-3} NaCl at a pH of 3.0.

The dicationic heptyl viologen showed a highly ordered two dimensional array structure on the chloride-modified Cu(100) electrode, while the dicationic EV did not show any evidence of a well-ordered compact structure. As detailed in Section 6.1.1, the EV diperchlorate salt was employed as the source of the viologen. However, it is unlikely that the perchlorate anion has any significant effect, as the chloride anion is in large excess and the initial dissolution of copper is controlled by the chloride anions. The possible participation of the perchlorate anions in the formation of the viologen films was explored by adding a comparable concentration of perchlorate salt to the MV solution. However, there was little difference between the data

recorded in the presence and absence of the perchlorate, suggesting that the observed results for the EV system are connected with the nature and structure of the deposited films.

6.2.3 The Influence of pH

As previously discussed in Chapter 1, the pH of the solution has a significant effect on the stability of copper in aqueous solutions. In acidic or slightly acidic solution, dissolution of copper is observed, Equation 6.1, as the stable domain is the Cu^{2+} phase, while the oxides are the stable phases at higher pH values, as shown in the Pourbaix diagram, Chapter 1.

$$Cu(s) \rightarrow Cu^{2+} + 2e^{-} \tag{6.1}$$

It is generally accepted that the anodic dissolution of copper is influenced by chloride concentration independently of pH [85, 360]. However, it is also observed that the chloride ions have less influence on the dissolution of copper at higher pH values. The E-pH diagram compiled by Tromans and Sun [361] shows that the $CuCl_2^-$ complex is stable at low applied potentials and it becomes increasingly more stable with decreasing pH, while at higher pH it does not form at all. Instead copper oxides and hydroxy-containing species are generated [85, 361, 362]. Therefore, another factor that was considered in the synthesis of the viologens at the copper surface was the pH of the solution.

The pH was varied between pH 2.0 and 9.0. This covers a wide pH range extending from the soluble Cu^{2+} phase to the Cu_2O and hydrated copper oxides. Moreover, it is well known that OH^- adsorption is facilitated at higher pH values to give passivation of the copper surface [78, 278, 279]. The pH of the 0.10 mol dm^{-3} NaCl with 2.0×10^{-3} mol dm^{-3} viologen solution was adjusted using either HCl or NaOH, ensuring that no additional anions were introduced into the solution. The viologen films were deposited by cycling the copper electrode from -0.20 to 1.00 V vs. SCE at 1 mV s^{-1}. Representative data are presented in Figure 6.8, for copper cycled in the absence of the viologens and in Figure 6.9 for the BV system at pH values from 2.0 to 9.0.

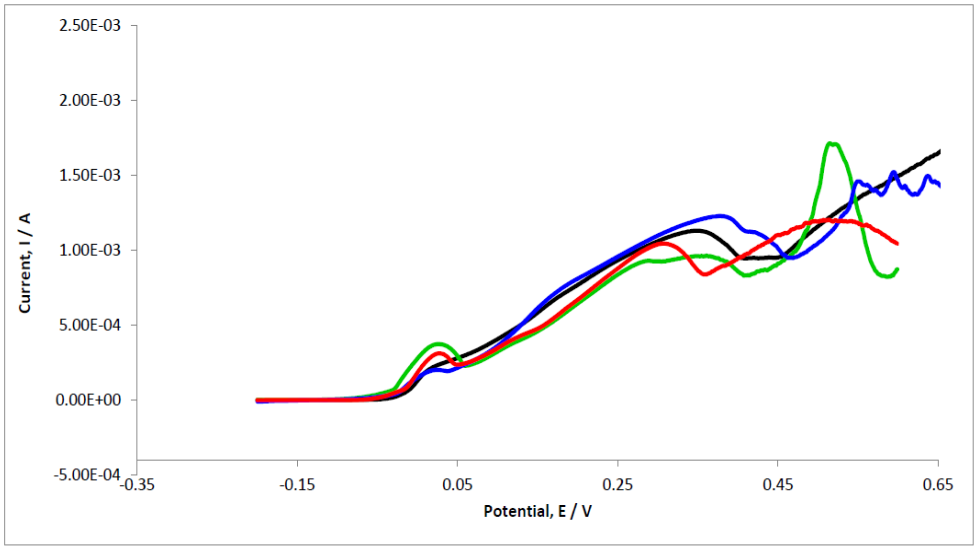

Figure 6.8: Current plotted as a function of increasing applied potential for Cu cycled at 1 mV s^{-1} in 0.10 mol dm^{-3} NaCl at pH values of 3.0 (black), 4.0 (green), 5.0 (blue) and 7.0 (red).

The data presented for copper cycled in the absence of the viologens is typical of active dissolution of the copper substrate. The current continues to increase from about 0.05 V vs. SCE to the final potential of 0.60 V vs. SCE. The characteristic peak seen at about 0.02 V vs. SCE, Figure 6.4, is observed at pH 3.0 to 7.0 and there appears to be very little difference in either the peak position or indeed the peak current as the pH is varied. The current continues to increase on further polarisation and there appears to be little variation in either the charge or the current as the pH is varied over this pH range. This is evident from the data presented in Table 6.1 where the current and charge, measured from the voltammograms at 0.40 V vs. SCE, are presented for copper in the absence of the viologens.

The data presented for the BV system again are consistent with the formation of a pseudo-passive film and are significantly different to that obtained for copper in the absence of the viologens. The initial dissolution peak appears to be dependent on the pH of the solution, with higher peak currents measured in the more acidic solutions. At a pH of 9.0, this peak is no longer observed and the current remains higher from about 0.10 to 0.80 V vs. SCE, but then the current decays as the potential is cycled to values in the vicinity of 1.00 V vs. SCE, Figure 6.9. This is consistent with the adsorption of OH^- and the formation of oxides at pH 9.0. This inhibits the formation of the initial chloride-containing anionic layer and consequently the BV-containing films are slower to form at the surface.

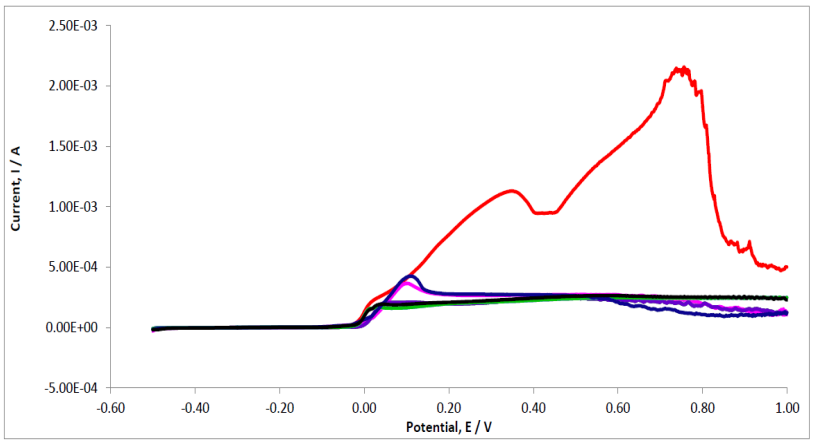

(a)

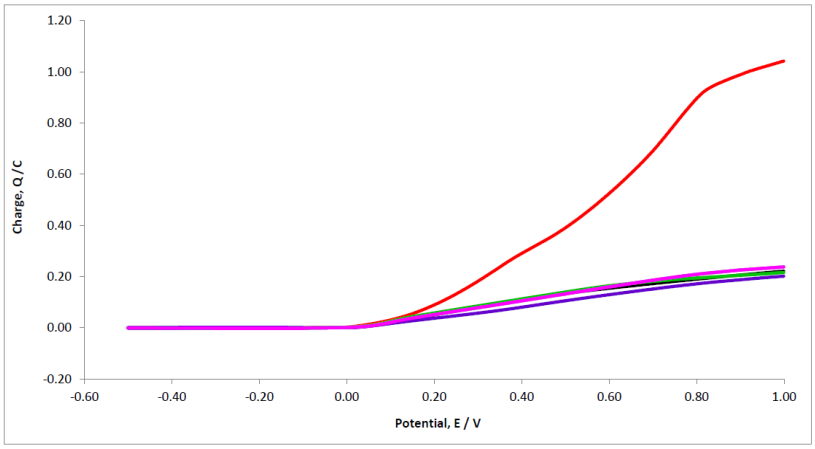

(b)

Figure 6.9: (a) Current plotted as a function of increasing applied potential and (b) charge plotted as a function of applied potential for Cu cycled at 1 mV s^{-1} in 0.10 mol dm^{-3} NaCl with the addition of 2.0 × 10^{-3} mol dm^{-3} BV at pH values of 2.0 (green), 3.0 (purple), 5.0 (black), 6.0 (blue), 7.0 (grey), 8.0 (pink) and 9.0 (blue) and at a pH of 7.0 in the absence of the viologen (red).

Although the pH has some influence at the lower applied potentials, the formation of the pseudo-passive layer seems to have little influence on the pH of the solution. Indeed, this is clearly evident in the charge plots where essentially identical charges are computed as a function of the pH. Similar data were recorded for the MV and EV and these are summarised in Tables 6.1, 6.2, 6.3 and 6.4. There is no significant variation in the charge or the current, measured at 0.40 V vs. SCE, as a function of the pH of the solution, indicating that the pH has little influence on the formation of the viologen films or on the stability and protective properties of the films. This is significant as the viologen-containing films have the potential to protect the copper from dissolution over a wide pH range, extending from pH 2.0 to 9.0.

Table 6.1: Current and charge recorded at 0.40 V vs. SCE for Cu in the absence of viologens.

Copper (Cu)		
pH	**Current/A**	**Charge/C**
3.0	9.59×10^{-4}	2.90×10^{-1}
4.0	8.58×10^{-4}	2.61×10^{-1}
5.0	1.66×10^{-3}	3.02×10^{-1}
7.0	9.46×10^{-4}	2.62×10^{-1}

Table 6.2: Current and charge recorded at 0.40 V vs. SCE for Cu in the presence of BV.

Benzyl viologen (BV)		
pH	**Current/A**	**Charge/C**
2.0	2.71×10^{-4}	1.05×10^{-1}
3.0	2.71×10^{-4}	1.13×10^{-1}
5.0	2.44×10^{-4}	8.45×10^{-2}
6.0	2.26×10^{-4}	7.80×10^{-2}
7.0	2.46×10^{-4}	8.04×10^{-2}
8.0	2.54×10^{-4}	8.04×10^{-2}
9.0	2.59×10^{-4}	1.10×10^{-2}

Table 6.3: Current and charge recorded at 0.40 V vs. SCE for Cu in the presence of EV.

Ethyl viologen (EV)		
pH	**Current/A**	**Charge/C**
2.0	2.74×10^{-4}	5.55×10^{-2}
3.0	2.38×10^{-4}	6.00×10^{-2}
5.0	2.28×10^{-4}	8.66×10^{-2}
6.0	1.51×10^{-4}	8.26×10^{-2}
7.0	1.82×10^{-4}	7.72×10^{-2}
8.0	1.86×10^{-4}	8.76×10^{-2}
9.0	1.88×10^{-4}	8.11×10^{-2}

Table 6.4: Current and charge recorded at 0.40 V vs. SCE for Cu in the presence of MV.

Methyl viologen (MV)		
pH	**Current/A**	**Charge/C**
3.0	3.72×10^{-5}	5.00×10^{-2}
5.0	8.42×10^{-5}	7.28×10^{-2}
7.0	1.78×10^{-5}	7.00×10^{-2}
9.0	6.66×10^{-5}	6.88×10^{-2}

6.2.4 The Influence of the Chloride Concentration

The concentration of chloride anions is well known to influence the corrosion products formed at copper. Different soluble and insoluble chloride-containing copper species have been observed and identified, and it has been shown that the nature of the corrosion products is highly dependent on the concentration of the chloride anions.

A number of studies on the mechanism of copper electro-dissolution in chloride media has been reported [8, 165, 338] and the role of various chloride-containing corrosion products has been discussed. At chloride concentrations lower than 1.0 mol dm^{-3}, the dissolution of copper proceeds with the formation of CuCl, as shown in Equation 6.2 [363]. However, several authors have observed the formation of $CuCl_2^-$ species, Equations 6.3 and 6.4, and have proposed that it is these soluble species that control the kinetics of the anodic dissolution of copper in inhibitor-free solutions. It has also been proposed that the soluble $CuCl_2^-$ species arise from the oxidation of copper to the cuprous ion, as shown in Equations 6.5 and 6.6.

$$Cu + Cl^- \rightarrow CuCl + e^- \tag{6.2}$$

$$CuCl + Cl^- \rightarrow CuCl_2^- \tag{6.3}$$

$$Cu + 2Cl^- \rightarrow CuCl_2^- + e^- \tag{6.4}$$

$$Cu \rightarrow Cu^+ + e^- \tag{6.5}$$

$$Cu^+ + 2Cl^- \rightarrow CuCl_2^- \tag{6.6}$$

At chloride concentrations higher than 1.0 mol dm^{-3}, complexes such as $CuCl_3^{2-}$ and $CuCl_4^{3-}$ are formed [262, 363]. However, in alkaline solutions containing chloride ions the mechanism can be very different, with the additional formation of various oxides and hydroxy-containing species [338, 364]. Indeed in alkaline solutions the formation of Cu_2O films can be favoured over the formation of CuCl [338, 364]. This suggests that the electrochemical behaviour of copper is governed by two parallel reactions leading to either the formation of the Cu_2O film, that leads to passivity, or nucleation and growth of CuCl layers [91, 365].

The influence of chloride concentration on the breakdown of passive films formed on copper has been reported. Anodic polarisation data obtained by Thomas and Tiller [80] in

0.01 and 0.10 mol dm^{-3} NaCl reveal that although copper is passive in a wide potential region, breakdown of the passive film occurs and the breakdown potential shifts to more negative potentials as the chloride concentration is increased. It was also shown that the breakdown resulted in localised corrosion, or pitting attack. Starosvetsky *et al.* [282] investigated the effect of varying the concentration of chloride ions and found that at higher concentrations of NaCl the anodic current rapidly increased with a positive potential shift, reaching a maximum current density of approximately 20 mA cm^{-2} at 50 mV vs. SCE. A reduction in the anodic current was then observed. This type of anodic behaviour is associated with copper dissolution through a soluble chloride complex of $CuCl_2^-$ [338]. Indeed, these $CuCl_2^-$ species have been discussed [85, 361] in the dissolution of copper. A linear relationship between the electrode potential and the logarithm of the current density was obtained and this was explained in terms of the diffusion of soluble $CuCl_2^-$ species as the rate-determining step. It was concluded that dissolution of the copper was diffusion controlled [85, 361]. In addition, the formation of a CuCl film was proposed [85] in agreement with Equation 6.2.

As chloride anions were used to prepare the viologen films and the concentration of chloride clearly has a significant influence on the dissolution of copper, the influence of the chloride concentration on the formation of the viologen films was studied. The chloride concentration was varied from 2.5×10^{-3} to 0.30 mol dm^{-3}, the concentration of the viologen was maintained at 2.0×10^{-3} mol dm^{-3} and the pH of the final solution was adjusted with HCl to pH 3.0. The viologen-containing films were formed by cycling the copper electrode at a scan rate of 1 mV s^{-1} from an initial potential of -0.20 V to 1.00 V vs. SCE. Representative data are shown in Figure 6.10a where the voltammograms recorded in 0.0125 mol dm^{-3} NaCl are presented, for the MV, EV and BV, while data recorded for the BV in the presence of 0.0125, 0.0250 and 0.0500 mol dm^{-3} NaCl are shown in Figure 6.10b.

It is clear on comparing the data recorded for copper in the absence of the viologen, Figure 6.10a, to that data presented in Figure 6.4 at the higher concentration, that the concentration of chloride has a significant influence on the rate of copper dissolution. At the lower concentration, the current begins to increase at about 0.05 V vs. SCE and relatively high currents in the vicinity of 0.80 mA cm^{-2} are observed at 0.80 V vs. SCE, indicating dissolution of the copper. However, there is no evidence of any peak at the lower potentials, instead the current increases in a near linear manner with increasing potential. The data recorded for the

violgens are also very different. The peak observed at 0.08 V vs. SCE, Figure 6.4, is again evident in the data shown in Figure 6.10. However the peak is considerably broader and occurs at higher potentials, at approximately 0.22 V vs. SCE. This effect is more clearly evident in Figure 6.10b. Indeed, the peak currents depend on the chloride concentration, giving a peak current of 0.14 mA cm^{-2} in the presence of 0.0125 mol dm^{-3} NaCl, but increasing to 0.23 and 0.40 mA cm^{-2} as the chloride concentration is increased from 0.025 to 0.050 mol dm^{-3}. It is clear that the chloride concentration has a significant influence on the initial dissolution of copper and as this dissolution is extended over a wider potential range the formation of the viologen films is somewhat inhibited. This effect is observed for the three viologens, as highlighted in Figure 6.10a.

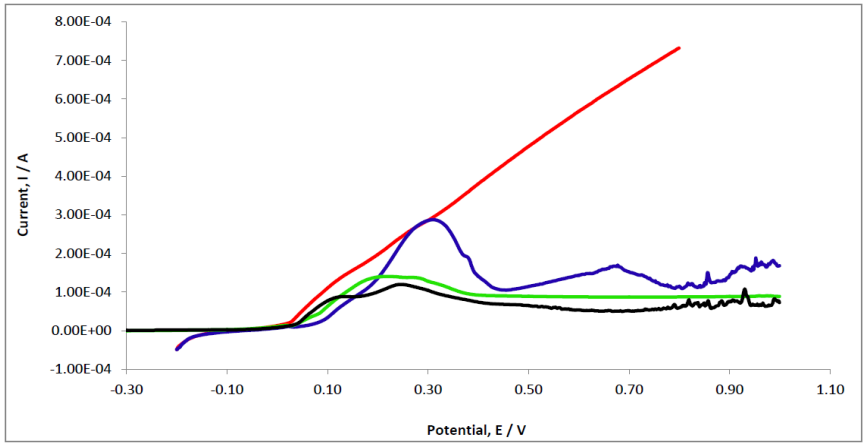

(a)

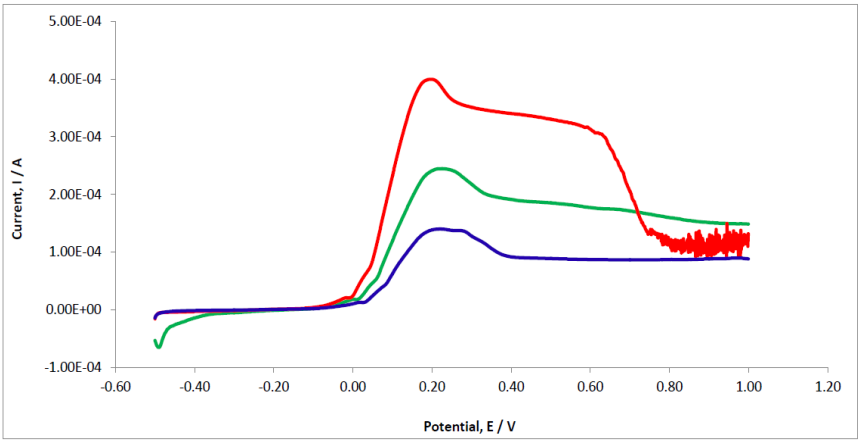

(b)

Figure 6.10: Current plotted as a function of increasing applied potential for Cu cycled at 1 mV s^{-1} in (a) 0.0125 mol dm^{-3} NaCl in the absence (red) and presence of 2.0×10^{-3} mol dm^{-3} BV (green), EV (black), MV (blue) at a pH of 3.0, (b) 2×10^{-3} mol dm^{-3} BV and 0.0125 (blue), 0.025 (green) and 0.050 (red) mol dm^{-3} NaCl, at a pH of 3.0.

The influence of higher concentrations of chloride on the formation of the BV films are shown in Figure 6.11, where data are presented for the BV in 0.10, 0.20 and 0.30 mol dm^{-3} NaCl. Relatively sharp peaks are observed, indicating the deposition of a stable CuCl complex, in a relatively short period, that facilitates the deposition of the viologen. However, at these higher concentrations, the formation of various soluble copper-chloride species, such as $CuCl_2^-$, $CuCl_3^{2-}$ and $CuCl_4^{3-}$, is possible [283]. Again, the peak current is clearly dependent on the concentration of the chloride anion and increases to approximately 1 mA cm^{-2} in the presence of 0.30 mol dm^{-3} NaCl. The BV-containing films are formed successfully at these higher chloride concentrations and accordingly good corrosion protection of the underlying copper is observed. It appears that 0.10 mol dm^{-3} is the optimum concentration of the chloride electrolyte. At this concentration the formation of the CuCl layer is efficient, but the chloride anion concentration is not sufficiently high to convert the CuCl layer to the soluble $CuCl_2^-$, $CuCl_3^{2-}$ and $CuCl_4^{3-}$ species. Similar results were obtained with the MV, while the EV films were only protective with higher concentrations of the viologen. Again, a 0.10 mol dm^{-3} concentration of chloride was found to be the optimum in depositing the MV and EV films.

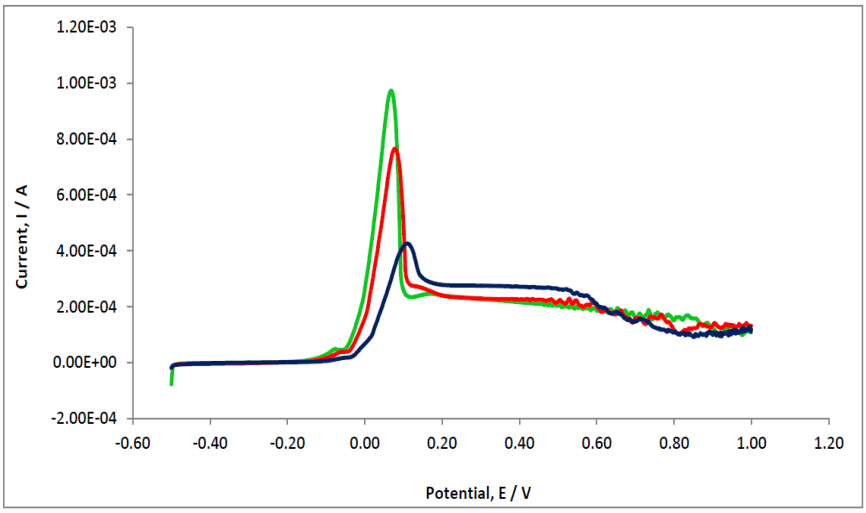

Figure 6.11: Current plotted as a function of increasing applied potential for Cu cycled at 1 mV s^{-1} in 2.0×10^{-3} mol dm^{-3} BV and 0.10 (blue), 0.20 (red) and 0.30 (blue) mol dm^{-3} NaCl, at a pH of 3.0.

6.2.5 The Influence of the Immersion Time and Electrochemical Window

The influence of the immersion period in the viologen-containing solution was studied to determine if the initial immersion in the presence of viologen had any influence on the formation and protective properties of the viologen-containing films. In these experiments the copper was immersed in the 2.0×10^{-3} mol dm^{-3} viologen solution in 0.10 mol dm^{-3} NaCl at a pH of 3.0 for periods ranging from 0 to 30 min, then the copper was polarised from an initial potential of -0.20 V vs. SCE. Representative data are presented in Figure 6.12 for the BV, EV and MV systems. The data recorded for the BV, Figure 6.12a, clearly show that the initial immersion period has no influence on the voltammograms, or on the formation of the BV film at the copper. Likewise, the immersion period has little or no significant influence on the data recorded for the EV and MV systems. In particular, the initial immersion in the EV solution does not give rise to any additional protective properties to the film. The current increases as the potential is increased and the rate of this increase is independent of the immersion period. It is clear that protective EV-containing films can only be deposited with higher viologen concentrations. Furthermore, with the longer immersion periods there is no significant variation in the second broad peak, observed from about 0.10 to 0.30 V vs. SCE, for the MV system, Figure 6.12.

Studies on the influence of the electrochemical window, in particular the initial potential, were carried out. Voltammograms were recorded by varying the initial potential from -0.50 to -0.20 V, and then the copper was cycled at 1 mV s^{-1} from this initial potential to 1.00 V vs. SCE in the MV, EV and BV-containing solutions. Although, not shown here, data identical to that presented in Figure 6.12 were obtained, indicating that the initial potential has no influence on the formation of the viologen-containing films.

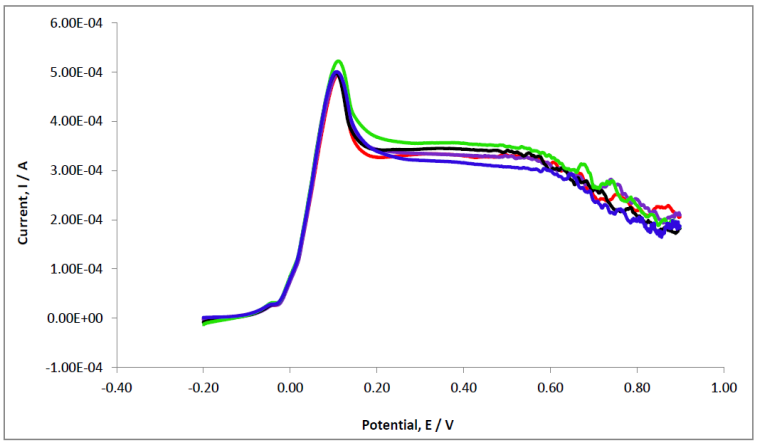

(a)

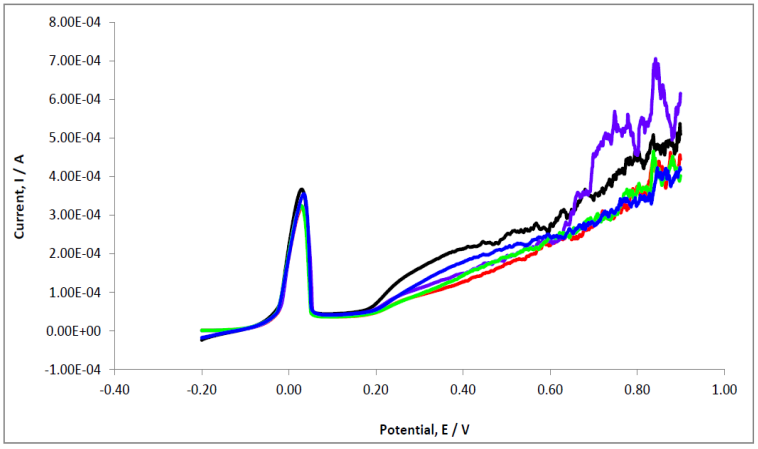

(b)

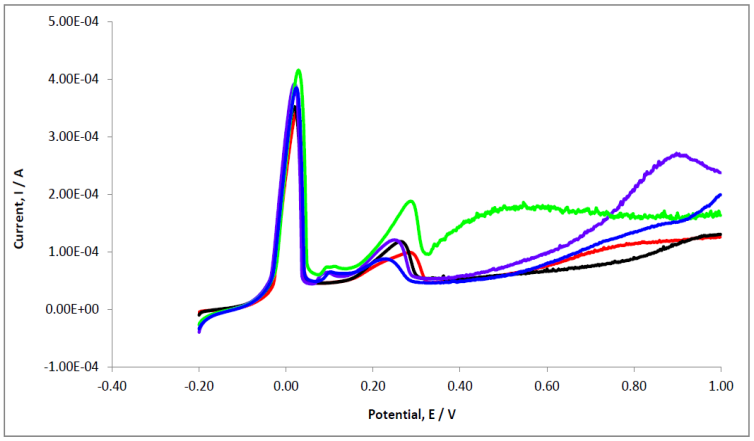

(c)

Figure 6.12: Current plotted as a function of increasing applied potential for Cu cycled at 1 mV s^{-1} in 0.10 mol dm^{-3} NaCl, pH 3.0 solution as a function of the immersion period in the presence of (a) 2.0×10^{-3} mol dm^{-3} BV (b) 2.0×10^{-3} mol dm^{-3} EV and (c) 2.0×10^{-3} mol dm^{-3} MV (5 min-red, 10 min-black, 15 min-purple, 20 min-green and 30 min-blue).

6.2.6 Morphology and Surface Analysis of the Benzyl Viologen Films

It is evident from the data presented in Sections 6.2.1 to 6.2.5 that the BV films and, to a somewhat lesser extent, the MV films are stable and protective, while the EV films are only protective when higher concentrations of the viologen are employed. Therefore, a surface analytical study was carried out with the BV system.

As shown in Figure 6.13, the measured current depends on the applied potential, with relatively high currents from about 0.00 to 0.20 V vs. SCE, then a pseudo-like passive region, which extends from about 0.20 to 0.60 V vs. SCE and then a further more gradual decay in the current from 0.60 to 1.00 V vs. SCE, in the presence of the BV. However, as shown in Figures 6.4 and 6.5, this third region depends on the nature of the viologen and it is not observed in the absence of the viologen. Instead, there is a considerable increase in the current from 0.60 to 1.00 V vs. SCE in the absence of the viologen, indicating active dissolution of the copper. In an attempt to determine the morphology and composition of the films deposited at the copper electrode during this cycling period, the copper electrode was cycled from an initial potential of -0.20 V vs. SCE to higher potential limits of 0.00, 0.20 and 0.60 V vs. SCE as highlighted in Figure 6.13, and removed from the solution. The morphology of the modified copper surface was then analysed using scanning electron microscopy (SEM), while information on the composition of the viologen-containing films was obtained using energy dispersive X-Ray analysis (EDX). The copper electrode was immersed in the 0.10 mol dm^{-3} NaCl solution or a 0.10 mol dm^{-3} NaCl solution containing 2.0×10^{-3} mol dm^{-3} BV and cycled from -0.20 V vs. SCE to upper potential limits of 0.00 V, 0.20 V or 0.60 V vs. SCE at 1 mV s^{-1}. The electrode was then removed from the electrochemical cell, rinsed several times with distilled water to ensure a clean surface that was free from any viologens that were not incorporated within the film and finally dried in a stream of air. This procedure was repeated a number of times in order to achieve more accurate and reliable EDX results as shown in Figure 6.14.

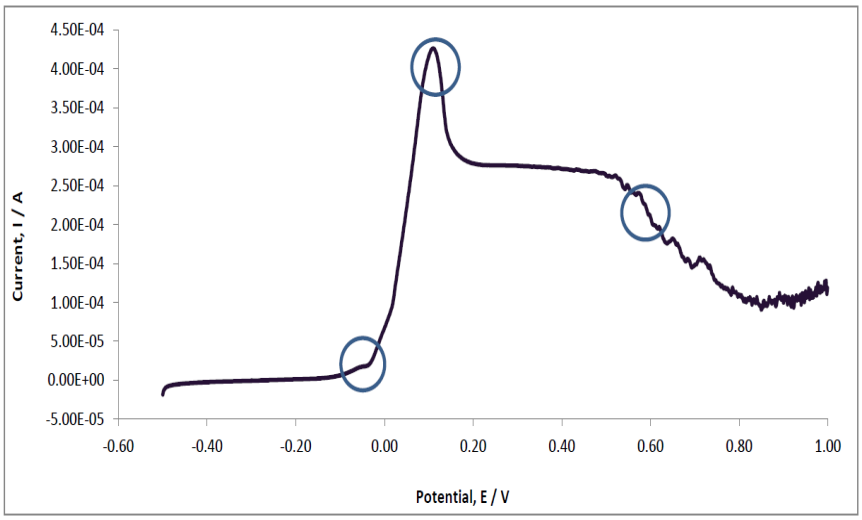

Figure 6.13: A typical voltammogram for the formation of BV at the Cu interface. The areas circled on the plot indicate the potential where the surface analyses were performed.

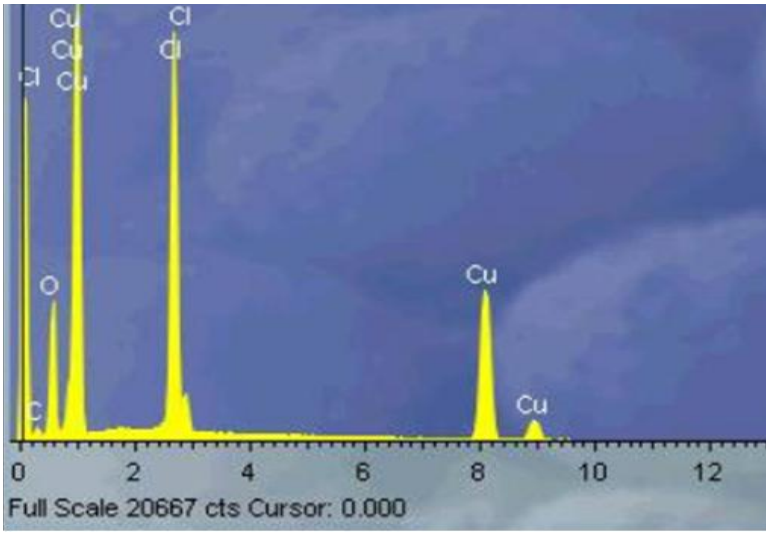

Figure 6.14: EDX spectrum of Cu cycled from -0.20 to 0.00 V vs. SCE in 0.10 mol dm^{-3} NaCl, 2.0×10^{-3} mol dm^{-3} BV, at pH 3.0.

In Figure 6.15 scanning electron micrographs are shown for the copper electrode polarised from -0.20 to 0.00 V vs. SCE in the chloride solution and in the BV-containing solution, while the EDX spectrum recorded for the BV modified copper is shown in Figure 6.14. There is a considerable difference between the micrographs presented in Figure 6.15 for the copper cycled in the chloride solution and in the BV solution. A layer or film is clearly evident on the copper cycled in the BV-containing solution and as shown in the EDX spectrum, Figure 6.14, this layer is composed of chloride, at a relatively high concentration, oxygen and carbon. The presence of the chloride is consistent with the formation of a CuCl complex layer, while the oxygen indicates the formation of copper oxides or hydroxides, possibly Cu_2O, Cu(OH), or hydrated oxides of Cu_2O. Although Cu_2O is in equilibrium with CuO, it is unlikely given the Pourbaix diagram of Cu, Chapter 1, Section 1.3.1, that significant amounts of CuO are formed as the potential was only cycled to 0.00 V vs SCE. The presence of the carbon, which was not detected when the copper was cycled in the simple chloride solution, is evidence for the presence of the BV.

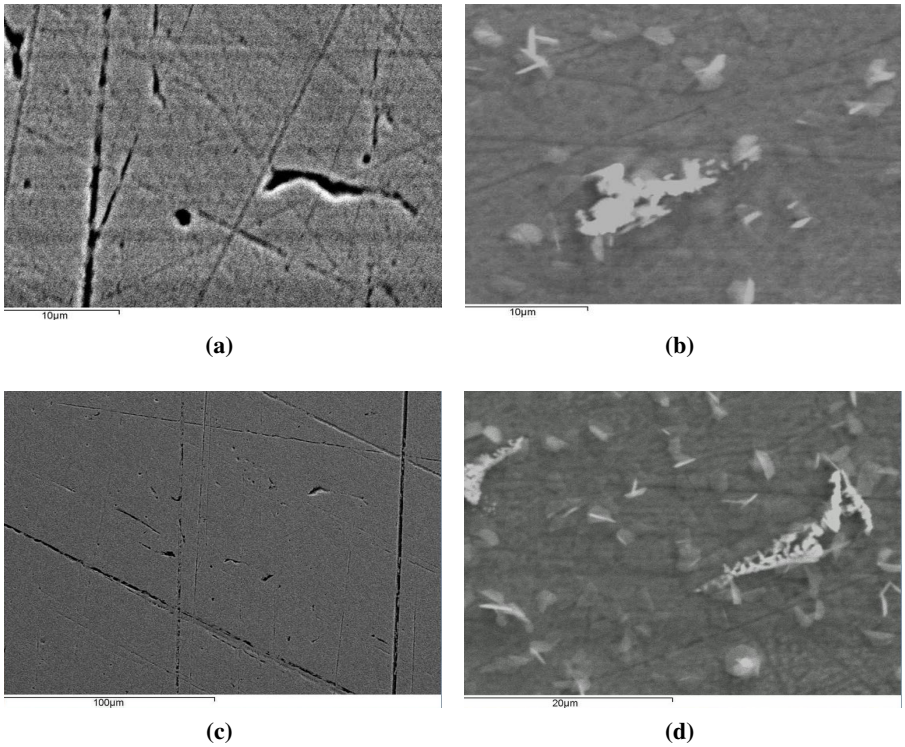

(a) **(b)** **(c)** **(d)**

Figure 6.15: SEM micrographs of Cu cycled from -0.20 to 0.00 V vs. SCE in (a) 0.10 mol dm^{-3} NaCl, pH 3.0 at 10 μm (b) 0.10 mol dm^{-3} NaCl, 2.0×10^{-3} mol dm^{-3} BV, pH 3.0, at 10 μm (c) 0.10 mol dm^{-3} NaCl, pH 3.0 at 100 μm and (d) 0.10 mol dm^{-3} NaCl. 2.0×10^{-3} mol dm^{-3} BV, pH 3.0 at 20 μm.

The EDX spectrum, presented in Figure 6.14, for the viologen-modified surface clearly shows the formation of a CuCl layer, or film, at the surface, while the carbon signal indicates the presence of the BV. The EDX spectrum was recorded at a number of different points on the surface and the spectra collected were similar. In particular, carbon was detected in all analyses, indicating a uniform or near uniform viologen-containing film at the copper surface. Although not shown, the EDX spectra of the copper cycled in the acidified chloride solution but in the absence of the BV, indicate the formation of the chloride layer, however the intensity of the signal at 2.7 keV is somewhat reduced, which may indicate that the formation of the CuCl complex is facilitated in the presence of the BV. In addition, there was no evidence of carbon in any of the spectra, suggesting that the carbon is indeed related to the presence of the BV.

The SEM micrographs obtained for the copper cycled in the presence and absence of the BV from -0.20 to 0.20 V vs. SCE are shown in Figure 6.16. These micrographs are very different compared to the micrographs depicted in Figure 6.15, showing a considerable change in the surface morphology, when the copper is polarised to 0.20 V vs. SCE. At this potential, significant dissolution of the copper is observed, as shown in Figure 6.4 and this alters the morphology of the surface. At this potential, there is little difference between the morphology of the copper cycled in the presence and absence of the BV. The EDX spectrum recorded for the BV-modified surface is presented in Figure 6.17. Again, the C signal indicates the presence of the viologen, while the O and Cl arise from the formation of copper oxides and the CuCl layer. At this potential, the copper oxides, are likely to be dominated by the Cu(II) oxide species, such as CuO, $Cu(OH)_2$, $Cu_2(OH)_3Cl$, as indicated in the Pourbaix diagram of copper, Chapter 1, Section 1.1. Interestingly, the ratio of the Cu to Cl signals is similar to that observed in Figure 6.14, where the potential was cycled to 0.00 V vs. SCE. This indicates that a higher concentration of chloride-containing species is not observed on cycling the copper to 0.20 V vs. SCE in the BV solution. The EDX spectrum of the copper cycled to 0.20 V vs. SCE, but in the absence of the BV, showed evidence for the presence of the oxides and again no carbon was detected. However, the ratio of Cl to Cu was considerably higher. This indicates a significant increase in the concentration of chloride-containing species at the higher potential of 0.20 V vs. SCE. This is not surprising as significant dissolution of the copper is observed at this potential, as shown in Figure 6.4.

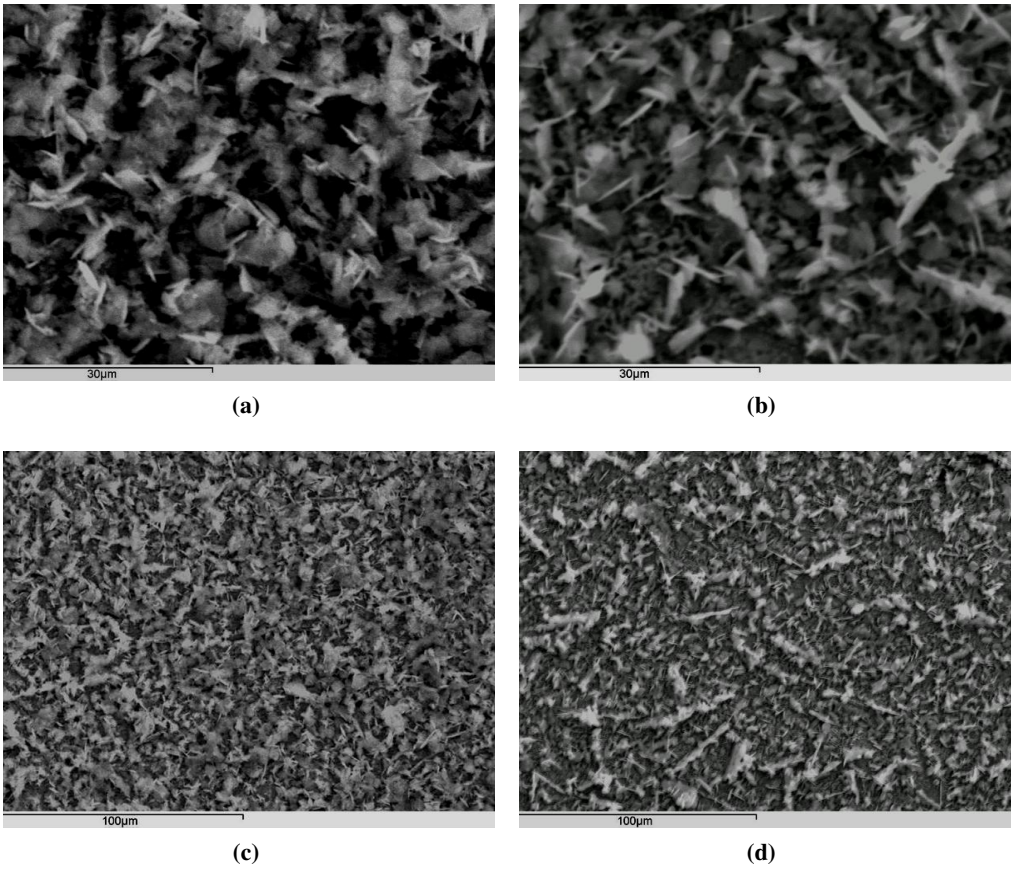

(a) **(b)**

(c) **(d)**

Figure 6.16: SEM micrographs of Cu cycled from -0.20 to 0.20 V vs. SCE in (a) 0.10 mol dm^{-3} NaCl, pH 3.0 at 30 μm (b) 0.10 mol dm^{-3} NaCl, 2.0×10^{-3} mol dm^{-3} BV, pH 3.0, at 30 μm (c) 0.10 mol dm^{-3} NaCl, pH 3.0 at 100 μm and (d) 0.10 mol dm^{-3} NaCl. 2.0×10^{-3} mol dm^{-3} BV, pH 3.0 at 100 μm.

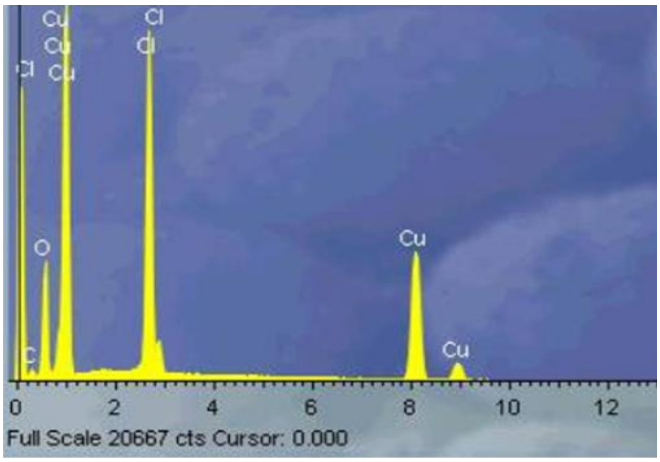

Figure 6.17: EDX spectrum of Cu cycled from -0.20 to 0.20 V vs. SCE in 0.10 mol dm^{-3} NaCl, 2.0×10^{-3} mol dm^{-3} BV, pH 3.0.

The morphology of the copper cycled in the absence and presence of the BV from -0.20 to 0.60 V vs. SCE is shown in the micrographs presented in Figure 6.18. Again, there is little difference between the morphology in the absence and presence of the BV. On comparing these micrographs to those presented in Figure 6.16, it is clear that the morphology is slightly different, with clear leaf-like structures formed at the higher potential in the presence of the viologen. These are somewhat less developed in the simple chloride-containing solution, Figure 6.18. Although, not shown, the EDX spectra are dominated by the CuCl complex at this potential in the absence of the viologen. Again, the CuCl complex is evident in the presence of the viologen and the main difference between the spectra is the carbon signal, which indicates the presence of the BV.

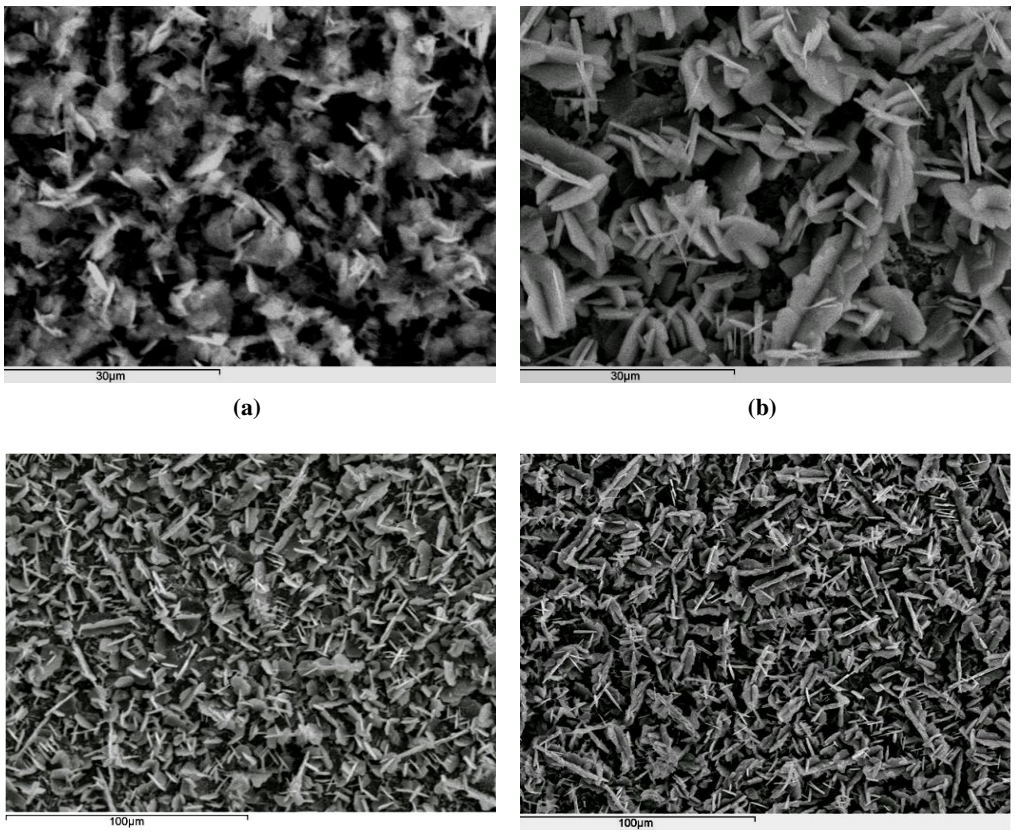

(a) **(b)**

(c) **(d)**

Figure 6.18: SEM micrographs of Cu cycled from -0.20 to 0.60 V vs. SCE in (a) 0.10 mol dm^{-3} NaCl, pH 3.0 at 30 μm (b) 0.10 mol dm^{-3} NaCl, 2.0×10^{-3} mol dm^{-3} BV, pH 3.0, at 30 μm (c) 0.10 mol dm^{-3} NaCl, pH 3.0 at 100 μm and (d) 0.10 mol dm^{-3} NaCl. 2.0×10^{-3} mol dm^{-3} BV, pH 3.0 at 100 μm.

Although it is well known that EDX is only a qualitative technique [260, 366], a quantitative analysis was attempted to obtain information on the composition of the films as the potential was varied. The EDX analyses were repeated several times on different samples and at different points on the surface. Very good reproducibility was obtained at different points on the same sample, indicating uniform coverage of the copper. The intensity of the Cl and Cu signals for both the copper and the viologen-modified copper electrode were recorded, while the C signal was monitored in the case of the viologen-modified surface. The results for the copper cycled in the chloride solution, and in the absence of the BV are summarised in Tables 6.5, 6.6 and 6.7, while the data recorded in the presence of the viologen are shown in Tables 6.8, 6.9 and 6.10, where the upper potential limits are 0.00, 0.20 and 0.60 V vs. SCE. The data shown in these tables correspond to different samples. There is reasonably good reproducibility and the standard deviations, which are provided in the table, are relatively small, indicating that while this analysis may not be appropriate to determine the actual composition of the films, trends as the potential is varied and the viologen is added can be observed.

At -0.20 V vs. SCE, the EDX spectra are dominated by the Cu signal and only low amounts of the CuCl complex are formed, with the Cl signal at about 0.16 ± 0.04%, Table 6.5. This is consistent with the micrographs, presented in Figure 6.15, which show no evidence of corrosion. However, as the potential is increased to 0.20 V vs. SCE, a considerable increase in the concentration of chloride-containing species is evident, Tables 6.5, 6.6 and 6.7. This is consistent with the dissolution of copper and the generation of corrosion products, such as CuCl, $CuCl_2^-$ and $Cu_2(OH)_3Cl$ species. It is also evident from Tables 6.5, 6.6 and 6.7, that the Cu signal is reduced from approximately 90% to 69% on increasing the potential from -0.20 to 0.60 V vs. SCE. This indicates the formation of a layer of corrosion products on the surface, which is clearly visible in the SEM micrographs, shown in Figures 6.16 and 6.18.

The data obtained in the presence of the BV are presented in Tables 6.8, 6.9 and 6.10 and in this case the C signal is also monitored as a function of the upper potential limit. From the results presented it is obvious that the carbon content increases slightly as the potential is increased from -0.20 to 0.60 V vs. SCE. This suggests that although the BV is adsorbed onto the copper at -0.20 V vs. SCE, slightly higher amounts are incorporated as the potential is increased. There is a significant reduction in the concentration of chloride-containing species in the presence of the BV, particularly at the higher applied potentials, Tables 6.8, 6.9 and 6.10.

This clearly shows that very good corrosion protection is achieved by incorporating the BV into the films. The data obtained at -0.20 V vs. SCE, shows that the BV adsorbs onto the chloride-modified copper surface, but there is no further increase in the chloride content as the potential is increased. The presence of the viologen at the surface seems to stabilise the initial CuCl complex layer that is formed at -0.20 V vs. SCE to give good corrosion protection of the underlying copper substrate.

Table 6.5: The % of Cl and Cu (n = 4) for Cu cycled to 0.00 V vs. SCE in 0.10 mol dm^{-3} NaCl.

	% Cl	**% Cu**
	0.20	93.8
	0.16	86.0
	0.10	97.4
	0.16	86.0
Average	0.16	90.8
Standard Deviation	0.04	5.7

Table 6.6: The % of Cl and Cu (n = 13) for Cu cycled to 0.20 V vs. SCE in 0.10 mol dm^{-3} NaCl.

	% Cl	**% Cu**
	27.9	72.3
	27.0	63.7
	15.4	82.2
	20.9	71.3
	23.0	66.8
	13.0	81.4
	19.0	74.4
	30.7	57.9
	26.5	64.2
	26.2	71.7
	20.3	70.3
	20.0	80.3
	20.7	78.3
Average	22.3	71.4
Standard Deviation	5.1	7.4

Table 6.7: The % of Cl and Cu (n = 7) for Cu cycled to 0.60 V vs. SCE in 0.10 mol dm^{-3} NaCl.

	% Cl	**% Cu**
	31.8	75.2
	21.6	64.0
	21.5	71.9
	16.5	72.5
	22.5	65.5
	22.7	65.7
	21.8	70.3
Average	22.5	69.3
Standard Deviation	4.5	4.2

Table 6.8: The % of Cl, C and Cu (n = 12) for Cu cycled to 0.00 V vs. SCE in 0.10 mol dm^{-3} NaCl and 2.0×10^{-3} mol dm^{-3} BV.

	% C	**% Cl**	**% Cu**
	3.7	7.1	89.0
	1.9	4.0	90.7
	2.3	7.8	81.0
	0.6	7.4	82.6
	0.6	1.8	91.9
	1.5	7.4	81.0
	1.8	7.1	81.6
	0.5	1.2	93.4
	2.6	6.3	81.0
	0.5	4.9	88.2
	0.9	6.2	85.8
	1.2	4.1	90.9
Average	1.5	5.4	86.4
Standard Deviation	0.9	2.2	4.8

Table 6.9: The % of Cl, C and Cu (n = 6) for Cu cycled to 0.20 V vs. SCE in 0.10 mol dm^{-3} NaCl and 2.0×10^{-3} mol dm^{-3} BV.

	% C	**% Cl**	**% Cu**
	4.4	3.8	90.4
	4.1	4.7	90.3
	5.8	4.4	90.1
	6.5	3.5	89.6
	4.4	3.6	89.6
	5.3	4.1	90.4
Average	5.1	4.0	90.1
Standard Deviation	0.9	0.4	0.3

Table 6.10: The % of Cl, C and Cu (n = 8) for Cu cycled to 0.60 V vs. SCE in 0.10 mol dm^{-3} NaCl and 2.0×10^{-3} mol dm^{-3} BV.

	% C	**% Cl**	**% Cu**
	4.9	3.7	87.1
	4.1	3.4	92.1
	5.9	3.9	89.2
	7.6	3.7	89.5
	6.7	3.4	90.8
	5.3	3.6	89.1
	6.7	3.5	83.5
	6.0	3.9	90.8
Average	5.91	3.6	89.0
Standard Deviation	1.1	0.19	2.6

6.2.7 Comparison with Benzotriazole (BTA)

Benzotriazole (BTA) is one of the most widely used inhibitors in the corrosion protection of copper and its alloys [7], and for this reason the properties of the viologen system were compared to this well-known and documented corrosion inhibitor. BTA is a heterocyclic compound, as shown in Figure 6.19, and it appears to function as an inhibitor through chemical bonding to the metal or metal oxide surface [83]. The presence of the nitrogen atoms in the triazole ring enables bonding with copper and this gives a highly stable film with good corrosion protection properties.

Commencing with the pioneering work of Cotton and co-workers [367] many investigations relating to the inhibition phenomenon observed with BTA have been published [69, 90]. These include comparative electrochemical and corrosion studies in the presence and absence of BTA. The early work published by Cotton *et al.* [70, 82] postulated that the corrosion inhibition effect of BTA is due to the formation of a strongly bonded chemisorbed two-dimensional barrier film less than 50 Å thick. This insoluble film, which may be a monomolecular layer, protects copper and its alloys in aqueous media, and also in the presence of lubricants, and hydraulic fluids. BTA has been described as an anodic corrosion inhibitor and its deposition at the copper surface has been shown to follow the Langmuir isotherm, followed by the formation of complex Cu(I)-BTA [368, 369]. Coordination between the BTA molecule and the copper occurs through the nitrogen atom of the triazole ring. BTA molecules can be oriented in parallel or vertical to the surface [90, 370]. The orientation of the inhibitor molecule is important because of the possibility of formation of stronger bonds if

the orientation is parallel due to interaction of the π electrons of the ring with vacant *d* orbitals of copper [90, 368, 370, 371]. The complex formation can be described by Equation 6.7, where Cu-BTAH$_{(ads)}$ corresponds to the adsorbed BTA at the copper surface. In the presence of oxidants or by anodic polarisation, the adsorbed BTAH is transformed to the Cu(I)-BTA complex, as shown in Equation 6.8.

$$Cu_{(s)} + BTAH \rightarrow Cu - BTAH_{(ads)} \tag{6.7}$$

$$Cu - BTAH_{(ads)} \rightarrow Cu(I) - BTA + H^{+} + e^{-} \tag{6.8}$$

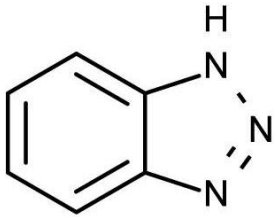

Figure 6.19: Chemical structure of benzotriazole (BTA).

From this equation it can be seen that an increase in the BTA concentration shifts the reaction towards formation of larger amounts of protective complex, Cu(I)-BTA. Indeed, this is confirmed in numerous experiments. For example, Tromans and Sun [85] constructed the E-pH diagrams for systems containing copper and BTA that provide an indication when the protective action can be expected, and when not, depending on pH, potential and inhibitor concentration. As the adsorption is an exothermic process an increase in temperature has an adverse effect on the inhibition efficiency.

In these experiments the protective properties of the viologen films were compared to that afforded by the BTA in 0.10 mol dm^{-3} NaCl with pH values ranging from 2.0 to 9.0. The concentration of the BTA was 2.0×10^{-3} mol dm^{-3}. This is typical of the concentrations used in literature reports [313], and compares well with the values given by Tromans and Sun [85], but in some cases BTA concentrations as high as 0.01 mol dm^{-3} have been employed [313, 368]. In addition, the BTA solutions were not de-oxygenated, as it has been reported that the presence of dissolved oxygen facilitates the formation of the Cu(I)-BTA [313, 369]. This is connected with the oxidising properties of the adsorbed oxygen, which gives rise to Cu(I) and the formation

of the Cu(I)-BTA complex [372, 373]. The data recorded in the acidified solution, at a pH of 3.0, are shown in Figure 6.20. Here the data recorded for copper in the 0.10 mol dm^{-3} NaCl solution, in the absence and presence of the viologens, and in the presence of BTA are shown. Again the potential was cycled at 1 mV s^{-1} from -0.20 to 1.00 V vs. SCE. Apart from the EV system, the BV and MV and the BTA show good corrosion protection. However, the charge plots indicate the formation of a highly stable and protective film in the presence of BTA. Accordingly, under these slightly acidic conditions the BTA provides the more protective film. The protective properties of the BTA are more clearly shown in Figure 6.21, where the results recorded under identical conditions are compared [7]. There is no evidence of the characteristic peak at about 0.08 V vs. SCE observed for the viologen system. Instead, the currents remain low until the breakdown of the film occurs between 0.20 and 0.80 V vs. SCE.

It has been shown that relatively thick BTA films are formed under slightly acidic conditions and that these films can be porous and permeable to oxygen and indeed other species [371]. This might account for the difference observed in the breakdown potentials recorded in Figure 6.21, which vary by about 600 mV. It has also been reported by Musiani *et al.* [374] that the degree of Cu(I)-BTA polymerisation is pH dependent, with higher rates at higher pH values due to the presence of stable copper oxides. The role of copper oxides in the adsorption of BTA is controversial with several reports indicating that oxides are essential for the adsorption of BTA [375, 376], while other reports indicate that these oxide phases are not particularly important [69, 70, 90, 377, 378, 379, 380]. In the presence of 0.10 mol dm^{-3} NaCl and at a pH of 3.0, these copper oxides are not stable. However, Tromans and Sun [85] have shown that the Cu(I)-BTA complex can be formed on oxide-free copper in the presence of chloride anions, in accordance with Equations 6.9, 6.10 and 6.11.

$$Cu + BTAH \rightarrow Cu - BTAH_{(ads)} \tag{6.9}$$

$$nCuCl_2^- + nBTAH \rightarrow (Cu(I) - BTA)_n + nH^+ + 2nCl^- \tag{6.10}$$

$$Cu - BTAH_{(ads)} + Cu(I) - BTA_n \rightarrow [Cu - BTAH + (Cu(I) - BTA)_n]_{(ads)} \tag{6.11}$$

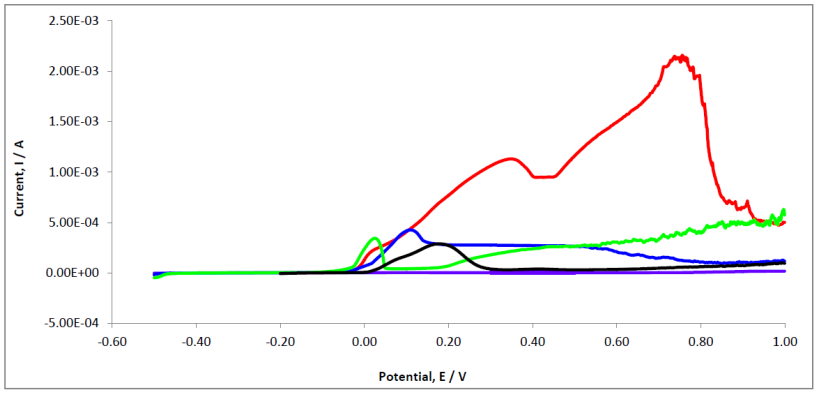

(a)

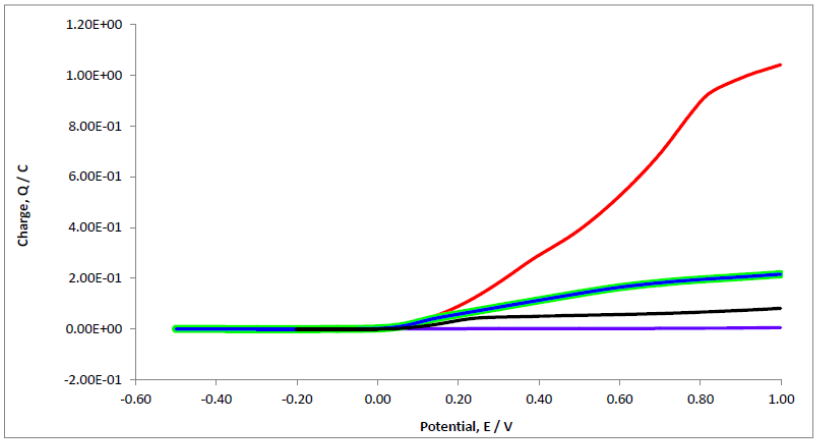

(b)

Figure 6.20: Current and charge plotted as a function of increasing applied potential for Cu cycled at 1 mV s^{-1} in 0.10 mol dm^{-3} NaCl, pH 3.0 solution in the absence (red) and in the presence of 2.0×10^{-3} mol dm^{-3} BV (blue), 2.0×10^{-3} mol dm^{-3} EV (green), 2.0×10^{-3} mol dm^{-3} MV (black) and 2.0×10^{-3} mol dm^{-3} BTA (purple).

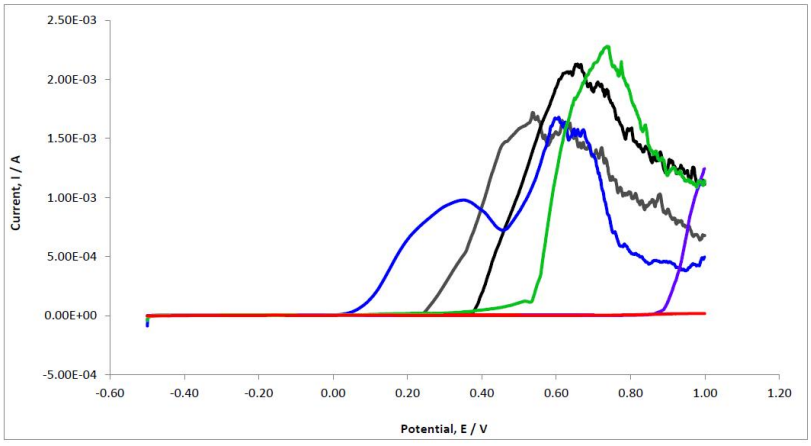

Figure 6.21: Current plotted as a function of increasing applied potential for Cu cycled at 1 mV s^{-1} in 0.10 mol dm^{-3} NaCl, pH 3.0 solution in the presence of 2.0×10^{-3} mol dm^{-3} BTA.

The adsorption of BTA occurs as shown in Equation 6.9, while the Cu(I)-BTA complex is formed in the diffusion layer through reaction with $CuCl_2^-$, Equation 6.10. Then, this complex is adsorbed on the initial Cu-$BTAH_{(ads)}$ monolayer to form a polymeric film, Equation 6.11. The protective properties observed with the BTA molecule, Figures 6.20 and 6.21, are consistent with this sequence of reactions.

The protective properties of the MV, EV and BV films are compared with the BTA inhibitor in 0.10 mol dm^{-3} NaCl solutions at a pH of 5.0 in Figure 6.22 and at a pH of 7.0 in Figure 6.23. Again, there is no evidence of the initial dissolution of copper in the presence of BTA at pH 5.0 or at pH 7.0. Indeed, this may be related to Equations 6.9 and 6.10, where the adsobed BTA inhibits the dissolution of copper and complexes with any $CuCl_2^-$ species that are generated. The data recorded at a pH of 5.0 show the breakdown of the film at about 0.58 V vs. SCE. This is followed by significant dissolution of the copper.

The data shown for the pH 7.0 solution indicate little difference between the copper cycled in the presence of the BTA and in the absence of the BTA, this is particularly evident in the charge-potential profile. Similar results were obtained as the pH was increased further [368]. This is somewhat surprising as many reports indicate that BTA is more effective at higher pH values. However, at these higher pH values the copper oxides are more stable and the BTA action may be hindered, and under these conditions the reactions highlighted in Equations 6.9, 6.10 and 6.11 will no longer be the predominant steps in the formation of the Cu(I)-BTA complex.

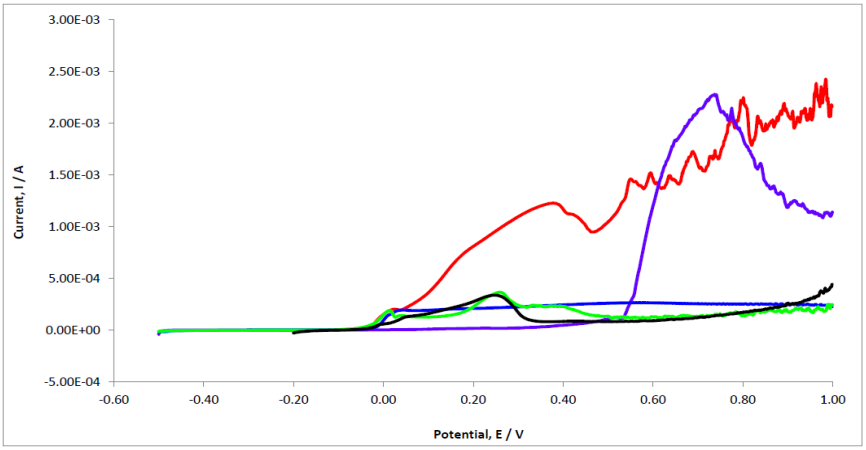

Figure 6.22: Current plotted as a function of increasing applied potential for Cu cycled at 1 mV s^{-1} in 0.10 mol dm^{-3} NaCl, pH 5.0 solution in the absence (red) and presence of 2.0×10^{-3} mol dm^{-3} BV (blue), EV (green) , MV (black) or BTA (purple).

This lack of corrosion protection at the higher pH values may also be connected to the nature of the BTA molecule and the initial adsorption of the BTA at the copper surface. The BTA molecule can exist in three different forms depending on the pH in aqueous solution, as shown in Equations 6.12 and 6.13 [368]. It is clear that in alkaline conditions the molecule is predominantly present as the anionic form, while at a pH of 7.0 a mixture of the neutral and anionic species are present. At a pH of 3.0, a significant concentration of the cationic species exists.

$$BTAH_2^+ \rightarrow BTAH + H^+, \quad pK = 1.0 \tag{6.12}$$

$$BTAH \rightarrow BTA^- + H^+, \quad pK = 8.2 \tag{6.13}$$

As the CuCl complex layer is anionic, the adsorption of the BTA^- is inhibited due to the unfavourable electrostatic interactions. This, in turn, will give rise to poor or weak adsorption on the CuCl layer [380].

The breakdown of the BTA film is clearly very different to that observed with the EV system. A rapid increase in the current is observed with the BTA system, as shown in Figures 6.21 and 6.22. This breakdown has been described in terms of the local rupture of the Cu(I)-BTA film [368]. It has been proposed that once the initial Cu(I)-BTA film is formed, a Cu_2O underlayer is formed. As the potential is increased the higher flux of Cu(I) ions gives rise to the precipitation of CuCl between the Cu_2O and the Cu(I)-BTA overlayer. As the Cu_2O is doped with chloride anions, the conductivity of the layer is increased and this enhances the rate of CuCl formation between the Cu_2O and the Cu(I)-BTA layers. At some point the mechanical stress and tension between the layers gives rise to the local rupture of the Cu(I)-BTA film and significant dissolution of the underlying copper is observed. This is consistent with the results presented in Figures 6.20, 6.21 and 6.22, while the data presented in Figure 6.23 are more consistent with poor adsorption of BTA at the CuCl layer and the loss of the resulting Cu(I)-BTA due to poor adhesion of the film to the surface. These effects are not observed with the BV-containing film. Indeed, it has been shown in the literature that once the viologen adsorbs at the CuCl complex layer there is no further uptake of chloride anions [17]. This is in good agreement with the EDX analyses presented in Tables 6.8, 6.9 and 6.10 which clearly show no increase in the chloride content with increasing potential. Consequently, the local rupture of the BV film or indeed the EV or MV films is not observed.

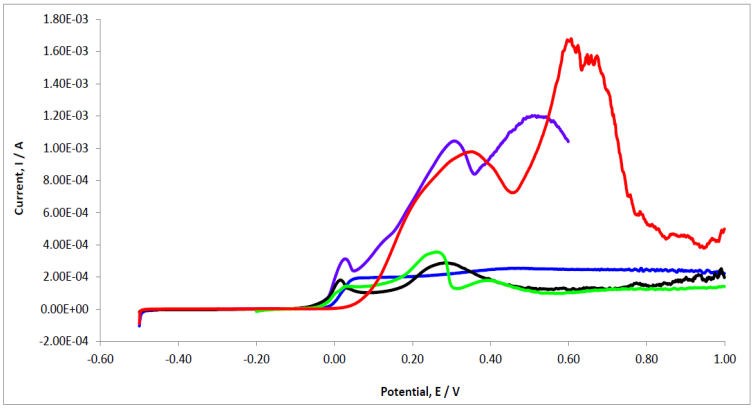

(a)

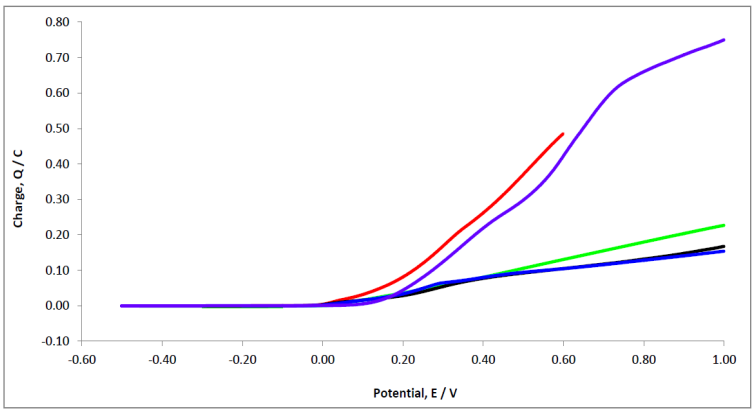

(b)

Figure 6.23: Current and charge plotted as a function of increasing applied potential for Cu cycled at 1 mV s^{-1} in 0.10 mol dm^{-3} NaCl, pH 7.0 solution in the absence (red) and presence of 2.0×10^{-3} mol dm^{-3} BV (blue), 2.0×10^{-3} mol dm^{-3} EV (green), 2.0×10^{-3} mol dm^{-3} MV (black) and 2.0×10^{-3} mol dm^{-3} BTA (purple).

6.3 Summary of Results

In this chapter results are presented and discussed on the electrochemical deposition of three viologens, MV, BV and EV at copper in the presence of a 0.10 mol dm^{-3} NaCl supporting electrolyte. Sodium chloride was found to be a suitable electrolyte for the electrochemical formation of these viologen-containing films at the copper interface. There was no need for the addition of any further supporting electrolyte. A 2.0×10^{-3} mol dm^{-3} solution of each viologen was sufficient to enable its formation in a highly reproducible manner at the copper electrode.

The formation of the viologen films was achieved by cycling the copper electrode from the potential of -0.20 to 1.00 V vs. SCE at a scan rate of 1 mV s^{-1}. For comparison, the copper was cycled under the same conditions in the 0.10 mol dm^{-3} NaCl solution, but in the absence

of the viologens. Significant dissolution of the copper was observed in the absence of the viologens, with currents as high as 0.30 mA cm^{-2} recorded as copper was cycled to potentials in the vicinity of 0.60 V vs. SCE at the relatively slow scan rate of 1 mV s^{-1}. However, considerably lower currents were measured in the presence of the viologens, indicating a reduction in the rate of dissolution and the formation of a protective film. The voltammograms, recorded in the presence and absence of the viologens, had similar characteristics at the lower applied potentials. At relatively low potentials, -0.02 V vs. SCE, there was no evidence of any dissolution, but as the potential was increased, the current increased to give a peak centered at about 0.08 V vs. SCE. This peak has been explained in terms of the dissolution of copper and the nucleation of copper oxides, hydroxides and chloride-containing species. Indeed, these species were identified and confirmed using EDX analysis. However, once these chloride species are initially formed it appears that the adsorbed viologens inhibit any further dissolution of the copper substrate.

The formation of the MV and BV-containing films at the copper surface appears to be independent of the pH of the solution, between a pH of 2.0 and 9.0, the concentration of the viologen, from 2.0×10^{-3} to 5.0×10^{-3} mol dm^{-3}, and the immersion time in the viologen-containing solution prior to formation of the film by cycling the copper electrode in the same solution. However, the formation of the EV-containing film is dependent on the viologen concentration and protective films are only formed using the higher viologen concentration of 5.0×10^{-3} mol dm^{-3}.

In order to establish the role of the chloride anion in the formation of the viologens at the copper surface, the concentration of the chloride solution was varied from 1.25×10^{-3} mol dm^{-3} to 0.30 mol dm^{-3}. The optimum chloride concentration was determined as 0.10 mol dm^{-3}. At the lower concentrations, the formation of the viologen films was inhibited by the slow formation of the CuCl complex layer. This was clearly evident from the appearance of broad oxidation waves, at the lower chloride concentrations. At concentrations higher than 0.10 mol dm^{-3}, the CuCl complex was formed and stable viologen-containing films were formed.

Although it is well known that EDX analysis is strictly a qualitative technique, a quantitative study was carried out to determine if the concentration of the BV and the composition of the initial chloride adsorbed layer varied with the applied potential. There was a significant increase in the concentration of chloride-containing species as the copper electrode

was polarised to higher potentials in the absence of the viologen, indicating dissolution and corrosion of the copper substrate. However, on addition of the BV to the solution, the concentration of the chloride-containing species was reduced significantly and varied little with the applied potential, indicating a stable and protective film. Moreover, clear evidence for the presence of the BV was obtained using EDX analysis. Carbon was detected in all samples cycled in the BV solution, however no carbon was observed for the copper electrode cycled in the chloride solution.

The protective properties of the viologen films were compared to the well-known copper inhibitor, BTA. While the BTA offered very good corrosion protection of the copper substrate at pH values ranging from 3.0 to 5.0, the performance of the inhibitor was considerably reduced at pH values below 3.0 and higher than a pH of 5.0. In contrast, the viologen-containing films were protective across a much wider pH range, extending from a pH of 2.0 to 9.0.

CHAPTER 7

Analysis of the Corrosion Protective Performance of the Viologen Films

It was clearly shown in Chapter 6, that MV, EV and BV can be deposited successfully at a chloride-modified copper surface. Preliminary investigations into the protective nature of these films were presented, and it was concluded that the BV forms the more protective films. In this chapter, the results of a more in-depth study into the corrosion performance of the BV films are presented and discussed. An assessment of the corrosion protection properties of the films is made using an array of electrochemical, spectrophotometric and surface-analytical techniques that are well known in the field of corrosion science [2, 186, 240].

As the chloride interface between the viologen and the copper appears to enhance the stability of the film, Chapter 6, the formation and stability of the BV films in the presence of acetates, sulfates, oxalates and bromides were studied. There are no reports in the literature on the formation of viologen films in the presence of these anions and this was important in determining the role of the chloride anions in the formation of stable viologen films. Then, the electrochemical properties of the BV films were studied in NaOH, and the influence of the electrochemical window, particularly at potentials from -0.20 to -1.50 V vs. SCE, was explored. Again, there are no reports in the literature on the stability of viologen films in alkaline conditions or at potentials in the vicinity of -1.50 V vs. SCE.

Finally, the films were examined for their stability and corrosion protection properties using a spectrophotometric analysis of the copper ion concentrations, open-circuit potential measurements, electrochemical impedance spectroscopy (EIS), potentiodynamic polarisation measurements and Tafel analyses [4, 40, 260, 277, 381, 382]. These results are examined and discussed with reference to the uncoated copper, while in some cases the EV and MV films are included for comparison.

7.1 Experimental

The experimental approach used in recording the data is similar to that outlined previously in Section 6.1, Chapter 6. All chemicals were obtained from Aldrich and in addition to the reagents described in Section 6.1.1, sodium oxalate ($Na_2C_2O_2$), sodium acetate (CH_3COONa), sodium sulfate (Na_2SO_4), sodium hydroxide (NaOH) and sodium bromide (NaBr) were used. The electrodes were prepared, as outlined in Section 6.1.2, while the equipment and procedures, described in Sections 6.1.2 and 6.1.3 were employed. Unless otherwise stated, the BV films were deposited from 2.0×10^{-3} mol dm^{-3} BV in 0.10 mol dm^{-3} NaCl at a pH of 3.0 by cycling the copper from -0.20 to 1.00 V vs. SCE at 1 mV s^{-1} for a single sweep.

A spectrophotometric analysis was used to monitor the concentration of dissolved copper. This involved complexing the copper ions with the well-known chelating agent, bathocuproine disulfonate [383, 384, 385], as detailed in Section 4.3.1, Chapter 4. The complexing reagent was added, at a known concentration, to the solution. An orange-coloured complex, with a λ_{max} at 480 nm was formed and this was monitored using UV-Vis spectroscopy. A Cary UV-Vis spectrometer was used to record all the data. A quartz crystal cuvette was used with a diameter of 1 cm and the wavelength was scanned from 300 to 800 nm.

The stability of the complex was monitored as a function of time, by recording the absorbance of the complex over a 72 h period. Calibration curves were obtained using stock solutions of $CuSO_4$, and a typical calibration curve is shown in Section 4.3.1, Figure 4.10. The pH of the solution was increased to 7.0, as it is possible that H^+ ions may hinder the complexation reaction between the copper ion and the bathocuproine, as indicated in Equation 7.1. Another consideration was the presence of chloride anions in the electrolyte. It has been reported that chloride anions can participate in the bathocuproine reaction [307], in

accordance with Equation 7.2. Therefore, the influence of chloride anions on the calibration curve was studied and the optimum conditions for monitoring the copper ion concentration were found, as detailed in Section 4.3.1.

$$Cu(bathocuproine)_2^+ + 2H^+ \rightarrow Cu^+ + 2H(bathocuproine)^+ \tag{7.1}$$

$$CuCl_n^{(n-1)} + (bathocuproine) \rightarrow Cu(bathocuproine)Cl + (n-1)Cl^- \tag{7.2}$$

Electrochemical impedance spectroscopy (EIS) was used to study the stability of the BV films at the open-circuit potential (OCP) and at applied potentials ranging from -0.20 to 0.60 V vs. SCE. These data were recorded in 0.10 mol dm^{-3} NaCl following an initial 30 min polarisation period at the desired potential to give steady-state conditions. This was tested further by recording the impedance data from high to low frequencies, then reversing the sweep and recording the data from low to high frequencies. The impedance data were recorded using a Solartron Model SI 1285 or Model SI 1287 potentiostat coupled with a frequency response analyser, Model SI 1250. A potential perturbation of 5 mV was used to ensure a pseudo-linear response of the system, while the frequency was varied from 65 kHz to 10 mHz. Similar data were recorded for copper immersed and polarised in the 0.10 mol dm^{-3} NaCl solution. The data were fitted to equivalent circuits as detailed in Chapter 2, Section 2.5.3.

7.2 Results and Discussion

7.2.1 Influence of the Nature of the Anion on the Formation of BV Films

It was clearly shown in Section 6.2.4 that the concentration of the chloride anion influences the formation of the viologen films and that specific concentrations of the chloride anion are required for the successful formation of a stable and protective viologen film. The influence of this anionic layer, between the viologens and the copper substrate, was further investigated by varying the nature of the anion. This was an obvious step before a more detailed study on the corrosion performance of the films was carried out [5, 364, 386, 387]. A number of anions was examined and these included the oxalate, acetate, sulfate, bromide and chloride anions. In order to assess the effect of each of the anions on the formation of the viologen film at the copper surface, the formation of the BV film in the presence of the anions was

investigated using cyclic voltammetry [4, 186, 240, 336]. A 0.10 mol dm^{-3} solution of the anion was prepared, a concentration of 2.0×10^{-3} mol dm^{-3} BV was added and the pH of the solution was adjusted to a value of 3.0. The copper electrode was then immersed in the solution and polarised from -0.20 V vs. SCE, at 1 mV s^{-1} up to a final potential of 1.00 V vs. SCE, as detailed in Chapter 6, Section 6.1.3. The voltammograms were recorded for copper polarised in the presence and absence of the BV. Then, the modified copper electrodes were removed and placed in a fresh solution of the corresponding anion, and cycled in the anion-containing electrolyte. This analysis gives an indication of the stability of the films formed at the copper interface in both the anion solution and in the BV solution.

In Figure 7.1a and 7.1b, data are presented for the oxalate system. The formation of an insoluble copper oxalate film, which gives rise to the passivation of the copper surface, is clearly evident in Figure 7.1a [1]. Dissolution of the copper starts at -0.05 V vs. SCE and continues until potentials in the vicinity of 0.30 V vs. SCE are reached. This indicates that the dissolution continues until a sufficient concentration of Cu^{2+} ions are generated at the surface for precipitation of the insoluble copper oxalate. Once this oxalate layer is formed, the dissolution of copper is inhibited, giving good stability from 0.40 to 1.00 V vs. SCE. However, when the oxalate-modified copper is transferred to a new oxalate solution and cycled from the potential of -0.20 V vs. SCE, the protective properties of the oxalate layer are no longer evident or retained. In the presence of the BV, the initial precipitation of the copper oxalate is clearly inhibited. There is a significant increase in the peak potential from -0.01 V to 0.15 V vs. SCE, Figure 7.1a, and the rapid decay in the current, which is consistent with the precipitation of the copper oxalate deposit, is not observed. Instead, there is a more gradual decay in the current indicating a slower rate of copper oxalate deposition in the presence of the BV. However, when this BV-modified surface is cycled in the oxalate solution, but in the absence of the viologen, Figure 7.1b, there is little evidence for the dissolution of copper, indicating the formation of a protective viologen containing film.

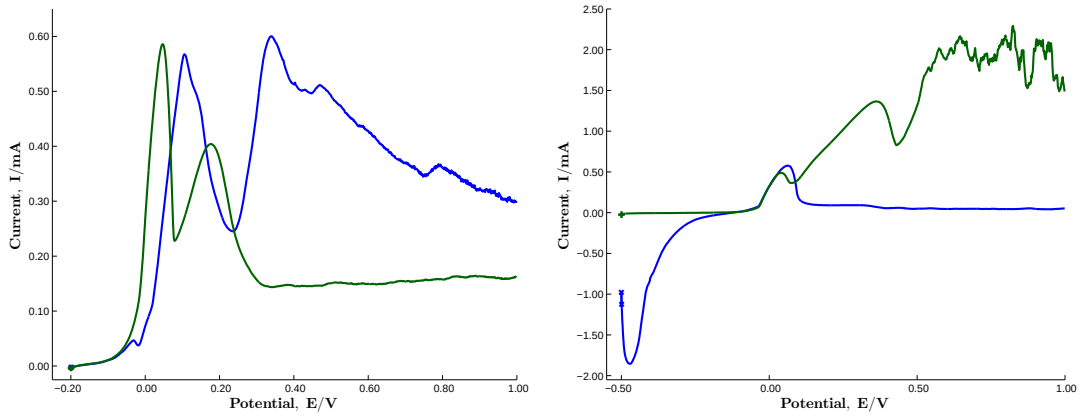

(a) **(b)**

Figure 7.1: (a) Cyclic voltammograms recorded for Cu at 1 mV s^{-1} in 0.10 mol dm^{-3} $Na_2C_2O_2$ adjusted to a pH of 3.0 in the presence (blue) and absence (green) of 2.0×10^{-3} mol dm^{-3} BV and (b) cyclic voltammogram recorded for BV-modified Cu (blue) and oxalate-modified Cu (green) in 0.10 mol dm^{-3} $Na_2C_2O_2$ adjusted to a pH of 3.0.

The surface morphology of the copper electrode polarised in the presence of the BV and oxalate anion is shown in the micrographs presented in Figure 7.2. This morphology is very different to that observed in the chloride-containing solutions, Section 6.2.6, Chapter 6, indicating that the nature of the anion has a significant effect on the morphology of the surface. The surface is reasonably homogeneous, and is crack and defect free. The surface is clearly covered with a deposit and this is consistent with the deposition of insoluble copper oxalate species. As shown in the accompanying EDX spectrum, Figure 7.3, this layer is sufficiently thin to observe the signal from the copper, while the intensity of the O and C signals is low, again indicating a relatively thin layer of insoluble copper oxalate. Indeed, the apparent protective nature of the deposited viologen film, Figure 7.1b, may be connected to the formation of these insoluble copper oxalates at the surface.

Similar data were recorded for the acetate system and these are shown in Figure 7.4. Again, dissolution of copper is observed in the acetate solution and this dissolution extends from the initial potential of -0.01 V to the final potential of 1.00 V vs. SCE. However, there are several reports in the literature which show that copper acetates are formed during the dissolution of copper and these have relatively low solubility and consequently give rise to the deposition of copper acetates at the surface [84, 388]. Compounds, such as $Cu(CH_3COO)_2CuO.\times H_2O$, have been identified on copper exposed to acetates [84, 389]. While this passivation effect is not very evident in Figure 7.4a, it is clearly seen in Figure 7.4b, where there is a significant decay in the

current at about 0.75 V vs. SCE. This is consistent with the precipitation of copper acetates at the surface, which inhibit further dissolution of the underlying copper. Again, in the presence of the BV, the voltammograms are very different. A considerable reduction in the dissolution rate is observed in the presence of the viologen in Figure 7.4a, while the deposited BV film shows reasonably good stability when cycled in 0.1 mol dm^{-3} CH_3COONa, Figure 7.4b. However, in this case, the presence of the BV has little effect on the peak potential or peak current as shown in Figure 7.4b.

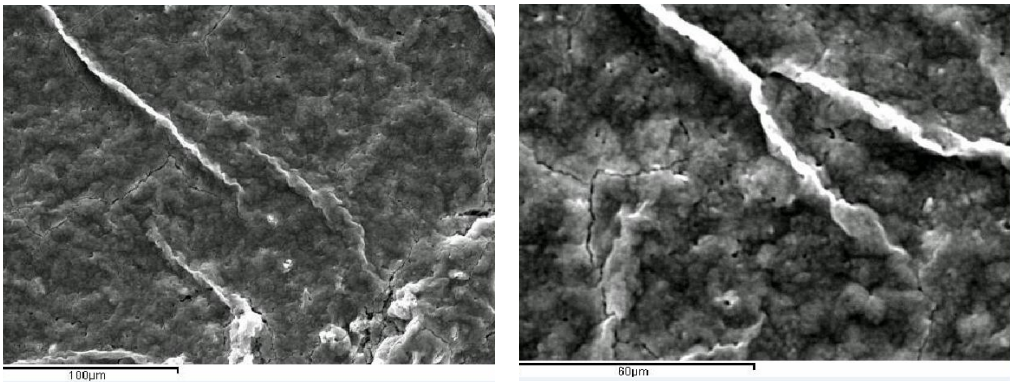

(a) **(b)**

Figure 7.2: SEM micrographs recorded for Cu cycled in 2.0×10^{-3} mol dm^{-3} BV and 0.1 mol dm^{-3} $Na_2C_2O_2$, (a) the scale bar corresponds to 100 μm and (b) the scale bar corresponds to 60 μm.

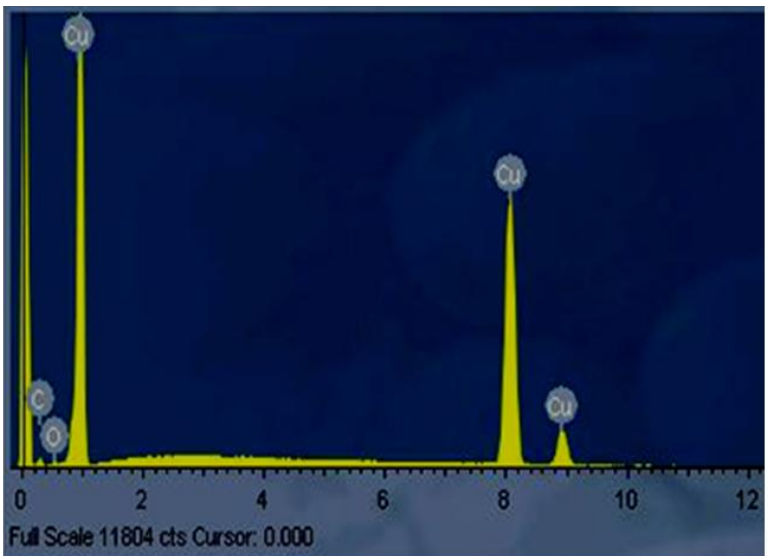

Figure 7.3: EDX spectrum of BV-oxalate modified Cu electrode.

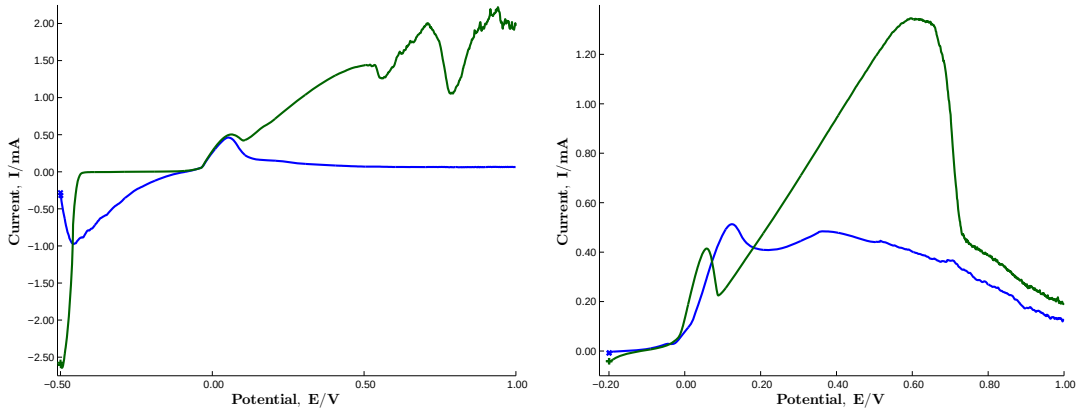

(a) **(b)**

Figure 7.4: (a) Cyclic voltammograms recorded for Cu at 1 mV s^{-1} in 0.10 mol dm^{-3} CH_3COONa at a pH of 3.0 in the presence (blue) and absence (green) of 2.0×10^{-3} mol dm^{-3} BV and (b) cyclic voltammogram recorded for BV-modified Cu (green) and acetate-modified Cu (blue) in 0.10 mol dm^{-3} CH_3COONa at a pH of 3.0.

The data recorded for the halide and sulfate systems are shown in Figures 7.5, 7.6 and 7.7 and are consistent with dissolution of copper in the absence of the BV. The voltammograms shown in Figures 7.5a, 7.6a and 7.7a, have similar shapes, with an initial peak followed by further dissolution and higher currents. Although relatively high concentrations of Cu^{2+} are generated, there is no evidence for the formation of protective layers or deposits on the surface. The dissolution mechanism of copper in bromide solutions is similar to that proposed in chloride media [274, 280, 282, 283]. It has been suggested that soluble $CuBr_2^-$ species are generated through the oxidation of copper, however at higher current densities, CuBr precipitates onto the copper surface. This CuBr layer reacts with Br^- ions to generate soluble complex anions, such as $CuBr_2^-$, $CuBr_3^{2-}$ and $CuBr_n^{(n-1)-}$, and it is the diffusion of these species into the bulk solution that controls the rate of dissolution. The anodic current eventually reaches a limiting value that is dependent on the rate of dissolution of the CuBr layer. Indeed, this sequence of steps is consistent with the data presented in Figure 7.5a.

On addition of the BV to the solution, the dissolution of copper is clearly inhibited. Similar data are recorded for the bromide and chloride systems, Figures 7.5a and 7.6a, indicating the formation of stable viologen films. The formation of the BV film in the sulfate solution is somewhat different and less efficient, as shown in Figure 7.7a. An increase in the current is observed at about -0.03 V vs. SCE, and this continues to increase to give a peak current at

0.10 V vs. SCE. The subsequent decay in the current is slow, and stable conditions are only achieved at 0.35 V vs. SCE, Figure 7.7a. This suggests that the formation of the BV film in the sulfate solution is slow, compared to the chloride or bromide solutions.

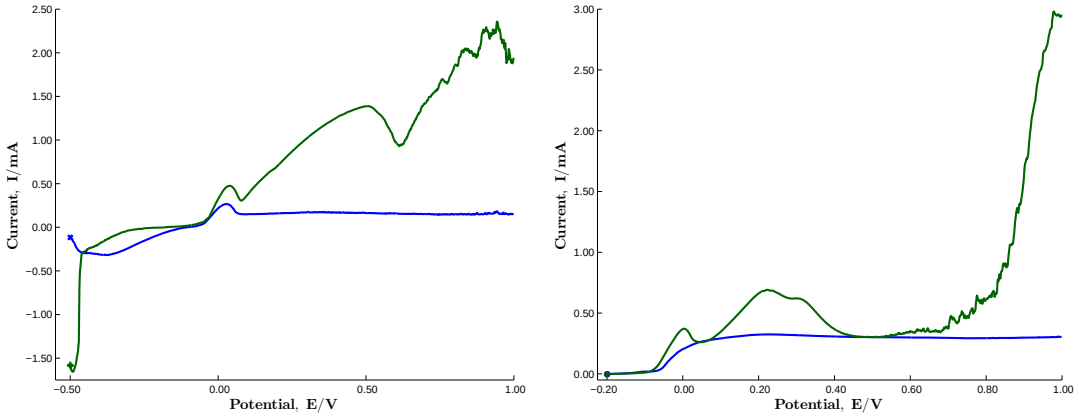

(a) **(b)**

Figure 7.5: (a) Cyclic voltammograms recorded for Cu at 1 mV s^{-1} in 0.10 mol dm^{-3} NaBr adjusted to a pH of 3.0 in the presence (blue) and absence (green) of 2.0×10^{-3} mol dm^{-3} BV and (b) cyclic voltammogram recorded for BV-modified Cu (blue) and Br-modified Cu (green) in 0.10 mol dm^{-3} NaBr at a pH of 3.0.

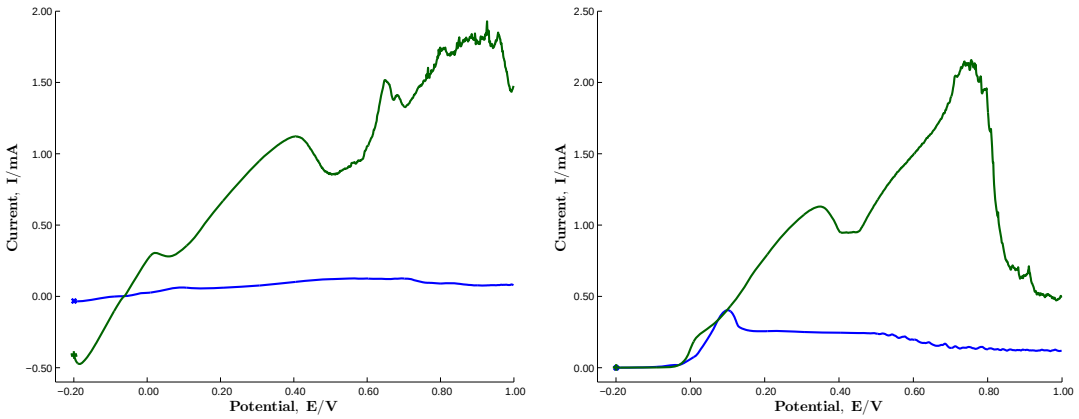

(a) **(b)**

Figure 7.6: (a) Cyclic voltammograms recorded for Cu scanned in the forward direction → at 1 mV s^{-1} in 0.10 mol dm^{-3} NaCl adjusted to a pH of 3.0 in the presence (blue) and absence (green) of 2.0×10^{-3} mol dm^{-3} BV and (b) cyclic voltammogram recorded for BV-modified Cu (blue) and Cl-modified Cu (green) in 0.10 mol dm^{-3} NaCl at a pH of 3.0.

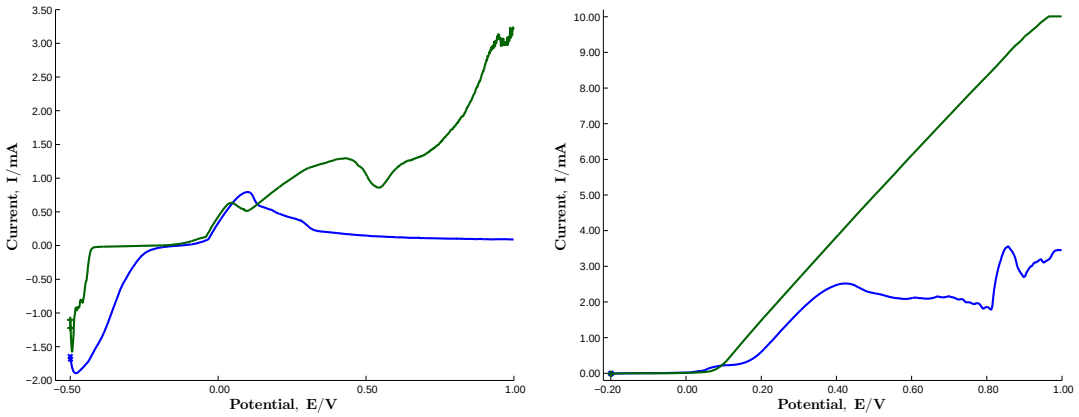

(a) **(b)**

Figure 7.7: (a) Cyclic voltammograms recorded for Cu at 1 mV s^{-1} in 0.10 mol dm^{-3} Na_2SO_4, at a pH of 3.0 in the presence (blue) and absence (green) of 2.0 × 10^{-3} mol dm^{-3} BV and (b) cyclic voltammogram recorded for BV-modified Cu (blue) and sulfate-modified Cu (green) in 0.10 mol dm^{-3} Na_2SO_4 at a pH of 3.0.

The stability of the viologen films and the bromide, chloride or sulfate-modified copper are shown in Figures 7.5b, 7.6b and 7.7b. The data recorded for the chloride-modified copper are similar to that recorded for copper in the chloride solution and are dominated by dissolution and the generation of chloride-containing corrosion products. Similar effects are observed with the sulfate-modified copper. Indeed, very high dissolution rates were observed, with currents as high as 8 mA cm^{-2} at 0.70 V vs. SCE, as highlighted in Figure 7.7b. The behaviour of the bromide-modified copper is somewhat surprising compared to the chloride-modified surface. However, this may be connected to the buildup of a CuBr layer that is only converted to the more soluble $CuBr_n^{(n-1)-}$ species at the higher potential. High currents are observed when the potential is increased to 0.80 V vs. SCE and then a rapid increase in the current is seen, indicating significant dissolution.

The BV films formed in the chloride or bromide solutions show very good stability and corrosion protective properties when cycled in the halide solutions, with low currents of about 0.5 mA cm^{-2} from 0.10 to 1.0 V vs. SCE. However, the viologen film formed in the sulfate solution has poor protective properties, as shown in Figure 7.7b. Dissolution of copper is observed at 0.20 V vs. SCE and while this dissolution is limited compared to the sulfate-modified copper the currents reach a limiting value with some fluctuations, which are consistent with dissolution of the underlying copper. This is probably connected with the nature of the film deposited in the presence of the sulfate anions, and as shown in Figure 7.7a, the deposition

of the BV film is inhibited.

The surface morphology of the copper electrode cycled in the presence of the BV and sulfate anions is evident in the micrographs shown in Figure 7.8. Again, this morphology is very different to that observed in the chloride-containing solutions, Section 6.2.6, Chapter 6, or the oxalate solution, Figure 7.2. The morphology is consistent with the high rate of dissolution, which was observed in Figure 7.7. Randomly oriented scale-like deposits are seen distributed over the surface. Again, this clearly shows that the surface morphology is dominated by the nature of the anions.

It is clear from these data that significant dissolution of copper occurs in the sulfate solutions and that the formation and deposition of the BV films are inhibited in the presence of the sulfate anions. In the acetate and oxalate solutions the formation of the BV films is influenced by the formation of copper oxalate and acetate species and in direct competition with the formation of insoluble copper oxalates and acetates at the copper surface. Although the BV films deposited from these solutions have protective properties, these results are in good agreement with the data presented in Chapter 6 which show that the adsorption of chloride anions and the formation of a CuCl complex layer at the copper surface is critical in the formation of stable and protective BV films.

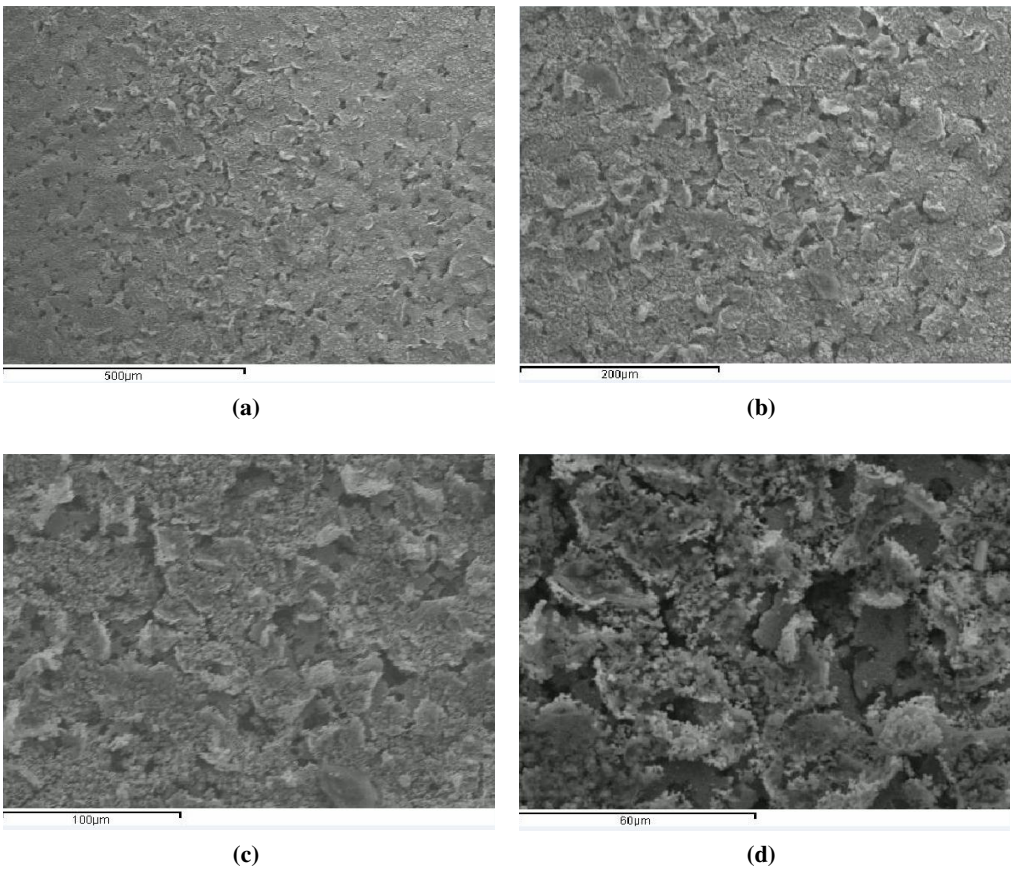

Figure 7.8: SEM micrographs recorded for Cu cycled in 2.0×10^{-3} mol dm^{-3} BV and 0.10 mol dm^{-3} Na_2SO_4 (a) the scale bar corresponds to 500 μm (b) the scale bar corresponds to 200 μm (c) the scale bar corresponds to 100 μm and (d) the scale bar corresponds to 60 μm.

7.2.2 Electrochemical Properties of the Viologen-Coated Copper in Sodium Hydroxide

It is well known that the formation of copper oxide species, such as CuO and Cu_2O, can be followed by cycling copper in NaOH solutions [64, 390, 391, 392]. Sinapi *et al.* [393] achieved distinct peaks for both the oxidation and the reduction of copper oxides in NaOH. In the forward sweep three anodic peaks were observed, a first oxidation peak and a broader feature composed of two oxidation waves. The first peak was assigned to the oxidation of Cu to Cu_2O, and the broader feature to the formation of CuO and its conversion to $Cu(OH)_2$. In the reverse sweep, two cathodic peaks were observed and these were attributed to the reduction of the CuO and Cu_2O oxides that were formed during the anodic process.

Cyclic voltammograms were recorded for copper in 0.10 and 0.15 mol dm^{-3} NaOH, with a pH at approximately 12.0, at 20, 50 and 100 mV s^{-1}. The peaks increased with

increasing scan rate, which is in good agreement with the studies reported by Marchiano *et al.* [64]. Representative voltammogram recorded at 20 mV s^{-1} are shown in Figure 7.9, where the data presented in Figure 7.9a were recorded in 0.10 mol dm^{-3} NaOH and the voltammograms depicted in Figure 7.9b were recorded in 0.15 mol dm^{-3} NaOH. It is evident that the voltammograms are similar in 0.10 and 0.15 mol dm^{-3} NaOH and the slight change in the NaOH concentration has little influence on the peak positions and only a slight effect on the peak currents.

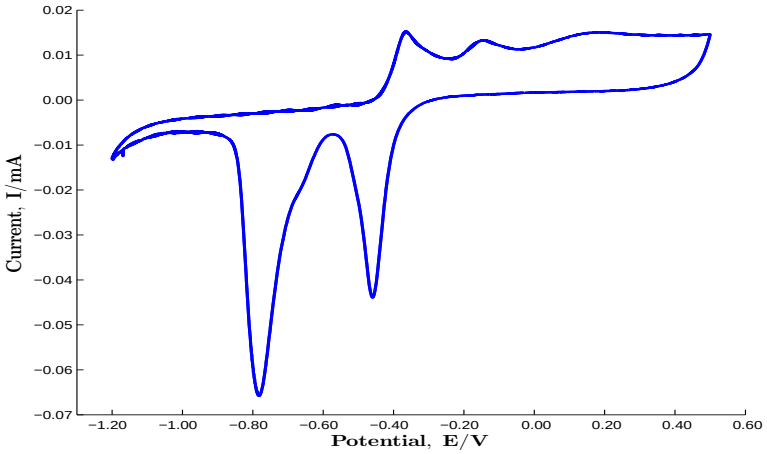

(a)

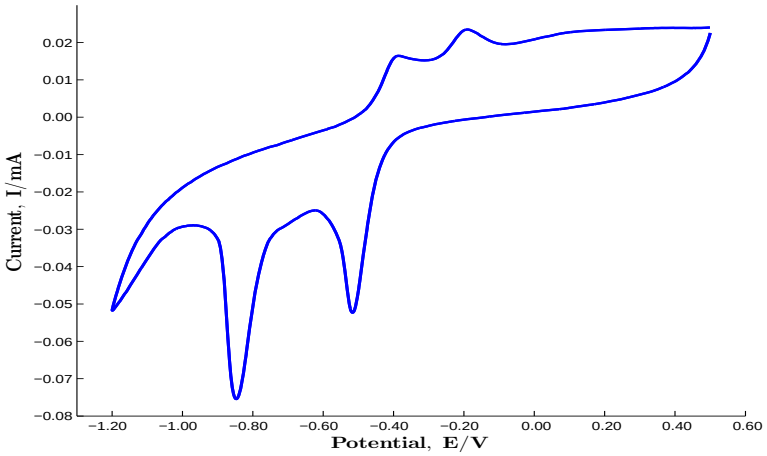

(b)

Figure 7.9: Cyclic voltammograms recorded at 20 mV s^{-1} of Cu in (a) 0.10 and (b) 0.15 mol dm^{-3} NaOH.

Two reduction peaks, at approximately -0.50 V and -0.90 V vs. SCE, are clearly observed and these were attributed to the reduction of the Cu(II) oxide (CuO or $Cu(OH)_2$) to the Cu(I) oxide (Cu_2O or Cu(OH)), and the further reduction of Cu(I) to Cu. The position and magnitude of these peaks are in good agreement with the reduction peaks reported in the literature, [64,

382, 391, 393, 394]. Using integration to estimate the charge associated with the reduction waves, a higher charge was computed for the reduction of the copper (I) species (either from Cu_2O or from Cu(OH) or $Cu(OH)_2^-$ species). This is to be expected since some of the Cu(I) is generated from the reduction of the Cu(II) species and this will contribute to the total charge computed for the reduction of the Cu(I) species. Two clear oxidation peaks at about -0.40 and -0.20 V vs. SCE are observed and these are in good agreement with those reported by Marchiano *et al.* [64], Schwartz and Muller [395, 396] and Wilhelm *et al.* [397] and were attributed to the reactions, which are given in Equations 7.3 and 7.4.

$$2Cu + 2OH^- \rightarrow Cu_2O + H_2O + 2e^- \tag{7.3}$$

$$Cu_2O + 2OH^- \rightarrow 2CuO + H_2O + 2e^- \tag{7.4}$$

The BV-modified copper electrode was analysed under the same conditions. The modified copper was prepared using 2.0×10^{-3} mol dm^{-3} BV in 0.10 mol dm^{-3} NaCl and adjusted to pH 3.0 with a few drops of concentrated HCl. The copper electrode was cycled in this solution from -0.20 to 1.00 V vs. SCE at a scan rate of 1 mV s^{-1} for a single sweep, as detailed in Section 7.1. The BV-modified copper was then rinsed thoroughly in distilled water and transferred to the NaOH solutions. The resulting voltammograms recorded in 0.10 and 0.15 mol dm^{-3} NaOH at 20 mV s^{-1} are shown in Figure 7.10. Although the NaOH concentration had little influence on the voltammograms recorded for copper, it is clear from Figure 7.10b that the NaOH concentration has a more significant influence on the redox reactions taking place at the BV-modified copper electrode. In the more concentrated 0.15 mol dm^{-3} NaOH solution, two oxidation waves, centred at -0.40 and -0.10 V vs. SCE are clearly evident and these correspond with the data recorded for the unmodified copper, Figure 7.9b and Equations 7.3 and 7.4. The two reduction peaks observed at about -0.90 and -0.50 V vs. SCE, are in good agreement with the reduction peaks reported elsewhere, [64, 76] and are similar to that recorded in Figure 7.9b. However, there is evidence of a shoulder peak at -0.70 V vs. SCE, which is not seen for the copper system, or at the lower NaOH concentration for the BV coated copper electrode. Complex cathodic reduction peaks in highly alkaline solutions have been reported previously by Marchiano *et al.* [64], Schwartz *et al.* [395] and Park and Pyun [76]. They attributed such peaks to the reduction of copper hydroxide species.

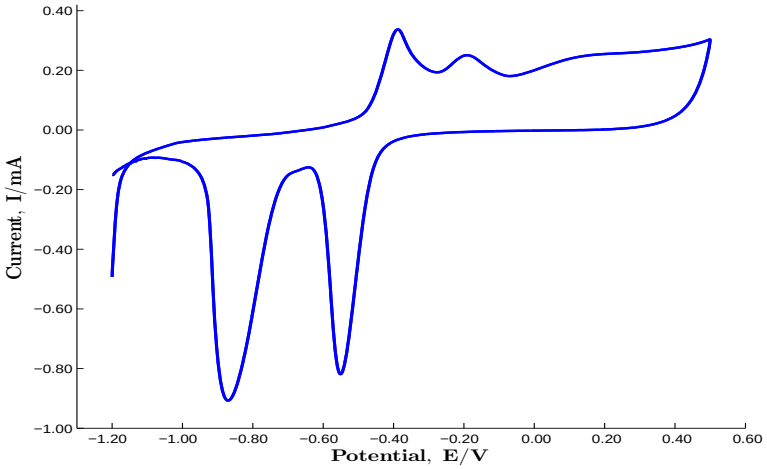

(a)

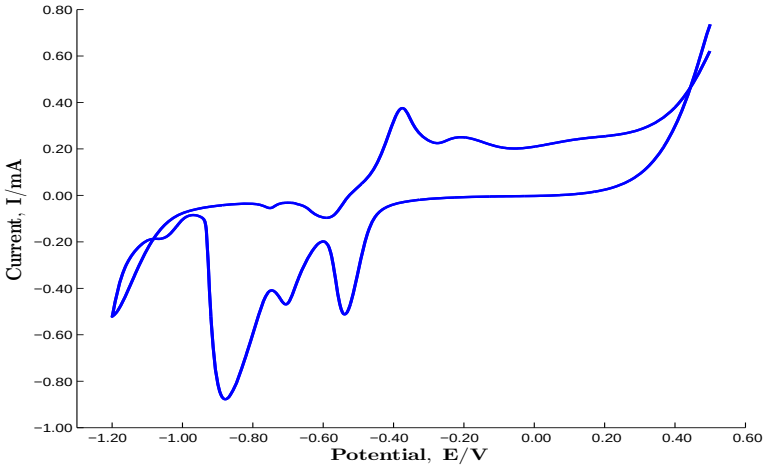

(b)

Figure 7.10: Cyclic voltammograms recorded at 20 mV s^{-1} for BV-modified Cu in (a) 0.10 and (b) 0.15 mol dm^{-3} NaOH.

The data recorded in 0.10 mol dm^{-3} NaOH, Figure 7.10a are similar to that recorded at the copper electrode, Figure 7.9. In the forward scan the oxidation waves appear as two distinct peaks and a very broad wave extending from 0.0 to 0.50 V vs. SCE. These peaks are attributed to the oxidation of copper metal (Cu^0) to Cu_2O at -0.40 V vs. SCE, Equation 7.3, and the oxidation of Cu_2O to CuO at -0.20 V vs. SCE, Equation 7.4, and the wave centred at approximately 0.25 V vs. SCE can be assigned to the further oxidation and dissolution of copper. This oxidation reaction may be connected to the formation of soluble Cu(I) or soluble Cu(II) species from the underlying copper substrate and soluble Cu(II) species from Cu(I) oxides or hydroxides. However, the currents are low indicating that these dissolution reactions are not significant and at the higher NaOH concentration these reactions are further inhibited

and protective CuO and Cu_2O oxides and hydroxides are only formed. Two reduction waves are observed at approximately -0.90 V and -0.50 V vs. SCE. When compared to the reduction peaks recorded for the uncoated copper, Figure 7.9, the peak positions are similar. These results show that the BV-modified copper is stable in both the 0.15 and 0.10 mol dm^{-3} NaOH solutions and the only significant difference between the data recorded for copper and the viologen-modified copper is the presence of a shoulder peak in the more concentrated solution, which may indicate the formation of copper hydroxide species. The influence of the concentration of the NaOH solution on the peak currents for the two reduction reactions is summarised in Table 7.1. In all cases, the peak currents are higher for the second reduction wave, seen at -0.90 V vs. SCE. It is also evident that the peak currents are higher for the copper cycled in 0.15 mol dm^{-3} NaOH, while the concentration of NaOH has less influence on the peak currents of the viologen-modified copper electrodes.

Table 7.1: Peak currents of Cu and BV-modified Cu in 0.10 mol dm^{-3} NaOH.

Concentration of NaOH / mol dm^{-3}	Peak current / A cm^{-2} (at -0.50 V vs. SCE)		Peak current / A cm^{-2} (at -0.90 V vs. SCE)	
	BV-modified Cu	Cu	BV-modified Cu	Cu
0.15	3.12×10^{-4}	7.19×10^{-5}	8.63×10^{-4}	1.32×10^{-4}
0.10	8.22×10^{-4}	4.34×10^{-5}	9.11×10^{-4}	6.61×10^{-5}

7.2.3 Influence of the Electrochemical Window on the Stability of the Viologen-Coated Copper in the Presence of Chloride Anions

Given the results obtained in the alkaline NaOH solution, the stability and properties of the BV-modified copper were compared to the unmodified copper under similar applied potential conditions, but in the presence of chloride anions. A 0.10 mol dm^{-3} NaCl solution, adjusted to a pH of 7.0, was employed as the chloride-containing solution and the copper and BV-modified copper electrodes were cycled from -1.50 to 0.00 V vs. SCE at scan rates varying from 1 to 200 mV s^{-1}. Again the BV film was prepared using the method highlighted in Section 7.1. Once the film was prepared the surface was well rinsed with distilled water and then transferred to the neutral 0.10 mol dm^{-3} NaCl solution.

Typical voltammograms are shown in Figure 7.11 for data recorded at 50 and 25 mV s^{-1}. Similar data and features were recorded at higher scan rates and these data are summarised

in Table 7.2. The data recorded for copper show a clear reduction wave at about -0.50 V vs. SCE, however there is no evidence of any oxidation wave. Two reduction peaks are clearly evident for the BV-modified copper, at about -0.70 and -0.50 V vs. SCE and the corresponding oxidation waves are seen at approximately -0.50 and -0.40 V vs. SCE. These reduction waves are somewhat different to that observed in the NaOH solutions, Figures 7.9 and 7.10. The first reduction wave, at about -0.50 V vs. SCE, is broad, while the second reduction peak has a somewhat lower current and charge. It is clear that the charge associated with the first peak is higher than that arising from the second reduction wave and again this is very different to that observed in the NaOH solution. The broad reduction wave observed with the unmodified copper is probably related to the formation of CuCl at the surface. Indeed, this is consistent with the EDX analysis presented in Figure 7.12a, where a strong Cl signal is seen. However, it is also evident from the EDX spectrum that oxide species are generated and these are probably related to the formation of Cu_2O or hydrated Cu_2O species. Similar EDX spectra were recorded for the viologen-modified film, as shown in Figure 7.12b. Again, the spectrum is consistent with the presence of Cu_2O and CuCl, however carbon is also detected, which indicates the presence of the viologen. As shown in Table 7.2, the peak currents associated with these oxidation and reduction waves increase with an increase in the scan rate, while the peaks are not well defined or visible at 1 mV s^{-1}.

Table 7.2: Peak currents for the BV-modified Cu as a function of the scan rate in 0.10 mol dm^{-3} NaCl.

BV-modified Cu	Peak current I/A			
Scan rate/ mV s^{-1}	Oxidation		Reduction	
	Peak 1	Peak 2	Peak 1	Peak 2
200	2.82×10^{-4}	2.35×10^{-4}	1.94×10^{-4}	2.11×10^{-4}
100	1.91×10^{-4}	$1{,}91 \times 10^{-4}$	1.49×10^{-4}	1.59×10^{-4}
50	1.31×10^{-4}	1.48×10^{-4}	1.05×10^{-4}	1.02×10^{-4}
25	9.43×10^{-5}	9.43×10^{-5}	7.42×10^{-5}	5.90×10^{-5}
10	7.19×10^{-5}	6.98×10^{-5}	5.18×10^{-5}	3.35×10^{-5}
1	-	-	2.12×10^{-5}	-

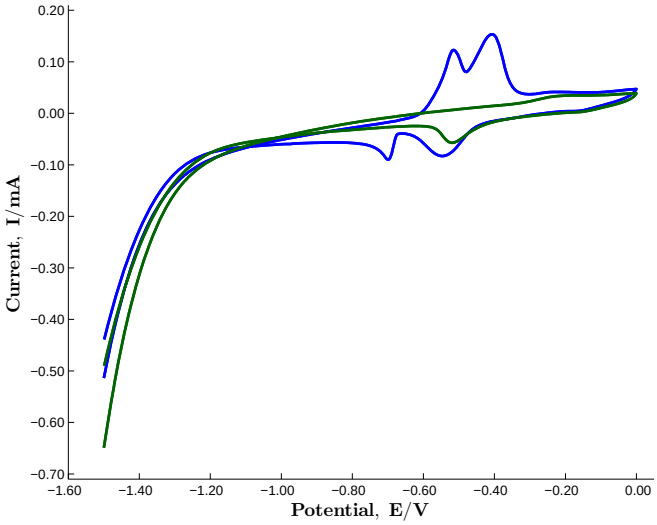

(a)

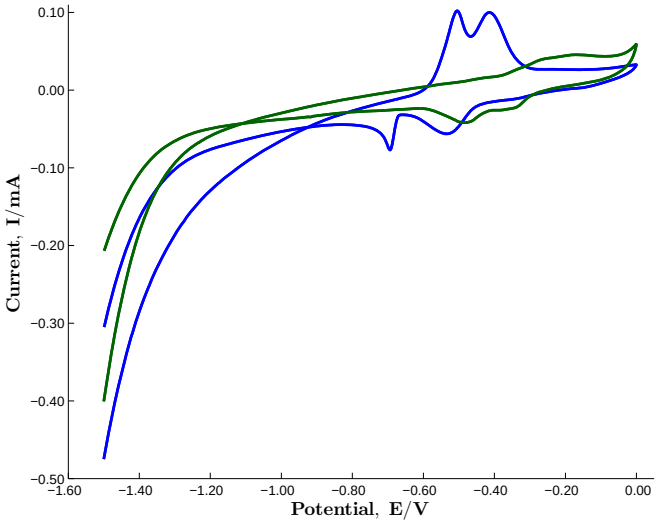

(b)

Figure 7.11: Cyclic voltammograms recorded for Cu (green) and the BV-modified Cu (blue) in 0.10 mol dm^{-3} NaCl, at a pH of 7.0 (a) scanned in the forward direction at 50 mV s^{-1} and (b) at 25 mV s^{-1}.

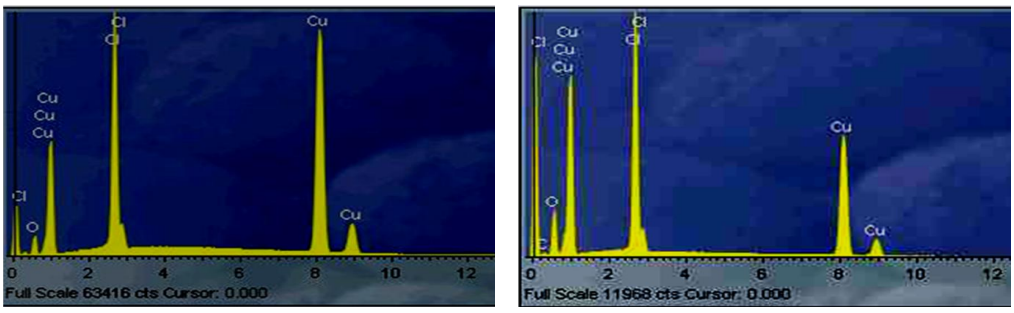

(a) **(b)**

Figure 7.12: EDX spectra recorded for (a) Cu and (b) BV-modified Cu on cycling the electrodes in 0.10 mol dm^{-3} NaCl, at a pH of 7.0 from -1.50 to 0.00 V vs. SCE.

The surface morphology of the copper and the viologen-modified copper electrodes, which was recorded following this cycling from -1.50 to 0.00 V vs. SCE, is evident from the micrographs presented in Figures 7.13 and 7.14. There is little difference between the micrographs recorded for the copper and the viologen-modified copper, as shown from a comparison of these micrographs. The surface is covered by a high density of rod like deposits, which consist of CuCl and copper oxide species, such as Cu_2O and CuO and the corresponding hydroxyl species, as shown from the EDX analyses, Figure 7.12. These are observed with copper and the viologen-modified copper. However, the high signal from the copper indicates that this layer is sufficiently thin for detection of the copper substrate.

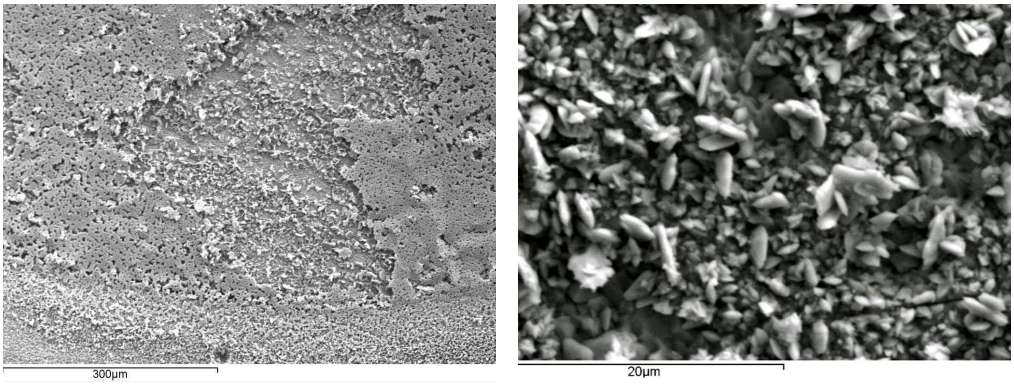

(a) **(b)**

Figure 7.13: SEM micrographs recorded of Cu on cycling the Cu in 0.10 mol dm^{-3} NaCl, at a pH of 7.0 from -1.50 to 0.00 V vs. SCE (a) the scale bar corresponds to 300 μm and (b) the scale bar corresponds to 20 μm.

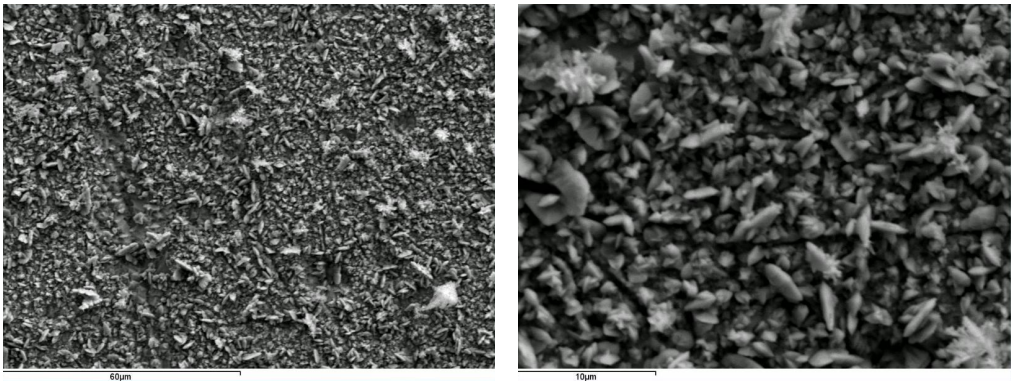

(a) **(b)**

Figure 7.14: SEM micrographs recorded of BV-modified Cu on cycling the electrode in 0.10 mol dm^{-3} NaCl, at a pH of 7.0 from -1.50 to 0.00 V vs. SCE (a) the scale bar corresponds to 60 μm and (b) the scale bar corresponds to 10 µm.

The influence of the electrochemical window on the stability of the electrodes is shown in Figure 7.15. Here, the copper and viologen-modified copper electrodes were cycled from -1.50 to 1.00 V vs. SCE at a scan rate of 1 mV s^{-1} in the neutral 0.10 mol dm^{-3} NaCl solution. Significant dissolution is observed for the copper electrode. At potentials higher than about 0.05 V vs. SCE, the current increases and continues to rise as the potential is further increased. On the reverse cycle, a distinct reduction wave is evident. The data recorded for the viologen-modified copper electrode are very different. Dissolution of copper is observed at about 0.05 V vs. SCE and the current increases to give a broad-like wave, which extends from about 0.05 to 0.35 V vs. SCE. However, at higher applied potentials the current decays and limited dissolution of the copper is observed. On the reverse cycle a clear and well defined reduction peak is seen. Interestingly, this peak is observed at a potential that is considerably lower than that measured for the unmodified copper electrode. Moreover, the peak current is higher in magnitude. These peaks are probably connected to the formation of CuCl at the surface.

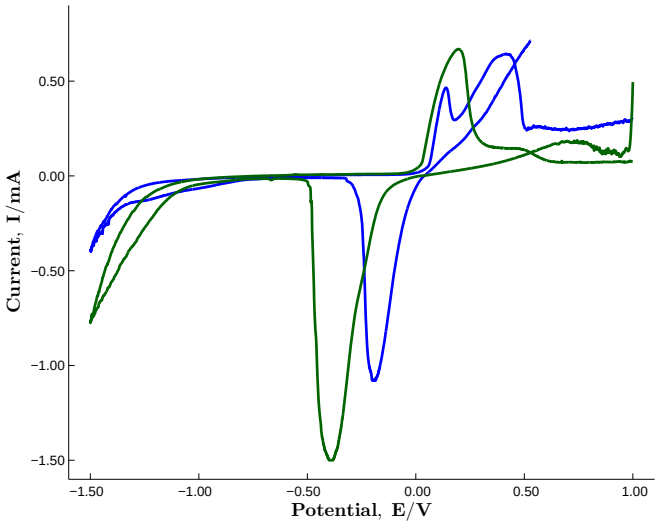

Figure 7.15: Cyclic voltammogram recorded of uncoated Cu (blue) and BV-modified Cu electrode (green) at a scan rate of 1 mV s^{-1} in 0.10 mol dm^{-3} NaCl solution at a pH of 7.0.

The surface morphologies of the viologen-modified copper and the copper electrodes were studied and recorded, and typical micrographs for the copper system are shown in Figure 7.16, while the micrographs recorded under identical conditions are shown in Figure 7.17 for the viologen-modified copper electrode. These micrographs were recorded after the electrodes were cycled from -1.50 to 1.00 V vs. SCE. The micrograph presented for the copper electrode shows a high density of rod and cube-like deposits across the entire surface, and although

not presented, the recorded EDX spectra show the presence of CuCl and copper oxides, such as CuO and hydrated CuO species which are formed at these higher applied potentials. The micrographs recorded for the viologen-modified copper are similar. However, it is evident that the surface has a lower density of these rod and cube-like structures. Again, the EDX spectra confirmed the presence of copper oxides, such as CuO or hydrated CuO, chloride species, consistent with the formation of CuCl and higher chloride containing copper species and carbon, which can be explained by the presence of the BV.

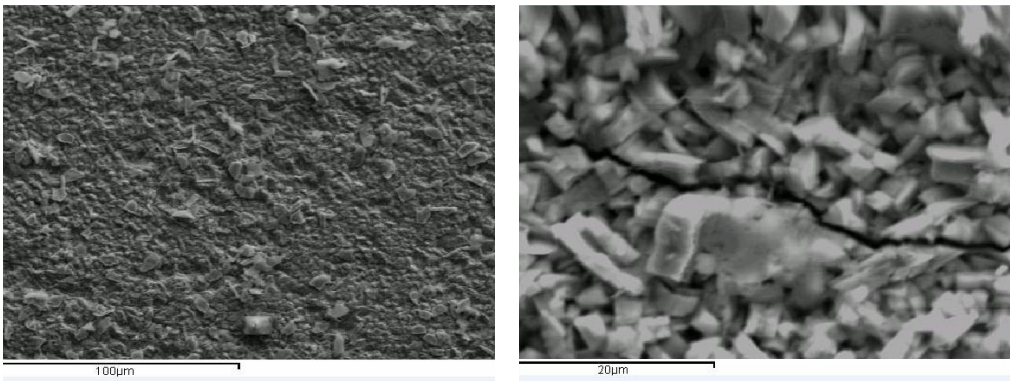

(a) **(b)**

Figure 7.16: SEM micrographs recorded of Cu on cycling the electrode in 0.10 mol dm^{-3} NaCl, at a pH of 7.0 from -1.50 to 1.00 V vs. SCE (a) the scale bar corresponds to 100 μm and (b) the scale bar corresponds to 20 μm.

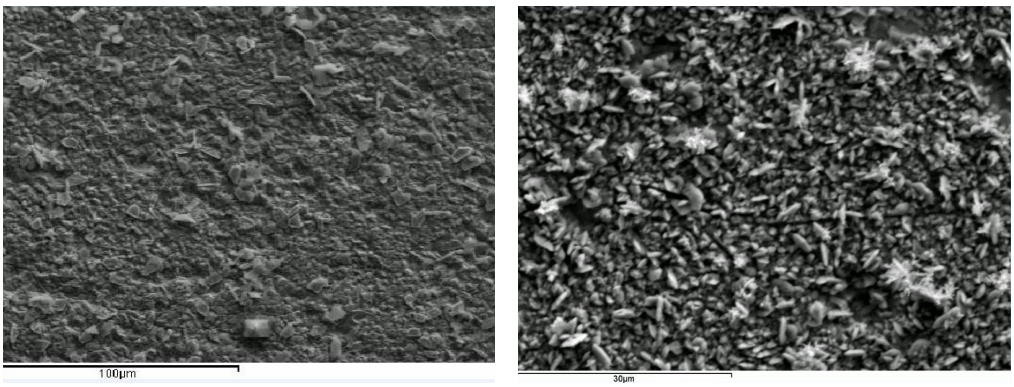

(a) **(b)**

Figure 7.17: SEM micrographs recorded for BV-modified Cu on cycling the electrode in 0.10 mol dm^{-3} NaCl, at a pH of 7.0 from -1.50 to 1.00 V vs. SCE (a) the scale bar corresponds to 100 μm and (b) the scale bar corresponds to 30 μm.

7.3 Corrosion Assessment of the Viologen Films

The corrosion protection properties of the viologen-modified copper was studied using a combination of electrochemical techniques, some of these included cyclic voltammetry, open-circuit potential measurements, potentiodynamic polarisation plots, Tafel analyses and electrochemical impedance spectroscopy. In addition, a spectrophotometric analysis was used to monitor the copper ion concentration.

7.3.1 Spectrophotometric Analysis of the Copper Ion Concentration

The concentration of copper dissolved from the BV-modified copper and copper electrodes was monitored using the spectrophotometric approach described in Section 7.1. The first test involved a study on the stability of the complex. Test solutions with different concentrations of copper ions were prepared in the 0.10 mol dm^{-3} NaCl solution and the bathocuproine was added to form the complex, as detailed in Section 4.3.1. The absorbance was recorded at 480 nm as a function of time to monitor the stability of the complex. These data are summarised in Table 7.3 and show that the absorbance varies only slightly with time, indicating good stability of the complex. Moreover, this stability is observed at a range of copper ion concentrations, indicating that the presence of chloride anions has little influence on the stability of the complex. Indeed, the concentration of the chloride anion was varied and the absorbance of the complex was followed, as a function of time, and again very good reproducibility and stability was observed, making this approach suitable in the quantitative analysis of the copper ion concentration.

Table 7.3: Stability of the complex as a function of time and concentration of Cu ions.

Concentration mol dm^{-3}	Absorbance t = 5 min	Absorbance t = 5 h	Absorbance t = 24 h
5.25×10^{-7}	0.0940	0.0969	0.0969
1.07×10^{-6}	0.1650	0.1667	0.1676
1.14×10^{-6}	0.2021	0.2062	0.2106

The copper and BV-modified copper electrodes were cycled in 0.10 mol dm^{-3} NaCl from -0.20 V vs. SCE up to final potentials of 0.00, 0.20 and 0.60 V vs. SCE and then the solutions were treated with the bathocuproine reagent, as detailed in Section 4.3.1. However, poor reproducibility was observed, as shown in Table 7.4. In this table the absorbance recorded at 480 nm is shown as a function of the upper applied potential for the copper electrode. Although

there is a general increase in the absorbance with increasing applied potentials, consistent with higher dissolution rates at the higher applied potentials, the reproducibility is poor. The absorbance varies from 0.0988 to 0.1415 at 0.00 V vs. SCE and from 0.1650 to 0.2021 at 0.60 V vs. SCE. These variations may be related to the dissolution and precipitation of corrosion products at the copper surface.

Table 7.4: Absorbance recorded as a function of the upper potential for Cu cycled in 0.10 mol dm^{-3} NaCl at 1 mV s^{-1}.

Upper potential/ V vs. SCE	Absorbance t = 5 min	Absorbance t = 5 h
0.00	0.0998	0.1027
	0.1106	0.1129
	0.1415	0.1506
0.20	0.0925	0.0939
	0.0995	0.1011
	0.1611	0.1639
	0.1650	0.1699
0.60	0.1694	0.1699
	0.2021	0.2026

Although not shown, poor reproducibility was also observed for the data recorded with the BV-modified copper. For example, the absorbance varied from 0.1337 to 0.1695, when the BV-modified copper was polarised to 0.60 V vs. SCE and from 0.1462 to 0.1971 when polarised to 1.0 V vs. SCE. When these data are compared with the results obtained with the copper system, Table 7.4, it is clear that lower absorbance values are obtained for the BV-modified copper, indicating a lower rate of copper dissolution. However, the reproducibility is poor and it is difficult to assess the corrosion protection properties of the BV film.

In an attempt to increase the reproducibility of the data, the copper and BV-modified copper were polarised at fixed potentials of 0.00, 0.20, 0.60 and 1.00 V vs. SCE for 30 min and then the resulting solution was treated with the bathocuproine reagent and the absorbance was recorded at 480 nm. These data are summarised in Table 7.5. A considerable improvement in the reproducibility was observed and trends in the data can now be seen. It is clear that higher concentrations of copper are measured when the copper and viologen modified copper are polarised at higher applied potentials. This corresponds well with the SEM and EDX analyses presented in Section 6.2.6, Chapter 6. It is also evident that lower concentrations of dissolved copper ions are measured for the viologen-modified films. However, these

concentrations are influenced by the deposition of copper-containing corrosion products at the copper electrode. Indeed, this can be seen from the data presented for the copper system, where similar concentrations of dissolved copper ions are evident at 0.60 and 1.00 V vs. SCE. In this case, the deposition of corrosion products inhibits the release of the dissolved copper ions into the solution giving solution concentrations that are lower than the true rate of dissolution. This is not seen with the viologen-modified copper and in this case, the copper ion concentration represents the true rate of copper dissolution. Consequently, the final concentrations are not significantly different from the values recorded for the copper system, as shown in Table 7.5.

Table 7.5: Concentration of dissolved Cu ions (n = 4) from Cu and BV-modified Cu as a function of the applied potential.

System	Applied Potential / V vs. SCE	Concentration μmol dm^{-3}
Cu	0.00	3.65 ± 0.15
	0.20	4.19 ± 0.20
	0.60	4.68 ± 0.17
	1.00	4.58 ± 0.21
BV-modified Cu	0.00	3.21 ± 0.10
	0.20	3.66 ± 0.16
	0.60	4.09 ± 0.14
	1.00	4.13 ± 0.16

7.3.2 Cyclic Voltammetry

It is well known that chloride anions affect the passivation of copper, resulting in the breakdown of the passive film. It is also well accepted that copper rapidly dissolves through the formation of soluble $CuCl_2^-$ complex species [80, 85, 313, 321, 338, 398]. This dissolution occurs at more positive potentials, compared to the potential values where the oxide films are formed or detected [39, 65, 67, 284, 399, 400]. These breakdown events can be easily monitored using cyclic voltammetry and this technique was employed to study the stability of the viologen-modified copper and copper electrodes. A neutral 0.10 mol dm^{-3} NaCl solution was used and the electrodes were cycled from -0.20 V to 1.00 V vs. SCE at a scan rate of 1 mV s^{-1}. The viologen-modified copper electrodes were prepared as detailed in Section 7.1. Representative data are presented in Figure 7.18, where the current-potential and charge-potential plots are compared for the BV-modified copper and uncoated copper. Similar data are shown in

Figure 7.19. However, in this case a plot recorded for the viologen-modified copper, which was previously cycled in the chloride solution, is compared with the freshly deposited viologen film and the uncoated copper.

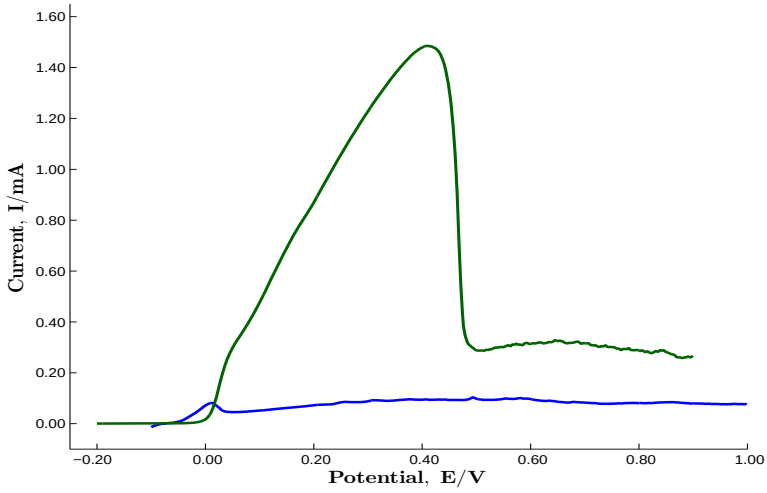

(a)

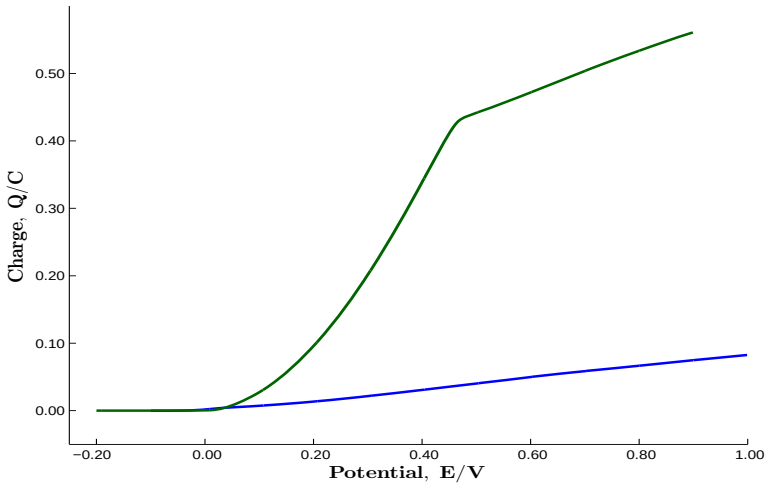

(b)

Figure 7.18: Voltammograms at 1 mV s^{-1} for Cu (green) and BV-modified Cu (blue) in 0.10 mol dm^{-3} NaCl, at a pH of 7.0, (a) current-potential plots and (b) charge-potential plots.

Dissolution of copper is observed for the uncoated copper and the current continues to rise with increasing applied potential, as shown in Figures 7.18 and 7.19. The initial dissolution is observed at about 0.02 V vs. SCE, however this potential varies slightly from -0.03 to 0.12 V vs. SCE. The charge-time plots show that the rate of dissolution varies with the applied potential and at higher potentials the charge increases at a slower rate, which is consistent with the deposition of corrosion products [32, 50, 68, 285], such as CuCl and

copper oxides. The formation of these CuCl deposits has been observed on the electrode surface at potentials corresponding to dissolution [6, 48, 280, 282]. These data are in good agreement with literature reports and are connected with the adsorption of chloride ions and the formation of a two-dimensional salt layer that is known to play an important role in the passivity breakdown of copper [78, 390, 401]. Indeed, the adsorption of chloride ions has been detected at potentials negative to that of active dissolution by several authors [351, 359, 402]. For example, Becerra *et al.* [403] reported the formation of a chloride adsorbed layer on the copper surface at -0.60 V vs. SCE in 0.10 mol dm^{-3} NaCl, while Marchiano *et al.* [64] detected chloride adsorption in 0.3 mol dm^{-3} NaCl at potentials as low as -0.80 V vs. SCE. It was suggested that the onset of copper dissolution is connected with the degree of metal surface coverage by chloride and hydroxide electro-adsorbates. Benedetti *et al*. [394] have shown that the chloride adsorption/desorption equilibrium precedes active dissolution, while Starosvetsky *et al*. [282] have shown that dissolution is initiated when the potential exceeds a breakdown value, consistent with the data presented in Figures 7.18 and 7.19.

In contrast, very good stability is observed when the viologen modified copper electrodes are cycled under the same conditions. There is no evidence of these dissolution reactions and the charge remains essentially constant and independent of the applied potential, signifying a highly protective coating. It is also significant that the protective properties of the viologen coating are maintained even though the viologen-modified copper was previously cycled at the scan rate of 1 mV s^{-1} from -0.20 to 1.00 V vs. SCE in the chloride-containing solution. This is shown clearly in Figure 7.19, where the protective properties of a freshly deposited coating are compared with the aged film. Clearly, the current-potential and charge-potential profiles are similar, indicating that the BV has indeed very good protective properties.

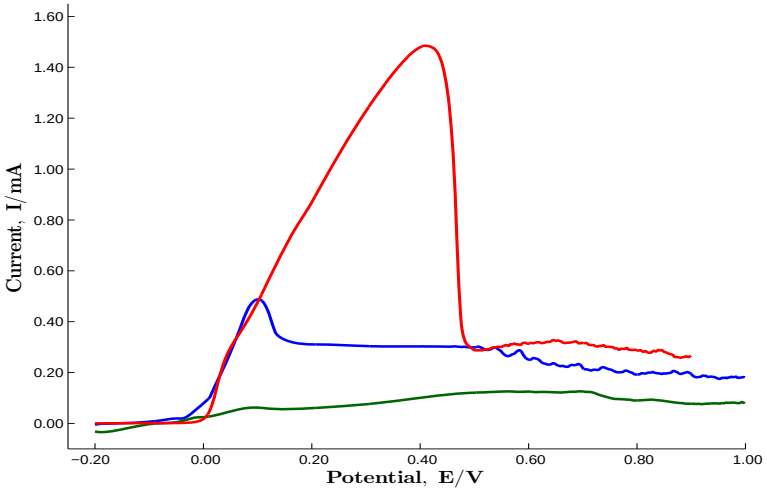

(a)

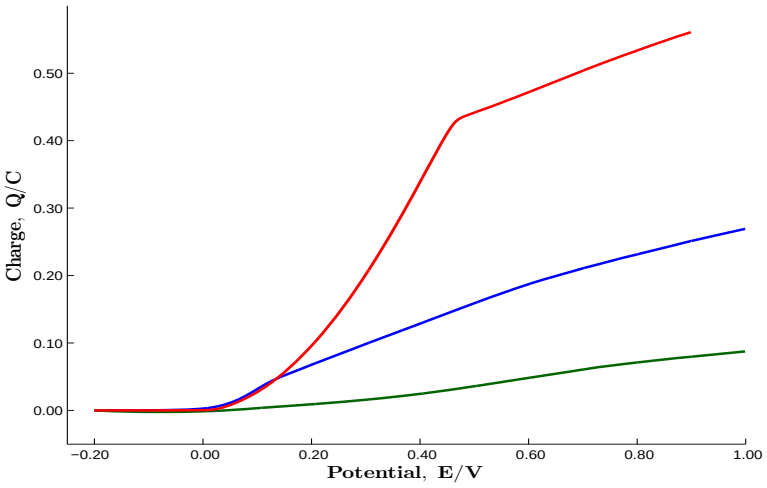

(b)

Figure 7.19: Voltammograms at 1 mV s^{-1} in 0.10 mol dm^{-3} NaCl, at a pH of 7.0 for Cu (red), BV-modified Cu (green), previously cycled in the chloride solution, and BV-modified Cu (blue), (a) current-potential plots and (b) charge-potential plots.

7.3.3 Open-Circuit Potential (OCP) Measurements

In order to investigate the corrosion protection properties further and the stability of the viologen-modified copper, immersion experiments were performed and the potential adopted was recorded as a function of time in the aggressive chloride-containing solution. Typically in corrosion, the principle of charge conservation dictates that the sum of all the oxidation currents must equal the sum of all the reduction currents, to avoid the accumulation of charge on a freely immersed electrode. Therefore, at the corrosion potential, the oxidation currents,

I_a, are equal in magnitude to the reduction currents, I_c, Equation 7.5.

$$\sum Ia + \sum Ic = 0 \tag{7.5}$$

The corrosion potential is a mixed potential and it depends on the rate of the anodic and the cathodic half reactions. This can be explained by the Evans diagram, depicted in Figure 7.20 [44]. The relative values of the slopes of the anodic or cathodic polarisation curves determine whether the anodic, cathodic, or both reactions control the rate of the corrosion process and, in turn, the adopted corrosion potential.

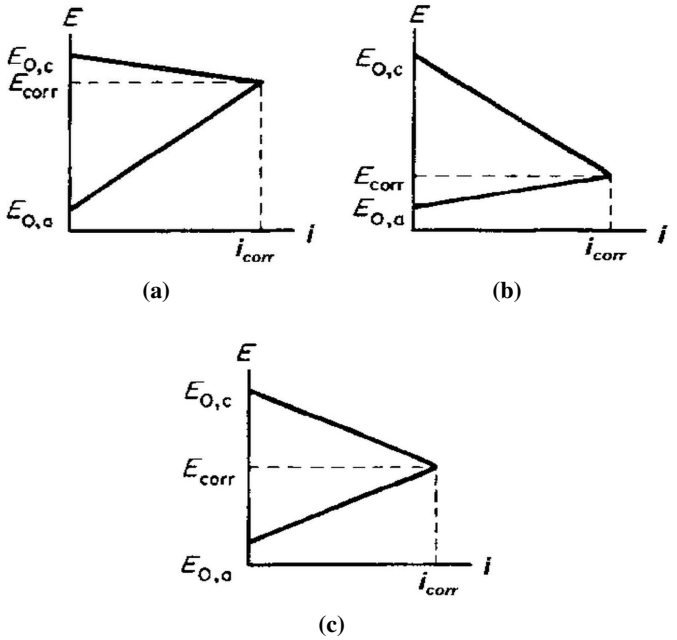

Figure 7.20: Evans diagram illustrating three main ways in which the corrosion potential can be influenced (a) control by the reactions on the anode (b) control by the reactions on the cathode and (c) control by a mixture of both [44].

As shown in Figure 7.20, the corrosion potential can be used to give information on the protective properties of a metal, which is susceptible to dissolution or corrosion. Accordingly, the open-circuit potentials adopted by copper and the BV-modified copper were recorded as a function of time in 0.10 mol dm^{-3} NaCl solutions adjusted to pH values between 3.0 and 7.0. These results are summarised in Figures 7.21 and 7.22. The results presented in Figure 7.21 correspond to the copper and BV-modified copper immersed at a pH of 5.0 and 3.0. For the data presented at a pH of 3.0, the results recorded for the viologen-modified copper following

approximately 96 h period in the chloride solution are also included. In this case, the electrode was stored for approximately 96 h in the acidified 0.10 mol dm^{-3} NaCl solution, it was then transferred to fresh 0.10 mol dm^{-3} NaCl and the open-circuit potential was recorded for 7000 s. In Figure 7.22, the data recorded at a pH of 6.0 are shown on initial immersion in Figure 7.22a, while the data recorded following a 4 day immersion period are presented in Figure 7.22b.

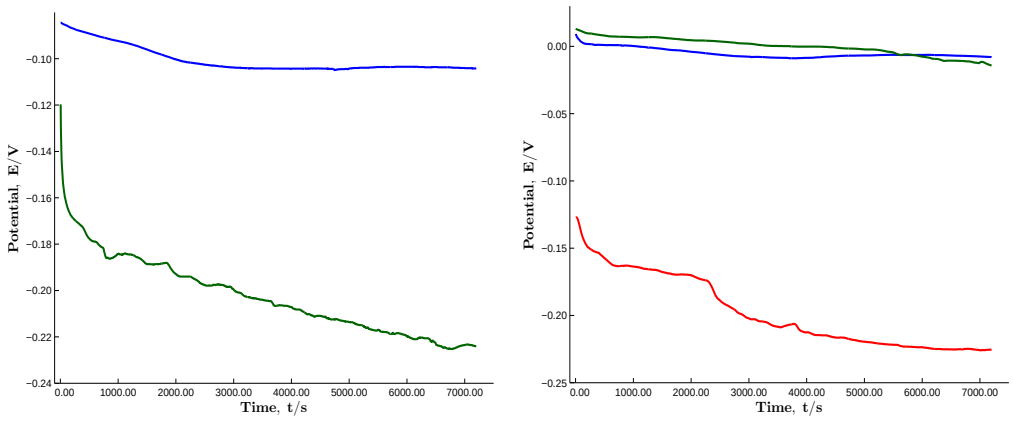

Figure 7.21: Open-circuit potential plotted as a function of immersion times for Cu and the BV-modified Cu immersed in 0.10 mol dm^{-3} NaCl (a) uncoated Cu (green) and BV-modified Cu (blue) at a pH of 5.0 and (b) pH of 3.0, uncoated Cu (red), the BV-coated Cu (green) and the BV-coated Cu (blue) after 96 h immersion.

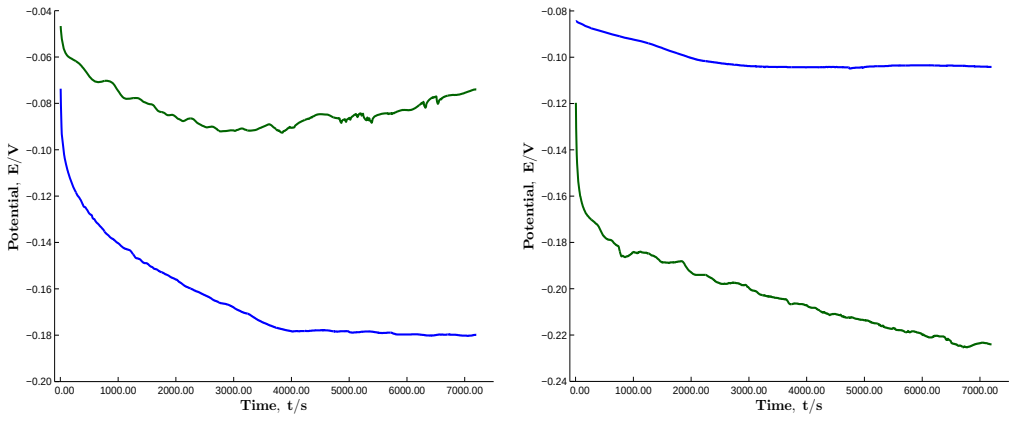

Figure 7.22: Open-circuit potential plotted as a function of immersion time for Cu and the BV-modified Cu immersed in 0.10 mol dm^{-3} NaCl at a pH of 6.0 (a) data recorded on immersion, uncoated Cu (blue) and BV-modified Cu (green) (b) data recorded following 4 days of immersion, uncoated Cu (green) and BV-modified Cu (blue).

On examination of these figures, it can be seen that the open-circuit potentials recorded for the BV-modified copper are significantly higher than that recorded for the uncoated copper. This is observed at pH values of 3.0, 5.0 and 6.0, and although the data are not shown, similar results were obtained at pH values of 4.0 and 7.0. On immersion of the uncoated copper in the chloride-containing solutions, the potential decays to reach near steady-state conditions at about 5000 to 7000 s. This slow decay in the potential is consistent with the adsorption of chloride anions and the formation of copper-containing corrosion products at the surface. However, at this potential the dissolution rate of copper is very low, as shown in Figure 7.18. A similar potential-time profile is observed for the viologen-modified copper electrodes. However, in this case, steady-state conditions are attained at much shorter times. For example, the potential reaches a near constant value within 100 s at a pH of 3.0, and 2500 s at a pH of 5.0 and 6.0, Figures 7.21 and 7.22. This suggests that while the surface of the uncoated copper electrode is modified on immersion in the chloride solutions, these modifications do not occur, or at least they occur to a lesser extent, for the viologen-modified copper. This is consistent with the protective properties of the viologen films. Furthermore, these open-circuit potentials are stable for considerable periods of time for the viologen-modified copper. As shown in Figure 7.22, the open-circuit potential adopts values of approximately -0.08 to -0.09 V vs. SCE from 2000 s to periods exceeding 4 days. This indicates very good stability over extended periods of time.

As the OCP value is determined by the rate of both the anodic and cathodic reactions, according to the electro-neutrality theory and the Evans diagram in Figure 7.20, a decrease in the rate of the anodic current will give rise to more positive OCP values. This clearly shows that the rate of the anodic dissolution of copper at the viologen-modified copper is reduced and this is consistent with the cyclic voltammetry data, presented in Section 7.3.2 and the spectrophotometric data presented in Section 7.3.1. Furthermore, the OCP values of the viologen-modified copper remain at these more positive values and do not decay to the values adopted by the uncoated copper electrodes, indicating very good stability over extended periods.

7.3.4 Potentiodynamic Polarisation Curves and Tafel Analyses

The corrosion protection properties of the viologen-modified copper electrodes were also compared to the uncoated electrodes in 0.1 mol dm^{-3} NaCl at a pH of 7.0 using potentiodynamic polarisation curves and Tafel analyses. These data were recorded at a relatively slow scan rate of 1 mV s^{-1} and the electrodes were polarised from below the corrosion potential to higher potential values to monitor the cathodic reduction and anodic dissolution reactions at the surface.

Shown in Figure 7.23b is a typical polarisation curve recorded for copper. It is evident that on polarising the copper in the anodic direction that dissolution of the copper occurs. The anodic current increases rapidly at potentials higher than the corrosion potential. The plots depicted in Figure 7.23a, show the corresponding data recorded for the BV-modified copper. Again, an increase in the current is observed when the electrode is polarised above the corrosion potential. The current increases rapidly to give a peak current and then the current decays to give a pseudo-passive film. These data are similar to the voltammetry measurements presented and discussed in Section 7.3.2. However, the corrosion potentials observed in Figure 7.23 are somewhat different to the values measured in Section 7.3.3, but this is probably connected with the manner in which the electrodes were polarised in the chloride-containing solutions.

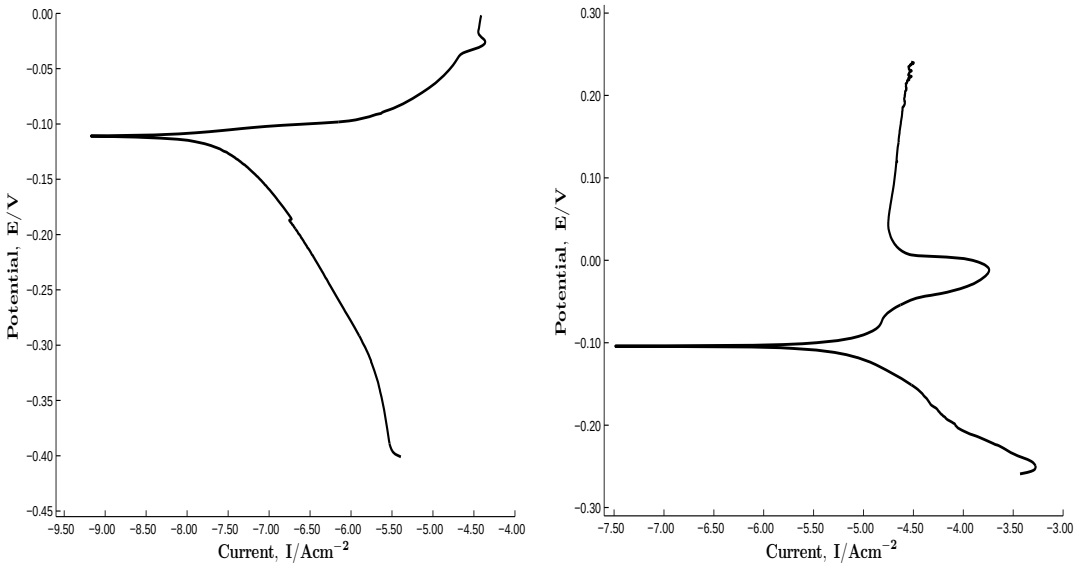

Figure 7.23: Potentiodynamic polarisation plots recorded in 0.1 mol dm^{-3} NaCl at 1 mV s^{-1}, (a) uncoated Cu and (b) BV-modified Cu.

Using the data presented in Figure 7.23, the corrosion current and corrosion potential were obtained by computing the Tafel slopes of the cathodic and anodic polarisation curves [263, 310]. At the corrosion potential, the rate of the reduction reaction is equal to the rate of the metal dissolution, and this point corresponds to the corrosion rate of the system expressed in terms of current density. The reduction reaction depends on the pH of the solution and involves either the reduction of hydrogen ions or the reduction of dissolved oxygen to hydroxide ions, Equations 7.6 and 7.7.

$$2H^+ + 2e^- \rightarrow H_2^+ \tag{7.6}$$

$$O_2 + 2H_2O + 4e^- \rightarrow 4OH^- \tag{7.7}$$

However, it should be pointed out that this analysis is strictly only applicable to activation controlled corrosion processes. It is well known that the dissolution of copper in chloride-containing solutions is under mixed activation and diffusion control [280, 282] and this may impair the usefulness of this approach. However, on inspection of the data presented in Figure 7.23, there appears to be sufficient linear regions for the analysis for both the uncoated copper and the viologen-modified copper. The computed corrosion potential, E_{corr}, corrosion current, I_{corr} and Tafel slopes, b_a and b_c are summarised in Table 7.6, where values for the uncoated copper and the BV coated copper are presented. Included are data for the EV-modified copper and the MV-modified copper, while the data obtained in the presence of the BTA inhibitor are also provided for comparison. The proportionality constant, B, which can be calculated from the anodic and cathodic Tafel slopes, b_a and b_c using Equation 7.8, [310, 404], is also shown for each system.

$$B = \frac{b_a b_c}{2.303(b_a + b_c)} \tag{7.8}$$

The Tafel slopes and corrosion current obtained for copper are in relatively good agreement with the data obtained by Mansfeld *et al*. [310] for copper in chloride solutions, where b_a was calculated as 68 mV, b_c as 81 mV, B as 16.1 mV and I_{corr} as 2.0 μA cm^{-2}. On comparing the different systems in Table 7.6, there is little variation in the I_{corr} values, except slightly lower values were recorded for the MV modified copper. Indeed, on computing, R_p, where $R_p = B/I_{corr}$, a relatively high value of 15 kΩ was obtained compared to a value of 11 kΩ recorded for the uncoated copper. The I_{corr} value recorded for the BV-modified copper is somewhat

high at 1.67 μA cm^{-2}, giving a relatively low R_p value of 10 kΩ . This indicates that the BV-modified copper has no significant influence on the rate of corrosion, but as pointed out earlier these analyses are only appropriate for activation-controlled processes. On the other hand, it is seen from the voltammetry data, presented in Figures 7.15, 7.18 and 7.19, the SEM micrographs, presented in Figures 7.16, and 7.17 and the open-circuit potential data presented in Figures 7.21 and 7.22, that the viologen-modified copper has indeed corrosion protection properties and these are particularly evident at higher applied potentials.

Table 7.6: Tafel analysis in 0.10 mol dm^{-3} NaCl, at a pH of 7.0.

System	b_a mV decade^{-1}	b_c mV decade^{-1}	E_{corr} V vs. SCE	I_{corr} μA cm^{-2}	B mV
Uncoated Cu	54	89	-0.111	1.29	14.8
BV-modified Cu	83	94	-0.104	1.67	16.8
EV-modified Cu	74	57	-0.102	4.83	14.1
MV-modified Cu	51	59	-0.149	0.81	11.9
BTA in solution	37	72	-0.135	1.24	10.7

7.3.5 Electrochemical Impedance Spectoscopy

Electrochemical impedance spectroscopy (EIS) was used to investigate and compare the properties and stability of the BV-modified copper with copper. The data were recorded over a range of potentials in 0.10 mol dm^{-3} NaCl, but only at potentials where the copper and viologen-modified copper were stable. The BV-modified copper was prepared as detailed in Section 7.1.

Representative impedance plots of the uncoated copper and the viologen-modified copper recorded at 0.00 V vs. SCE are shown in Figures 7.24 and 7.25, respectively. This corresponds to a potential where the dissolution of copper is first observed, as shown from the data presented in Figures 7.18 and 7.19. The modulus of the impedance, Z, and the phase angle presented as a function of the frequency result in the Bode plot, while the imaginary and real components of the impedance are plotted to give the complex plane. In all cases, the data were recorded as a function of the immersion period for a total of 12 h in 0.10 mol dm^{-3} NaCl. Three traces are shown in Figure 7.24 for the uncoated copper and these correspond to the data recorded after 60, 120 and 180 min. The data presented for the viologen-modified copper were recorded following 240 min at 0.00 V vs. SCE. For the uncoated copper, Figure 7.24, the Nyquist plot shows two

merged semi-circles at high and low frequency and this is typical of a corroding surface [405]. At longer times, the radius of the semicircle, corresponding to the film resistance, increases. Again, this is consistent with the behaviour of a corroding surface, where the dissolution gives rise to the deposition of a corrosion product layer, comprising copper oxides, hydroxides and various copper chloride species, such as CuCl. As this layer increases in thickness and ages, there is a corresponding increase in the film resistance, as shown in Figure 7.24. Indeed, impedance studies have been performed on copper in the near-active and active dissolution regions and these data have been interpreted in terms of the diffusion through the copper chloride salt layer, CuCl, deposited at the surface [260, 345, 401]. The impedance data recorded for the viologen-coated copper are very different, as shown in Figure 7.25. Although not shown on this plot, the impedance remained essentially constant and did not vary with the polarisation period. This indicates that the corrosion products are not formed on continued polarisation at 0.00 V vs. SCE. Instead, the viologen film protects the underlying copper and minimises the formation of these corrosion products. The impedance data are characterised by a single depressed semi-circle.

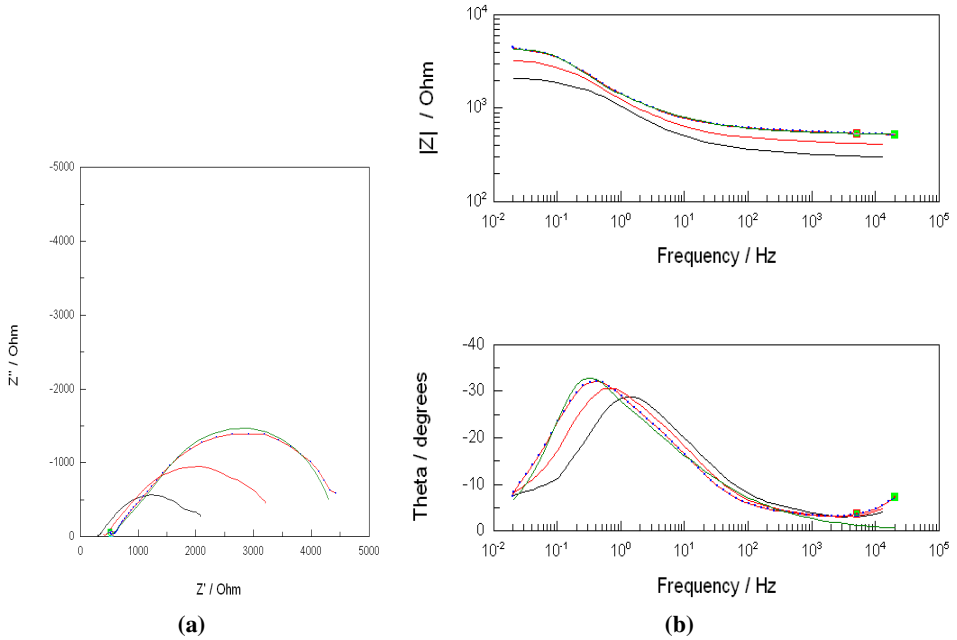

Figure 7.24: (a) Complex plane and (b) Bode plots recorded for uncoated Cu in 0.10 mol dm^{-3} NaCl at 0.00 V vs. SCE. Both the experimental data (red/blue dot trace) and the simulated fitted traces (green) are shown, data shown as a function of time at 60, 120 and 180 min.

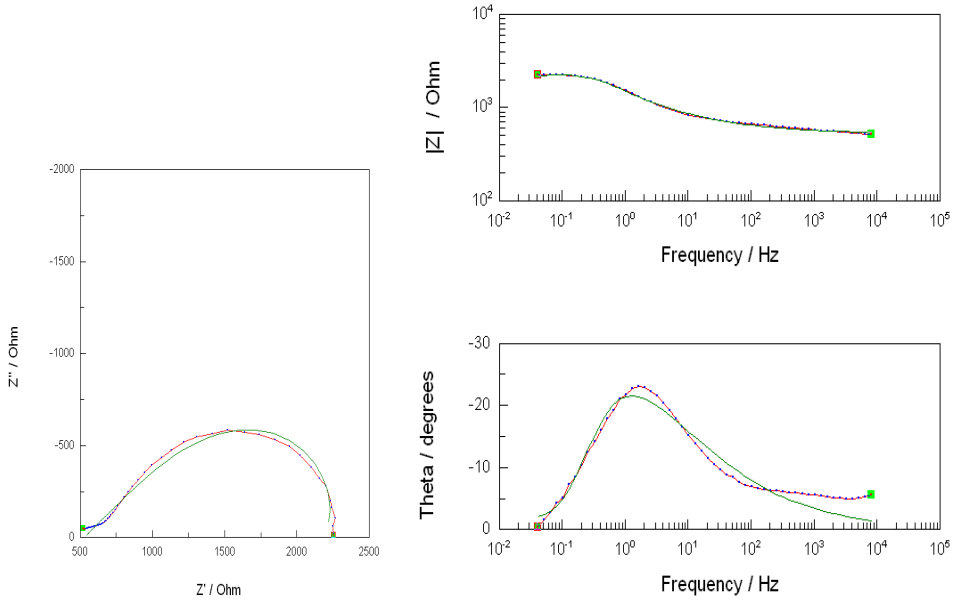

Figure 7.25: (a) Complex plane and (b) Bode plots recorded for the BV-modified Cu in 0.10 mol dm^{-3} NaCl at 0.00 V vs. SCE. Both the experimental data (red/blue dot trace) and the simulated fitted traces (green) are shown.

These impedance data were fitted to the equivalent circuit depicted in Figure 7.28 using a non-linear least squares fitting minimisation method in the ZView fitting programme, as detailed in Section 2.5.3. In this circuit, R_s represents the solution resistance, R_1 represents the charge-transfer resistance, while CPE_1 and CPE_2 are constant phase elements. Very good agreement between the experimental and the simulated data was obtained as shown in the figure, where the experimental data are compared to the simulated traces. In addition, the % errors obtained were < 3% suggesting a good fit for the data. In this fitting routine, constant phase elements were used to determine the capacitance of the interface and also to model the diffusional processes. These were used rather than pure capacitors to take into account the inhomogeneity of the surface of the electrode. The impedance of a constant phase element, Z_{CPE} is defined in accordance with Equation 7.9, with the fractional exponent, n, having values between 0 and 1 [256, 344]. Here, j is the imaginary number, ω is the angular frequency and n represents a phase shift that is a measure of surface inhomogeneity.

$$Z_{CPE} = \frac{1}{Q(j\omega)^n} \tag{7.9}$$

When the exponent is zero, $n = 0$, the CPE describes an ideal resistor and when the exponent is unity, $n = 1.0$, the CPE is equivalent to an ideal capacitor, while an exponent of 0.5, $n = 0.5$, corresponds to homogeneous semi-infinite diffusion. The higher exponent values, $n > 0.95$, point to a relatively high degree of surface homogeneity, while lower values, $0.85 < n < 0.95$, indicate poor surface homogeneity, which may be related to a more porous structure. Excellent agreement between the experimental data and the theoretical fitted data was obtained when these frequency-dependent constant phase elements (CPE) were used, as opposed to ideal capacitors or Warburg elements. For the uncoated copper, the parallel combination between CPE_1 and R_1 is related to the mid-frequency range, where CPE_1 represents the double layer capacitance. The low frequency Warburg response, modelled by CPE_2, is probably due to the intermediate species generated during the dissolution of copper, which are then adsorbed or precipitated on the surface forming a layer. The dissolution is thus limited by the formation of this layer. In the case of copper, the n value is close to unity in the case of CPE_1, at 0.92, indicating that CPE_1 represents a capacitor while the n value of CPE_2 is close to 0.5 signifying that this is a Warburg diffusional term. For the viologen-modified copper, R_1 represents the resistance of the viologen film and the resistance of the initial CuCl layer formed on copper prior to the deposition of the viologen, while CPE_1 corresponds to the capacitance of the film. The capacitance was computed as 1.50×10^{-4} F cm^{-2} and this remained constant during the polarisation period, from 30 to 720 min. The resistance, R_1, was calculated as 500 Ω cm^2, and again there was little change in this resistance with continued polarisation.

The impedance data recorded at -0.20 V vs. SCE are depicted in Figures 7.26 for the uncoated copper and in Figure 7.27 for the viologen-modified copper. At this potential, the copper is stable and the potential is sufficiently removed from the active dissolution region, as shown in Figures 7.18 and 7.19, that the copper remains stable as a function of time. Indeed this was observed on recording the data as a function of the polaristion period from 30 to 720 min. The impedance data for the viologen-coated and uncoated copper are similar and consist of a depressed semi-circle and a diffusion tail and can be fitted to the two-time constant model shown in Figure 7.28. Again, the simulated data are compared with the experimental data and very good agreement is seen over the entire frequency range. The fitted parameters are provided in Tables 7.7 and 7.8.

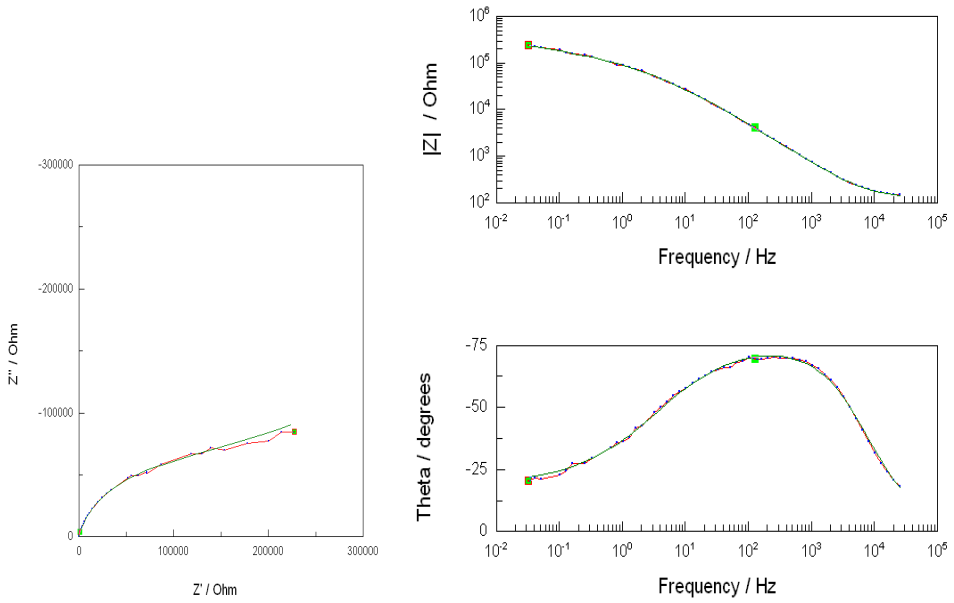

(a) **(b)**

Figure 7.26: (a) Complex plane and (b) Bode plots recorded for the uncoated Cu in 0.10 mol dm^{-3} NaCl at -0.20 V vs. SCE. Both the experimental data (red/blue dot trace) and the simulated fitted traces (green) are shown.

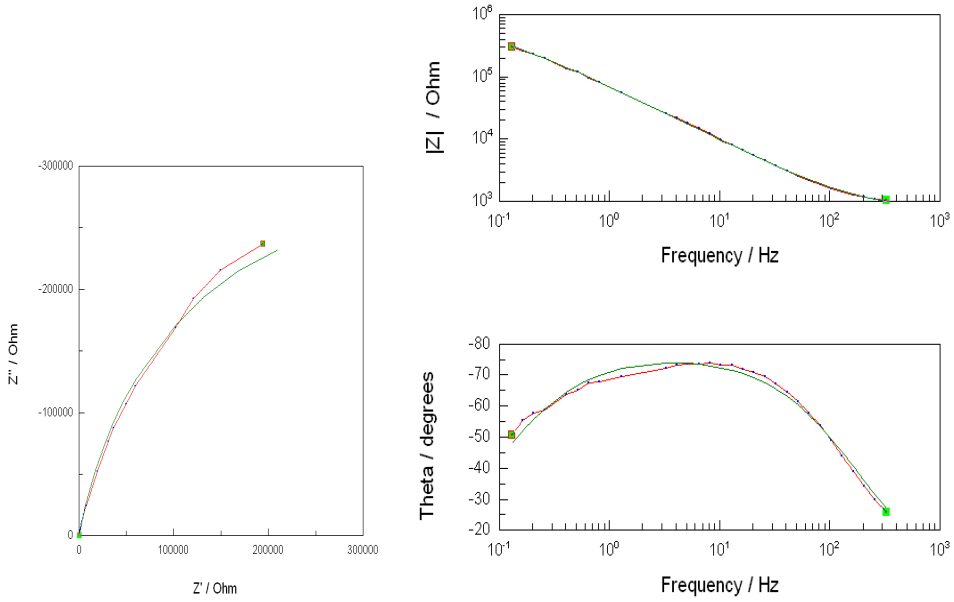

(a) **(b)**

Figure 7.27: (a) Complex plane and (b) Bode plots recorded for the BV-modified Cu in 0.10 mol dm^{-3} NaCl at -0.20 V vs. SCE. Both the experimental data (red/blue dot trace) and the simulated fitted traces (green) are shown.

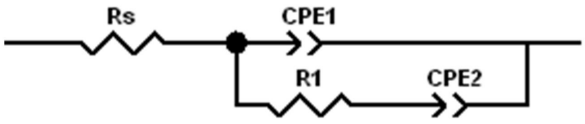

Figure 7.28: Equivalent circuit used in the fitting of the experimental data.

Table 7.7: Fitted parameters for the BV-modified Cu at -0.20 V vs. SCE in 0.10 mol dm^{-3} NaCl solution.

BV-modified R_1Cu	R_s/Ω	CPE_2/F cm^{-2}	n	R_1/Ω
60 min	132	1.17 ×10 $^{-4}$	0.67	910
180 min	134	1.15 ×10 $^{-4}$	0.69	991
300 min	136	1.12 ×10 $^{-4}$	0.70	1096

Table 7.8: Fitted parameters for Cu at -0.20 V vs. SCE in 0.10 mol dm^{-3} NaCl solution.

Cu	R_s/Ω	CPE_2/F cm^{-2}	n	R_1/Ω
60 min	112	1.77 ×10 $^{-3}$	0.42	21167
180 min	109	1.71 ×10 $^{-3}$	0.46	17342
300 min	105	1.66 ×10 $^{-3}$	0.52	14411

Under these applied potential conditions, chloride adsorption occurs at the surface of the bare electrode. This slows down the electron kinetics and the adsorbed chloride acts like an insulation layer affecting the rate at which redox species are oxidised or reduced at the surface. The capacitance of the uncoated copper, represented as CPE_1 in Figure 7.28, with n = 0.81, is 40 μF cm^{-2}, and this is in good agreement with the double-layer capacitance of bare electrodes [27, 174]. The CPE_2 represents a diffusional process at the adsorbed chloride layer, while R_1 corresponds to the resistance of this adsorbed layer. A lower resistance is measured for the viologen-modified copper, as shown in Tables 7.7 and 7.8. From the analysis presented in Tables 7.7 and 7.8, it is clear that the circuit parameters remain nearly constant. This suggests good stability and the establishment of steady-state conditions after 180 min.

Babioc and Metikos-Hukovioc [2] have reported an increase in total resistance with increasing inhibitor and immersion times. The increase in charge transfer resistance is generally associated with improved corrosion protection. Babic *et al*. [84] have shown a decrease in the capacitance for both Cu and CuNi in a BTA-containing acetate solution and have attributed this decrease to the formation of a protective film on the electrodes. Subramanian *et al*. [95] have proposed that the double layer capacitance reduces after absorption of the

inhibitor since the absorbed layer reduces the dielectric constant (K) between the metal and the electrolyte as shown in Equation 7.10. This is consistent with the data presented in Tables 7.7 and 7.8.

$$C = K\frac{\epsilon_0 A}{d} \tag{7.10}$$

At higher applied potentials the uncoated copper was unstable and the impedance response varied with the polarisation period as corrosion products were formed and deposited at the surface. On the other hand, the viologen-modified copper electrode continued to remain stable up until a fixed potential of 0.60 V vs. SCE was applied. This breakdown potential is slightly lower than that observed in the polarisation plots and cyclic voltammetry analysis, Figures 7.18 and 7.19. However, this can be related to the relatively long periods of time at these high applied potentials. The stability of the viologen-modified copper is summarised in Figure 7.29, where the resistance of the film is plotted as a function of the polarisation period at 0.00, 0.20 and 0.60 V vs. SCE. Steady-state conditions are achieved after approximately 80 min and then the resistance remains constant with no evidence for modification of the film or dissolution of copper from the underlying substrate. These data clearly show that the BV film has corrosion protection properties and the film is stable for considerable periods of time.

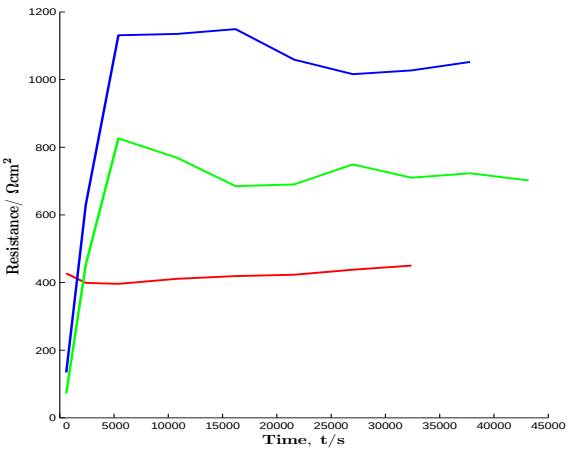

Figure 7.29: Resistance, R_1, for BV-modified Cu, plotted as a function of the polarisation period at 0.00 V (red), 0.20 V (blue) and 0.60 (green) V vs. SCE in 0.10 mol dm^{-3} NaCl.

7.4 Summary of Results

From the results presented in this chapter it can be concluded that stable and protective BV films are readily deposited from a chloride solution. The formation and deposition of the BV films are inhibited in the presence of sulfates, while in acetate and oxalate solutions the formation of insoluble copper oxalates and acetates at the copper surface, inhibits the deposition of the viologen. Although the BV films deposited from these acetate and oxalate solutions have some protective properties, these results are in good agreement with the data presented in Chapter 6 and highlight that the adsorption of chloride anions and the formation of a CuCl complex layer at the copper surface is critical in the formation of stable and protective BV films. The BV-modified copper showed good stability on cycling to -1.50 V vs. SCE in 0.10 and 0.15 mol dm^{-3} NaOH. The formation of CuO and Cu_2O oxides were observed, but there was no evidence of the dissolution of the underlying copper on cycling the modified electrode to an upper potential of 0.50 V vs. SCE. Good stability was also observed when the modified electrode was cycled from -1.50 to 1.00 V vs. SCE in the presence of 0.10 mol dm^{-3} NaCl.

In the assessment of the corrosion protection properties of the BV films it appears that the film offers relatively good corrosion protection to the copper. This was observed using a combination of a spectrophotometric analysis of the copper ion concentration and electrochemical techniques, ranging from OCP measurements, cyclic voltammetry, polarisation curves, Tafel analyses and electrochemical impedance spectroscopy. The spectrophotometric analysis of the dissolved copper ion concentration showed higher copper ion concentrations for the uncoated copper. However, in the absence of the viologen coating, the deposition of insoluble copper-containing corrosion products limits the release of the copper ions into the solution phase, giving ion concentrations that are lower than the true rate of dissolution of the uncoated copper. Nevertheless, the copper ion concentration was lower for the BV-modified copper, indicating good corrosion protection properties. Very good stability was observed on cycling the BV-modified copper from -0.20 to 1.00 V vs. SCE in the presence of 0.10 mol dm^{-3} NaCl. There was no evidence of copper dissolution, low currents and nearly constant charges were observed throughout the electrochemical window. The OCP data, recorded at pH values from 3.0 to 7.0, showed that the potential adopted by the BV-modified copper was higher than that recorded for the uncoated copper. This potential remained constant, highlighting the stability of the film

over time in highly aggressive solutions. Moreover, the characteristic decay of the potential to the value adopted by the uncoated electrode, which indicates loss in the protective properties, was not observed for the BV films over a 5 day period. Tafel analyses, which are routinely applied to compute corrosion currents and rates of corrosion, were difficult to interpret as these are limited to activation controlled conditions. However, the impedance study showed that the BV films remained stable for periods in excess of 12 h, when polarised to potentials in the vicinity of 0.60 V vs. SCE, highlighting the good protective properties of the BV films.

CHAPTER 8

Conclusions

In the research presented in this thesis, corrosion protection films were synthesised and characterised. The films were based on polypyrrole coatings doped with combinations of tartrate, oxalate and DBS along with the incorporation of MWCNT and viologen films adsorbed at copper. The corrosion protective properties of these films were studied and compared to the uncoated pure copper substrate.

As copper is easily oxidised it was challenging to obtain a protective film at the copper interface without the possibility of the dissolution of the copper substrate. However, polypyrrole films were successfully deposited at copper from a 0.10 mol dm^{-3} oxalate solution at pH 8.0 and a 0.10 mol dm^{-3} tartrate solution at pH 7.0 to generate PPy-Tartrate and PPy-Oxalate films on copper. Highly adherent polymer films were formed using these optimised conditions. SEM micrographs confirmed that the polymers were homogeneous, defect and crack-free. It was also possible to deposit the PPy-Tartrate film at pH values of 6.0 and 8.0. In addition, bi-layers comprising PPy-Tartrate/PPy-Oxalate and PPy-Oxalate/PPy-Tartrate were successfully formed at the copper surface. The PPy-Tartrate and PPy-Oxalate films were also deposited at platinum, however a more acidic pH was required. Adherent and homogeneous polymer films were only formed at a pH of 4.0 in the presence of either the oxalate or tartrate anions.

The electropolymerisation period was varied from 200 s to 3600 s to give polymer films with different thickness. The breakdown potential of the PPy-Tartrate film was approximately 0.45 V vs. SCE and this remained essentially independent of the electropolymerisation period. However, more protective PPy-Oxalate films were formed with electropolymerisation periods between 2400 and 3600 s. The bi-layer coating was also more protective with increasing electropolymerisation periods. The bi-layer provided the more corrosion protective coatings. Higher breakdown potentials were observed with the bi-layer. Furthermore, the open-circuit potential recorded for the bi-layer remained constant at about 0.10 V vs. SCE for a 30 day period in a neutral 0.10 mol dm^{-3} NaCl solution. Slightly lower open-circuit potentials were recorded for the PPy-Tartrate and the PPy-Oxalate film, but again the open-circuit potentials remained essentially constant over a 12-day period. However, at longer immersion times, the open-circuit potentials decayed to the values adopted by the uncoated copper electrode, indicating a loss in the protective properties of the films. This loss in corrosion protection was not observed with the PPy-Oxalate/PPy-Tartrate bi-layer, highlighting the more corrosion protective properties of the bi-layer.

In an attempt to further improve the corrosion protective properties of the bi-layer coatings, multi-walled carbon nanotubes, MWCNT, were incorporated into the polymer films. The dispersion of the MWCNT proved difficult; however, they were successfully dispersed using dodecylbenzene sulfonate (DBS) [218]. The concentration ratio of the MWCNT to DBS was important in forming a stable and well dispersed solution of MWCNT, in agreement with several literature reports [298]. Stable and well dispersed solutions were obtained using a 0.05 mol dm^{-3} DBS solution with 0.02 mg of MWCNT. The critical micelle content (CMC), which is defined as the concentration of surfactants above which micelles are formed, was obtained using conductivity and fluorescence measurements. The CMC was computed as 6.8×10^{-3} mol dm^{-3} and the aggregation number, N, which gives information on the number of surfactant molecules contained within the micelle, was estimated at 52.7. These values correspond well with literature reports [305, 406] and show that the micelles are present together with the DBS monomer in the MWCNT dispersed DBS solutions.

Once dispersed in the DBS solution and in the presence of pyrrole, the MWCNT were successfully incorporated within the polypyrrole films. Highly adherent and protective coatings were formed by incorporating the MWCNT in polypyrrole films deposited at tartrate

and oxalate doped polymer films. The PPy-Tartrate/PPy-DBSCNT and PPy-Oxalate/PPy-DBSCNT were deposited at a constant potential of 0.75 V vs. SCE from a solution containing 0.1 mol dm^{-3} tartrate or 0.1 mol dm^{-3} oxalate and 0.30 mol dm^{-3} pyrrole. The initial PPy-Tartrate or PPy-Oxalate films were deposited for 300 s and then the PPy-DBSCNT polymer films were formed for an additional 300 s. Both bi-layers and multi-layers, which consisted of four consecutive layers deposited for 300 s to give a total electropolymerisation time period of 1200 s, were successfully formed. In addition, PPy-Tartrate/DBSCNT and PPy-Oxalate/DBSCNT were formed by adsorbing the MWCNT onto the initial PPy-Oxalate or PPy-Tartrate films at a fixed potential in a solution containing DBS and MWCNT.

The corrosion protection properties of the polymer films PPy-Tartrate/PPy-DBSCNT, PPy-Tartrate /DBSCNT, PPy-Oxalate/PPy-DBSCNT and PPy-Oxalate/DBSCNT multi-layers were assessed. Excellent corrosion protection properties were observed for copper with the tartrate-based system, with the PPy-Tartrate/PPy-DBSCNT and PPy-Tartrate/DBSCNT multi-layers providing similar corrosion protection. Breakdown of the polymer films was only observed at approximately 0.80 V vs. SCE, while the open-circuit potential measurements indicated excellent long-term corrosion protection properties exceeding 30 days. A spectrophotometric analysis using bathocuproine was employed to monitor the concentration of dissolved copper. Low concentrations of dissolved copper were observed, consistent with low rates of copper dissolution and very good corrosion protection properties. The corrosion protective capabilities of the tartrate based polymers were further studied by forming a scratch in the polymer coating to expose the copper substrate. Then potentiodynamic polarisation tests were carried out on this scratched polymer in 0.10 mol dm^{-3} NaCl at a pH of 7.0 and the results were compared to an unscratched polymer under the same experimental conditions. However, the excellent corrosion protective properties were somewhat lost and dissolution of the copper substrate was evident. Lower breakdown potentials were recorded with the oxalate-based system and the corrosion protection properties were lost following a 15 day immersion period in 0.10 mol dm^{-3} NaCl. Nevertheless, the tartrate-based polymer films were stable and highly adherent, and exhibited excellent corrosion protection properties.

As DBS was used to disperse the MWCNT, it was difficult to determine if the DBS or the MWCNT was responsible for the corrosion protection observed with the PPy-Tartrate/PPy-DBSCNT polymer films. Accordingly, a PPy-DBS film was studied as the outer polymer film

in a bi-layer structure. The PPy-Tartrate/PPy-DBS bi-layer was readily formed at copper. The initial PPy-Tartrate layer was formed at 0.75 V vs. SCE for 600 s in 0.30 mol dm^{-3} pyrrole and 0.10 mol dm^{-3} tartrate. The PPy-DBS layer was then deposited at the PPy-Tartrate film at 0.75 V vs. SCE for an additional 600 s from 0.30 mol dm^{-3} pyrrole and 0.05 mol dm^{-3} DBS at pH of 7.0, to give the bi-layered films. Freshly prepared solutions were used to deposit the polypyrrole bi-layers, giving very good reproducibility. EDX analysis confirmed that the DBS was successfully incorporated within the PPy-DBS layer. The influence of the applied potential and deposition times on the formation of the outer PPy-DBS polymer film was studied and it was shown that highly adherent and corrosion protective films were deposited at 0.70 V vs. SCE for time periods ranging from 300 to 1000 s and at 0.90 V vs. SCE for times between 300 and 400 s. At lower electropolymerisation periods the polymer was not sufficiently thick to protect the copper substrate and at longer growth times less stable polymer films were formed. The concentration of DBS was varied from 0.001 to 0.090 mol dm^{-3} and adherent bi-layers were formed regardless of the concentration of DBS. However, a DBS concentration of 0.05 mol dm^{-3} gave the best corrosion protection properties and as shown from SEM micrographs of the surface morphology, a compact PPy-DBS was deposited at this concentration. The cauliflower morphology was observed at the higher DBS concentrations, however, when the concentration of DBS was reduced to 0.001 mol dm^{-3}, oval-like structures were observed at the surface and the rate of electropolymerisation was reduced, giving thinner PPy-DBS layers.

The direct electropolymerisation of pyrrole in the DBS-containing solution, to generate the PPy-DBS film at the copper, was successful at a pH of 6.0 in a 0.30 mol dm^{-3} pyrrole and 0.05 mol dm^{-3} DBS solution. Homogenous, adherent and stable PPy-DBS films were formed directly at the copper substrate at applied potentials from 0.60 V to 0.90 V vs. SCE. Although these PPy-DBS films showed good corrosion protection properties, somewhat more protective properties were observed with the PPy-Tartrate/PPy-DBS bi-layers.

The corrosion protective properties of the PPy-Tartrate/PPy-DBS bi-layers were assessed and studied using a combination of cyclic voltammetry, polarisation curves, Tafel analysis, open-circuit potential measurements and electrochemical impedance spectroscopy. The bi-layer adopted a more positive open-circuit potential compared to the open-circuit potential of the uncoated copper. In addition, the open-circuit potential was stable and constant and did not decay to the potentials of the uncoated copper, indicating high stability and good corrosion

protection properties. Breakdown of the bi-layer was only observed at potentials higher than 0.85 V vs. SCE, highlighting the stability and excellent corrosion protection properties of the bi-layers. Using Tafel analysis the corrosion current for the bi-layer protected copper was estimated at 0.11 μA cm^{-2} in a neutral 0.10 mol dm^{-3} NaCl solution. Good stability of the bi-layer was also observed in the electrochemical impedance spectroscopy study. The impedance data were recorded at potentials from -0.20 V to 0.60 V vs. SCE. However, breakdown of the bi-layer coating was observed at 0.60 V vs. SCE. This is probably connected with the extended polarisation periods, at 0.60 V vs. SCE, in the chloride-containing electrolyte. It appears from the results obtained that the PPy-DBS film is the key factor in the formation of a highly protective bi-layer polymer. The incorporation of the MWCNT into the outer polymer film appears to have little additional influence on the protective properties of the films.

An alternative approach was then considered. The electrochemical deposition of three viologens, MV, BV and EV at copper in the presence of a 0.10 mol dm^{-3} NaCl supporting electrolyte was studied. Sodium chloride was found to be a suitable electrolyte for the electrochemical formation of these viologen-containing films at the copper substrate. There was no need for the addition of any further supporting electrolyte. A 2.0 $\times$ 10^{-3} mol dm^{-3} solution of each viologen was sufficient to enable its formation in a highly reproducible manner at the copper electrode.

The formation of the viologen films was achieved by cycling the copper electrode from the potential of -0.20 to 1.00 V vs. SCE at of 1 mV s^{-1}. For comparison, the copper was cycled under the same conditions in the 0.10 mol dm^{-3} NaCl solution, but in the absence of the viologens. Significant dissolution of the copper was observed in the absence of the viologens. However, considerably lower currents were measured in the presence of the viologens, indicating a reduction in the rate of dissolution and the formation of a protective film. Dissolution of copper, and the nucleation of copper oxides, hydroxides and chloride-containing species, was observed in the absence of the viologens. Indeed, these species were identified and confirmed using EDX analysis. However, once these chloride species were initially formed the adsorbed viologens inhibited any further dissolution of the copper substrate.

The formation of the MV and BV-containing films at the copper surface appeared to be independent of the pH of the solution, between pH 2.0 and 9.0, the concentration of the viologen, from 2.0 $\times$ 10^{-3} to 5.0 $\times$ 10^{-3} mol dm^{-3}, and the immersion time in the viologen-

containing solution prior to formation of the film by cycling the copper electrode in the same solution. However, the formation of the ethyl viologen-containing film was dependent on the viologen concentration and protective films were only formed using the higher viologen concentration of 5.0×10^{-3} mol dm^{-3}.

In order to establish the role of the chloride anion in the formation of the viologens at the copper surface, the concentration of the chloride solution was varied from 1.25×10^{-3} mol dm^{-3} to 0.30 mol dm^{-3}. The optimum chloride concentration was determined as 0.10 mol dm^{-3}. At the lower concentrations, the formation of the viologen films was inhibited by the slow formation of the CuCl complex layer. At concentrations higher than 0.10 mol dm^{-3}, the CuCl complex was formed and stable viologen-containing films were formed. Although it is well known that EDX analysis is strictly a qualitative technique, a quantitative study was carried out to determine if the concentration of the BV and the composition of the initial chloride adsorbed layer varied with the applied potential. There was a significant increase in the concentration of chloride-containing species as the copper electrode was polarised to higher potentials in the absence of the viologen, indicating dissolution and corrosion of the copper substrate. However, on addition of the BV to the solution, the concentration of the chloride-containing species was reduced significantly and varied little with the applied potential, indicating a stable and protective film. Moreover, clear evidence for the presence of the BV was obtained using EDX analysis. Carbon was detected in all samples cycled in the BV solution, however no carbon was observed for the copper electrode cycled in the chloride solution.

The protective properties of the viologen films were compared to the well-known corrosion inhibitor benzotriazole (BTA). The BTA offered very good corrosion protection of the copper substrate at pH values ranging from 3.0 to 5.0, the performance of the inhibitor was considerably reduced at pH values below 3.0 and higher than 5.0. In contrast, the viologen-containing films were protective across a much wider pH range, extending from pH 2.0 to 9.0. The formation and deposition of the BV films were inhibited in the presence of sulfates, while in acetate and oxalate solutions the formation of insoluble copper oxalates and acetates at the copper surface, inhibited the deposition of the viologen. Although the BV films deposited from these acetate and oxalate solutions did exhibit some protective properties, it was found that the formation of a CuCl complex layer at the copper surface was critical in forming stable and protective BV films. The BV modified copper showed good stability on cycling to -1.50 V vs.

SCE in 0.10 and 0.15 mol dm^{-3} NaOH. The formation of CuO and Cu_2O oxides were observed, but there was no evidence of the dissolution of the underlying copper on cycling the modified electrode to an upper potential of 0.50 V vs. SCE. Good stability was also observed when the modified electrode was cycled from -1.50 to 1.00 V vs. SCE in the presence of 0.10 mol dm^{-3} NaCl.

In the assessment of the corrosion protection properties of the BV films it appeared that the film offered relatively good corrosion protection to the copper. This was observed using a combination of a spectrophotometric analysis of the copper ion concentration and electrochemical techniques, ranging from open-circuit potential measurements, cyclic voltammetry, polarisation curves, Tafel analyses and electrochemical impedance spectroscopy. The spectrophotometric analysis of the dissolved copper ion concentration showed higher copper ion concentrations for the uncoated copper. However, in the absence of the viologen coating, the deposition of insoluble copper-containing corrosion products limited the release of the copper ions into the solution phase, giving ion concentrations that were lower that the true rate of dissolution of the uncoated copper. Nevertheless, the copper ion concentration was lower for the BV modified copper, indicating good corrosion protection properties. Very good stability was observed on cycling the BV modified copper from -0.20 to 1.00 V vs. SCE in the presence of 0.10 mol dm^{-3} NaCl. There was no evidence of copper dissolution.

The OCP data, recorded at pH values between 3.0 and 7.0, showed that the potential adopted by the BV modified copper was higher than that recorded for the uncoated copper. This potential remained constant, highlighting the stability of the film over time. Moreover, the characteristic decay of the potential to the value adopted by the uncoated electrode, which indicates loss in the protective properties, was not observed for the BV films over a 5 day period. The impedance study showed that the BV films remained stable for periods in excess of 12 h, when polarised to potentials in the vicinity of 0.60 V vs. SCE, highlighting the good protective properties of the BV films deposited at copper.

8.1 Conference Presentations

8.2 Poster Presentations

Ursula Carragher and Carmel Breslin; Studies on the Development of a Suitable Protective Conducting Polymer Coating, using Polypyrrole against the Corrosion of Copper, 216th ECS symposium Vienna, Austria, October 4th-9th 2009.

Ursula Carragher and Carmel Breslin; Development and Analysis of a Suitable Protective Conducting Polymer Coating, using Polypyrrole against the Corrosion of Copper, 61st Annual meeting of the International Society of Electrochemistry (ISE), Nice, France, September 26th-October 1st 2010.

Ursula Carragher and Carmel Breslin; Inhibition of Copper corrosion using Conducting Polymer Coatings, 220th ECS Meeting and Electrochemical Energy Summit, Boston Massachusetts, October 9th-14th 2011.

8.3 Oral Presentations

Ursula Carragher and Carmel Breslin; Advancements in and Analysis of a Suitable Conducting Polymer Coating, using Polypyrrole against the Corrosion of Copper. Eirlec' 11 Electrochemistry- The Future, Dunraven Arms hotel, Adare, Co. Limerick, May 16th-18th 2011.

Ursula Carragher and Carmel Breslin; Corrosion Protection of Copper using a suitable Protective Conducting Polymer Coating, 220th ECS Meeting and Electrochemical Energy Summit, Boston Massachusetts, October 9th-14th 2011.

References

[1] A. M. Fenelon and C. B. Breslin, "The Electrochemical Synthesis of Polypyrrole at a Copper Electrode: Corrosion Protection Properties," *Electrochimica Acta*, vol. 47, no. 28, pp. 4467 – 4476, 2002.

[2] R. Babic and M. Metikovs-Hukovic, "Spectroelectrochemical Studies of Protective Surface Films Against Copper Corrosion," *Thin Solid Films*, vol. 359, no. 1, pp. 88–94, 2000.

[3] M. Desai, S. Rana, and M. Gandhi, "Corrosion Inhibitors for Copper," *Anti-Corrosion Methods and Materials*, vol. 18, no. 2, pp. 19 – 23, 1971.

[4] J. Ambrose, R. Barradas, and D. Shoesmith, "Investigations of Copper in Aqueous Alkaline Solutions by Cyclic Voltammetry," *Journal of Electroanalytical Chemistry and Interfacial Electrochemistry*, vol. 47, no. 1, pp. 47 – 64, 1973.

[5] S. Awad, K. Kamel, Z. A. El-Hadi, and H. Bayumi, "Mechanism of Anodic Dissolution of Copper in Aqueous Acidified Solutions of Different Anions," *Journal of Electroanalytical Chemistry and Interfacial Electrochemistry*, vol. 199, no. 2, pp. 341 – 350, 1986.

[6] L. Abrantes, L. Araujo, and M. Levi, "Voltammetric Studies on Copper Deposition/Dissolution Reactions in Aqueous Chloride Solutions," *Minerals Engineering*, vol. 8, no. 12, pp. 1467 – 1475, 1995.

[7] A. Al-Hinai and K. Osseo-Asare, "Corrosion of Copper in BTA Solutions," *Electrochemical and Solid-State Letters*, vol. 6, no. 5, pp. B23–B24, 2003.

[8] M. Al-Abdallah, A. Maayta, M. Al-Qudah, and N. Al-Rawashdeh, "Corrosion Behavior of Copper in Chloride Media," *The Open Corrosion Journal*, vol. 2, pp. 71–76, 2009.

[9] L. Nunez, E. Reguera, F. Corvo, E. Gonzalez, and C. Vazquez, "Corrosion of Copper in Seawater and its Aerosols in a Tropical Island," *Corrosion Science*, vol. 47, no. 2, pp. 461 – 484, 2005.

[10] E. M. Sherif and S.-M. Park, "Inhibition of Copper Corrosion in 3.0 % NaCl Solution by N-Phenyl-1,4-phenylenediamine," *Journal of the Electrochemical Society*, vol. 152, pp. B428–B433, 2005.

[11] A. Shaban, E. Klman, J. Telegdi, G. Plinkas, and G. Dora, "Corrosion and Inhibition of Copper in Different Electrolyte Solutions," *Applied Physics A: Materials Science and Processing*, vol. 66, pp. 545–549, 1998.

[12] R. Ansari Khalkhali, "Electrochemical Synthesis and Characterisation of Electroactive Conducting Polypyrrole Polymers," *Russian Journal of Electrochemistry*, vol. 41, no. 9, pp. 950–955, 2004.

[13] T. Patois, B. Lakard, S. Monney, X. Roizard, and P. Fievet, "Characterisation of the Surface Properties of Polypyrrole Films: Influence of Electrodeposition Parameters," *Synthetic Metals*, vol. 161, pp. 2498 – 2505, 2011.

[14] M. Sharifirad, A. Omrani, A. Rostami, and M. Khoshroo, "Electrodeposition and Characterisation of Polypyrrole Films on Copper," *Journal of Electroanalytical Chemistry*, vol. 645, no. 2, pp. 149–158, 2010.

[15] H. Arami, M. Mazloumi, R. Khalifehzadeh, S. H. Emami, and S. Sadrnezhaad, "Polypyrrole/Multiwall Carbon Nanotube Nanocomposites Electropolymerised on Copper Substrate," *Materials Letters*, vol. 61, no. 22, pp. 4412 – 4415, 2007.

[16] J. Wang, Y. Xu, X. Sun, S. Mao, and F. Xiao, "Polypyrrole Films Electrochemically Doped with Dodecylbenzene sulfonate for Copper Protection," *Journal of the Electrochemical Society*, vol. 154, no. 8, pp. C445–C450, 2007.

[17] C. Bird and A. Kuhn, "Electrochemistry of the Viologens," *Chemical Society Review*, vol. 10, no. 1, pp. 49–82, 1981.

[18] S. Asavapiriyanont, G. Chandler, G. Gunawardena, and D. Pletcher, "The Electrodeposition of Polypyrrole Films from Aqueous Solutions," *Journal of Electroanalytical Chemistry and Interfacial Electrochemistry*, vol. 177, pp. 229 – 244, 1984.

[19] A. M. Fenelon and C. B. Breslin, "The Electropolymerisation of Pyrrole at a CuNi Electrode: Corrosion Protection Properties," *Corrosion Science*, vol. 45, no. 12, pp. 2837 – 2850, 2003.

[20] Y. Geng, M. Y. Liu, J. Li, X. M. Shi, and J. K. Kim, "Effects of Surfactant Treatment on Mechanical and Electrical Properties of CNT/Epoxy Nanocomposites," *Composites Part A: Applied Science and Manufacturing*, vol. 39, no. 12, pp. 1876–1883, 2008.

[21] B. R. Priya and H. J. Byrne, "Investigation of Sodium Dodecyl Benzene Sulfonate Assisted Dispersion and Debundling of Single-Wall Carbon Nanotubes," *Journal of Physical Chemistry*, vol. 112, pp. 332–337, 2008.

[22] R. Aitout, L. Makhloufi, and B. Saidani, "Kinetics of Copper Electrodeposition onto Polypyrrole Films Previously Synthesised onto Iron in Oxalic Aqueous Solution. Application to Electrocatalysis," *Thin Solid Films*, vol. 515, no. 4, pp. 1992 – 1997, 2006.

[23] A. H. El-Shazly and H. A. Al-Turaif, "Investigation for the Corrosion Resistance of the Galvanic Coupling of Steel with Polypyrrole Coated Galvanized Steel," *Canadian Journal on Chemical Engineering and Technology*, vol. 2, no. 1, pp. 105–119, 2011.

[24] C. Ferreira, S. Aeiyach, J. Aaron, and P. Lacaze, "Electrosynthesis of Strongly Adherent Polypyrrole Coatings on Iron and Mild Steel in Aqueous Media," *Electrochimica Acta*, vol. 41, pp. 1801 – 1809, 1996.

[25] D. Tallman, G. Bierwagen, and Y. Pae, "Conducting Polymers and Corrosion: Part 2 Polyaniline on Aluminum Alloys," *Corrosion*, vol. 56, no. 04, pp. 401–410, 2000.

[26] A. S. Liu, M. C. Bezerra, and L. Y. Cho, "Electrodeposition of Polypyrrole Films on Aluminum Surfaces from a p-Toluene Sulfonic Acid Medium," *Materials Research*, vol. 12, no. 4, pp. 503–507, 2009.

[27] S. S. A. E. Rehim, M. A. Amin, S. Moussa, and A. S. Ellithy, "The Corrosion Inhibition of Aluminum and its Copper Alloys in 1.0 M H_2SO_4 Solution using Linear-Sodium Dodecyl Benzene Sulfonate as Inhibitor," *Materials Chemistry and Physics*, vol. 112, no. 3, pp. 898 – 906, 2008.

[28] D. Tallman, G. Spinks, A. Dominis, and G. Wallace, "Electroactive Conducting Polymers for Corrosion Control," *Journal of Solid State Electrochemistry*, vol. 6, pp. 73–84, 2001.

[29] M. Kendig, M. Hon, and L. Warren, "'Smart' Corrosion Inhibiting Coatings," *Progress in Organic Coatings*, vol. 47, pp. 183 – 189, 2003.

[30] J. N. Barisci, T. W. Lewis, G. M. Spinks, C. O. Too, and G. G. Wallace, "Conducting Polymers as a Basis for Responsive Materials Systems," *Journal of Intelligent Material Systems and Structures*, vol. 9, no. 9, pp. 723–731, 1998.

[31] F. Mansfeld, *Corrosion Mechanisms (Hardback)*, F. Mansfeld and H. Heinemann, Eds. CRC (Dekker), 1987, vol. 28.

[32] Y. Feng, K. Tan, A. Hsieh, W. Teo, and K. Siow, "Corrosion Mechanisms and Products of Copper in Aqueous Solutions at Various pH Values," *Corrosion*, vol. 53, no. 5, 1997.

[33] J. Galvele, R. Torresi, and R. Carranza, "Passivity Breakdown, its Relation to Pitting and Stress-Corrosion-Cracking Processes," *Corrosion Science*, vol. 31, pp. 563 – 571, 1990.

[34] S. Mahmoud, "Electrochemical Studies of Pitting Corrosion of Cu-Fe Alloy in Sodium Chloride Solutions," *Journal of Alloys and Compounds*, vol. 457, pp. 587 – 592, 2008.

[35] C. A. C. Sequeira, *Copper and Copper Alloys*. John Wiley and Sons, Inc., 2011, pp. 757–785.

[36] B. D. Craig, *Fundamental Aspects of Corrosion Films in Corrosion Science*, B. D. Craig, Ed. Springer, 1991.

[37] F. Corvo, J. Minotas, J. Delgado, and C. Arroyave, "Changes in Atmospheric Corrosion Rate Caused by Chloride Ions Depending on Rain Regime," *Corrosion Science*, vol. 47, no. 4, pp. 883 – 892, 2005.

[38] N. Allam, A. Nazeer, and E. Ashour, "A Review of the Effects of Benzotriazole on the Corrosion of Copper and Copper Alloys in Clean and Polluted Environments," *Journal of Applied Electrochemistry*, vol. 39, pp. 961–969, 2009.

[39] A. J. Bard, M. Stratmann, and G. S. Frankel, *Corrosion and Oxide Films*, M. Stratmann and G. S. Frankel, Eds. Wiley, VCH, 2003.

[40] A. Bard and L. Faulkner, *Electrochemical Methods: Fundamentals and Applications*, D. Harris, E. Swain, C. Robey, and E. Aiello, Eds. Wiley New York, 1980, vol. 2.

[41] A. J. Bard and M. Stratmann, *Thermodynamics and Electrified Interfaces*, E. Gileadi and M. Urbakah, Eds. Wiley, VCH, 2007.

[42] A. Hillier, S. Kim, and A. Bard, "Measurement of Double-Layer Forces at the Electrode/Electrolyte Interface using the Atomic Force Microscope: Potential and Anion Dependent Interactions," *The Journal of Physical Chemistry*, vol. 100, no. 48, pp. 18 808–18 817, 1996.

[43] A. J. Bard and M. Stratmann, *Interfacial Kinetics and Mass Transport*, E. Calvo, Ed. Wiley-VCH, 2003.

[44] N. Prez, *Electrochemistry and Corrosion Science*, N. Prez, Ed. Springer, 2004.

[45] Z. Ahmad, *Principles of Corrosion Engineering and Corrosion Control*, Z. Ahmad, Ed. Butterworth-Heinemann, 2006.

[46] C. M. A. Brett and A. M. Brett, *Electrochemistry: Principles, Methods, and Applications*. Oxford University Press, 1993.

[47] O. Barcia, O. Mattos, N. Pafobare, and B. Tribollet, "Anodic Dissolution of Metals Under Mass Transport Control," *Electrochimica Acta*, vol. 41, no. 7-8, pp. 1385 – 1391, 1996.

[48] J. Bockris and M. Enyo, "Mechanism of Electrodeposition and Dissolution Processes of Copper in Aqueous Solutions," *Transactions of the Faraday Society*, vol. 58, pp. 1187–1202, 1962.

[49] J. Galvele, "Tafel's Law in Pitting Corrosion and Crevice Corrosion Susceptibility," *Corrosion Science*, vol. 47, no. 12, pp. 3053 – 3067, 2005.

[50] L. Lu and X.-g. Li, "Corrosion Products of Reverse Crevice Corrosion of Copper," *International Journal of Minerals, Metallurgy, and Materials*, vol. 18, pp. 320–324, 2011.

[51] A. E. Warraky, H. E. Shayeb, and E. Sherif, "Pitting Corrosion of Copper in Chloride Solutions," *Anti-Corrosion Methods and Materials*, vol. 51, no. 1, pp. 52 – 61, 2004.

[52] D. A. Lytle, D. Williams, and C. White, "A simple Approach to Assessing Copper Pitting Corrosion Tendencies and Developing Control Strategies," *Journal of Water Supply: Research and Technology*, vol. 61, no. 3, pp. 164–175, 2012.

[53] S.-H. Lee, J.-G. Kim, and J.-Y. Koo, "Investigation of Pitting Corrosion of a Copper Tube in a Heating System," *Engineering Failure Analysis*, vol. 17, no. 6, pp. 1424 – 1435, 2010.

[54] T. Burleigh, E. Ludwiczak, and R. Petri, "Intergranular Corrosion of an Aluminum-Magnesium-Silicon-Copper Alloy," *Corrosion*, vol. 51, no. 1, pp. 50–56, 1995.

[55] A. M. Abdullah, F. M. Al-Kharafi, and B. G. Ateya, "Intergranular Corrosion of Copper in the Presence of Benzotriazole," *Scripta Materialia*, vol. 54, no. 9, pp. 1673 – 1677, 2006.

[56] R. Baboian, *Corrosion Tests and Standards: Application and Interpretation*. Astm International, 2005, vol. 20.

[57] G. Bianchi and J. Galvele, "Embrittlement of Copper by the Surface Mobility Mechanism," *Corrosion Science*, vol. 27, no. 6, pp. 631 – 635, 1987.

[58] J. R. Davis, *Copper and Copper Alloys*, J. R. Davis, Ed. Asm International, 2001.

[59] W. Huijbregts, "Effect Of Copper and Copper Oxide on Corrosion of Bolier Steel," *Mitteilungen der V.G.B.*, vol. 51, no. 3, pp. 229–235, 1971.

[60] A. El-Meligi, "Corrosion Behaviours of Copper Alloy in Solutions Containing Na_2SO_4 and NaCl with Different Concentrations," *Journal of Materials Sciences and Technology*, vol. 18, no. 06, pp. 549–551, 2002.

[61] S. Guy, C. Broadbent, G. Lawson, and J. Jackson, "Cupric Chloride Leaching of a Complex Copper/Zinc/Lead Ore," *Hydrometallurgy*, vol. 10, no. 2, pp. 243–255, 1983.

[62] Q. Luo, R. Mackay, and S. Babu, "Copper Dissolution in Aqueous Ammonia-Containing Media During Chemical Mechanical Polishing," *Chemistry of Materials*, vol. 9, no. 10, pp. 2101–2106, 1997.

[63] F. Habashi, "Kinetics and Mechanism of Copper Dissolution in Aqueous Ammonia," *Berichte der Bunsengesellschaft für Physikalische Chemie*, vol. 67, no. 4, pp. 402–406, 1963.

[64] S. L. Marchiano, C. I. Elsner, and A. J. Arvia, "The Anodic Formation and Cathodic Reduction of Cuprous Oxide Films on Copper in Sodium Hydroxide Solutions," *Journal of Applied Electrochemistry*, vol. 10, pp. 365–377, 1980.

[65] L. D. Burke, M. J. G. Ahern, and T. G. Ryan, "An Investigation of the Anodic Behavior of Copper and its Anodically Produced Oxides in Aqueous Solutions of High pH," *Journal of the Electrochemical Society*, vol. 137, no. 2, pp. 553–561, 1990.

[66] M. Shirkhanzadeh, G. Thompson, and V. Ashworth, "A study of the Initial Stages in Oxidation of Copper in Alkaline Solutions," *Corrosion Science*, vol. 31, pp. 293 – 298, 1990.

[67] H.-H. Strehblow, V. Maurice, and P. Marcus, "Initial and Later stages of Anodic Oxide Formation on Cu, Chemical Aspects, Structure and Electronic Properties," *Electrochimica Acta*, vol. 46, no. 24-25, pp. 3755 – 3766, 2001.

[68] R. Ericsson and T. Sydberger, "Corrosion Products Formed on Copper Exposed to Humid SO_2-Containing Atmospheres," *Materials and Corrosion*, vol. 28, no. 11, pp. 755–757, 1977.

[69] D. Chadwick and T. Hashemi, "Adsorbed Corrosion Inhibitors Studied by Electron Spectroscopy: Benzotriazole on Copper and Copper Alloys," *Corrosion Science*, vol. 18, no. 1, pp. 39 – 51, 1978.

[70] J. Cotton and I. Scholes, "Benzotriazole and Related Compounds as Corrosion Inhibitors for Copper," *British Corrosion Journal*, vol. 2, no. 1, pp. 1–5, 1967.

[71] F. Zucchi, G. Trabanelli, and M. Fonsati, "Tetrazole Derivatives as Corrosion Inhibitors for Copper in Chloride Solutions," *Corrosion Science*, vol. 38, no. 11, pp. 2019 – 2029, 1996.

[72] S. Umoren, "Polymers as Corrosion Inhibitors for Metals in Different Media-A Review," *The Open Corrosion Journal*, vol. 2, pp. 175–188, 2009.

[73] M. Pourbaix, "Applications of Electrochemistry in Corrosion Science and in Practice," *Corrosion Science*, vol. 14, no. 1, pp. 25 – 82, 1974.

[74] D. W. Shoesmith, T. E. Rummery, D. Owen, and W. Lee, "Anodic Oxidation of Copper in Alkaline Solutions," *Journal of the Electrochemical Society*, vol. 123, no. 6, pp. 790–799, 1976.

[75] D. Shoesmith, S. Sunder, M. Bailey, G. Wallace, and F. Stanchell, "Anodic Oxidation of Copper in Alkaline solutions: Nature of the Passivating Film," *Journal of Electroanalytical Chemistry and Interfacial Electrochemistry*, vol. 143, no. 1-2, pp. 153 – 165, 1983.

[76] C.-H. Pyun and S.-M. Park, "In Situ Spectroelectrochemical Studies on Anodic Oxidation of Copper in Alkaline Solution," *Journal of The Electrochemical Society*, vol. 133, no. 10, pp. 2024–2030, 1986.

[77] G. Capobianco, P. Fabris, A. Glisenti, and G. Granozzi, "A study on the Initial Stages of Oxidation of Copper in Alkaline Solution by Electrochemical and XPS Analysis," *Materials Science Forum*, vol. 192, pp. 207–212, 1995.

[78] S. Sathiyanarayanan, S. Manoharan, G. Rajagopal, and K. Balakrishnan, "Characterisation of Passive Films on Copper," *British Corrosion Journal*, vol. 27, no. 1, pp. 72–74, 1992.

[79] L. Abrantes, L. Castillo, C. Norman, and L. Peter, "A photoelectrochemical Study of the Anodic Oxidation of Copper in Alkaline Solution," *Journal of Electroanalytical Chemistry and Interfacial Electrochemistry*, vol. 163, no. 1-2, pp. 209 – 221, 1984.

[80] J. Thomas and A. Tiller, "Formation and Breakdown of Surface Films on Copper in Sodium Hydrogen Carbonate and Sodium Chloride Solutions: Effects of Anion Concentrations," *British Corrosion Journal*, vol. 7, no. 6, pp. 256–262, 1972.

[81] F. J. Cornwell, G. Wildsmith, and P. T. Gilbert, "Pitting Corrosion in Copper Tubes in Cold Water Service," *British Corrosion Journal*, vol. 8, no. 5, pp. 202–209, 1973.

[82] I. Dugdale and J. Cotton, "An Electrochemical Investigation on the Prevention of Staining of Copper by Benzotriazole," *Corrosion Science*, vol. 3, no. 2, pp. 69 – 74, 1963.

[83] A. Modestov, G.-D. Zhou, Y.-P. Wu, T. Notoya, and D. Schweinsberg, "A study of the Electrochemical Formation of Cu(I)-BTA Films on Copper Electrodes and the Mechanism of Copper Corrosion Inhibition in Aqueous Chloride/Benzotriazole Solutions," *Corrosion Science*, vol. 36, no. 11, pp. 1931 – 1946, 1994.

[84] R. Babic, M. Metikos-Hukovic, and M. Loncar, "Impedance and Photoelectrochemical Study of Surface Layers on Cu and CuNi in Acetate Solution Containing Benzotriazole," *Electrochimica Acta*, vol. 44, no. 14, pp. 2413 – 2421, 1999.

[85] D. Tromans and R. hong Sun, "Anodic Polarisation Behavior of Copper in Aqueous Chloride/Benzotriazole Solutions," *Journal of the Electrochemical Society*, vol. 138, no. 11, pp. 3235–3244, 1991.

[86] D. Tromans and J. C. Silva, "Anodic Behavior of Copper in Chloride/Tolytriazole and Chloride/Benzotriazole Solutions," *Corrosion*, vol. 53, no. 1, pp. 16–25, 1997.

[87] G. Hope, D. Schweinsberg, and P. Fredericks, "Application of FT-Raman Spectroscopy to the Study of the Benzotriazole Inhibition of Acid Copper Corrosion," *Spectrochimica Acta Part A: Molecular Spectroscopy*, vol. 50, no. 11, pp. 2019 – 2026, 1994.

[88] E. A. Ashour, S. M. Sayed, and B. G. Ateya, "Inhibiting Effects of Benzotriazole on the Corrosion of α-Al-Bronze in Saline Water," *Journal of Applied Electrochemistry*, vol. 25, no. 2, pp. 137–141, 1995.

[89] S. Sayed, E. Ashour, and B. Ateya, "Inhibitive Effects of Benzotriazole on the Stress Corrosion Cracking of α-Brass in Nitrite Solution," *Corrosion Science*, vol. 36, no. 2, pp. 221–230, 1994.

[90] F. Mansfeld and T. Smith, "Benzotriazole as Corrosion Inhibitor for Copper: Acid NaCl Solutions," *Corrosion*, vol. 29, no. 3, pp. 105–107, 1973.

[91] G. Zhou, H. Shao, and B. Loo, "A study of the Copper Electrode Behavior in Borax Buffer Solutions Containing Chloride Ions and Benzotriazole-type Inhibitors by Voltammetry and the Photocurrent Response Method," *Journal of Electroanalytical Chemistry*, vol. 421, no. 1, pp. 129–135, 1997.

[92] N. Bellakhal and M. Dachraoui, "Study of the Benzotriazole Efficiency as a Corrosion Inhibitor for Copper in Humid Air Plasma," *Materials Chemistry and Physics*, vol. 85, no. 2, pp. 366–369, 2004.

[93] G. Cicileo, B. Rosales, F. Varela, and J. Vilche, "Comparative Study of Organic Inhibitors of Copper Corrosion," *Corrosion Science*, vol. 41, no. 7, pp. 1359 – 1375, 1999.

[94] G. K. Gomma, "Effect of Azole Compounds on Corrosion of Copper in Acid Medium," *Materials Chemistry and Physics*, vol. 56, no. 1, pp. 27 – 34, 1998.

[95] R. Subramanian and V. Lakshminarayanan, "Effect of Adsorption of Some Azoles on Copper Passivation in Alkaline Medium," *Corrosion Science*, vol. 44, no. 3, pp. 535 – 554, 2002.

[96] M. Metikos-Hukovic, R. Babic, Z. Petrovic, and D. Posavec, "Copper Protection by a Self-Assembled Monolayer of Alkanethiol," *Journal of the Electrochemical Society*, vol. 154, no. 2, pp. C138–C143, 2007.

[97] A. Guenbour, A. Kacemi, and A. Benbachir, "Corrosion Protection of Copper by Polyaminophenol Films," *Progress in Organic Coatings*, vol. 39, no. 2, pp. 151–155, 2000.

[98] R. Zhang, W. Lin, K.-S. Moon, Q. Liang, and C. Wong, "Highly Reliable Copper-Based Conductive Adhesives Using an Amine Curing Agent for in Situ Oxidation/Corrosion Prevention," *Components, Packaging and Manufacturing Technology, IEEE Transactions*, vol. 1, no. 1, pp. 25 –32, 2011.

[99] D. Taneichi, R. Haneda, and K. Aramaki, "A Novel Modification of an Alkanethiol Self-Assembled Monolayer with Alkylisocyanates to Prepare Protective Films Against Copper Corrosion," *Corrosion Science*, vol. 43, no. 8, pp. 1589–1600, 2001.

[100] V. Singh and R. Singh, "Corrosion and Inhibition Studies of Copper in Aqueous Solutions of Formic Acid and Acetic Acid," *Corrosion Science*, vol. 37, no. 9, pp. 1399–1410, 1995.

[101] A. Patel, N. Patel, and J. Vora, "2-Mercaptothiazoline as Corrosion Inhibitor for Copper in Acidic Media," *Corrosion Science*, vol. 14, no. 3, pp. 233 – 237, 1974.

[102] V. V. Walatka, M. M. Labes, and J. H. Perlstein, "Polysulfur Nitride-a One-Dimensional Chain with a Metallic Ground State," *Physical Review Letters*, vol. 31, no. 18, pp. 1139–1142, 1973.

[103] H. Shirakawa, E. J. Louis, A. G. MacDiarmid, C. K. Chiang, and A. J. Heeger, "Synthesis of Electrically Conducting Organic Polymers: Halogen Derivatives of Polyacetylene," *Journal of the Chemical Society, Chemical Commmunications*, pp. 578–580, 1977.

[104] J.-M. Pernaut and J. R. Reynolds, "Use of Conducting Electroactive Polymers for Drug Delivery and Sensing of Bioactive Molecules. A Redox Chemistry Approach," *The Journal of Physical Chemistry B*, vol. 104, no. 17, pp. 4080–4090, 2000.

[105] A. Malinauskas, J. Malinauskiene, and A. Ramanavičius, "Conducting Polymer-Based Nanostructurised Materials: Electrochemical Aspects," *Nanotechnology*, vol. 16, pp. R51–R62, 2005.

[106] M. R. Abidian, D.-H. Kim, and D. C. Martin, "Conducting-Polymer Nanotubes for Controlled Drug Release," *Advanced Materials*, vol. 18, no. 4, pp. 405–409, 2006.

[107] N. K. Guimard, N. Gomez, and C. E. Schmidt, "Conducting Polymers in Biomedical Engineering," *Progress in Polymer Science*, vol. 32, no. 8, pp. 876 – 921, 2007.

[108] J. L. Bredas and G. B. Street, "Polarons, Bipolarons, and Solitons in Conducting Polymers," *Accounts of Chemical Research*, vol. 18, no. 10, pp. 309–315, 1985.

[109] D. Wise, *Electrical and Optical Polymer Systems*, D. Wise, G. Wnek, D. J. Tarntolo, T. M. Cooper, and J. D. Gresser, Eds. CRC Press, 1998.

[110] L. Alcacer, *Conducting Polymers: Special Applications (Hardback)*, L. Alcacer, Ed. D Reidel Pub Co, 1998.

[111] A. L. Briseno, A. Baca, Q. Zhou, R. Lai, and F. Zhou, "Quantification of Dopant Ions in Polypyrrole Films with Electrochemical ICP-Atomic Emission Spectrometry and Comparison to Electrochemical Quartz Crystal Microbalance Studies," *Analytica Chimica Acta*, vol. 441, no. 1, pp. 123 – 134, 2001.

[112] P. Chandrasekhar, *Conducting Polymers, Fundamentals and Applications: A Practical Approach (Hardback)*, P. Chandrasekhar, Ed. Kluwer Academic publications (Springer), 1999.

[113] S. Machida, S. Miyata, and A. Techagumpuch, "Chemical Synthesis of Highly Electrically Conductive Polypyrrole," *Synthetic Metals*, vol. 31, no. 3, pp. 311–318, 1989.

[114] P. Subramanian, N. B. Clark, L. Spiccia, D. R. MacFarlane, B. Winther-Jensen, and C. Forsyth, "Vapour Phase Polymerisation of Pyrrole Induced by Iron(III) Alkylbenzenesulfonate Salt Oxidising Agents," *Synthetic Metals*, vol. 158, no. 17-18, pp. 704 – 711, 2008.

[115] A. Malinauskas, "Chemical Deposition of Conducting Polymers," *Polymer*, vol. 42, no. 9, pp. 3957–3972, 2001.

[116] J. Petitjean, S. Aeiyach, J. Lacroix, and P. Lacaze, "Ultra-Fast Electropolymerisation of Pyrrole in Aqueous Media on Oxidisable Metals in a One-Step Process," *Journal of Electroanalytical Chemistry*, vol. 478, no. 1, pp. 92–100, 1999.

[117] M. Suarez and R. Compton, "In Situ Atomic Force Microscopy Study of Polypyrrole Synthesis and the Volume Changes Induced by Oxidation and Reduction of the Polymer," *Journal of Electroanalytical Chemistry*, vol. 462, no. 2, pp. 211–221, 1999.

[118] C. Longo, J. Freitas, and M.-A. D. Paoli, "Performance and Stability of TiO_2/Dye Solar Cells Assembled with Flexible Electrodes and a Polymer Electrolyte," *Journal of Photochemistry and Photobiology A: Chemistry*, vol. 159, no. 1, pp. 33 – 39, 2003.

[119] H. S. Nalwa, *Handbook of Advanced Electronic and Photonic Materials and Devices*, H. S. Nalwa, Ed. Academic press (Elsevier), 2001, vol. 8.

[120] A. Dall'olio, Y. Dascola, V. Varacco, V. Bocchi, and C. R. Acad, *Comptes Rendus de l'Academie des Sciences*, vol. C267, pp. 433–435, 1968.

[121] A. Diaz and J. Castillo, "A Polymer Electrode with Variable Conductivity: Polypyrrole," *Journal of the Chemical Society, Chemical Communications*, no. 9, pp. 397–398, 1980.

[122] S. K. Ghosh, *Functional Coatings and Microencapsulation: A General Perspective*. Wiley-VCH Verlag GmbH & Co. KGaA, 2006, pp. 1–28.

[123] A. Mohammadi, M.-A. Hasan, B. Liedberg, I. Lundstrm, and W. Salaneck, "Chemical Vapour Deposition (CVD) of Conducting Polymers: Polypyrrole," *Synthetic Metals*, vol. 14, no. 3, pp. 189 – 197, 1986.

[124] B. Winther-Jensen, J. Chen, K. West, and G. Wallace, "Vapor Phase Polymerisation of Pyrrole and Thiophene Using Iron(III) Sulfonates as Oxidising Agents," *Macromolecules*, vol. 37, no. 16, pp. 5930–5935, 2004.

[125] C. Baker and J. Reynolds, "A Quartz Microbalance Study of the Electrosynthesis of Polypyrrole," *Journal of Electroanalytical Chemistry and Interfacial Electrochemistry*, vol. 251, no. 2, pp. 307–322, 1988.

[126] S. Sadki, P. Schottland, N. Brodie, and G. Sabouraud, "The Mechanisms of Pyrrole Electropolymerisation," *Chemical Society Review*, vol. 29, no. 5, pp. 283–293, 2000.

[127] M. Pournaghi-Azar and R. Ojani, "Preparation of Polypyrrole-Coated Platinum Modified Electrode in Chloroform in the Presence of Various Supporting Electrolytes and its use for the Catalytic Oxidation of Hydroquinone in Aqueous and Chloroform Solutions," *Talanta*, vol. 42, no. 4, pp. 657 – 662, 1995.

[128] E. W. Jager, E. Smela, O. Ingans, and I. Lundstrm, "Polypyrrole Micro Actuators," *Synthetic Metals*, vol. 102, no. 1, pp. 1309 – 1310, 1999.

[129] G. Cheng, J. Zhao, Y. Tu, P. He, and Y. Fang, "A Sensitive DNA Electrochemical Biosensor Based on Magnetite with a Glassy Carbon Electrode Modified by Muti-Walled Carbon Manotubes in Polypyrrole," *Analytica Chimica Acta*, vol. 533, no. 1, pp. 11 – 16, 2005.

[130] P. Mavinakuli, S. Wei, Q. Wang, A. B. Karki, S. Dhage, Z. Wang, D. P. Young, and Z. Guo, "Polypyrrole/Silicon Carbide Nanocomposites with Tunable Electrical Conductivity," *The Journal of Physical Chemistry C*, vol. 114, no. 9, pp. 3874–3882, 2010.

[131] L. Tian, Y. Qi, and B. Wang, "Electrochemical Preparation and Structural Characterisation of Platinum Thin Film on a Polypyrrole Film Modified ITO Electrode," *Journal of Colloid and Interface Science*, vol. 333, no. 1, pp. 249 – 253, 2009.

[132] A. A. A. Almario and R. L. T. Caceres, "Study of Kinetic Formation and the Electrochemical Behaviour of Polypyrrole Films," *Journal of the Chilean Chemical Society*, vol. 54, no. 1, pp. 14–19, 2009.

[133] X. Li, Y. Jiao, and S. Li, "The Syntheses, Properties and Application of New Conducting Polymers," *European Polymer Journal*, vol. 27, no. 12, pp. 1345 – 1351, 1991.

[134] R. Stankovic, O. Pavlovic, M. Vojnovic, and S. Jovanovic, "The Effects of Preparation Conditions on the Properties of Electrochemically Synthesized Thick Films of Polypyrrole," *European Polymer Journal*, vol. 30, no. 3, pp. 385–393, 1994.

[135] F. Vork and L. Janssen, "Structural Effects in Polypyrrole Synthesis," *Electrochimica Acta*, vol. 33, no. 11, pp. 1513 – 1517, 1988.

[136] F. Beck and P. Hulser, "Electrodeposition of Polypyrrole on Aluminium From Non-Aqueous Solutions," *Journal of Electroanalytical Chemistry and Interfacial Electrochemistry*, vol. 280, no. 1, pp. 159 – 166, 1990.

[137] K. Vidanapathirana, M. Careem, S. Skaarup, and K. West, "Ion Movement in Polypyrrole/Dodecylbenzene Sulfonate Films in Aqueous and Non-Aqueous Electrolytes," *Solid State Ionics*, vol. 154-155, pp. 331 – 335, 2002.

[138] L. A. Samuelson and M. A. Druy, "Kinetics of the Degradation of Electrical Conductivity in Polypyrrole," *Macromolecules*, vol. 19, no. 3, pp. 824–828, 1986.

[139] D. Kaplin and S. Qutubuddin, "Electrochemically Synthesized Polypyrrole Films: Effects of Polymerisation Potential and Electrolyte Type," *Polymer*, vol. 36, no. 6, pp. 1275–1286, 1995.

[140] A. Kassim, Z. Basar, and H. Mahmud, "Effects of Preparation Temperature on the Conductivity of Polypyrrole Conducting Polymer," *Indian Academy of Sciences*, vol. 114, no. 2, pp. 155–162, 2002.

[141] F. Beck, P. Braun, and M. Oberst, "Organic Electrochemistry in the Solid State-Overoxidation of Polypyrrole," *Berichte der Bunsengesellschaft/Physical Chemistry Chemical Physics*, vol. 91, no. 9, pp. 967–974, 1987.

[142] A. Diaz, J. I. Castillo, J. Logan, and W.-Y. Lee, "Electrochemistry of Conducting Polypyrrole Films," *Journal of Electroanalytical Chemistry and Interfacial Electrochemistry*, vol. 129, no. 1-2, pp. 115 – 132, 1981.

[143] R. Ansari, "Polypyrrole Conducting Electroactive Polymers: Synthesis and Stability Studies," *E-Journal of Chemistry*, vol. 3, no. 13, pp. 186–201, 2006.

[144] C. C. Bof Bufon, T. Heinzel, P. Espindola, and J. Heinze, "Influence of the Polymerisation Potential on the Transport Properties of Polypyrrole Films," *The Journal of Physical Chemistry B*, vol. 114, no. 2, pp. 714–718, 2010.

[145] T. Hernandez-Perez, M. Morales, N. Batina, and M. Salmon, "Effect of the Electrosynthesis Method on the Surface Morphology of the Polypyrrole Film an Atomic Force Microscopy Study," *Journal of the Electrochemical Society*, vol. 148, no. 5, pp. C369–C375, 2001.

[146] M. Zhou and J. Heinze, "Electropolymerisation of Pyrrole and Electrochemical Study of Polypyrrole: Evidence for Structural Diversity of Polypyrrole," *Electrochimica Acta*, vol. 44, no. 11, pp. 1733 – 1748, 1999.

[147] R. Ansari Khalkhali, W. Price, and G. Wallace, "Quartz Crystal Microbalance Studies of the Effect of Solution Temperature on the Ion-Exchange Properties of Polypyrrole Conducting Electroactive Polymers," *Reactive and Functional Polymers*, vol. 56, no. 3, pp. 141–146, 2003.

[148] L. H. Ningping Chen, "A Study on Polypyrrole-Polystyrene Sulfonic Acid Microspheres-a Proton Electrolyte," *European Polymer Journal*, vol. 37, pp. 1027–1035, 2001.

[149] H. Ge and G. Wallace, "Ion Exchange Properties of Polypyrrole," *Reactive Polymers*, vol. 18, no. 2, pp. 133–140, 1992.

[150] T. Skotheim, *Handbook of Conducting Polymers*, 3rd ed., T. Skotheim and J. Reynolds, Eds. CRC Press, 1998.

[151] G. Inzelt, *Conducting Polymers: A New Era in Electrochemistry (Hardback)*, F. Scholz, Ed. Springer Verlag, 2008.

[152] A. J. Heeger, "Nobel Lecture: Semi-Conducting and Metallic Polymers: The Fourth Generation of Polymeric Materials," *Review of Modern Physics*, vol. 73, pp. 681–700, Sep 2001.

[153] A. MacDiarmid, "Nobel Lecture: "Synthetic Metals": A Novel Role for Organic Polymers," *Reviews of Modern Physics*, vol. 73, no. 3, pp. 701–712, 2001.

[154] H. Shirakawa, "Nobel Lecture: The Discovery of Polyacetylene Film¯The Dawning of an Era of Conducting Polymers," *Review of Modern Physics*, vol. 73, pp. 713–718, 2001.

[155] P. Zarras, N. Anderson, C. Webber, D. Irvin, J. Irvin, A. Guenthner, and J. Stenger-Smith, "Progress in using Conductive Polymers as Corrosion-Inhibiting Coatings," *Radiation Physics and Chemistry*, vol. 68, no. 3, pp. 387 – 394, 2003.

[156] M. Rohwerder and A. Michalik, "Conducting Polymers for Corrosion Protection: What Makes the Difference Between Failure and Success," *Electrochimica Acta*, vol. 53, no. 3, pp. 1300 – 1313, 2007.

[157] C. Tan and D. Blackwood, "Corrosion Protection by Multilayered Conducting Polymer Coatings," *Corrosion Science*, vol. 45, no. 3, pp. 545 – 557, 2002.

[158] D. R. A. and F. F. Louis, *Polymeric Materials for Corrosion Control: An Overview*, D. R. A. and F. F. Louis, Eds. ACS Publications, 1986, vol. 322.

[159] B. Garcia, A. Lamzoudi, F. Pillier, H. Nguyen, T. Le, and C. Deslouis, "Oxide/Polypyrrole Composite Films for Corrosion Protection of Iron," *Journal of the Electrochemical Society*, vol. 149, no. 12, pp. B560–B566, 2002.

[160] H. Nguyen Thi Le, B. Garcia, C. Deslouis, and Q. Le Xuan, "Corrosion Protection and Conducting Polymers: Polypyrrole Films on Iron," *Electrochimica Acta*, vol. 46, no. 26-27, pp. 4259–4272, 2001.

[161] A. El-Shazly and A. Wazzan, "Using Polypyrrole Coating for Improving the Corrosion Resistance of Steel Buried in Corrosive Mediums," *International Journal of the Electrochemical Society*, vol. 7, pp. 1946 – 1957, 2012.

[162] I. Dehri, "Impedance Measurements of Polyester-Coated Galvanised Mild Steel in 10xAcid Rainwater After an Accelerated Wet-Dry Test," *Turkish Journal of Chemistry*, vol. 24, no. 3, pp. 239–246, 2000.

[163] P. Herrasti, F. Recio, P. Ocón, and E. Fatás, "Effect of the Polymer Layers and Bilayers on the Corrosion Behaviour of Mild Steel: Comparison with Polymers Containing Zn Microparticle," *Progress in Organic Coatings*, vol. 54, no. 4, pp. 285–291, 2005.

[164] S. Biallozor and A. Kupniewska, "Conducting Polymers Electrodeposited on Active Metals," *Synthetic Metals*, vol. 155, no. 3, pp. 443 – 449, 2005.

[165] A. Alfantazi, T. Ahmed, and D. Tromans, "Corrosion Behavior of Copper Alloys in Chloride Media," *Materials and Design*, vol. 30, no. 7, pp. 2425 – 2430, 2009.

[166] V. Haase and F. Beck, "Electrodeposition of N-Substituted Polypyrroles on Iron and the CIPL Strategy," *Electrochimica Acta*, vol. 39, no. 8-9, pp. 1195–1205, 1994.

[167] F. Beck, R. Michaelis, F. Schloten, and B. Zinger, "Filmforming Electropolymerisation of Pyrrole on Iron in Aqueous Oxalic Acid," *Electrochimica Acta*, vol. 39, no. 2, pp. 229–234, 1994.

[168] M. Schirmeisen and F. Beck, "Electrocoating of Iron and other Metals with Polypyrrole," *Journal of Applied Electrochemistry*, vol. 19, no. 3, pp. 401–409, 1989.

[169] B. Duran and G. Bereket, "Cyclic Voltammetric Synthesis of Poly(N-methyl Pyrrole) on Copper and Effects of Polymerisation Parameters on Corrosion Performance," *Industrial and Engineering Chemistry Research*, vol. 51, no. 14, pp. 5246–5255, 2012.

[170] M. Redondo, E. S. de la Blanca, M. Garcia, and M. Gonzalez-Tejera, "Poly(N-methylpyrrole) Electrodeposited on Copper: Corrosion Protection Properties," *Progress in Organic Coatings*, vol. 65, no. 3, pp. 386 – 391, 2009.

[171] M. M. Gvozdenovic, B. Z. Jugovic, J. S. Stevanovic, B. Grgur, T. L. Triovic, and Z. S. Jugovic, "Electrochemical Synthesis and Corrosion Behavior of Polyaniline-Benzoate Coating on Copper," *Synthetic Metals*, vol. 161, pp. 1313 – 1318, 2011.

[172] V. Shinde, S. Sainkar, and P. Patil, "Corrosion Protective Poly(o-toluidine) Coatings on Copper," *Corrosion Science*, vol. 47, no. 6, pp. 1352 – 1369, 2004.

[173] A. Cascalheira, S. Aeiyach, P. Lacaze, and L. Abrantes, "Electrochemical Synthesis and Redox Behaviour of Polypyrrole Coatings on Copper in Salicylate Aqueous Solution," *Electrochimica Acta*, vol. 48, no. 17, pp. 2523 – 2529, 2003.

[174] D. Patil and P. P. Patil, "Electrodeposition of Poly(o-toluidine) on Brass from Aqueous Salicylate Solution and its Corrosion Protection Performance," *Journal of Applied Polymer Science*, vol. 118, no. 4, pp. 2084–2091, 2010.

[175] P. Pawar, A. Gaikwad, and P. Patil, "Corrosion Protection Aspects of Electrochemically Synthesized Poly(o-anisidine-co-o-toluidine) Coatings on Copper," *Electrochimica Acta*, vol. 52, no. 19, pp. 5958 – 5967, 2007.

[176] F. M. Menger, "The Structure of Micelles," *Accounts of Chemical Research*, vol. 12, no. 4, pp. 111–117, 1979.

[177] B. L. Bales, F. H. Quina, P. M. Nassar, J. B., and S. Bonilha, "Growth of Sodium Dodecyl Sulfate Micelles with Detergent Concentration," *Journal of Physical Chemistry*, vol. 99, no. 46, pp. 17 028–17 031, 1995.

[178] X. Zhang, J. K. Jackson, and H. M. Burt, "Determination of Surfactant Critical Micelle Concentration by a Novel Fluorescence Depolarisation Technique," *Journal of Biochemical and Biophysical Methods*, vol. 31, pp. 145 – 150, 1996.

[179] S. Sitaram, J. Stoffer, and T. O'Keefe, "Application of Conducting Polymers in Corrosion Protection," *Journal of Coatings Technology*, vol. 69, no. 866, pp. 65–69, 1997.

[180] M. Rohwerder, "Intelligent Corrosion Protection by Conducting Polymers," in *ACS symposium series*, vol. 1002. ACS Publications, 2009.

[181] D. Tallman, G. Bierwagen, and Y. Pae, "Conducting Polymers and Corrosion: Polyaniline on Steel," *Corrosion*, vol. 55, no. 8, pp. 73–84, 1999.

[182] P. Camille Lacaze, J. Ghilane, H. Randriamahazaka, and J.-C. Lacroix, *Electroactive Conducting Polymers for the Protection of Metals against Corrosion: from Micro- to Nanostructured Films (Hardback)*, 1st ed. John Wiley and Sons, Ltd, 2010.

[183] U. Rammelt, P. Nguyen, and W. Plieth, "Corrosion Protection by Ultrathin Films of Conducting Polymers," *Electrochimica Acta*, vol. 48, no. 9, pp. 1257 – 1262, 2003.

[184] G. Paliwoda-Porebska, M. Stratmann, M. Rohwerder, K. Potje-Kamloth, Y. Lu, A. Pich, and H.-J. Adler, "On the Development of Polypyrrole Coatings with Self-Healing Properties for Iron Corrosion Protection," *Corrosion Science*, vol. 47, no. 12, pp. 3216 – 3233, 2005.

[185] A. Michalik and M. Rohwerder, "Conducting Polymers for Corrosion Protection: A Critical View," *Journal of Physical Chemistry*, vol. 219, no. 11, pp. 1547–1559, 2005.

[186] K. Arihara, F. Kitamura, K. Nukanobu, T. Ohsaka, and K. Tokuda, "Voltammetric and Spectroscopic Study of the Adsorption of Alkyl Viologens on a HOPG Electrode," *Journal of Electroanalytical Chemistry*, vol. 473, no. 1, pp. 138–144, 1999.

[187] A. Jorio, G. Dresselhaus, and M. Dresselhaus, *Carbon Nanotubes: Advanced Topics in the Synthesis, Structure, Properties and Applications (Hardback)*, A. Jorio, M. S. Dresselhaus, and G. Dresselhaus, Eds. Springer Verlag, 2008, vol. 111.

[188] M. Monthioux, *Introduction to Carbon Nanotubes*. John Wiley and Sons, Ltd, 2011, vol. 1.

[189] S. Iijima, "Helical Microtubules of Graphitic Carbon," *Nature*, vol. 354, no. 6348, pp. 56–58, 1991.

[190] P. M. Ajayan, "Nanotubes from Carbon," *Chemical Review*, vol. 99, no. 7, pp. 1787–1799, 1999.

[191] T. Wu, H. Chang, and Y. Lin, "Synthesis and Characterisation of Conductive Polypyrrole/Multi-Walled Carbon Nanotubes Composites with Improved Solubility and Conductivity," *Composites Science and Technology*, vol. 69, no. 5, pp. 639–644, 2009.

[192] R. Reilly, "Carbon Nanotubes: Potential Benefits and Risks of Nanotechnology in Nuclear Medicine," *Journal of Nuclear Medicine*, vol. 48, no. 7, pp. 1039–1042, 2007.

[193] L. Kavan and L. Dunsch, "Electrochemistry of Carbon Nanotubes," *Carbon Nanotubes*, vol. 111, pp. 567–603, 2008.

[194] R. Andrews, D. Jacques, D. Qian, and T. Rantell, "Multiwall Carbon Nanotubes:Synthesis and Application," *Accounts of Chemical Research*, vol. 35, no. 12, pp. 1008–1017, 2002.

[195] H. Dai, "Carbon Nanotubes: Synthesis, Integration, and Properties," *Accounts of Chemical Research*, vol. 35, no. 12, pp. 1035–1044, 2002.

[196] S. Bandow, A. M. Rao, K. A. Williams, A. Thess, R. E. Smalley, and P. C. Eklund, "Purification of Single-Wall Carbon Nanotubes by Microfiltration," *The Journal of Physical Chemistry B*, vol. 101, no. 44, pp. 8839–8842, 1997.

[197] G.-Z. Fang, J.-X. He, and S. Wang, "Multiwalled Carbon Nanotubes as Sorbent for on-line Coupling of Solid-Phase Extraction to High-Performance Liquid Chromatography for Simultaneous Determination of 10-Sulfonamides in Eggs and Pork," *Journal of Chromatography A*, vol. 1127, no. 1, pp. 12 – 17, 2006.

[198] J. A. Fagan, M. L. Becker, J. Chun, P. Nie, B. J. Bauer, J. R. Simpson, A. Hight-Walker, and E. K. Hobbie, "Centrifugal Length Separation of Carbon Nanotubes," *Langmuir*, vol. 24, no. 24, pp. 13 880–13 889, 2008.

[199] X.-L. Xie, Y.-W. Mai, and X.-P. Zhou, "Dispersion and Alignment of Carbon Nanotubes in Polymer Matrix: A Review," *Materials Science and Engineering: Reports*, vol. 49, no. 4, pp. 89 – 112, 2005.

[200] L. Agui, P. Ynez-Sedeno, and J. M. PingarrOn, "Role of Carbon Nanotubes in Electroanalytical Chemistry: A Review," *Analytica Chimica Acta*, vol. 622, no. 1, pp. 11 – 47, 2008.

[201] M. Deyab, "Effect of Cationic Surfactant and Inorganic Anions on the Electrochemical Behavior of Carbon Steel in Formation Water," *Corrosion Science*, vol. 49, no. 5, pp. 2315–2328, 2007.

[202] M. Malik, M. Hashim, F. Nabi, S. AL-Thabaiti, and Z. Khan, "Anti-Corrosion Ability of Surfactants: A Review," *International Journal of the Electrochemical Science*, vol. 6, pp. 1927–1948, 2011.

[203] H. El-Kashlan, "Kinetic Study of the Effect of Selected Surfactants on Corrosion of Copper," *American Journal of Applied Sciences*, vol. 5, no. 4, pp. 347–354, 2008.

[204] Y. Moroi, *Micelles: Theoretical and Applied Aspects*, Y. Moroi, Ed. Springer, 1941.

[205] F. M. Menger and D. W. Doll, "On the Structure of Micelles," *Journal of the American Chemical Society*, vol. 106, no. 4, pp. 1109–1113, 1984.

[206] G. D. Halsey, "On the Structure of Micelles," *The Journal of Physical Chemistry*, vol. 57, no. 1, pp. 87–89, 1953.

[207] M. Free, "A New Corrosion Inhibition Model for Surfactants that More Closely Accounts for Actual Adsorption than Traditional Models that Assume Physical Coverage is Proportional to Inhibition," *Corrosion Science*, vol. 46, no. 12, pp. 3101–3113, 2004.

[208] N. Smirnova, "Macroscopic Properties and Self-Organisation in Mixed Solutions of Surfactants," *Russian Journal of Physical Chemistry A, Focus on Chemistry*, vol. 80, no. 10, pp. 1608–1616, 2006.

[209] A. M. Khan and S. S. Shah, "Determination of Critical Micelle Concentration (CMC) of Sodium Dodecyl Sulfate (SDS) and the Effect of Low Concentration of Pyrene on its CMC Using Origin Software," *Chemical Society*, vol. 30, no. 2, pp. 186–191, 2007.

[210] R. Zielinski, "Effect of Temperature on Micelle Formation in Aqueous NaBr Solutions of Octyltrimethylammonium Bromide," *Journal of Colloid and Interface Science*, vol. 235, no. 2, pp. 201 – 209, 2001.

[211] M. J. Schick, "Effect of Temperature on the Critical Micelle Concentration of Non Ionic Detergents. Thermodynamics of Micelle formation," *The Journal of Physical Chemistry*, vol. 67, no. 9, pp. 1796–1799, 1963.

[212] E. Ruckenstein. and R. Nagarajan, "Critical Micelle Concentration. A Transition Point for Micellar Size Distribution," *Journal of Physiscal Chemistry*, vol. 79, no. 24, pp. 2622–2626, 1975.

[213] J.-Y. Shin, T. Premkumar, and K. Geckeler, "Dispersion of Single-Walled Carbon Nanotubes by Using Surfactants: Are the Type and Concentration Important," *A European Journal*, vol. 14, no. 20, pp. 6044–6048, 2008.

[214] M. S. Strano, V. C. Moore, M. K. Miller, M. J. Allen, E. H. Haroz, C. Kittrell, R. H. Hauge, and R. Smalley, "The Role of Surfactant Adsorption during Ultrasonication in the Dispersion of Single-Walled Carbon Nanotubes," *Journal of Nanoscience and Nanotechnology*, vol. 1, no. 2, pp. 81–86, 2003.

[215] A. Dominguez, A. Fernandez, N. Gonzalez, E. Iglesias, and L. Montenegro, "Determination of Critical Micelle Concentration of Some Surfactants by Three Techniques," *Journal of Chemical Education*, vol. 74, no. 10, p. 1227, 1997.

[216] L. Vaisman, H. D. Wagner, and G. Marom, "The Role of Surfactants in Dispersion of Carbon Nanotubes," *Advances in Colloid and Interface Science*, vol. 128-130, pp. 37 – 46, 2006.

[217] M. D. Clark, S. Subramanian, and R. Krishnamoorti, "Understanding Surfactant Aided Aqueous Dispersion of Multi-Walled Carbon Nanotubes," *Journal of Colloid and Interface Science*, vol. 354, no. 1, pp. 144 – 151, 2011.

[218] H. Wang, "Dispersing Carbon Nanotubes using Surfactants," *Current Opinion in Colloid; Interface Science*, vol. 14, no. 5, pp. 364 – 371, 2009.

[219] V. C. Moore, M. S. Strano, E. H. Haroz, R. H. Hauge, R. E. Smalley, J. Schmidt, and Y. Talmon, "Individually Suspended Single-Walled Carbon Nanotubes in Various Surfactants," *Nano Letters*, vol. 3, no. 10, pp. 1379–1382, 2003.

[220] V. Datsyuk, P. Landois, J. Fitremann, A. Peigney, A. M. Galibert, B. Soula, and E. Flahaut, "Double-walled Carbon Nanotube Dispersion via Surfactant Substitution," *Journal of Materials Sciences and Technology*, vol. 19, no. 18, pp. 2729–2736, 2009.

[221] J. Yu, N. Grossiord, C. E. Koning, and J. Loos, "Controlling the Dispersion of Multi-wall Carbon Nanotubes in Aqueous Surfactant Solution," *Carbon*, vol. 45, no. 3, pp. 618–623, 2006.

[222] O. Matarredona, H. Rhoads, Z. Li, J. H. Harwell, L. Balzano, and D. E. Resasco, "Dispersion of Single-Walled Carbon Nanotubes in Aqueous Solutions of the Anionic Surfactant NaDDBS," *The Journal of Physical Chemistry B*, vol. 107, no. 48, pp. 13 357–13 367, 2003.

[223] R. Rastogi, R. Kaushal, S. Tripathi, A. L. Sharma, I. Kaur, and L. M. Bharadwaj, "Comparative Study of Carbon Nanotube Dispersion using Surfactants," *Journal of Colloid and Interface Science*, vol. 328, no. 2, pp. 421 – 428, 2008.

[224] P. P. Infelta, "Fluorescence Quenching in Micellar Solutions and its Application to the Determination of Aggregation Numbers," *Chemical Physics Letters*, vol. 61, no. 1, pp. 88 – 91, 1979.

[225] C. Thevenot, B. Grassl, G. Bastiat, and W. Binana, "Aggregation Number and Critical Micellar Concentration of Surfactant Determined by Time-Dependent Static Light Scattering (TDSLS) and Conductivity," *Colloids and Surfaces A: Physicochemical and Engineering Aspects*, vol. 252, pp. 105 – 111, 2005.

[226] N. J. Turro and A. Yekta, "Luminescent Probes for Detergent Solutions. A Simple Procedure for Determination of the Mean Aggregation Number of Micelles," *Journal of the American Chemical Society*, vol. 100, no. 18, pp. 5951–5952, 1978.

[227] P. J. Tummino and A. Gafni, "Determination of the Aggregation Number of Detergent Micelles using Steady-State Fluorescence Quenching," *Biophysical Journal*, vol. 64, no. 5, pp. 1580–1587, 1993.

[228] A. Yekta, B. Xu, J. Duhamel, H. Adiwidjaja, and M. A. Winnik, "Fluorescence Studies of Associating Polymers in Water: Determination of the Chain end Aggregation Number and a Model for the Association Process," *Macromolecules*, vol. 28, no. 4, pp. 956–966, 1995.

[229] M. Maestri, P. P. Infelta, and M. Gratzel, "Kinetics of Fast Light-Induced Redox Processes in Micellar Systems: Intramicellar Electron Transfer," *Journal of Chemical Physics*, vol. 69, no. 4, pp. 1522–1526, 1978.

[230] L. Michaelis and E. Hill, "The Viologen Indicators," *The Journal of General Physiology*, vol. 16, no. 6, pp. 859–873, 1933.

[231] R. Mortimer, "Electrochromic Materials," *Chemical Society Review*, vol. 26, no. 3, pp. 147–156, 1997.

[232] E. Engelman and D. Evans, "Investigation of the Nature of Electrodeposited Neutral Viologens Formed by Reduction of the Dications," *Journal of Electroanalytical Chemistry*, vol. 349, no. 1-2, pp. 141–158, 1993.

[233] P. Hale, L. Boguslavsky, H. Karan, H. Lan, H. Lee, Y. Okamoto, and T. Skotheim, "Investigation of Viologen Derivatives as Electron-transfer Mediators in Amperometric Glucose Sensors," *Analytica Chimica Acta*, vol. 248, no. 1, pp. 155 – 161, 1991.

[234] C. Gomez-Moreno and M. Bes, "Structural Requirements for the Electron Transfer between a Flavoprotein and Viologens," *Biochimica et Biophysica Acta (BBA) - Bioenergetics*, vol. 1187, no. 2, pp. 236 – 240, 1994.

[235] S. Cosnier, B. Galland, and C. Innocent, "New Electropolymerisable Amphiphilic Viologens for the Immobilisation and Electrical Wiring of a Nitrate Reductase," *Journal of Electroanalytical Chemistry*, vol. 433, no. 1, pp. 113–119, 1997.

[236] M. Vidotti and S. I. C. de Torresi, "Nanochromics: Old Materials, New Structures and Architectures for High Performance Devices," *Journal of the Brazilian Society*, vol. 19, no. 7, pp. 1248–1257, 2008.

[237] R. Bromilow, "Paraquat and Sustainable Agriculture," *Pest Management Science*, vol. 60, no. 4, pp. 340–349, 2004.

[238] D. Lee, A. Kafi, S. Park, and Y. Kwon, "Charge Transfer Property of Self-assembled Viologen Derivative by Electrochemical Quartz Crystal Microbalance Response," *Journal of Nanoscience and Nanotechnology*, vol. 6, no. 11, pp. 3657–3660, 2006.

[239] K. Arihara and F. Kitamura, "Adsorption States of Heptyl Viologen on an Au (111) Electrode Surface Studied by Infrared Reflection Absorption Spectroscopy," *Journal of Electroanalytical Chemistry*, vol. 550-551, pp. 149–159, 2003.

[240] M. Jiang, E. Sak, K. Gentz, A. Krupski, and K. Wandelt, "Redox Activity and Structural Transition of Heptyl Viologen Adlayers on Cu(100)," *A Eurppean Journal of Chemical Physics and Physical Chemistry*, vol. 11, no. 7, pp. 1542–1549, 2010.

[241] S. Breuer, D. Pham, S. Huemann, K. Gentz, C. Zoerlein, R. Hunger, K. Wandelt, and P. Broekmann, "Organic Layers at Metal/Electrolyte Interfaces: Molecular Structure and Reactivity of Viologen Monolayers," *New Journal of Physics*, vol. 10, pp. 1–24, 2008.

[242] S. Tsay, J. Tsay, T. Fu, P. Broekmann, T. Sagara, and K. Wandelt, "Molecular Structures of Dicarboxylated Viologens on a Cu (100) Surface During an Ongoing Charge Transfer Reaction," *Physical Chemistry Chemical Physics*, vol. 12, no. 45, pp. 14 950–14 959, 2010.

[243] S. Yuan, F. Xu, E. Kang, and S. Pehkonen, "Modification of Surface-Oxidised Copper Alloy by Coupling of Viologens for Inhibiting Microbiologically Influenced Corrosion," *Journal of the Electrochemical Society*, vol. 154, no. 11, pp. C645–C657, 2007.

[244] J. Ballesteros, E. Chainet, P. Ozil, Y. Meas, and G. Trejo, "Electrodeposition of Copper from Non-Cyanide Alkaline Solution Containing Tartrate," *International Journal Electrochemical Science*, vol. 6, pp. 2632–2651, 2011.

[245] V. Annibaldi, A. Rooney, and C. Breslin, "Corrosion Protection of Copper using Polypyrrole Electrosynthesised from a Salicylate Solution," *Corrosion Science*, vol. 59, no. 4, pp. 179–185, 2011.

[246] E. Garfias-García, M. Romero-Romo, M. Ramírez-Silva, J. Morales, and M. Palomar-Pardavé, "Eletrochemical Nucleation of Polypyrrole onto Different Substrates," *International Journal Electrochemical Science*, vol. 5, pp. 763–773, 2010.

[247] F. Mansfeld, "Electrochemical Impedance Spectroscopy (EIS) as a new tool for Investigation methods of Corrosion Protection," *Electrochimica Acta*, vol. 35, no. 10, pp. 1533–1537, 1990.

[248] G. Li, H. Ma, Y. Jiao, and S. Chen, "An Impedance Investigation of Corrosion Protection of Copper by Self-assembled Monolayers of Alkanethiols in Aqueous Solution," *Journal of the Serbian Chemical Society*, vol. 69, no. 10, pp. 791–805, 2004.

[249] A. Amirudin and D. Thieny, "Application of Electrochemical Impedance Spectroscopy to Study the Degradation of Polymer-Coated Metals," *Progress in Organic Coatings*, vol. 26, no. 1, pp. 1 – 28, 1995.

[250] A. Srivastava and R. Balasubramaniam, "Electrochemical Impedance Spectroscopy Study of Surface Films formed on Copper in Aqueous Environments," *Materials and Corrosion*, vol. 56, no. 9, pp. 611–618, 2005.

[251] F. Mansfeld and M. W. Kendig, "Electrochemical Impedance Spectroscopy of Protective Coatings," *Materials and Corrosion*, vol. 36, no. 11, pp. 473–483, 1985.

[252] J. R. Scully and D. C. Silverman, *Electrochemical Impedance: Analysis and Interpretation*, J. R. Scully and D. C. Silverman, Eds. ASTM International, 1993, no. 1188.

[253] I. Epelboin, M. Keddam, and H. Takenouti, "Use of Impedance Measurements for the Determination of the Instant Rate of Metal Corrosion," *Journal of Applied Electrochemistry*, vol. 2, no. 1, pp. 71–79, 1972.

[254] X. Ren and P. Pickup, "Coupling of Ion and Electron Transport during Impedance Measurements on a Conducting Polymer with similar Ionic and Electronic Conductivities," *Journal Chemical Society, Faraday Transactions*, vol. 89, no. 2, pp. 321–326, 1993.

[255] J. F. Rubinson and Y. P. Kayinamura, "ChemInform Abstract: Charge Transport in Conducting Polymers: Insights from Impedance Spectroscopy," *ChemInform*, vol. 41, no. 14, pp. 2110–2123, 2010.

[256] E. Barsoukov and J. Macdonald, *Impedance Spectroscopy: Theory, Experiment, and Applications (Hardback)*, 2nd ed., E. Barsoukov and J. Macdonald, Eds. John Wiley and Sons, 2005.

[257] B. T. Mark E. Orazem, *Electrochemical Impedance Spectroscopy*, B. T. Mark E. Orazem, Ed. John Wiley and Sons, 2008, vol. 48.

[258] M. Bazzaoui, J. Martins, E. Bazzaoui, L. Martins, and E. Machnikova, "Sweet Aqueous Solution for Electrochemical Synthesis of Polypyrrole part 1B: On copper and its Alloy," *Electrochimica Acta*, vol. 52, no. 11, pp. 3568 – 3581, 2007.

[259] M. Abdulhay and A. Al-Suhybani, "Open-circuit Potential for Copper Electrode in 1 M NaCl Solutions," *Materials Science and Engineering Technology*, vol. 23, no. 11, pp. 407–412, 1992.

[260] M. Amin, "Weight Loss, Polarisation, Electrochemical Impedance Spectroscopy, SEM and EDX Studies of the Corrosion Inhibition of Copper in Aerated NaCl Solutions," *Journal of Applied Electrochemistry*, vol. 36, no. 2, pp. 215–226, 2006.

[261] R. Bandy, "The Simultaneous Determination of Tafel Constants and Corrosion Rates-A New Method," *Corrosion Science*, vol. 20, no. 8-9, pp. 1017 – 1028, 1980.

[262] G. Kear and F. Walsh, "The Characteristics of a True Tafel Slope," *Corrosion and Materials*, vol. 30, no. 6, pp. 51–55, 2005.

[263] G. Rocchini, "The Determination of Tafel Slopes by the Successive Approximation Method," *Corrosion Science*, vol. 37, no. 6, pp. 987–1003, 1995.

[264] K. Keiji Kanazawa, A. Diaz, W. Gill, P. Grant, G. Street, G. Piero Gardini, and J. Kwak, "Polypyrrole: An Electrochemically Synthesised Conducting Organic Polymer," *Synthetic Metals*, vol. 1, no. 3, pp. 329–336, 1980.

[265] S. Yuan, F. Xu, S. Pehkonen, Y. Ting, K. Neoh, and E. Kang, "Grafting of Antibacterial Polymers on Stainless Steel via Surface-Initiated Atom Transfer Radical Polymerisation for Inhibiting Biocorrosion by Desulfovibrio Desulfuricans," *Biotechnology and Bioengineering*, vol. 103, no. 2, pp. 268–281, 2009.

[266] I. Lehr and S. Saidman, "Corrosion Protection of Iron by Polypyrrole Coatings Electrosynthesised from a Surfactant Solution," *Corrosion Science*, vol. 49, no. 5, pp. 2210–2225, 2006.

[267] C. Breslin, A. Fenelon, and K. Conroy, "Surface Engineering: Corrosion Protection using Conducting Polymers," *Materials and Design*, vol. 26, no. 3, pp. 233 – 237, 2005.

[268] M. Raso, M. Gonzalez-Tejera, I. Carrillo, E. S. de la Blanca, M. Garcia, and M. Redondo, "Electrochemical Nucleation and Growth of Poly-N-Methylpyrrole on Copper," *Thin Solid Films*, vol. 519, no. 8, pp. 2387 – 2392, 2011.

[269] T. Raudsepp, "Influence of Dopant Anions on the Electrochemical Properties of Polypyrrole Films," Ph.D. dissertation, University of Tartu, 2010.

[270] D. Cossement, F. Plumier, J. Delhalle, L. Hevesi, and Z. Mekhalif, "Electrochemical Deposition of Polypyrrole Films on Organosilane-modified ITO Substrates," *Synthetic Metals*, vol. 138, no. 3, pp. 529 – 536, 2003.

[271] T. O. L. Sunde, E. Garskaite, B. Otter, H. E. Fossheim, R. Sterli, R. Holmestad, M.-A. Einarsrud, and T. Grande, "Transparent and Conducting ITO Thin Films by Spin Coating of an Aqueous Precursor Solution," *Journal of Materials Chemistry*, vol. 22, pp. 15 740–15 749, 2012.

[272] H. N. Cong, K. E. Abbassi, J. Gautier, and P. Chartier, "Oxygen Reduction on Oxide/Polypyrrole Composite Electrodes: Effect of Doping Anions," *Electrochimica Acta*, vol. 50, no. 6, pp. 1369 – 1376, 2005.

[273] W. Prissanaroon, N. Brack, P. Pigram, and J. Liesegang, "Electropolymerisation of Pyrrole on Copper in Aqueous Media," *Synthetic Metals*, vol. 142, no. 1, pp. 25 – 34, 2004.

[274] R. Verdieck, S. Ksycki, and L. Yntema, "The Deposition Potentials of Cobalt, Nickel, and Copper from Chloride and Bromide Solutions," *Journal of the Electrochemical Society*, vol. 80, no. 1, pp. 41–54, 1941.

[275] M. Antonijevic, S. Alagic, M. Petrovic, M. Radovanovic, and A. Stamenkovic, "The Influence of pH on Electrochemical Behavior of Copper in Presence of Chloride Ions," *International Journal of Electrochemical Science*, vol. 4, pp. 516–524, 2009.

[276] I. DKez-Perez, F. Sanz, and P. Gorostiza, "In Situ Studies of Metal Passive Films," *Current Opinion in Solid State and Materials Science*, vol. 10, no. 3-4, pp. 144–152, 2006.

[277] A. Nasseer and A. Y. Khan, "Electrochemical Impedance Spectroscopic Studies of the Passive Layer on the Surface of Copper as a Function of Potential," *Turkish Journal of Chemistry*, vol. 34, pp. 815–824, 2009.

[278] H. Strehblow and H. Speckmann, "Corrosion and Layer Formation of Passive Copper in Alkaline Solutions," *Materials and Corrosion*, vol. 35, no. 11, pp. 512–519, 1984.

[279] A. Naseer and A. Khan, "Stability Study of Passive Film on Copper Surface as a Function of Anodic Potential," *Turkish Journal of Chemistry*, vol. 35, pp. 225–235, 2011.

[280] C. Bonfiglio, H. Albaya, and O. Cobo, "The kinetics of the Anodic Dissolution of Copper in Acid Chloride Solutions," *Corrosion Science*, vol. 13, no. 10, pp. 717–724, 1973.

[281] F. Crundwell, "The Anodic Dissolution of Copper in Hydrochloric Acid Solutions," *Electrochimica Acta*, vol. 37, no. 15, pp. 2707 – 2714, 1992.

[282] D. Starosvetsky, O. Khaselev, M. Auinat, and Y. Ein-Eli, "Initiation of Copper Dissolution in Sodium Chloride Electrolytes," *Electrochimica Acta*, vol. 51, no. 26, pp. 5660–5668, 2005.

[283] J. Y. Josefowicz, L. Xie, and G. C. Farrington, "Observation of Intermediate Cuprous Chloride Species during the Anodic Dissolution of Copper using Atomic Force Microscopy," *The Journal of Physical Chemistry*, vol. 97, no. 46, pp. 11 995–11 998, 1993.

[284] I. Casella and M. Gatta, "Anodic Electrodeposition of Copper Oxide/Hydroxide Films by Alkaline Solutions Containing Cuprous Cyanide Ions," *Journal of Electroanalytical Chemistry*, vol. 494, no. 1, pp. 12 – 20, 2000.

[285] Y. V. Ingelgem, I. Vandendael, J. Vereecken, and A. Hubin, "Study of Copper Corrosion Products Formed During Localised Corrosion usingFeld Emission Auger Electron Spectroscopy," *Surface and Interface Analysis*, vol. 40, no. 3-4, pp. 273–276, 2008.

[286] P. Herrasti, A. del Rio, and J. Recio, "Electrodeposition of Homogeneous and Adherent Polypyrrole on Copper for Corrosion Protection," *Electrochimica Acta*, vol. 52, no. 23, pp. 6496 – 6501, 2007.

[287] L. Martins dos Santos, J. Lacroix, K. Chane-Ching, A. Adenier, L. Abrantes, and P. Lacaze, "Electrochemical Synthesis of Polypyrrole Films on Copper Electrodes in Acidic and Neutral Aqueous Media," *Journal of Electroanalytical Chemistry*, vol. 587, no. 1, pp. 67–78, 2006.

[288] H. Xie, M. Yan, and Z. Jiang, "Transition of Polypyrrole from Electroactive to Electroinactive State Investigated by use of in situ FTIR Spectroscopy," *Electrochimica Acta*, vol. 42, no. 15, pp. 2361 – 2367, 1996.

[289] A. Toyota, N. Nakashima, and T. Sagara, "UV Visible Transmission Absorption Spectral Study of Au Nanoparticles on a Modified ITO Electrode at Constant Potentials and under Potential Modulation," *Journal of Electroanalytical Chemistry*, vol. 565, no. 2, pp. 335 – 342, 2004.

[290] R. Davidson and T. Turner, "An IR Spectroscopic Study of the Electrochemical Reduction of Polypyrrole Doped with Dodecylsulfate Anion," *Synthetic Metals*, vol. 72, no. 2, pp. 121–128, 1995.

[291] H. Eisazadeh, "Studying the Characteristics of Polypyrrole and its Composites," *World Journal of Chemistry*, vol. 2, no. 2, pp. 67–74, 2007.

[292] F. Beck and M. Oberst, "Electrodeposition and Cycling of Polypyrrole," *Makromolekulare Chemie. Macromolecular Symposia*, vol. 8, no. 1, pp. 97–125, 1987.

[293] M. Bozlar, F. Miomandre, and J. Bai, "Electrochemical Synthesis and Characterisation of Carbon Nanotube/Modified Polypyrrole Hybrids using a Cavity Microelectrode," *Carbon*, vol. 47, no. 1, pp. 80 – 84, 2009.

[294] Y. Y. Huang and E. M. Terentjev, "Dispersion of Carbon Nanotubes: Mixing, Sonication, Stabilisation, and Composite Properties," *Polymers*, vol. 4, no. 1, pp. 275–295, 2012.

[295] C.-J. Ko, C.-Y. Lee, F.-H. Ko, H.-L. Chen, and T.-C. Chu, "Highly Efficient Microwave-Assisted Purification of Multiwalled Carbon Nanotubes," *Microelectronic Engineering*, vol. 73, pp. 570 – 577, 2004.

[296] G. Han and G. Shi, "Conducting polymer Electrochemical Actuator made of High-Strength Three-layered Composite films of Polythiophene and Polypyrrole," *Sensors and Actuators B: Chemical*, vol. 99, pp. 525 – 531, 2004.

[297] S. Pegel, P. Potschke, G. Petzold, I. Alig, S. Dudkin, and D. Lellinger, "Dispersion, Agglomeration, and Network Formation of Multiwalled Carbon Nanotubes in Polycarbonate Melts," *Polymer*, vol. 49, no. 4, pp. 974–984, 2008.

[298] M. F. Islam, E. Rojas, D. M. Bergey, A. T. Johnson, and A. G. Yodh, "High Weight Fraction Surfactant Solubilisation of Single-Wall Carbon Nanotubes in Water," *Nano Letters*, vol. 3, no. 2, pp. 269–273, 2003.

[299] N. Grossiord, J. Loos, O. Regev, and C. E. Koning, "Toolbox for Dispersing Carbon Nanotubes into Polymers to get Conductive Nanocomposites," *Chemistry of Materials*, vol. 18, no. 5, pp. 1089–1099, 2006.

[300] K. Yurekli, C. A. Mitchell, and R. Krishnamoorti, "Small-Angle Neutron Scattering from Surfactant-Assisted Aqueous Dispersions of Carbon Nanotubes," *Journal of the American Chemical Society*, vol. 126, no. 32, pp. 9902–9903, 2004.

[301] M. O'Connell, B. P., E. L.M., C. Huffman, Y. Wang, E. Haroz, C. Kuper, J. Tour, K. D. Ausman, and R. E. Smalley, "Reversible Water-Solubilisation of Single-Walled Carbon Nanotubes by Polymer Wrapping," *Chemical Physics Letters*, vol. 342, no. 3, pp. 265–271, 2001.

[302] N. F. intao Zhu and R. C. Hayward, "Tuning the Assembly of Amphiphilic Block Copolymers through Instabilities of Solvent/Water Interfaces in the Presence of Aqueous Surfactants," *Soft Matter*, vol. 5, no. 12, pp. 2471–2478, 2009.

[303] K. Furton and A. Norelus, "Determining the Critical Micelle Concentration of Aqueous Surfactant Solutions: Using a Novel Colorimetric Method," *Journal of Chemical Education*, vol. 70, no. 3, pp. 254–257, 1993.

[304] D. Cheng and E. Gulari, "Micellisation and Intermicellar Interactions in Aqueous Sodium Dodecylbenzene Sulfonate Solutions," *Journal of Colloid and Interface Science*, vol. 90, no. 2, pp. 410–423, 1982.

[305] S. W. H. Shah, B. Naseem, W. Rehman, N. Bashir, and S. S. Shah, "Investigation of 1-Alkanols in Organised Solutions," *Chemical Society of Ethiopia*, vol. 25, no. 3, pp. 469–474, 2011.

[306] J. W. Moffett, R. G. Zika, and R. G. Petasne, "Evaluation of Bathocuproine for the Spectro-Photometric Determination of Copper(I) in Copper Redox Studies with Applications in Studies of Natural Waters," *Analytica Chimica Acta*, vol. 175, pp. 171 – 179, 1985.

[307] T. Saito, "Sensing of Trace Copper Ion by a Solid Phase Extraction-Spectrophotometry using a Poly(vinyl chloride) Membrane Containing Bathocuproine," *Talanta*, vol. 41, no. 5, pp. 811 – 815, 1994.

[308] A. Iseki, F. Kambe, K. Okumura, S. Niwata, R. Yamamoto, T. Hayakawa, and H. Seo, "Pyrrolidine Dithiocarbamate Inhibits TNF-α-Dependent Activation of NF-*k*B by Increasing Intracellular Copper Level in Human Aortic Smooth Muscle Cells," *Biochemical and Biophysical Research Communications*, vol. 276, no. 1, pp. 88 – 92, 2000.

[309] X. Zhang, Z. Jiang, Z. Yao, Y. Song, and Z. Wu, "Effects of Scan Rate on the Potentiodynamic Polarisation Curve Obtained to Determine the Tafel Slopes and Corrosion Current Density," *Corrosion Science*, vol. 51, no. 3, pp. 581 – 587, 2009.

[310] F. Mansfeld, "Tafel Slopes and Corrosion Rates Obtained in the Pre-Tafel Region of Polarisation Curves," *Corrosion Science*, vol. 47, no. 12, pp. 3178–3186, 2005.

[311] ——, "Fundamental aspects of the polarisation resistance technique the early days," *Journal of Solid State Electrochemistry*, vol. 13, no. 4, pp. 515–520, 2009.

[312] G. Badea, A. Caraban, M. Sebesan, S. Dzitac, P. Cret, and A. Setel, "Polarisation Measurements used for Corrosion rates Determination," *Journal of Sustainable Energy*, vol. 1, no. 1, pp. 140–144, 2010.

[313] M. M. Antonijevic, S. M. Milic, and M. B. Petrovic, "Films Formed on Copper Surface in Chloride Media in the Presence of Azoles," *Corrosion Science*, vol. 51, no. 6, pp. 1228 – 1237, 2009.

[314] R. Vergaz, D. Barrios, J.-M. Snchez-Pena, C. Pozo-Gonzalo, and M. Salsamendi, "Relating Cyclic Voltammetry and Impedance Analysis in a Viologen Electrochromic Device," *Solar Energy Materials and Solar Cells*, vol. 93, no. 12, pp. 2125 – 2132, 2009.

[315] E. McCafferty, "Validation of Corrosion Rates Measured by the Tafel Extrapolation Method," *Corrosion Science*, vol. 47, no. 12, pp. 3202–3215, 2005.

[316] L. Miller, B. Zinger, and Q. Zhou, "Electrically Controlled Release of Hexacyanoferrate (4-) from Polypyrrole," *Journal of the American Chemical Society*, vol. 109, no. 8, pp. 2267–2272, 1987.

[317] G. Appel, D. Schmeiafaer, J. Bauer, M. Bauer, H. Egelhaaf, and D. Oelkrug, "The Formation of Oligomers in the Electrolyte upon Polymerisation of Pyrrole," *Synthetic Metals*, vol. 99, no. 1, pp. 69 – 77, 1999.

[318] D. Kim, H. Cho, and C. Kim, "Mechanism of Redox Reaction on Polypyrrole," *Journal of Intelligent Material Systems and Structures*, vol. 5, no. 5, pp. 626–630, 1994.

[319] D. M. Soares, S. Wasle, K. G. Weil, and K. Doblhofer, "Copper ion reduction catalyzed by chloride ions," *Journal of Electroanalytical Chemistry*, vol. 532, no. 1, pp. 353 – 358, 2002.

[320] R. W. Ramette, "Copper(II) Complexes with Chloride Ion," *Inorganic Chemistry*, vol. 25, no. 14, pp. 2481–2482, 1986.

[321] F. King and S. kärnbränslehantering AB., *Corrosion of Copper in Alkaline Chloride Environments*, F. King and S. kärnbränslehantering AB., Eds. Swedish Nuclear Fuel and Waste Management Company, 2002.

[322] C. Deslouis, B. Tribollet, G. Mengoli, and M. M. Musiani, "Electrochemical Behaviour of Copper in Neutral Aerated Chloride Solution. I. Steady-state Investigation," *Journal of Applied Electrochemistry*, vol. 18, no. 3, pp. 374–383, 1988.

[323] M. Bazzaoui, E. Bazzaouib, and J. M. L Martinsc, "Electrochemical Synthesis of Adherent Polypyrrole films on Zinc Electrodes in Acidic and Neutral Organic Media," *Synthetic Metals*, vol. 128, no. 1, pp. 103 –114, 2001.

[324] W. Lewis, G. Wallace, Y. Kim, and D. Kim, "Studies of the Overoxidation of Polypyrrole," *Synthetic Metals*, vol. 84, no. 1-3, pp. 403–404, 1997.

[325] R. Paisal, R. Martinez, J. Padilla, and A. F. Romero, "Electrosynthesis and Properties of the Polypyrrole/Dodecylbenzene Sulfonate Polymer. Influence of Structural Micellar Changes of Sodium Dodecylbenzene Sulfonate at High Concentrations," *Electrochimica Acta*, vol. 56, no. 18, pp. 6345 – 6351, 2011.

[326] F. Kellou-Kerkouche, A. Benchettara, and S. Amara, "Effect of Sodium Dodecylbenzene Sulfonate on the Corrosion Inhibition of Fe-1Ti-20C Alloy in 0.5 M H_2SO_4," *Materials Chemistry and Physics*, vol. 110, no. 1, pp. 26–33, 2008.

[327] S. Abd El Rehim, H. Hassan, and M. Amin, "The Corrosion Inhibition Study of Sodium Dodecylbenzene Sulphonate to Aluminium and its Alloys in 1.0 M HCl Solution," *Materials Chemistry and Physics*, vol. 78, no. 2, pp. 337–348, 2003.

[328] R. Fuchs-Godec, "The Adsorption, CMC Determination and Corrosion Inhibition of some N-alkyl Quaternary Ammonium Salts on Carbon Steel Surface in 2M H_2SO_4," *Colloids and Surfaces A: Physicochemical and Engineering Aspects*, vol. 280, no. 1, pp. 130–139, 2006.

[329] M. Antonijevic, M. Petrovic, S. Serbula, S. Milic, and G. Bogdanovic, "Electrochemical Behavior of Copper in the Presence of Benzotriazole: Influence of pH and Chloride Ions," *Zastita Materijala*, vol. 47, no. 3, pp. 3–16, 2009.

[330] S. Shimoda and E. Smela, "The Effect of pH on Polymerisation and Volume Change in PPy(DBS)," *Electrochimica Acta*, vol. 44, no. 2-3, pp. 219 – 238, 1998.

[331] M. Careem, Y. Velmurugu, S. Skaarup, and K. West, "A Voltammetry Study on the Diffusion of Counter Ions in Polypyrrole Films," *Journal of Power Sources*, vol. 159, no. 1, pp. 210 – 214, 2006.

[332] Z. Nagy and D. A. Thomas, "Effect of Mass Transport on the Determination of Corrosion Rates from Polarisation Measurements," *Journal of the Electrochemical Society*, vol. 133, no. 10, pp. 2013–2017, 1986.

[333] H. P. Leckie, "The Anodic Polarisation Behavior of Copper," *Journal of the Electrochemical Society*, vol. 117, no. 12, pp. 1478–1483, 1970.

[334] A. Zhou, B. Xie, and N. Xie, "Comparison of Polarisation Curve and Electrochemical Quartz Crystal Microbalance Methods for Determination of Copper Corrosion Rate," *Corrosion Science*, vol. 42, no. 3, pp. 469 – 480, 1999.

[335] W. H. Gauvin and C. A. Winkler, "The Effect of Chloride Ions on Copper Deposition," *Journal of the Electrochemical Society*, vol. 99, no. 2, pp. 71–77, 1952.

[336] J. L. Anderson and I. Shain, "Cyclic Voltammetric Studies of the pH Dependence of Copper(II) Reduction in Acidic Aqueous Nitrate and Perchlorate Solutions," *Analytical Chemistry*, vol. 48, no. 9, pp. 1274–1282, 1976.

[337] J. Crousier, L. Pardessus, and J.-P. Crousier, "Voltammetry Study of Copper in Chloride Solution," *Electrochimica Acta*, vol. 33, no. 8, pp. 1039 – 1042, 1988.

[338] G. Kear, B. Barker, and F. Walsh, "Electrochemical Corrosion of Unalloyed Copper in Chloride Media–A Critical Review," *Corrosion Science*, vol. 46, no. 1, pp. 109–135, 2004.

[339] K. L. Mittal, *Adhesion Measurement of Films and Coatings*, K. L. Mittal, Ed. VSP, 1993.

[340] E. Kus and F. Mansfeld, "An Evaluation of the Electrochemical Frequency Modulation (EFM) Technique," *Corrosion Science*, vol. 48, no. 4, pp. 965 – 979, 2006.

[341] E. van Westing, G. Ferrari, and J. de Wit, "The Determination of Coating Performance with Impedance Measurements: Coating Polymer Properties," *Corrosion Science*, vol. 34, no. 9, pp. 1511 – 1530, 1993.

[342] K.-M. Yin and H. Wu, "Electrochemical Impedance Study of the Degradation of Organic-Coated Copper," *Surface and Coatings Technology*, vol. 106, no. 2, pp. 167 – 173, 1998.

[343] F. Mansfeld, "Use of Electrochemical Impedance Spectroscopy for the Study of Corrosion Protection by Polymer Coatings," *Journal of Applied Electrochemistry*, vol. 25, no. 3, pp. 187–202, 1995.

[344] Z. Stoynov and D. Vladikova, *Differential Impedance Analysis*, Z. Stoynov and D. Vladikova, Eds. Marin Drinov Academic Publishing House, 2005.

[345] A. Benedeti, P. Sumodjo, K. Nobe, P. Cabot, and W. Proud, "Electrochemical Studies of Copper, Copper-Aluminium and Copper-Aluminium-Silver Alloys: Impedance Results in 0.5M NaCl," *Electrochimica Acta*, vol. 40, no. 16, pp. 2657 – 2668, 1995.

[346] E. Genies and J. Pernaut, "Spectroelectrochemical Studies of the Redox and Kinetic Behaviour of Polypyrrole Film," *Synthetic Metals*, vol. 10, no. 2, pp. 117 – 129, 1984.

[347] X. Ren and P. G. Pickup, "Impedance Measurements of Ionic Conductivity as a Probe of Structure in Electrochemically Deposited Polypyrrole Films," *Journal of Electroanalytical Chemistry*, vol. 396, no. 1, pp. 359 – 364, 1995.

[348] Z. X.-B. Jinag Min, Zhang Hong-Yu, "Effect of Alkyl Chain Length on the Structure of Viologen Adsorbed on a Cu(100) Electrode," *Acta Physico-Chimica Sinica*, vol. 27, no. 1, pp. 163–168, 2011.

[349] C. Safarowsky, A. Rang, C. Schalley, K. Wandelt, and P. Broekmann, "Formation of 2D Supramolecular Architectures at Electrochemical Solid/Liquid Interfaces," *Electrochimica Acta*, vol. 50, no. 21, pp. 4257–4268, 2005.

[350] C. Safarowsky, L. Merz, A. Rang, P. Broekmann, B. Hermann, and C. Schalley, "Second-Order Templation: Ordered Deposition of Supramolecular Squares on a Chloride-Covered Cu (100) Surface," *Angewandte Chemie International Edition*, vol. 43, no. 10, pp. 1291–1294, 2004.

[351] D. Pham, S. Tsay, K. Gentz, C. Zoerlein, S. Kossmann, J. Tsay, B. Kirchner, K. Wandelt, and P. Broekmann, "Quasi-Reversible Chloride Adsorption/Desorption through a Polycationic Organic Film on Cu (100)," *The Journal of Physical Chemistry C*, vol. 111, no. 44, pp. 16 428–16 436, 2007.

[352] B. Wilde and G. Teterin, "Anodic Dissolution of Copper-Zinc Alloys in Alkaline Solutions," *British Corrosion Journal*, vol. 2, pp. 125–128, 1967.

[353] T. Tsuru, "Anodic Dissolution Mechanisms of Metals and Alloys," *Materials Science and Engineering: A*, vol. 146, no. 1-2, pp. 1–14, 1991.

[354] S. Kologo, M. Eyraud, L. Bonou, F. Vacandio, and Y. Massiani, "Voltametry and EQCM Study of Copper Oxidation in Acidic Solution in Presence of Chloride Ions," *Electrochimica Acta*, vol. 52, no. 9, pp. 3105 – 3113, 2007.

[355] S. Cere and M. Vazquez, "Properties of the Passive Films Present on Copper and Copper-Nickel Alloys in Slightly Alkaline Solutions," *Journal of Materials Science Letters*, vol. 21, no. 6, pp. 493–495, 2002.

[356] H.-D. Speckmann, M. M. Lohrengel, J. W. Schultze, and H.-H. Strehblow, "The Growth and Reduction of Duplex Oxide Films on Copper," *Berichte der Bunsengesellschaft fr Physikalische Chemie*, vol. 89, no. 4, pp. 392–402, 1985.

[357] R. L. Deutscher and R. Woods, "Characterisation of Oxide Layers on Copper by Linear Potential Sweep Voltammetry," *Journal of Applied Electrochemistry*, vol. 16, no. 3, pp. 413–421, 1986.

[358] A. Michalik, "Conductive Polymers for Corrosion Protection: A Critical Investigation," Ph.D. dissertation, Ruhr-Bochum University, 2009.

[359] M. Plavsic and B. cosovic, "The Effect of Surface Active Substances on the Electrochemical Behaviour of Copper Ions in Chloride Solutions and in Natural Waters," *Water Research*, vol. 23, no. 12, pp. 1545 – 1553, 1989.

[360] I. Milosev and M. Metikos-Hukovic, "Effect of Chloride Concentration Range on the Corrosion Resistance of Cu–xNi Alloys," *Journal of Applied Electrochemistry*, vol. 29, no. 3, pp. 393–402, 1999.

[361] D. Tromans and R. hong Sun, "Anodic Behavior of Copper in Weakly Alkaline Solutions," *Journal of the Electrochemical Society*, vol. 139, no. 7, pp. 1945–1951, 1992.

[362] D. Tromans, "Aqueous Potential-pH Equilibria in Copper-Benzotriazole Systems," *Journal of the Electrochemical Society*, vol. 145, no. 3, pp. L42–L45, 1998.

[363] H. Otmacic and E. Stupnisek-Lisac, "Copper Corrosion Inhibitors in Near Neutral Media," *Electrochimica Acta*, vol. 48, no. 8, pp. 985–991, 2003.

[364] O. Azzaroni, M. Cipollone, M. Vela, and R. Salvarezza, "Protective Properties of Dodecanethiol Layers on Copper Surfaces: The Effect of Chloride Anions in Aqueous Environments," *Langmuir*, vol. 17, no. 5, pp. 1483–1487, 2001.

[365] M. R. G. Chialvo, S. L. Marchiano, and A. J. Arva, "The Mechanism of Oxidation of Copper in Alkaline Solutions," *Journal of Applied Electrochemistry*, vol. 14, no. 2, pp. 165–175, 1984.

[366] F. Fay, I. Linossier, V. Langlois, D. Haras, and K. Vallee-Rehel, "SEM and EDX analysis: Two powerful Techniques for the Study of Antifouling Paints," *Progress in Organic Coatings*, vol. 54, no. 3, pp. 216 – 223, 2005.

[367] J. Cotton, P. Hayfield, and J. Morgan, "Corrosion. A Literature Review," *British Corrosion Journal*, vol. 1, no. 3, pp. 123–127, 1965.

[368] M. Finsgar and I. Milosev, "Inhibition of Copper Corrosion by 1, 2, 3-Benzotriazole: A Review," *Corrosion Science*, vol. 52, no. 9, pp. 2737–2749, 2010.

[369] F. Altaf, R. Qureshi, and S. Ahmed, "Surface Protection of Copper by Azoles in Borate Buffers-Voltammetric and Impedance Analysis," *Journal of Electroanalytical Chemistry*, vol. 659, no. 2, pp. 134–142, 2011.

[370] N. Morito and W. Suetaka, "Infra-Red and Ultra -Visible Reflection Spectra of the Surface Films on Cu Treated with Benzo-triazole," *Journal of Japan Institute of Metals*, vol. 35, no. 12, pp. 1165–1170, 1971.

[371] G. Poling, "Reflection Infra-Red Studies of Films Formed by Benzotriazole on Cu," *Corrosion Science*, vol. 10, no. 5, pp. 359 – 370, 1970.

[372] R. Roberts, "X-ray Photoelectron Spectroscopic Characterisation of Copper Oxide Surfaces Treated with Benzotriazole," *Journal of Electron Spectroscopy and Related Phenomena*, vol. 4, no. 4, pp. 273 – 291, 1974.

[373] N. Morito and W. Suetaka, "Infra-Red Reflection Studies of the Oxidation of Cu and the Inhibition by Benzotriazole," *Journal of Japan Institute of Metals*, vol. 36, no. 11, pp. 1131–1140, 1972.

[374] M. Musiani, G. Mengoli, M. Fleischmann, and R. Lowry, "An Electrochemical and SERS Investigation of the Influence of pH on the Effectiveness of some Corrosion Inhibitors of Copper," *Journal of Electroanalytical Chemistry and Interfacial Electrochemistry*, vol. 217, no. 1, pp. 187–202, 1987.

[375] B. Fang, C. Olson, and D. Lynch, "A Photoemission Study of Benzotriazole on Clean Copper and Cuprous Oxide," *Surface Science*, vol. 176, no. 3, pp. 476–490, 1986.

[376] G. Xue, J. Ding, P. Lu, and J. Dong, "SERS, XPS, and Electroanalytical Studies of the Chemisorption of Benzotriazole on a Freshly Etched Surface and an Oxidized Surface of Copper," *The Journal of Physical Chemistry*, vol. 95, no. 19, pp. 7380–7384, 1991.

[377] V. Brusic, M. Frisch, B. Eldridge, F. Novak, F. Kaufman, B. Rush, and G. Frankel, "Copper Corrosion With and Without Inhibitors," *Journal of the Electrochemical Society*, vol. 138, no. 8, pp. 2253–2259, 1991.

[378] T. Hashemi and C. Hogarth, "The Mechanism of Corrosion Inhibition of Copper in NaCl Solution by Benzotriazole Studied by Electron Spectroscopy," *Electrochimica Acta*, vol. 33, no. 8, pp. 1123 – 1127, 1988.

[379] D. Chadwick and T. Hashemi, "Benzotriazole Adsorption on Copper Studied by X-ray Photoelectron Spectroscopy," *Journal of Electron Spectroscopy and Related Phenomena*, vol. 10, no. 1, pp. 79 – 83, 1977.

[380] P. Fox, G. Lewis, and P. Boden, "Some Chemical Aspects of the Corrosion Inhibition of Copper by Benztriazole," *Corrosion Science*, vol. 19, no. 7, pp. 457–467, 1979.

[381] M. Antonijevic and M. Radovanovic, "Methods for Characterisation of Protective Films on the Copper Surface: A Review," *Zastita Materijala*, vol. 51, no. 2, pp. 111–122, 2010.

[382] F. H. Assaf, A. M. Zaky, and S. S. A. El-Rehim, "Cyclic Voltammetric Studies of the Electrochemical Behaviour of Copper-Silver Alloys in NaOH Solution," *Applied Surface Science*, vol. 187, pp. 18 – 27, 2002.

[383] G. Moretti and F. Guidi, "Tryptophan as Copper Corrosion Inhibitor in 0.5 M Aerated Sulfuric Acid," *Corrosion Science*, vol. 44, no. 9, pp. 1995 – 2011, 2001.

[384] G. Quartarone, T. Capobianco, A. Zingales, and G. Moretti, "Using Indole to Inhibit Copper Corrosion in Aerated 0.5 M Sulfuric Acid," *Corrosion*, vol. 54, no. 08, pp. 606–618, 1998.

[385] S. Olszowka, A. Barkatt, and M. Manning, "Copper Dissolution and Hydrogen Peroxide Formation in Aqueous Media," *Corrosion*, vol. 48, no. 5, pp. 411–418, 1992.

[386] M. Drogowska, L. Brossard, and H. Ménard, "Influence of Anions on the Passivity Behavior of Copper in Alkaline Solutions," *Surface and Coatings Technology*, vol. 34, no. 4, pp. 383–400, 1988.

[387] W. Shao, G. Pattanaik, and G. Zangari, "Influence of Chloride Anions on the Mechanism of Copper Electrodeposition from Acidic Sulfate Electrolytes," *Journal of the Electrochemical Society*, vol. 154, no. 4, pp. D201–D207, 2007.

[388] H. Dewald, P. Parmananda, and R. Rollins, "Periodic Current Oscillations in the Anodic Dissolution of Copper in Acetate Buffer," *Journal of Electroanalytical Chemistry and Interfacial Electrochemistry*, vol. 306, no. 1-2, pp. 297–300, 1991.

[389] E. Sutter, C. Fiaud, and D. Lincot, "Electrochemical and Photoelectrochemical Characterisation of Naturally Grown Oxide Layers on Copper in Sodium Acetate Solutions with and without Benzotriazole," *Electrochimica Acta*, vol. 38, no. 10, pp. 1471–1479, 1993.

[390] J. Kunze, V. Maurice, L. Klein, H. Strehblow, and P. Marcus, "In Situ STM Study of the Duplex Passive Films Formed on Cu (111) and Cu (001) in 0.1 M NaOH," *Corrosion Science*, vol. 46, no. 1, pp. 245–264, 2003.

[391] S. A. el Haleem and B. G. Ateya, "Cyclic Voltammetry of Copper in Sodium Hydroxide Solutions," *Journal of Electroanalytical Chemistry and Interfacial Electrochemistry*, vol. 117, no. 2, pp. 309 – 319, 1981.

[392] A. M. Castro Luna De Medina, S. L. Marchiano, and A. J. Arva, "The Potentiodynamic Behaviour of Copper in NaOH Solutions," *Journal of Applied Electrochemistry*, vol. 8, no. 2, pp. 121–134, 1978.

[393] F. Sinapi, S. Julien, D. Auguste, L. Hevesi, J. Delhalle, and Z. Mekhalif, "Monolayers and Mixed-Layers on Copper Towards Corrosion Protection," *Electrochimica Acta*, vol. 53, no. 12, pp. 4228–4238, 2008.

[394] A. Benedetti, R. Nakazato, P. Sumodjo, P. Cabot, F. Centellas, and J. Garrido, "Potentiodynamic Behaviour of Cu-Al-Ag Alloys in NaOH: A Comparative Study Related to the Pure Metals Electrochemistry," *Electrochimica Acta*, vol. 36, no. 9, pp. 1409 – 1421, 1991.

[395] D. T. Schwartz and R. H. Muller, "Oxidation Films on Copper in Alkaline Media: Intensity Modulated Photoelectrochemical and Raman Spectroscopy Studies," *Surface Science*, vol. 248, no. 3, pp. 349 – 358, 1991.

[396] D. Schwartz and R. Muller, "Photoelectrochemical Evidence for Saturated Optical Absorption in Electrolytic Cuprous Oxide," *Applied Physiscs Letters*, vol. 58, no. 16, pp. 1739–1741, 1991.

[397] S. Wilhelm, Y. Tanizawa, C.-Y. Liu, and N. Hackerman, "A photo-Electrochemical Investigation of Semi-conducting Oxide Films on Copper," *Corrosion Science*, vol. 22, no. 8, pp. 791 – 805, 1982.

[398] S. Milic and M. Antonijevic, "Some Aspects of Copper Corrosion in Presence of Benzotriazole and Chloride Ions," *Corrosion Science*, vol. 51, no. 1, pp. 28 – 34, 2008.

[399] D. Gimenez-Romero, J. J. Garcia-Jareno, J. Agrisuelas, C. Gabrielli, H. Perrot, and F. Vicente, "Formation of a Copper Oxide Layer as a Key Step in the Metallic Copper Deposition Mechanism," *The Journal of Physical Chemistry C*, vol. 112, no. 11, pp. 4275–4280, 2008.

[400] B. Millet, C. Fiaud, C. Hinnen, and E. Sutter, "A Correlation Between Electrochemical Behaviour, Composition and Semi-conducting Properties of Naturally Grown Oxide Films on Copper," *Corrosion Science*, vol. 37, no. 12, pp. 1903 – 1918, 1995.

[401] A. Naseer and A. Y. Khan, "A Study of Growth and Breakdown of Passive Flm on Copper Surface by Electrochemical Impedance Spectroscopy," *Turkish Journal of Chemistry*, vol. 33, pp. 739–750, 2007.

[402] J. Long, P. Searson, and P. Vereecken, "Electrochemical Characterisation of Adsorption-Desorption of the Cuprous-Suppressor-Chloride Complex During Electrodeposition of Copper," *Journal of the Electrochemical Society*, vol. 153, no. 4, pp. C258–C264, 2006.

[403] J. G. Becerra, R. Salvarezza, and A. Arvia, "The Influence of Slow $Cu(OH)_2$ Phase Formation on the Electrochemical Behaviour of Copper in Alkaline Solutions," *Electrochimica Acta*, vol. 33, no. 5, pp. 613 – 621, 1988.

[404] F. Walsh, C. P. de Len, C. Kerr, S. Court, and B. Barker, "Electrochemical Characterisation of the Porosity and Corrosion Resistance of Electrochemically Deposited Metal Coatings," *Surface and Coatings Technology*, vol. 202, no. 21, p. 5092 5102, 2009.

[405] Y. Feng, W.-K. Teo, K.-S. Siow, and A.-K. Hsieh, "The Corrosion Behaviour of Copper in Neutral Tap Water: Determination of Corrosion Rates," *Corrosion Science*, vol. 38, no. 3, pp. 387 – 395, 1997.

[406] K. Cheung, D. Bloor, and G. Stevens, "Characterisation of Polypyrrole Electropolymerised on Different Electrodes," *Polymer*, vol. 29, no. 9, pp. 1709–1717, 1988.